

Floods of Central Europe during the Late Quaternary

Dissertation

zur Erlangung des Grades

„Doktor der Naturwissenschaften“

im Promotionsfach Geologie/ Paläontologie

am Fachbereich Chemie, Pharmazie und Geowissenschaften

der Johannes Gutenberg-Universität

in Mainz

Heiko Brunck

geb. in Landstuhl

Mainz, Januar 2017

Dekan:

1. Gutachter:

2. Gutachter:

Tag der mündlichen Prüfung: 31.03.2017

„Es kommt nicht darauf an, mit dem Kopf durch die Wand zu rennen, sondern mit den Augen die Tür zu finden.“

Werner von Siemens (1816 – 1892)

Abstract

Since 1998, drill cores have been systematically extracted from the maar lakes and the dry maar structures of the Eifel region as part of the ELSA project (Eifel Laminated Sediment Archive) by the Institute for Geosciences of the Johannes Gutenberg University Mainz. In the maar structures, predominantly anoxic conditions are present in the deep water, thus reducing bioturbation to a minimum. For this reason, event layers remain undisturbed in the maar sediments. If the maars are additionally fed by a river or stream, the sediments can also be used as a flood archive.

Long time series of flood events are increasingly required on a time scale of hundreds or thousands of years in order to establish contexts and frequency in a larger climatic relationship than it would be possible using historical records and instrumental data. Lakes that allow a Holocene flood and climate reconstruction are widespread in Central Europe. However, continuous reconstructions of the climatic conditions for the period between 10 000 and 60 000 before AD 2000 (b2k) are only possible in the maar structures of the Eifel region. This study reconstructs the most significant flood stages in Central Europe by detecting flood markers in Holocene and Pleistocene maar sediments. For a better understanding of the sedimentation history, the focus of the "Palaeoflood project" was on the detection of event layers and the correlation of these layers between several maar structures. The frequency of flood deposits in the Eifel maar sediments allows a detailed reconstruction of the flood history in the context of climate development. The period of interest in this work includes, for the first time, a climate-related flood chronology based on recent gauge data from Cologne combined with palaeoflood events from the Holocene and the late Pleistocene.

The basis of this dissertation is the publication "The ELSA-Vegetation-Stack: Reconstruction of Landscape Evolution Zones (LEZ) from laminated Eifel maar sediments of the last 60 000 years", in which the stratigraphy of the Eifel maar structures could be tuned to the Greenland ice core chronology. The special sedimentation conditions in the maar structure of Auel explains the unique possibility of rediscovering all 17 Greenland interstadials in the data of the "Total Carbon Measurements". Furthermore, 5 different tephra layers of several centimetre have been identified in the sediments of Auel. These tephra layers have also been described in all other ELSA sediment cores, enabling one to

make a simple maar-to-maar to correlation. Based on this new stratigraphic concept, the landscape evolution of Central Europe could be directly compared with the Greenland climate history and so-called landscape development zones, short LEZ's, were defined. The LEZ's represent the largest vegetation- and climate changes during the last 60 000 years and were developed primarily on the basis of pollen and macroremains.

A comparison between gauge-time series from the Eifel region and Germany showed that the floods in the streams and rivers of the Eifel statistically correlate significantly with floods in the Rhine and Moselle. Therefore, local extreme precipitation events of the Eifel region can be transmitted to the supra-regional level of Central Europe. In total, 297 flood layers measuring more than 7.5 mm could be identified in the sediment cores from Schalkenmehren, Ulmen, Holzmaar, Roth, Merscheid and Auel.

In contrast to turbidites, suspension layers are not graduated from a coarse base layer to a fine top layer; instead, a heterogeneous particle-size gradient can be detected with several particle-size maxima within a flood layer. These observations can be explained by the repetitive occurrence of heavy rainfall during the days and weeks of a major flood event. Thus, flood layers can be distinguished from normal background sedimentation and seismites by the microscopic analysis of thin sections. In consequence of further sedimentological and/ or geochemical investigations (e.g. particle size, Camsizer[®] or μ -XRF analysis), it is also possible to clearly demarcate flood layers, turbidites and slumps.

The strongest flood events occurred in the Late Holocene (LEZ 1) and could be assigned to the years 658, 2800 and 4100 b2k (AD 1342, 800 BC and 2100 BC). By contrast, the flood layers in the Early Holocene are mostly weak. Nevertheless, a slight flood peak could be identified in the period between 6000 and 6500 b2k. For the Pleistocene, 33 flood layers could be dated from the LEZ 3 (10 500 – 14 700 b2k), 11 from the LEZ 4 (14 700 – 21 000 b2k), 20 from the LEZ 5 (21 000 – 28 500 b2k), 45 from the LEZ 6 (28 500 – 36 500 b2k), 25 from the LEZ 7 (36 500 – 49 000 b2k), 6 from the LEZ 8 (49 000 – 55 000 b2k), 0 from the LEZ 9 (55 000 – 60 000 b2k) and 10 older than 60 000 b2k. The analysis of the sediment cores showed 6 distinct flood phases in the glacial – interglacial cycle. These occur in the time periods 10 000 – 17 500 b2k, 21 500 – 24 000 b2k, 26 000 – 35 000 b2k, 39 000 – 47 000 b2k, 51 500 – 54 500 b2k and 60 500 – 64 000 b2k. A closer look at the results revealed that several maar structures are

suitable for the reconstruction of flood phases, while the highest resolution and most accurate results are only possible in the sediments of Auel.

The variation of the flood dynamics is primarily climatically controlled and predominantly associated with moister and colder periods in combination with vegetation changes. It turned out that low vegetation cover, which is related to Greenland stadials or anthropogenic influence, is mainly responsible for the formation of flood layers in the sediments of the maar structures. Consequently, flood events most likely document the erodibility of the soils to the first order, and climate events only to the second order.

Zusammenfassung

Seit 1998 werden die Maarseen und Trockenmaare der Eifel im Rahmen des ELSA Projektes (Eifel Laminated Sediment Archive) systematisch von dem Institut für Geowissenschaften der Johannes Gutenberg-Universität Mainz mittels Bohrkerne erschlossen. In den Maarstrukturen bilden sich vorwiegend anoxische Bedingungen im Tiefenwasser aus und reduzieren somit die Bioturbation auf ein Minimum. Aus diesem Grund bleiben Eventlagern in den Maarsedimente ungestört erhalten. Werden die Maare zusätzlich von einem Fluss oder Bach gespeist, sind die Sedimente auch als Hochwasserarchive nutzbar.

Lange Zeitreihen von Hochwasserevents werden immer häufiger auf hundert- oder tausendjähriger Zeitskala benötigt, um die Zusammenhänge und Frequenzen in einen größeren klimatischen Bezug zu setzen als es durch historische Aufzeichnungen und instrumentelle Daten möglich wäre. Seen, die eine holozäne Hochwasser- und Klimarekonstruktion ermöglichen, sind in Mitteleuropa weit verbreitet. Allerdings sind kontinuierliche Rekonstruktionen der klimatischen Bedingungen für den Zeitraum zwischen 10 000 und 60 000 vor dem Jahr AD 2000 (b2k) nur in den Maaren der Eifel möglich. Die vorliegende Studie rekonstruiert die bedeutendsten Flutphasen in Zentraleuropa mittels Detektion von Suspensionslagen in holozänen und pleistozänen Maarsedimenten der Eifel. Für ein besseres Verständnis der Sedimentationsgeschichte lag der Schwerpunkt des „Palaeoflood Projektes“ auf dem Nachweis der Eventlagen und der Korrelation dieser Schichten zwischen mehreren Maarstrukturen. Die Häufigkeit der Hochwasserevents in den Sedimenten der Eifel ermöglicht eine detaillierte Rekonstruktion der Hochwassergeschichte von Mitteleuropa im Kontext der Klimaentwicklung. Zum ersten Mal konnte eine klimabezogene Hochwasser-Chronologie für die letzten 60 000 Jahre durch die Verknüpfung von rezenten Pegeldaten aus Köln mit paläohydrologischen Ereignissen aus Sedimentkernen aufgestellt werden.

Die Grundlage der vorliegenden Dissertation bildet die mitveröffentlichte Publikation „The ELSA-Vegetation-Stack: Reconstruction of Landscape Evolution Zones (LEZ) from laminated Eifel maar sediments of the last 60 000 years“, in der erstmals die Stratigraphie der Eifel-Maare an die grönländische Eiskern-Chronologie angepasst werden konnte. Die speziellen Sedimentationsbedingungen in dem Maar Auel erklärt die einzigartige

Möglichkeit alle 17 Grönland Interstadiale in den Daten der „Total Carbon-Messungen“ wiederzufinden. Des Weiteren konnten in den Sedimenten von Auel 5 verschiedene Tephralagen von mehreren Zentimetern identifiziert werden. Diese Tephralagen wurden auch in allen anderen ELSA Sedimentkernen beschrieben, wodurch eine Maar zu Maar Korrelation möglich ist. Auf Basis dieses neuen stratigraphischen Konzepts konnte die landschaftliche Entwicklung von Mitteleuropa direkt mit der grönländischen Klimageschichte verglichen werden und sogenannte Landschaftsentwicklungszonen, kurz LEZ's, definiert werden. Dabei repräsentieren die LEZ's die größten Vegetations- und Klimaveränderungen der letzten 60 000 Jahre und wurden vor allem auf Basis von Pollen und Makroresten entwickelt.

Ein Vergleich zwischen Pegelzeitreihen aus der Eifel und Deutschland zeigte, dass die Hochwasserereignisse in den Bächen und Flüssen der Eifel statistisch signifikant mit Hochwässern in Rhein und Mosel korrelieren. Daher können diese lokalen Niederschlagsextremereignisse auf die überregionale Ebene von Mitteleuropa übertragen werden. Insgesamt konnten 297 Flutlagen über 7,5 mm in den Sedimentkernen von Schalkenmehren, Ulmen, Holzmaar, Roth, Merscheid und Auel identifiziert werden.

Suspensionslagen sind im Gegensatz zu Turbiditen nicht von einer groben Basisschicht zu einer feinen Deckschicht gradiert, stattdessen kann ein heterogener Korngrößengradient mit mehreren Korngrößenmaxima innerhalb einer Hochwasserlage detektiert werden. Diese Beobachtungen lassen sich durch den wiederholenden Starkregeneintrag während den Tagen und Wochen eines großen Hochwasserereignisses erklären. Somit lassen sich Hochwasserlagen von der normalen Hintergrundsedimentation und von Seismiten durch die mikroskopische Analyse von Dünnschliffen unterscheiden. In Folge von weiteren sedimentologischen und/ oder geochemischen Untersuchungen (z.B. Korngrößen-, Camsizer®- oder μ -XRF-Analysen) ist auch eine eindeutige Abgrenzung zwischen Hochwasserlagen, Turbiditen und Rutschungen möglich.

Die stärksten Flutereignisse traten im späten Holozän (LEZ 1) auf und konnten den Jahren 658, 2800 und 4100 b2k (AD 1342, 800 BC und 2100 BC) zugeordnet werden. Im Gegensatz dazu sind die Flutlagen im frühen Holozän überwiegend schwach ausgeprägt. Nichtsdestotrotz konnte ein leichtes Flutmaximum in der Zeit zwischen 6000 – 6500 b2k identifiziert werden. Für das Pleistozän konnten 33 Hochwasserlagen der LEZ 3 (10 500 – 14 700 b2k) zugeordnet werden, 11 der LEZ 4 (14 700 – 21 000 b2k), 20 der

LEZ 5 (21 000 – 28 500 b2k), 45 der LEZ 6 (28 500 – 36 500 b2k), 25 der LEZ 7 (36 500 – 49 000 b2k), 6 der LEZ 8 (49 000 – 55 000 b2k), 0 der LEZ 9 (55 000 – 60 000 b2k) und 10 älter als 60 000 b2k. Die Analyse der Sedimentkerne ergab 6 ausgeprägte Flutphasen im Glazialen – Interglazialen Zyklus. Diese belaufen sich auf die Zeitspannen von 10 000 bis 17 500 b2k, 21 500 bis 24 000 b2k, 26 000 bis 35 000 b2k, 39 000 bis 47 000 b2k, 51 500 bis 54 500 b2k und 60 500 bis 64 000 b2k. Bei der differenzierten Betrachtung der Ergebnisse fällt auf, dass mehrere Maarstrukturen für die Rekonstruktion von Hochwasserlagen geeignet sind, die höchst aufgelösten und präzisesten Ergebnisse aber nur in den Sedimenten von Auel möglich sind.

Die Variation der Hochwasserdynamik ist vor allem klimatisch gesteuert und vorwiegend mit feuchteren und kälteren Perioden sowie mit Vegetationsveränderungen verbunden. Dabei stellte sich heraus, dass die geringe Vegetationsbedeckung, welche im Zusammenhang mit Grönland Stadialen oder dem anthropogenen Einfluss steht, hauptverantwortlich für die Ausbildung von Flutlagen in den Sedimenten der Maare ist. Folglich dokumentieren die Hochwasserereignisse in erster Instanz die Erosionsanfälligkeit der Böden und nur untergeordnet die Klimaereignisse.

Table of Contents

List of Figures	II
List of Tables	VI
Preface	VII
1 Introduction	1
1.1 Flood reconstruction – State of the art	2
1.2 The geological setting of the Eifel	4
1.3 The formation of a maar lake	6
1.4 The Eifel region – Study area	8
1.5 Methods	10
1.6 Objectives	11
2 Manuscript 1	13
<i>The ELSA-Vegetation-Stack: Reconstruction of Landscape Evolution Zones (LEZ) from laminated Eifel maar sediments of the last 60,000 years</i>	
3 Manuscript 2	73
<i>Defining transport processes of the clastic sand fraction in lake sediments by rapid Camsizer® analysis</i>	
4 Manuscript 3	97
<i>The ELSA-Flood-Stack: A reconstruction from the laminated sediments of Eifel maar structures during the last 60 000 years</i>	
5 Manuscript 4	118
<i>Reconstruction of the Stadial – Interstadial flood frequency from dry maar structure Auel and laminated Eifel maar sediments</i>	
6 Conclusion and Outlook	141
7 Bibliography	145
8 Appendix	
Appendix A Core data table	175
Appendix B High resolution lithology	176
Appendix C Flood layer table	195
Appendix D Core correlation table	207
Acknowledgements	X
Curriculum vitae	XI
Eidesstattliche Erklärung	XII

List of Figures

Fig. 1.1:	Schematic cross-section of a maar lake (modified after Büchel, 1993)	7
Fig. 1.2:	Digital terrain model of the Eifel region with all core positions	9
Fig. 2.1:	a) Map of the modern North Atlantic b) Digital elevation map of the “Rheinisches Schiefergebirge”. c) Digital elevation model of the Eifel region with maar positions and coring sites	16
Fig. 2.2:	Photo of core HM1 from Lake Holzmaar with tephra marker layers.....	19
Fig. 2.3:	Photo of core DE3 from Dehner maar with tephra marker layers.....	20
Fig. 2.4a:	Photo of core AU2 from Auel (0-75 m) dry maar with tephra layers	22
Fig. 2.4b:	Photo of core AU2 from Auel (75-123 m) dry maar with tephra layers	22
Fig. 2.5:	Pollen concentrations, macroremains and marker tephra layer of core HM1 from Holzmaar versus depth	27
Fig. 2.6:	Pollen percent concentrations and marker tephra layer of core DE3 from Dehner dry maar versus depth	28
Fig. 2.7:	Pollen counts [$\#/ \text{cm}^3$] of sediment and marker tephra layer of core DE3 from Dehner dry maar versus depth.....	29
Fig. 2.8:	Pollen concentrations of core AU2 from Auel dry maar versus depth.....	29
Fig. 2.9:	Photos of selected macroremains typical for the LEZ.....	30
Fig. 2.10a:	Macroremains ($\#/ 200 \text{ g}$) of core HM1 from Holzmaar versus depth	31
Fig. 2.10b:	Macroremains ($\#/ 200 \text{ g}$) of core HM1 from Holzmaar versus depth	32
Fig. 2.10c:	Macroremains ($\#/ 200 \text{ g}$) of core HM1 from Holzmaar versus depth	33
Fig. 2.11:	Macroremains (presence/ absence) of core DE3 from Dehner dry maar versus depth	34
Fig. 2.12a:	Macroremains ($\#/ \text{kg}$) of core AU2 from Auel dry maar versus depth	35
Fig. 2.12b:	Macroremains ($\#/ \text{kg}$) of core AU2 from Auel dry maar versus depth	36
Fig. 2.13:	Diatoms of core DE3 from Dehner dry maar versus depth	37
Fig. 2.14:	Overview of main ELSA cores covering MIS 1 – 7.....	39
Fig. 2.15:	Schematic diagrams of annual varve composition during the last 60 000 years as visible on petrographic thin sections.....	41
Fig. 2.16:	Varve thickness and normalised varve stack in comparison with normalised flood stack (modified after Brunck et al., 2016).....	42

Fig. 2.17:	Age/ depth relations for cores AU2, DE2/ DE3 and HM1 with ¹⁴ C dates and the Picea-Carpinus-pollen-zones	43
Fig. 2.18:	Age/ depth relations for cores MS1, RM2, DE3 and AU2 with detected tephra marker layers (after Förster and Sirocko, 2016) and the Picea pollen zones.....	44
Fig. 2.19:	¹⁴ C dates and time series of total carbon concentrations from AU2 tuned to the Greenland ice core stratigraphy after Svensson et al. (2008).....	46
Fig. 2.20:	The ELSA-Vegetation stack	48
Fig. 2.21:	Synthesis of all ELSA stacks	49
Fig. 2.22:	Time series of the major forcings for the Central European climate during the last 60 000 years	55
Fig. 3.1:	Camsizer [®] device with sediment funnel and feeding channel on top left.....	76
Fig. 3.2:	Particle flow and detecting process in the Camsizer [®] (modified after Retsch Technology, 2011)	77
Fig. 3.3:	Illustration of the shape parameter sphericity.....	78
Fig. 3.4:	Illustration of the shape parameter symmetry	79
Fig. 3.5:	Illustration of the shape parameter breadth/ length	80
Fig. 3.6:	Illustration of the shape parameter convexity.....	80
Fig. 3.7:	Microscopic photo, grain size distribution and sphericity of Holocene interglacial sample from Holzmaar	81
Fig. 3.8:	Microscopic photo, grain size distribution and sphericity of Eemian interglacial sample from Maar westlich Hoher List	82
Fig. 3.9:	Microscopic photo, grain size distribution and sphericity of glacial loess with an aeolian coversand fraction from Dehner dry maar	83
Fig. 3.10:	Microscopic photo, grain size distribution and sphericity of glacial aeolian loess sample from Dehner dry maar.....	84
Fig. 3.11:	Microscopic photo, grain size distribution and sphericity of a flood event from the riparian zone at Auel dry maar	85
Fig. 3.12:	Microscopic photo, grain size distribution and sphericity of interstadial flood sample from Auel dry maar.....	86
Fig. 3.13:	Microscopic photo, grain size distribution and sphericity of tephra sample from Maar westlich Hoher List	87

Fig. 3.14:	Microscopic photo, grain size distribution and sphericity of turbidite sample from Dehner dry maar	89
Fig. 3.15:	Microscopic photo, grain size distribution and sphericity of slump sample from Dehner dry maar	89
Fig. 3.16:	Microscopic photo, grain size distribution and sphericity of a river sample from Heidelberg	91
Fig. 3.17:	Microscopic photo, grain size distribution and sphericity of a river sample from Ludwigshafen	91
Fig. 3.18:	Symmetry of the grain size classes for all studied samples	93
Fig. 3.19:	Sphericity of the grain size classes for all studied samples	94
Fig. 4.1:	a) Outline map of Germany. b) Digital terrain model West Germany c) Digital terrain model of the Eifel with the maar locations and the core positions	100
Fig. 4.2:	Age/ depth model of the cores SMf2, UM2, HM1 and AU2	102
Fig. 4.3:	Time series with transition points between the gauge analysis and the cores SMf2, UM2, HM1 and AU2	103
Fig. 4.4:	a) Pattern of an idealized flood layer. b) Pattern of an idealized turbidite. c) Pattern of an idealized slump	104
Fig. 4.5:	a) Summer suspension layer. b) Winter suspension layer. c) Turbidite. Modified after Sirocko and Dietrich (2009)	107
Fig. 4.6:	a) Core SMf2 with all detected flood events and varve counted years. b) Core HM1 with all detected flood events and tephra layers. c) Core UM2 with all detected flood events	109
Fig. 4.7:	a) Core AU2 with all detected flood events and tephra layers. b) Exemplary flood layer from the depth of 15.41 m	110
Fig. 4.8:	The ELSA-Flood-Stack	112
Fig. 5.1:	a) Outline map of Germany. b) Digital terrain model of central western Germany c) Digital terrain model of the Eifel showing maar locations after Büchel (1993) and core positions	121
Fig. 5.2:	Geological overview map of the maar structures Auel, Merscheid and Roth with the exact core position	122
Fig. 5.3:	Age/ depth model for cores AU2, MS1 and RM2. In addition, the C_{total} from Auel is directly tuned to the GI 1 – 17	125
Fig. 5.4:	Overview of the study area and field work location of Auel	126

Fig. 5.5:	Unconstrained inversion model of ERT 1 and DP EC logs 1 – 5 that were converted to electrical resistivities using the identical colour scale	127
Fig. 5.6:	Stratigraphical log of core AU8 and electrical conductivity values of DP3	128
Fig. 5.7:	Grain count ratios of the marker layers from Laacher See, Wartgesberg, Dreiser-Weiher, unknown origin UT1 and unknown origin UT2	129
Fig. 5.8:	Subdivision of the maar structures from the west Eifel region into groups according to their hydrological background	131
Fig. 5.9:	Core AU2 with all detected flood events and tephra layers	132
Fig. 5.10:	Core MS1 with all detected flood events and tephra layers	133
Fig. 5.11:	Core RM2 with all detected flood events and tephra layers	134
Fig. 5.12:	Comparison of the flood records from Auel with the results from the cores MS1 and RM2	136
Fig. 6.1:	The Elsa-Flood-Stack with new results from Merscheid and Roth	142

List of Tables

Tab. 1.1:	Morphometry of the 7 Eifel maar lakes, modified after Scharf and Oehms, (1992)	6
Tab. 2.1:	Top and base for LEZ 1 – 10 in all ELSA cores	50
Tab. 3.1:	Equations for mean grain size, the median, the sorting, the skewness and the kurtosis after Folk and Ward (1957) and Tucker (1996)	81
Tab. 3.2:	Descriptive statistical parameters of the sand fraction in lake sediments	93
Tab. 4.1:	Time overview of all flood events from the gauge analysis and the core SMf2, as well as the number of flood events per 1000 years from the cores HM1, UM2 and AU2.....	115
Tab. 5.1:	Number of flood events per 1000 years for the cores AU2, MS1 and RM2 from the Eifel region	135

Preface

My investigation focused on the main flood phases in Central Europe from event layers in sediment cores from Holocene Eifel maar lakes and Pleistocene dry maar structures. These reconstructions are combined with recent gauge time-series to cover the entire precipitation extremes of the last 60 000 years. This sedimentary record of flood events will help to understand flood variability under changing climate boundary conditions in Central Europe further back in time complementing instrumental and documentary archives.

This thesis is a “cumulative thesis” and includes four single manuscripts (Chapters 2 – 5), which are presented after the introduction (Chapter 1). These manuscripts represent the stratigraphy (Chapter 2), new methods to identify flood layers (Chapter 3) and the history of flood variations at various time scales, from modern instrumental time (last 200 years) to prehistoric time (60 000 b2k) by tuning the stratigraphy to the Greenland ice core chronology (Chapter 4 and Chapter 5).

The manuscripts have been either published or submitted for publication. Manuscript no. 1 is published, manuscript no. 2 has been submitted, manuscript no. 3 is published and manuscript no. 4 is submitted. A summary and conclusion of this thesis is presented in the final chapter (chapter 6). The references are listed in chapter 7.

Manuscript #1 (Chapter 2)

Title: The ELSA-Vegetation-Stack: Reconstruction of Landscape Evolution Zones (LEZ) from laminated Eifel maar sediments of the last 60 000 years

Authors: Frank Sirocko, Hannes Knapp, Frank Dreher, Michael Förster, Johannes Albert, Heiko Brunck, Daniel Veres, Stephan Dietrich, Michael Zech, Ulrich Hambach, Marieke Röhner, Saskia Rudert, Klaus Schwibus, Christel Adams, Petra Sigl

Published in *Global and Planetary Change*

Manuscript #1 presents the stratigraphy and the climate history of laminated sediment records from several maar lakes and dry maar structures of the Eifel (Germany) during the last 60 000 years. The time series of the last 30 000 years is based on a continuous varve counted chronology; the MIS 3 section is tuned to the Greenland ice core chronology.

Total carbon, pollen and plant macrofossils are employed to synthesize a vegetation-stack, which is used together with the stacks from seasonal varve formation, flood layers, aeolian dust content and volcanic tephra layers to define Landscape Evolution Zones (LEZ).

Manuscript #2 (Chapter 3)

Title: Defining transport processes of the clastic sand fraction in lake sediments by rapid Camsizer® analysis

Authors: Christel Adams, Marieke Röhner, Heiko Brunck, Frank Sirocko

Submitted to *The Depositional Record*

This study analyses different transport processes from lake sediments with a Retsch Camsizer® for the sand and gravel fraction to understand and reconstruct the climate and environment of the past. The coarse grain fractions have been photographed with the Extended Focal Imaging method to detect the texture of the rounded, frosted and pitted grain surfaces. The mode/ bimodality of the sand fraction together with the grain symmetry and sphericity allows to detect organic particles and characterizes the aeolian, fluvial and limnic transport processes.

Manuscript #3 (Chapter 4)

Title: The ELSA-Flood-Stack: A reconstruction from the laminated sediments of Eifel maar structures during the last 60 000 years

Authors: Heiko Brunck, Johannes Albert, Frank Sirocko

Published in *Global and Planetary Change*

The manuscript reconstructs the main flood phases in Central Europe from event layers in sediment cores from Holocene Eifel maar lakes (Schalkenmehren, Ulmen and Holzmaar) and a Pleistocene dry maar structure (Auel). These reconstructions are combined with recent gauge time-series from Cologne to cover the entire precipitation extremes of the last 60 000 years.

Manuscript #4 (Chapter 5)

Title: Reconstruction of the Stadial – Interstadial flood frequency from dry maar structure Auel and laminated Eifel maar sediments

Authors: Heiko Brunck, Peter Fischer, Tina Wunderlich, Andreas Vött, Frank Sirocko

Submitted to *Journal of Limnology*

This manuscript compares for the first time the main flood phases from three different Pleistocene dry maar structures. The cores were drilled in the Eifel region of western Germany and were dated by ^{14}C , luminescence, tephra markers and ice core tuning. Therefore, a clear inter-maar correlation of event layers can be done to define the main glacial – interglacial flood phases.

Author's contribution

I am the first author of manuscript #3 and manuscript #4 presented in this thesis. I led the interpretation of the results as well as the writing of the manuscripts. I organized and lead the coring campaign in collaboration with Peter Fischer. Helpful discussions and valuable comments on the manuscripts with constructive improvements were given by the co-authors. I conducted all analyses and established the flood chronology for the last 60 000 b2k based on the stratigraphy presented in manuscript #1. My work concerned the combined interpretation of core analyses with geochemical data and event layer identification.

Manuscript #1: I performed the core analyses and the lithoprofiles, especially for the core AU2 and the step by step tuning of the AU2- C_{total} time series to the Greenland ice core chronology GICC05 (Svensson et al., 2008). I wrote parts of the manuscript with flood relations and helped with the stratigraphic interpretation of the data.

Manuscript #2: I measured samples with the Camsizer[®] from three sediment cores and developed ideas about depositional processes in lake basins. I analysed the data, reviewed the relevant literature and compared the different event layer types. All authors took part in the evaluation and interpretation of the results and the writing of the manuscript.

Chapter 1

Introduction

Maars represent a high-resolution natural climate archive based on their annual varve sediments. The connection was first recognized in 1878 by the Swedish geologist Gerard de Geer, who presented the first geochronology of the past 12 000 years. Due to its proximity to the Eifel region and in view of the geological and climatological possibilities offered by investigations of sediments from maar structures, the drilling project ELSA (Eifel Laminated Sediment Archive) was established in 1998 at the University of Mainz and has been continuously expanded.

Initial researches were limited to dry maar structures and extended in 2004 to include the open maar lakes of the Eifel region. For this purpose, a special drilling method is applied, which makes it possible to core 2-metre-long undisturbed core samples from the upper water sediments. The core is drilled from a floating platform, on which a 2 m long sword is pressed by a rod into the sediment. Subsequently, an 800 °C cold liquid-gas mixture is pumped from the platform into the sword to freeze the sediment onto the metal surface (Sirocko, 2009). Longer cores of up to 12 metres are obtained with a Livingston piston corer. The core surfaces are disturbed by the pile-driving process, which is why several overlapping cores are drilled in order to obtain full coverage of the sediment profile.

Sediment cores from dry maar structures are extracted by using a wire line coring method. With this method, drilling is accomplished by rotating the outer piping. A 1 m long core barrel is latched onto the lowest metre of the piping, and the core sample is slid into this. After each metre of drilling, a 1-metre-long core section is brought to the surface with the wire line. Smaller dry maar structures are studied with pile cores of up to 20 m. Using this method, a penetrometer held from a mobile carriage is struck by a rod into the

ground and sampled in 1m core liners. In total, 2240 m of maar sediments are permanently archived in the core stock of the ELSA project.

1.1 Flood reconstruction – State of the art

Global climate models predict an increase of summer droughts and precipitation maxima combined with a higher risk of flash floods in creeks and rivers as a result of climate warming (IPCC report, 2014, 2007; Jacob et al., 2007; Piao et al., 2010). Furthermore, natural climate factors influence the intensity and frequency of such events on time scales from decades to millennia. For a comprehensive understanding of flood-generating climate mechanisms, long-term periods and regional patterns must be considered. Classical flood reconstruction is based on instrumental flood data of the last 50 to 100 years on a sub-daily resolution. Due to the time limitation of the instrumental time series, these studies offer only a limited insight into possible connections between climate and flood.

Palaeoflood hydrology is the reconstruction of the magnitude and frequency of recent, past, or ancient floods using geological archives instead of direct measurement or historical observation (Kochel and Baker, 1982). The Greek word “palaeo” means, literally translated, “old”. In the geosciences, this prefix is defined as indicating prehistoric time, the time before the written records of man. Thus, the collection of data from natural archives, not human, defines the term palaeoflood and distinguishes it from instrumental or historical floods records. The first scientific mention of palaeoflood layers is found in a paper by Bretz et al. (1956) about the Pleistocene lake Missoula. However, the term and the concept of palaeoflood layers was first introduced by Kochel and Baker (1982). The possibility of extending flood records into the past has opened new perspectives in the field of hydrology. Palaeoflood hydrology can produce the magnitude as well as the frequency of large flood events from the past.

Over the last 30 years, the historical flood archives as well as the palaeoflood investigations have become more and more important to understanding natural flood dynamics and variability. As studies by Glaser et al. (2010) show, the longest historical flood records in Europe document the last 500 years. The oldest historic flood record in the world is described from the flooding of the River Nile since 3000 BC (Bell, 1970). Problems of the historical data result from the subjective description of the recorded flood events and regional availability. Therefore, the scientific analyses of flood-climate

relations are strongly limited by both instrumental and historical data. A better understanding of how climatic variations might influence flood frequencies is possible by using the analysis of palaeoflood archives (Hoffmann et al., 2008; Macklin et al., 2006; Mudelsee et al., 2003; Starkel et al., 2002; Vandenberghe, 1995).

For palaeoflood reconstruction, lake sediments, river sediments, erosional landforms and high water marks (for example drift wood) can be analysed. In combination with an exact age model, the magnitude and the frequency of the flood events can be extended to the past. This method has already been successfully applied in many regions to extend instrumental and/ or histological flood data (Ely and Baker, 1985; Baker and Pickup, 1987; Kale et al., 2000; Sheffer et al., 2008; Yang et al., 2000). In contrast to river deposits, lake sediment records represent the final deposition of sediment particles, which have been transported from the catchment area into the lake during flood events (Gilli et al., 2013). Due to the reduced flow velocity, the sediment particles drop out and deposit on the ground of the lake as event layers, which contrast with the normal background sedimentation.

The event layers can be detected using optical methods, e.g. microscopy (Mangili et al., 2005; Marco et al., 1996; Moreno et al., 2008). Further sedimentological (e.g. grain size analysis) and geochemical (e.g. μ -XRF analysis) studies help to differentiate between flood layers, turbidites and slumps (Adams et al., 2016; Brunck et al., 2016; Gilli et al., 2003; Marco et al., 1996; Mulder et al., 2003; Sturm et al., 1995; Wirth et al., 2011). The first detailed flood record for Europe was reconstructed from the sediments of Lake Uri in Switzerland (Siegenthaler and Sturm, 1991). Coring in the maar lakes produced the first palaeoclimate records from Central Europe based on varve chronologies for the Holocene and late glacial (Brauer, 1994; Litt and Stebich, 1999; Negendank et al., 1990; Zolitschka, 1998). The Eifel maar structures provide an ideal climate and sediment archive with precise chronologies and seasonal resolution (Sirocko et al., 2016). Partly, the maar structures were fed by an inflow, which makes the reconstruction of flood layers possible. For the open maar lakes, it is even possible to link the sediment based flood record to the instrumental flood time series (Brunck et al., 2016).

There is large unexploited potential to improve our instrumental data sets with records from laminated lake sediments to develop long time series. Knowledge of palaeohydrology is an essential basis for understanding current and future environmental questions. Furthermore, the interpretation of modelling results for the impacts of climate and land use

change on the water system can be improved through the inclusion of palaeohydrological analogies.

1.2 The geological setting of the Eifel

The Eifel is a part of the Rhenish Massif situated on the left bank of the Rhine, which belongs to the Rhenohercynian Zone. The low mountain range is bordered in the east by the Middle Rhine Valley, in the south by the Moselle, in the west by the state border to Luxembourg and Belgium (or by the transition to the geologically related Ardennes) and in the north by the Lower Rhine Valley. The majority of the sedimentary rocks of the Eifel are Devonian sediments, mainly claystone and shale, sandstone, limestone and calcareous sediments.

In the early Phanerozoic, clastic sediments (shale and quartzite) were deposited in a shallow sea area of the later Eifel (Walter, 1980). The area was folded through the Caledonian orogeny during the Ordovician and formed together with the Ardennes the Ardennes ridge in the Silurian (Meyer, 1988). The Orogeny affected the Eifel region only to a limited extent, but formed the Old Red Continent in the north by the closure of the Iapetus Ocean.

In the north, the Central European Devonian Sea had two large basins, which were separated by the Central European islands from each other and interconnected by the Strait of Dinant. The strait extended to the east to "Rhenish Basin", which also included the present area of the Eifel. Due to the proximity of the Eifel to the Old Red Continent in the northwest and the "Siegerland Block" in the east, several thousand metres of fossil-free, red clastic sediments were deposited in this basin, which represents the basis of the Eifel.

The sedimentation rate decreased continuously until the Late Devonian and became increasingly replaced by carbonate sediments. During the Early Devonian, carbonates were deposited mainly in the lime depressions of the Eifel. In the further course of the Devonian, the Rhenish basin was visibly deepened by the middle Devonian marine transgression and a vast shelf platform formed with distinct reef growth. The change in the sedimentation and the abundance of fossils in the sediment layers mark the transition from the Early Devonian to Middle Devonian. These fossil-rich and calcareous sediments are now found only in the Eifel lime depressions. In the Rhenish bay, numerous species of coral were deposited, allowing one to subdivide the Middle Devonian and also to discern the transition to the marl slate of the Late Devonian. Already during the sedimentation of

the Devonian layers, the folding of the seabed began and reached its peak in the Carboniferous, when the Eifel was reached by Variscan orogeny. This event caused the uplifted of the seafloor into a mountain range. However, this did not occur as a whole, but rather in different fault blocks between which Variscan-oriented depressions formed (Meyer, 1988). With the uplift of the mountain range at the end of the Late Carboniferous, its erosion simultaneously began. The debris was deposited in the Variscan depressions during the Rotliegend formation and the mountain range was eroded into a truncated upland.

In the Triassic, the Eifel North-South zone developed into a pronounced depression area in which mainly Triassic and Jurassic sediments were deposited. The coarser sediments of the Middle Buntsandstein were washed together through widely branched river systems, whereas the finer sediments of the Upper Buntsandstein characterize a standing depositional environment. The remains of the deposits are the Buntsandstein layers on the Devonian deposits, which can be found mostly on the edge of lime depressions (Büchel and Mertes, 1982).

In the Early Jurassic, the Eifel was flooded for the last time, both from the Northwest German Basin and from the southern Paris Basin. However, in the Early Jurassic the Eifel became part of an elevated area and formed a slowly increasing undulating lowland until the end of the Cretaceous Period (Meyer, 1988).

In the Tertiary, there was a further uplifting of the Eifel region, which was accompanied by volcanic activity. The centre of the volcanic activity was in the Upper Eifel and according to K-Ar dating occurred about 42-34 million years ago (Meyer, 1988). Most of the approximately 300 Tertiary volcanoes feature basaltic composition, as well as the highest mountain in the Eifel, the Hohe Acht (747 m). The Pleistocene uplift phase ultimately led to the formation of steeply incised valleys (Fuchs et al., 2013).

Renewed volcanic activity continued in the Quaternary with two main centres. First, the Laacher Lake region was affected in the East Eifel and, second, and approximately 50 km long line of volcanoes in the West Eifel. Both volcanic areas are mainly SiO₂ undersaturated and predominantly alkali rich. According to Fuhrmann and Lippolt (1982), the oldest volcano, the Beuel in Zilsdorf, was dated at 960 000 years and the most recent eruption of the Ulmener Maar, at about 9000 years before the present day. The pre-volcanic underground was largely covered by lava flows and tuffs through this

eruption series. Therefore, the landscape of the Eifel is mainly characterized by numerous tuff and cinder cones together with the maar structures.

1.3 The formation of a maar lake

So far, 68 maar structures have been discovered in the Eifel. Most of these formations are already silted up and are therefore termed as dry maar structures. Currently, there are only 7 water-filled maar lakes in the Eifel region (Tab. 1.1).

Name	Height amsl [m]	Diameter [m]	Surface [ha]	Depth [m]
Gemündener Maar	407	309	7.2	39
Holzmaar	425	272	6.8	21
Meerfelder Maar	337	571	24	17
Pulvermaar	411	653	38.48	72
Schalkenmehrener Maar	421	528	21.6	21
Ulmener Maar	420	265	6	37
Weinfelder Maar	484	450	16.8	51

Tab 1.1: Morphometry of the 7 Eifel maar lakes, modified after Scharf and Oehms, (1992).

The term 'maar' is derived from the Latin word 'mare' (sea) and refers to a type of volcano caused by a phreatomagmatic eruption, which is negatively disseminated in the landscape surface. In the initial phase, there is a collision between the rising magma and water-bearing strata. The pore- or fissure water is abruptly transferred into a gaseous state, whereby it assumes a much larger volume. The resulting pressure blasts away the surrounding rock, so that magma continues to ascend and a mixture of magma and surrounding rock is jettisoned from the explosion crater. The crater is surrounded by a ring-shaped wall of ejected material. Typically, these maar deposits contain, apart from volcanic ash, a high proportion of surrounding rock material that was blasted into very

small pieces by the water vapour explosions. It is important to note here that the magma does not reach the earth's surface and no lava flows out. The magma remains in the explosion crater and is mixed with the rock material, whereby the explosion crater is sealed (Sirocko, 2009). The process can be repeated several times, as long as the underground pressure is large enough to cause another explosion. The maar craters become larger and deeper depending on the strength and frequency of eruptions. After the volcanic activity has subsided, the explosion crater fills with ground- and rainwater creating a maar lake (Fig. 1.1).

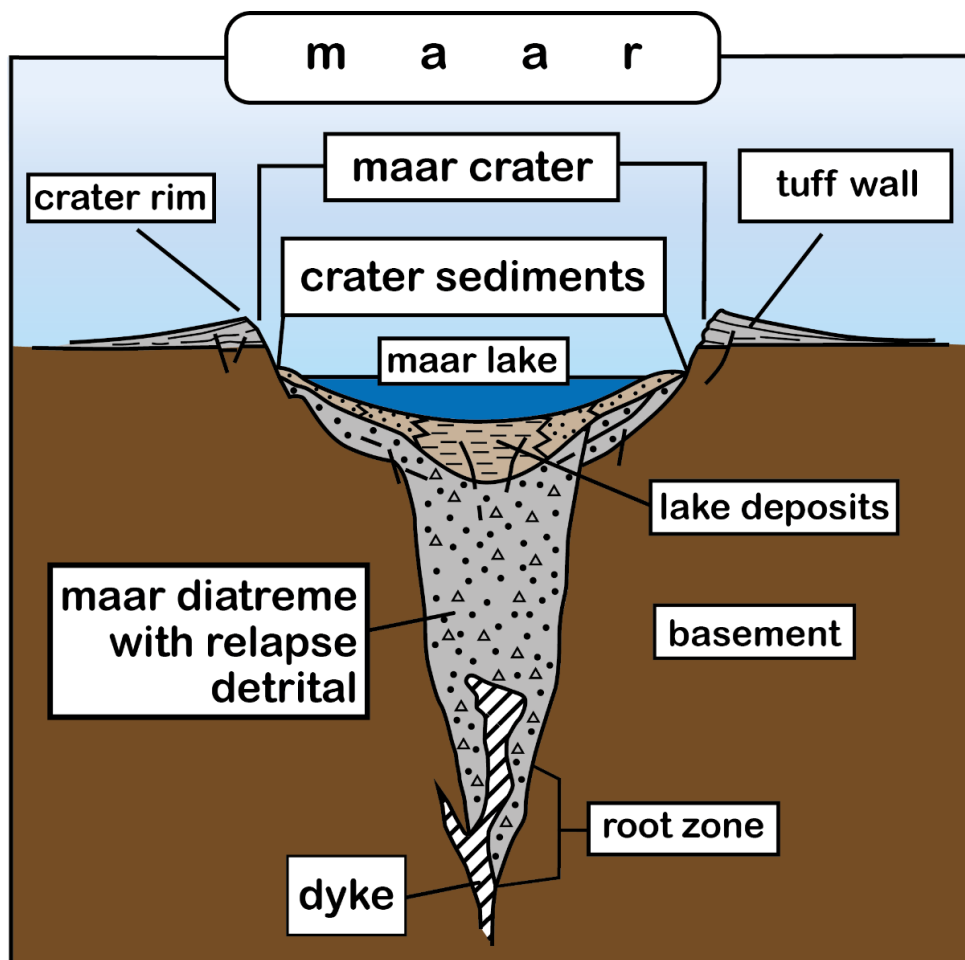


Fig. 1.1: Schematic cross-section of a maar lake (modified after Büchel, 1993).

The essential difference between a crater lake and a maar lake is in the surrounding strata and how the structure is filled with water. A normal volcanic crater fills with rainwater, as it sits as a positive form on the landscape surface. Thus, crater lakes are surrounded by volcanic rocks. On the other hand a maar lake has a negative landscape surface and fills mostly with groundwater from the surrounding strata. In the Eifel, the

maars are usually embedded in the Devonian rocks, whose clay and shale are water impermeable.

Maars are distinguished by their great depth due to the eruption structure and their lack of bioturbation. Because of their relatively small surface in proportion to great depth, they are able to incorporate thick sediment packages, whereby an ideal sedimentary archive is created. All the material that falls into a maar (volcanic ash, debris, material from streams or air) is deposited on the ground of the maar lake (Sirocko, 2009). In addition, the great depth benefits a lack of oxygen at the bottom of the maar lakes. The deep water body is not involved in the circulation and is thus depleted of oxygen, preventing benthic organisms from being present. Consequently, the seasonal deposits, so-called varves, remain undisturbed and can be used for analysis to reach conclusions about the climate of the past.

The thickness of the varve is defined by the seasonal sediment delivery to the drilling site, whereby the water constitutes the decisive factor of the material transport. For this reason, the sediment may be deposited on the spot or reach the drilling site through internal relocation in the lake. Furthermore, the particle size is defined by the flow rate of the water inflow, whereby conclusions about the strength of the floods are possible. Soil condition and vegetation density constitute decisive factors for soil erosion and the directly resulting sediment transport of the catchment area. Thus, human beings in the past and in the present represent an active influence on the material transport. Fallow or harvested fields boast an increased erosion potential, since the ground is not protected by roots.

1.4 The Eifel region – Study area

11 Sediment cores from three Holocene maar lakes and three Pleistocene dry maar structures are used to reconstruct the flood activity in the Eifel region for the last 60 000 years (Fig. 1.2). The total data for each drilling core is given in Appendix A. The morphology of the maar structures is described below.

1.4.1 Schalkenmehrener Maar

Lake Schalkenmehrener Maar is part of the “Dauner Maare”. It has a diameter of 528 m, an average depth of 14.5 m and a maximum depth of 21 m (Scharf and Oehms, 1992). With a lake surface of 219 000 m², it is one of the larger maar lakes of the Eifel. It has no large inflow or outflow stream. However, it is connected to a flanking dry maar,

which has been filled with sediment and peat since the middle Holocene (Straka, 1975) and drained since Roman times (Sirocko, 2009).

1.4.2 Holzmaar

The stratigraphy for this maar includes annual varve counting, which was constrained using ^{14}C -dating (Brauer, 1994; Hajdas et al., 1995; Zolitschka, 1998; Brauer et al., 1999a, 1999b). Holzmaar has a diameter of 272 m and a maximum depth of 20 m (Scharf and Oehms, 1992). It also has the smallest water volume of all maar lakes in the Eifel. The Sammetbach flows from the west into the maar. Just a few metres further south it flows out again. The small size of the maar and the direct inflow by the Sammetbach cause a relative high sedimentation rate (10 m Holocene).

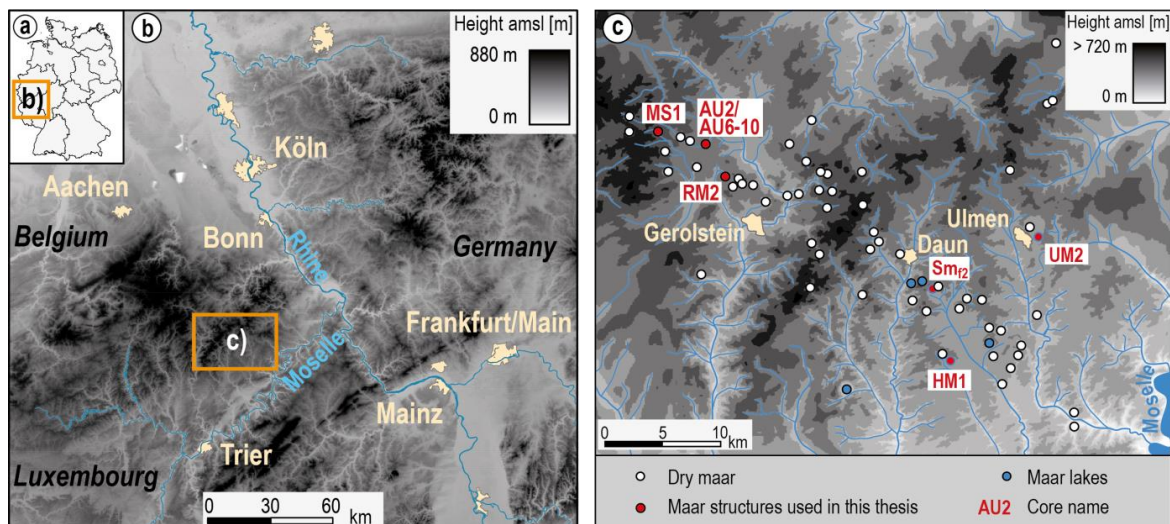


Fig. 1.2: Digital terrain model of the Eifel region with the core positions: SM_{f2} (German Grid Zone 2 (GK-System) 2561310/ 5559585); HM1 (GK-System 2562900/ 5554030); UM2 (GK-System 2570165/ 5564270), AU2 (GK-System 2542455/ 5572017), AU6 (GK-System 2542475/ 5572054), AU7 (GK-System 2542516/ 5572174), AU8 (GK-System 2542509/ 5572020), AU9 (GK-System 2542458/ 5572018), AU10 (GK-System 2542524/ 5571996), MS1 (GK-System 2538562/ 5573162) and RM2 (GK-System 2543958/ 5569786).

1.4.3 Ulmener Maar

The Ulmener Maar is slightly smaller than the Holzmaar with a diameter of 265 m (Scharf and Oehms, 1992). It is the smallest and youngest maar in the Eifel (about 11 000 before AD 2000 (b2k)). However, it is also one of the deepest with a maximum

depth of 39 m (Scharf and Oehms, 1992). The Ulmener Maar has the largest catchment area of the three analysed Holocene maars. Up to pre-Roman times, flood sediments were flushed from the Dellbach into the maar. Nowadays, the Dellbach flows west of the maar and had no contact to it since the founding of the city Ulmen. Consequently, the Ulmener Maar can only be applied to reconstruct the pre-Roman flood history.

1.4.4 Auel dry maar

The silted up basin of Auel is one of the largest dry maar structures of the Eifel with a diameter of 1325 m (Seib et al., 2013). The modern “Tiefer Bach” flows through the maar centre from west to east. This river has a catchment area of 12.187 km² and a total length of 9.4 km (Water management administration Rhineland-Palatinate: German river code 266374). The core AU2 from the centre of the maar is 123 m long and covers the time from the Laacher See eruption (Förster and Sirocko, 2016) back to 60 000 b2k. The average sedimentation rate of dry maar lake Auel is with $2 \frac{mm}{a}$ the highest of all Eifel maar structures, due to the abundant fluvial input.

1.4.5 Merscheid dry maar

The Merscheid dry maar is located approximately 4.5 km west of the Auel dry maar. The maar is slightly smaller than the Roth dry maar with a diameter of 771 m (Seib et al., 2013) and a sediment thickness of 50 m. The sedimentary record contains the time window between 24 000 and 70 000 b2k. The Mannebacher creek flows from west into the maar and turns to the south in the centre of the maar.

1.4.6 Roth dry maar

The Roth dry maar has a diameter of 823 m (Seib et al., 2013) and is located 5 km southeast from Auel. Thus, the maar is among the larger maar structures of the Eifel region. The core RM2 from the middle of the maar is 65 m long and covers the time from 10 000 back to 65 000 b2k. The Rother creek flows through the maar centre and leaves the dry maar at the opposite side, similar to the dry maar structure of Auel.

1.5 Methods

All analysed sediment cores have been drilled either from open maar lakes using the freeze core technology (Sm_{f2}) or the Niederreiter technology (HM1, SM3 and UM2), or from silted up dry maar structures using the Wireline coring technology (AU2, MS1 and

RM2) (Sirocko et al., 2013). Immediately after the drill core was prepared in the laboratory, 10 cm long samples were cut from the sediment. The samples were freeze-dried and impregnated with synthetic resin, which is why the samples are called resin impregnated samples (RIS). Thereafter, the RIS were processed into thin sections with a thickness of 30 μm , which were used for a detailed analysis of the event layers under the microscope.

For an accurate core-to-core correlation, it is necessary to describe the sediment cores lithologically. All lithological results of the sediment cores can be found in the lithoplots (Appendix B: High resolution lithology). Finally, the cores were correlated by lithological sequences, prominent layers, significant events or palynostratigraphic aspects (Appendix D: Core correlation table).

The age/ depth model is based on 8 different dating methods: varve counting, ^{137}Cs , ^{210}Pb , flood layer tuning, palynostratigraphy, tephrochronology, ^{14}C -dating and Greenland ice core tuning. Due to the precise age control, the flood layers can be directly compared with the climatic development of the Eifel region. For this purpose, the drilling cores were analysed visually and petrographically using various sedimentological methods (μ -XRF, microfacies analysis, Camsizer[®] samples, pollen analyses and in 10 cm long thin sections under the microscope) in order to identify possible event layers. Grain size distribution, sediment composition and thickness changes are used to distinguish turbidites, slumps and flood layers (Appendix C: Flood layer table). Additionally, instrumental and historical datasets are used to compare flood events with the flood layers in the maar sediments for the last 200 years. I refer to the single manuscripts for further information on the methods used for the analysis.

1.6 Objectives

For a better understanding of the processes and mechanisms, it is necessary to analyse long-term climate archives. For this purpose, the maar structures of the Eifel region offer unique insights into the past. Since climate change plays an important role on various times scales, the sensitivity of hydrological changes and the frequency of extreme events is analysed per millennium. Consequently, flood layers provide a proxy archive with unique environmental information, depending on regional conditions like vegetation and permafrost. The key objectives of this study are:

- (1) to develop a high resolution long time flood frequency record for Central Europe to define the main glacial – interglacial flood phases.
- (2) to analyse the correlation between flood variability and a) climate change, b) vegetation and c) precipitation.
- (3) the anthropogenic influence: Is the anthropogenic influence reflected in the flood frequency?

Chapter 2

The ELSA-Vegetation-Stack: Reconstruction of Landscape Evolution Zones (LEZ) from laminated Eifel maar sediments of the last 60 000 years

F. Sirocko¹, H. Knapp¹, F. Dreher¹, M.W. Förster¹, J. Albert¹, H. Brunck¹, D. Veres⁴, S. Dietrich², M. Zech³, U. Hambach³, M. Röhner¹, S. Rudert¹, K. Schwibus¹, C. Adams¹, P. Sigl¹

(1) Institute for Geosciences, Johannes Gutenberg-University, 55128 Mainz, Germany

(2) Bundesanstalt für Gewässerkunde, Am Mainzer Tor 1, 56068 Koblenz, Germany

(3) BayCEER and LS Geomorphologie Universität Bayreuth, 95440 Bayreuth, Germany

(4) Institute of Speleology, Romanian Academy, 400006 Cluj Napoca, Romania

A slightly modified version of this chapter has been published as Sirocko et al. (2016) in the journal “Global and Planetary Change”.

2.1 Abstract

Laminated sediment records from several maar lakes and dry maar lakes of the Eifel (Germany) reveal the history of climate, weather, environment, vegetation, and land use in Central Europe during the last 60 000 years. The time series of the last 30 000 years is based on a continuous varve counted chronology, the MIS 3 section is tuned to the Greenland ice – both with independent age control from ¹⁴C dates. Total carbon, pollen and plant macrofossils are used to synthesize a vegetation-stack, which is used together with the stacks from seasonal varve formation, flood layers, aeolian dust content and volcanic tephra layers to define Landscape Evolution Zones (LEZ). LEZ 1 encompasses the

landscape dynamics of the last 6000 years with widespread human influence. The natural oak and hazel forests of the early Holocene back to 10 500 b2k define LEZ 2. LEZ 3, the late glacial between 10 500 and 14 700 b2k, shows the development of a boreal forest with abundant grass and shallow water biomass in the lakes. The maximum of the last glaciation (LEZ 4: 14 700 – 23 000 b2k) was characterized by sparse vegetation of moss and characeae. These sediments are generally devoid of clay and sand and reveal no indication of snow-meltwater events. Accordingly, the Last Glacial Maximum (LGM) must have been extremely arid in Central Europe. The sediments of the subsequent LEZ 5 from 23 000 – 28 500 b2k preserve distinct layers of clay and coarse sand, which indicates running water with clay in suspension and ephemeral coarse-grained fluvial sediment discharge. Abundant Ranunculaceae macroremains (used for ^{14}C dating), insects, moss and fungi sclerotia reflect a tundra environment during a time of frequent strong snowmelt events. Total carbon content, *Betula-Pinus* pollen and diatoms reach increased concentrations during Marine Isotope Stage (MIS) 3 interstadials that occurred between 28 500 – 36 500 b2k (LEZ 6). The entire MIS 3 interstadials are well documented in the organic carbon record from the Auel dry maar. The main palaeobotanical indicators of MIS 3 are, however, grass pollen and heliophytes, which indicate a steppe environment with scattered/ patchy trees during the interstadials. The stadial phases inferred during LEZ 6 reveal initiation of aeolian dust deflation. The change of the early MIS 3 forested landscape to a steppe occurred with the LEZ 7 – LEZ 6 transition. This is when modern man spread in Central Europe. The principle vegetation change to a steppe at 36 500 b2k must have favoured the spread of horses, the favoured hunting prey of modern humans. We propose accordingly that the migration of the modern humans into Central Europe might have been at least partly driven by climate and associated vegetation change.

The LEZ 7 encompassed the time interval 36 500 to 49 000 b2k and was characterized by a boreal forest with high abundance of pine, birch, as well as spruce during the interstadial events. Abundant charcoal fragments indicate that this taiga was under frequent drought stress with regular burning. The most unexpected finding, but corroborated by all our maar records is the dominance of thermophilous tree taxa from 49 000 – 55 000 b2k (LEZ 8). Greenland interstadials 13 and 14 were apparently the warmest of MIS 3 according to the Eifel pollen records. The preceding LEZ 9 from 55 000 – 60 000 b2k is also dominated by spruce, but thermophilous trees were sparse. A warm early MIS 3 appears plausible, because summer insolation (at 60 °N) was higher in the early MIS 3 than

today, ice cover was low in Scandinavia and sea-surface temperatures of the North Atlantic were almost comparable to modern values during GI 14.

2.2 Introduction

The global climate of the past 60 000 years is well known from polar ice cores (e.g. Grootes et al., 1993; Johnsen et al., 2001; Petit et al., 2004; Andersen et al., 2004; Augustin et al., 2004) and ocean sediments (e.g. CLIMAP, 1981; Imbrie et al., 1984; SPECMAP, 1994; Lisiecki and Raymo, 2005). The stadial/ interstadial succession of the last glacial cycle was first documented in the Greenland ice cores, but became soon visible also in marine records (e.g. McManus et al., 1994; Behl and Kennett, 1996; Schulz et al., 1999; van Kreveland et al., 2004), reflecting that these sharp climate anomalies are a common feature of the entire Northern Hemisphere ice-ocean-land climate system.

The best chronologies for the last 60 000 years of climate change comes from the layer counted Greenland ice cores (e.g. Parannin et al., 2001; Svensson et al., 2008) and from Eifel maar sediments for the last 15 000 years (e.g. Zolitschka et al., 2015). Chronologies from the marine, land and glacier records have been recently synthesized into a common chronological framework by the INTIMATE project (e.g. Rasmussen et al., 2014) and summaries on the vegetation and environment of all of Europe have been presented by Moreno et al. (2014), Feurdean et al. (2014) and Heiri et al. (2014).

The extent of the European MIS 6 and MIS 2 maximum moraines is well mapped (CLIMAP, 1981; Ehlers and Gibbard, 2003, 2004) but the ice extent during MIS 4 is still poorly understood, even in Central Europe. Fluvial deposits (e.g. Kasse et al., 1995, 2003), palaeosol sequences (e.g. Haesarts et al., 2010; Schirmer, 2012) and loess deposits (e.g. Antoine et al., 2001; Frechen et al., 2001; Marković et al., 2008, 2015) have revealed the main stadial and interstadial characteristics in Europe, dated by luminescence methods (Kadereit et al., 2013; Lang et al., 2003; Timar-Gabor et al., 2011; Zöller et al., 2014).

Classical pollen analysis defines the late glacial and Holocene into distinct pollen zones, which have an almost common and identifiable succession all over Central Europe (e.g. Allen and Huntley, 2000; Litt et al., 2001; Guiter et al., 2003, 2005; Peyron et al., 2005; Tatau et al., 2005; Magny et al., 2006; Fletcher et al., 2010; Helmens, 2014). Pollen however, cannot be used to describe the climate of the Last Glacial Maximum (LGM) because most glacial lake sediments do not contain pollen or do not preserve them.

Accordingly, we will later in this paper introduce “Landscape Evolution Zones” (LEZs). The LEZ are a new approach to combine the palaeobotanic evidence with indicators of aeolian dust activity, flood events, seasonal varve composition and volcanic activity to arrive at a synthesis of all factors determining a landscape. In addition to these natural environmental processes, we include the archeological evidence for past land use. Accordingly, LEZs are an approach to integrate the various sources of information and reach a synthesis on the nature and evolution of past environments in Central Europe.

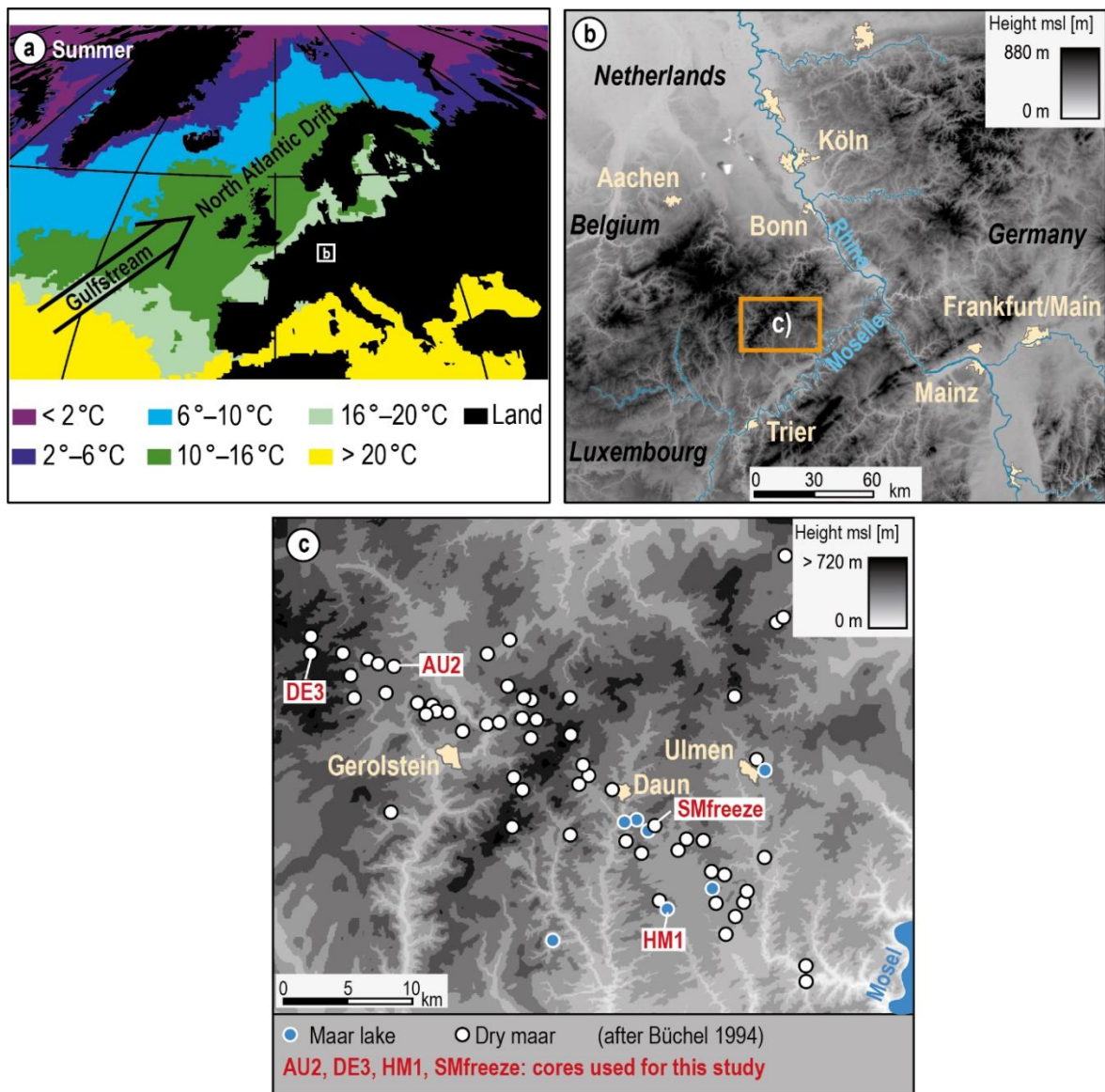


Fig. 2.1: a) Map of the modern North Atlantic sea surface temperatures and continental boundaries of Europe. b) Digital elevation map of the “Rheinisches Schiefergebirge”. c) Digital elevation model of the northwestern volcanic field with drainage system maar positions and coring sites.

2.2.1 Introduction to the ELSA Project

The west Eifel volcanic field (Germany) has six extant maar lakes and about 60 dry maar lakes (former maar lakes filled up with sediments) (Fig. 2.1). Most of these lakes and dry lakes have been systematically cored since 1998 by the ELSA Project (Eifel Laminated Sediment Archive) of the Institute for Geoscience, Johannes Gutenberg University Mainz, Germany. Today the core repository at Mainz hosts a total of 2700 metres of laminated lake sediments. Twenty-one scientific publications, one scientific book and one book for the general public have already been published from this core material.

All ELSA cores are laminated, but only the last 30 000 years, the early part of MIS 3 and the last interglacial sediments show continuous seasonal layering that can be varve counted (Rein et al., 2007; Sirocko et al., 2005, 2013). The absolute age control of all ELSA cores is based on ^{137}Cs , ^{210}Pb , ^{14}C , flood event tuning, magnetostratigraphy, ice core tuning, luminescence techniques and argon/ argon dating (Sirocko et al., 2013). An important further step for the ELSA chronology is accomplished with this work, because the new total carbon record of core AU2 from the dry maar of Auel is now the best (highest sediment rate) record from the Eifel to replicate the complete Greenland interstadial succession of the last 60 000 years. The other five Greenland ice tuned ELSA cores had used only the greyscale record, which is not always unequivocal (Sirocko et al., 2013).

The tuning of the AU2 time series to the Greenland ice core timescale in this paper is now the latest update of the age/ depth relations for all ELSA cores, because we transfer the ages of the distinct marker tephra in Auel to all other cores. Accordingly, this paper discusses the already published ELSA stacks, but on the new AU2 stratigraphy. All ELSA cores are now correlated to each other by means of tephrostratigraphy (see also Förster and Sirocko, 2016) to arrive at a consistent matrix of sediment records aligned within a common multi-method temporal framework.

The basins of the modern maar lakes are between 20 and 70 m deep. The average annual sedimentation rate is $1 \frac{\text{mm}}{\text{a}}$, which allows a typical maar sediment record of about 70 m length to cover about 70 000 years. Accordingly, it is necessary to splice overlapping cores into a composite stack in order to cover longer time series. At present, the stacked ELSA cores reach over the last 60 000 years, but with potential to extend back to the middle Pleistocene (Förster and Sirocko, 2016). The oldest ELSA sediment records date to

the time interval 400 000 – 500 000 years before present (Sirocko et al., 2013). A table with all published and on-going research is accessible on the web page of the ELSA-project <http://www.klimaundsedimente.geowissenschaften.uni-mainz.de>.

2.3 Coring sites and coring methods

Sediment cores have been recovered from open maar lakes with both Niederreiter piston core and freeze core technology (www.uwitec.at), while infilled dry maar basins have been drilled by the company “Stölben-Bohr” using ICDP drilling technology, however, not from a barge (www.stoelben-GmbH.de). Digital elevation models for all ELSA coring sites were presented in Sirocko et al. (2013); the drillings sites for AU2 and DE3 cores are shown with the larger catchment by Brunck et al. (2016).

2.3.1 *Schalkenmehrener Maar*

Lake Schalkenmehrener Maar is part of the Dauner Maar group. It has a diameter of 528 m, an average depth of 14.5 m, and a maximum depth of 21 m. The ELSA Project has drilled a total of 9 cores from this maar lake, including 3 freeze cores. Freeze core SM_{f1} is dated by ¹³⁷Cs and ²¹⁰Pb and shows clearly the 1986 and 1963 nuclear fallout maxima (Sirocko et al., 2013) (Fig. 2.2). Both cores reveal a unique thick layer with abundant botanical macroremains in the lower section of the cores, ¹⁴C dated to the first half of the 14th century; accordingly, this thick layer must represent the millennium flood of summer AD 1342 (Fig. 2.2). Freeze core SM_{f2} reveals a superb preservation of laminations, which have been shown by Fritz (2011) to be varves and reach back to the 11th century. Accordingly, the freezes cores from Schalkenmehren are best suited to monitor the modern and medieval landscape history and are used for the last 1000 years of the ELSA chronology.

2.3.2 *Holzmaar*

Holzmaar is well known since long for chronologies from annual varve counting (Negendank et al., 1990; Zolitschka et al., 1998; Brauer et al., 1999, 2001), however, constrained by ¹⁴C-dating (Hajdas et al., 1995). The ELSA project drilled a 2 m long freeze core, which was varve counted by Fritz (2011). This core together with core SM_{f2} from Schalkenmehrener Maar is presented in Fig. 2.2, however with a slightly updated

stratigraphy to match the observation of locust macroremains, which are known to have invaded Central Europe in 1338 and 1408.

The other core from Hozmaar is a 10 m long piston core from the Holzmaar, which is used in this study for the Holocene varve chronology, pollen and plant macrofossil analyses (Fig. 2.2). The piston core was retrieved in two-metre long sections, which were cut into one-metre lengths, so that minor sediment loss may have occurred between metres 2/ 3, 4/ 5, 6/ 7 and 8/ 9 in the core. The sediment record of HM1 reaches the Laacher See tephra (LST) at 9.57 m depth (Fig. 2.2).

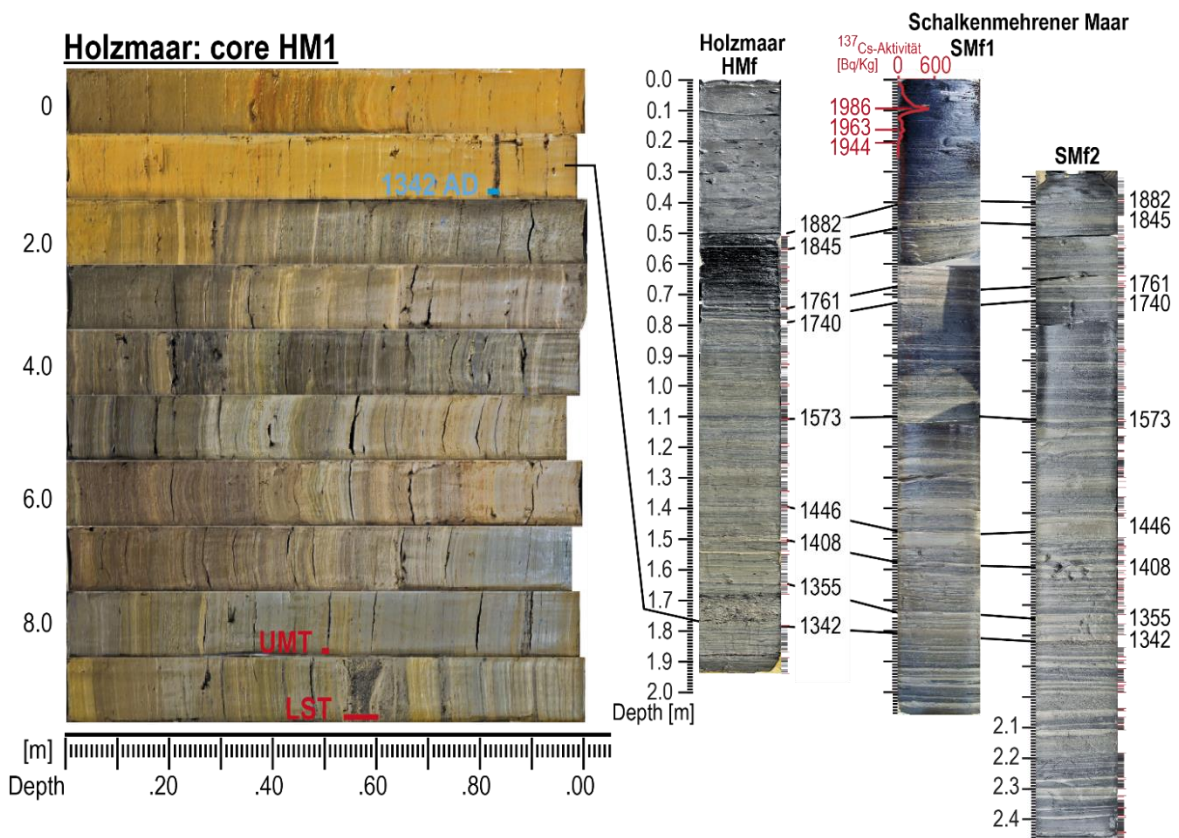


Fig. 2.2: Photo of core HM1 from Lake Holzmaar with tephra marker layers.

The varve time series for ELSA core HM1 is presented in this study. However, problems of missing varves and floating sections were encountered as in the earlier Holzmaar studies and solved by anchoring the floating varve chronologies to the well-dated flood layers at AD 1342 and 800 BC and the Laacher See tephra at 12 880 b2k (Fig. 2.2). The ELSA-pollen record from core HM1 is of century scale resolution, but resembles all important stratigraphic features of the decadal scale resolution pollen results from Kubitz (2000), Stebich (1999), Litt and Stebich (1999) and Litt et al. (2001, 2003) for Meerfelder Maar (Brauer, 1999, 2001).

2.3.3 Dehner dry maar

The Dehner dry maar (Figs. 2.1 and 2.3) is located in the northwestern part of the Western Eifel volcanic zone, north of the town of Reuth. The Dehner maar is still very well recognizable in the landscape, because it was infilled only during the early Holocene. It has a diameter of 950 metres and lies at an elevation of 565 m. The maar basin is near circular and does not display any recognizable traces of past inflow, however there is an outflow to the south. Accordingly, the Dehner maar structure is perfectly located to study the aeolian input over the Eifel region between the end of MIS 4 and the MIS 1/2 transition. The core DE3 from the Dehner dry maar is 87 m long and preserves the LST at 3.47 m depth (Fig. 2.3) and is paralleled by core DE2 drilled nearby. Both cores have a total of 18 radiocarbon ages, which are in agreement with chronological estimates derived from palaeomagnetic data (Sirocko et al., 2013).

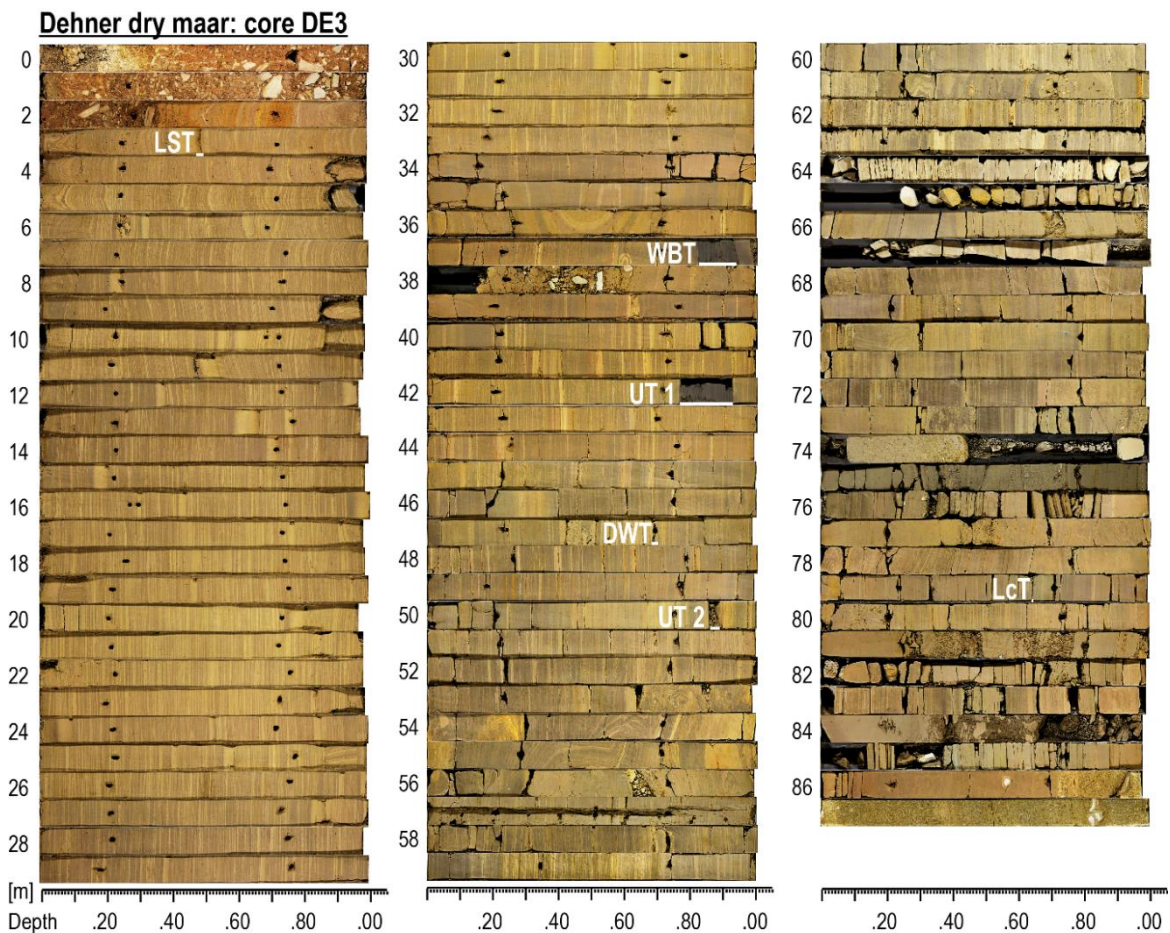


Fig. 2.3: Photo of core DE3 from Dehner dry maar with tephra marker layers.

The DE3 sediments display annual laminations from 12 900 b2k back to 32 000 b2k. Abundant thermophilous tree pollen occur between 60 m and 74 m depth, and pollen

continue during all of MIS 3. The stratigraphy of the *Picea*-dominated DE3 pollen profile was already presented by Sirocko et al. (2013), but is slightly modified in this paper, because the upper section back to 30 000 years is now on the varve counted time scale and the lower part on the new Greenland ice core-tuned Auel time scale. 550 samples from the Dehner dry maar were investigated for plant macroremains from 15 – 70 m depth. Samples cover 10 cm-long core sections and each represent 200 g of dry sediment. The DE3 samples contained only 61 non-carbonized and carbonized plant macrofossils, of which only a fraction could be identified to the species level. The macroremains in the sediment are recorded as present or absent, because the amount of 200 g of sediment was not large enough to find enough remains for calculation of concentration values.

The core DE3 is also used for the diatom analysis presented in this paper, because the diatoms can be well seen in the petrographic thin sections used for varve counting, which allows for annual resolution diatom analysis. The data presented in this paper are, however, done with discrete samples in 10 cm intervals.

2.3.4 Auel dry maar

The Auel dry maar is one of the largest infilled maar lakes in the Eifel with a diameter of 1325 m. The Tieferbach brook flows today through the centre of the maar. This river has a large catchment area and a length of 9.4 km so that the sediment record contained in Auel maar is well-suited for reconstructing the extent of past riverine input into the lake (see Brunck et al., 2017). Core AU2 is 123 m long (Figs. 2.1, 2.4a and 2.4b) and has the highest sedimentation rate ($2 \frac{mm}{a}$ on average) of all ELSA cores, due to the fluvial sediment influx to the basin. Half of each metre of core from AU2 (about 4 kg for each sample) was sieved and 3804 plant macrofossils were identified in total, including 2951 Characeae oogonia, 820 seed and fruits, of which 89 were identified to species level. Pollen in core AU2 were determined only in low resolution in 1 m increments (mix over entire 1 m core section).

The succession of pollen and tephra layer is identical between the Auel and the Dehner dry maar, but AU2 has much higher number of plant macrofossils due to the sample mass of 4 kg; accordingly macroremains are presented in counts (#) pro kg. Frequently encountered Ranunculaceae/ *Ranunculus* seeds were used to obtain four ¹⁴C dates from the glacial section, all of which reveal ages around 21 000 BP, the GI 2 interstadial.

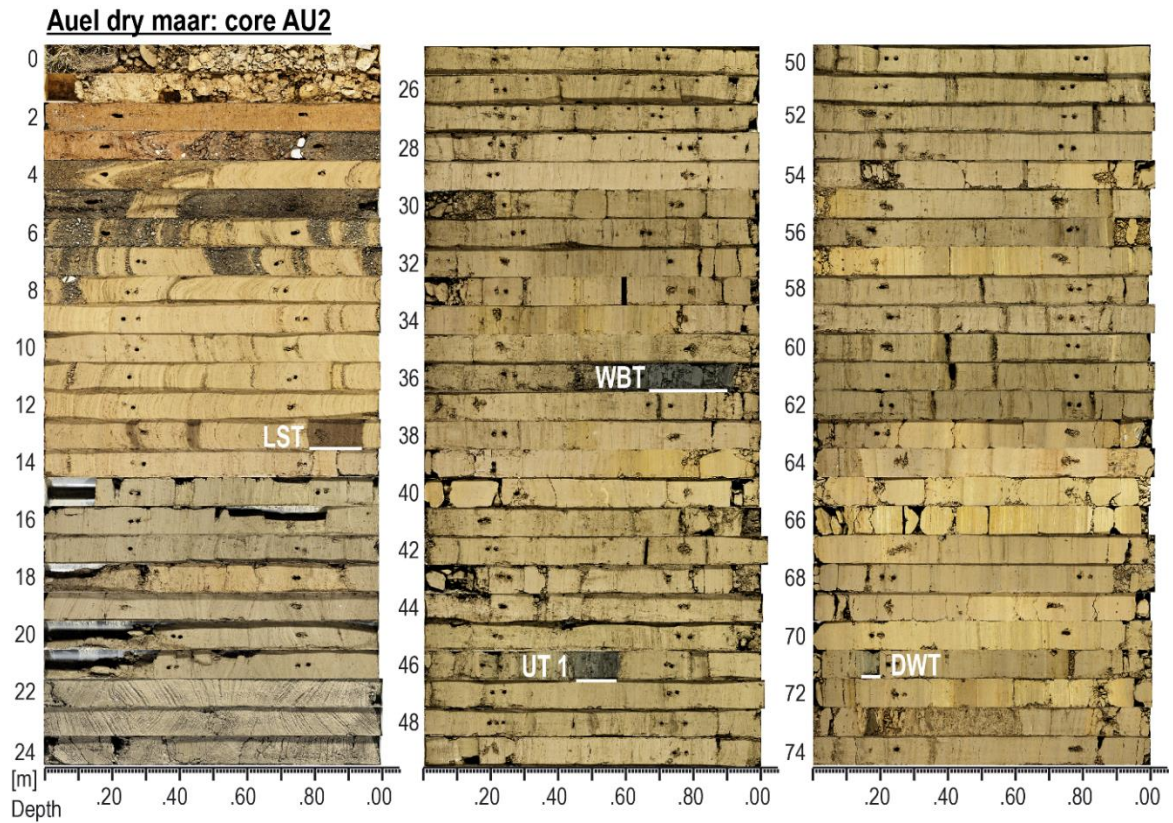


Fig. 2.4a: Photo of core AU2 from Auel (0-75m) dry maar with tephra marker layers.

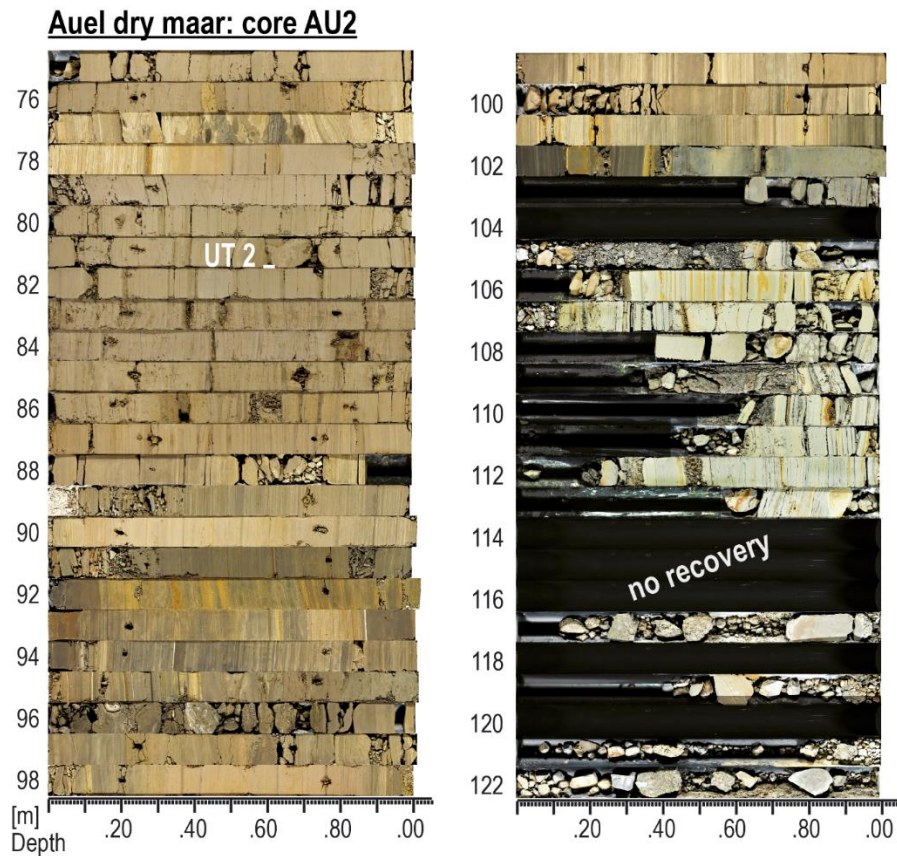


Fig. 2.4b: Photo of core AU2 from Auel (75-123m) dry maar with tephra marker layers.

2.3.5 The ELSA core stack

It was the intention of the ELSA Project to drill systematically all maar lakes and dry maar structures of the Eifel to obtain an understanding, which sites are best suited to form a matrix of correlated cores reaching from the modern back to the beginning of the Eifel volcanism in the middle Pleistocene.

The Core-Stack₂₀₁₆ is presented in this paper. It starts with the ¹³⁷Cs dated core SM_{f1} for the last 50 years (Fig. 2.2). It continues with the varve counted cores SM_{f2} and HM_f (Fig. 2.2) down to the AD 1342 millennium flood layer, which is used to anchor the varve counted Holocene time series of HM1. The Holocene varve counts in Holzmaar reach to the Laacher See Tephra at 12 900 b2k. This well visible layer with a distinct geochemical and mineral composition is found in the upper sections of core DE3 and AU2 from the dry maar sites of Dehner (Fig. 2.3) and Auel dry maar (Fig 2.4). The record from DE3 is varve counted from 12 900 back to 32 000 b2k. Accordingly, the ELSA varve chronology is continuous from today back to 32 000 b2k. The record of AU2 from Auel cannot be varve counted, despite varves are visibly occasionally. AU2, however, shows a succession of total carbon maxima, which is used to tune AU2 to the Svensson et al. (2008) time scale for the time interval 25 000 to 60 000 b2k, thus overlapping with the varve counted DE3 varve chronology.

The eruptions of Auel and Dehner occurred during the MIS 4 – 3 transition at 60 000 b2k, which is the lowest date included in the ELSA-Stacks₂₀₁₆. A continuation of the stack approach is shown for the Tephra-Stack₂₀₁₆ already in the paper by Förster and Sirocko (2016) and will be finally presented for all other stacks back to 220 000 b2k.

2.4 Proxies and Methods

2.4.1 Total carbon (C_{total})

C_{total} was determined in core AU2 using elemental analyses. Dry combustion of subsamples (up to 20 mg) was carried out with a Hekatech elemental analyzer coupled via a Conflo III Interface to a Delta V advantage IRMS. For 105 samples taken at lower-resolution, an additional pre-treatment using 24 h HCl fumigation in silver capsules at 60 °C was followed by 24 h KOH treatment at 60 °C under vacuum in order to remove carbonates and determine total organic carbon (TOC). C_{total} and TOC are highly correlated ($R= 0.98$) for the low-resolution samples, and the carbonate fraction does not exceed 2 %.

Thus only C_{total} is determined for the high-resolution time series and is interpreted as primarily presenting organic carbon.

2.4.2 Petrography of Tephra

The West Eifel volcanic field is part of the “Schiefergebirge” in central Germany and shows a total of about 280 volcanic structures, 68 of which are Pleistocene maar lakes (Fig. 2.1, after Büchel and Lorenz, 1982). The East Eifel volcanic field is geochemically and geodynamically characterized by much more differentiated magmas compared to the primitive West Eifel volcanic field magmas. Van den Boogard and Schmincke (1989) developed the general chronological framework of past volcanic activity in the East Eifel by argon/ argon dating of the most differentiated tephra layer from the East Eifel volcanic field. These volcanic layer can be clearly identified petrographically in the lake sediment records of the West Eifel volcanic field (Förster and Sirocko, 2016). Accordingly the ash plumes from these explosive East Eifel eruptions reached the maar lakes and provide robust marker tephra. The main tephra were distinguished geochemically by Sirocko et al. (2013), but can now also be quantified by fast and efficient analysis of the sand fraction mineralogy only (Förster and Sirocko, 2016).

Förster and Sirocko (2016) examined the visible tephra layers > 1 cm-thickness in all of the ELSA sediment core records. Bulk tephra samples of 2 g were sieved at 250 – 100 μm for petrographic characterization under a binocular microscope. A total of 100 identifiable crystals and grains were counted into ten groups including reddish sandstone, grayish sandstone, quartz, amphibole, pyroxene, scoria and pumice, sanidine, leucite and mica. The selection of these minerals and rock fragments was chosen based on their weathering resistance and characteristic appearance. Histograms of the count-results represent the volume percent (%) abundances for each grain type in the total from the 10 defined classes (Förster and Sirocko, 2016).

2.4.3 Varve counting

Varve counting was carried out in three different ways. Visible mm-thick laminae were counted directly from photographs of freeze core SM_{f2} from Schalkenmehrener Maar (Fritz, 2011). The photos were taken immediately after core recovery on the drilling platform, when the colour of the dark and light seasonal laminae was clearly visible. Direct counting from photographs is most efficient when sedimentation rate is more than $1 \frac{\text{mm}}{\text{a}}$

and sediment laminae are preserved by the freezing process up to the sediment/ water interface. The main advantage of this approach is the 20 cm core width of completely undisturbed sediment, which often allows the identification of problematic layers much better than on a 2 cm-wide petrographic thin section.

10 cm-long petrographic thin sections were prepared for cores HM1 and DE3. Both cores have an excellent preservation of laminae and allow counting of annual layers (varves) already at 20 times magnification under the petrographic microscope. The average thickness of well identifiable varves was determined and then applied to the entire length of the 10 cm thin section to calculate the number of years. These values are then stacked to floating chronologies between tie points. These tie points are the several cm-thick AD 1342 flood layer (658 b2k), which is clearly visible in the cores HM1 and freeze core SM_{f2} from Schalkenmehren (Fritz, 2011). The next anchor point is the 800 BC flood (2800 b2k) (see also Martin-Puertas al., 2012). The subsequent tie points were defined by pollen analysis. In particular, the spread of beech trees in the Eifel occurred at 3800 b2k (1800 BC) (Kubitz, 2000; Litt et al., 2001) whereas the elm decline is centred between 6300 and 6000 b2k. The 10 cm-thick sand layer with abundant grey pumice of the LST (12 880 b2k) is the tie point for the older cores from the dry maars covering MIS 2 and 3 (Figs. 2.2, 2.3 and 2.4). The only varve-countable sediment record below the LST is DE3. The DE3 varve chronology show 9000 layers below the LST (12 900 b2k) and place the UT1 at 28 900 b2k. The Greenland ice tuned age of the UT1 in AU2 is, however, 30 200 b2k. Accordingly, the missing varves in the glacial section are 4 % in comparison to the ice core tuned age model.

2.4.4 Pollen

Palaeobotanical investigations of the volcanic lake sediments in the Eifel region have a long scientific tradition (Straka, 1975; Usinger, 1982) and were concentrated on the extant maar lakes (Litt et al., 2001, 2003; Kubitz, 2000; Litt and Stebich, 1999; Stebich, 1999). Palynological data from older maar structures (infilled maar lakes) have been published for MIS 5e (Sirocko et al., 2005) and MIS 11 (Diehl and Sirocko, 2006).

Pollen preparation followed the techniques of Berglund and Ralska-Jasiewiczowa (1986) and Faegri and Iversen (1989). Each pollen sample spans a depth range of 1 cm (except for AU2, which was sampled as a mix for each complete core metre representing 500 years) and was of about 1 cm³ volume. The sediment was treated with potassium

hydroxide solution (KOH), hydrochloric acid (HCl) and hydrofluoric acid (HF). For acetolysis, acetic acid (C₂H₄O₂) and a mixture (9:1) of acetic anhydride (C₄H₆O₃) and sulphuric acid (H₂SO₄) were used. Centrifugation was done at 3000 – 3500 rpm for 5 minutes. The samples were sieved at 200 µm and later filtered at 10 µm. *Lycopodium*-spore tablets were added for calibration of absolute pollen concentration per cm³. The samples were mounted with liquid, anhydrous glycerol (C₃H₈O₃). Pollen counting was done under a maximum of six hundred-fold magnification. 300 pollen grains are counted for each sample. Percentages (% of all pollen) are presented only for those samples where the sum of all taxa exceeds 50 pollen grains. In addition, total pollen content (#/ cm³) have been calculated using the known numbers of lycopodium spores. The count data are presented, because the percentage data alone of *Pinus* and *Betula* are almost constant during MIS 3, but the pollen counts per ccm show clear maxima in the MIS 3 interstadials. All pollen data are plotted versus depth in Figs. 2.5 to 2.8.

2.4.5 Plant Macroremains

Pollen grains are dispersed by the wind over short or long distances and it can never be unambiguously inferred that the plants which produced a pollen grain grew near to the site of pollen deposition. This is different with plant macrofossils which always represent plants from within the catchment area of the lake. Thus, the combined evidence of a certain plant from both pollen and macroremains provides reliable evidence that this plant grew near the lake. However, plant macroremains and pollen can be reworked by slumping and turbidites, and thus could represent old components incorporated into younger sediment. Such events are episodic and have been identified and taken into account for the interpretation of isolated, rather unexpected spikes in all of the datasets presented.

Macroremains of aquatic plants or submerged macrophytes, like Characeae, which can drift, are dispersed within the lake naturally by surface currents. The other plant macroremains are transported by the fluvial inflow and represent the plants in the entire catchment. Thus, plant remains found in the sediments represent a mix of habitats, transported by different processes, but originate from within the catchment area of the maar lake.

Holzmaar: core HM1

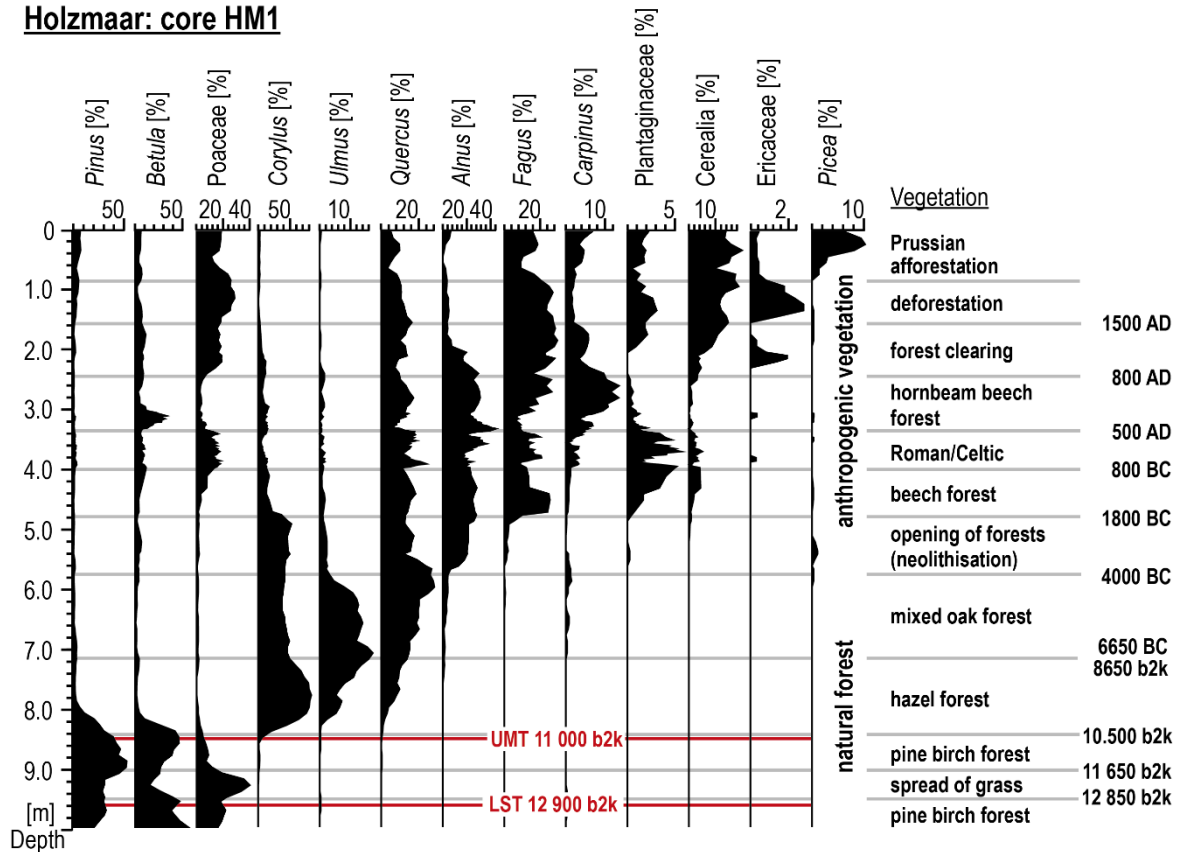


Fig. 2.5: Pollen concentrations, macroremains and marker tephra layer of core HM1 from Holzmaar versus depth.

Our study also includes macroscopic charcoal fragments resulting from lake proximal fires linked to human activity in the Eifel during late Holocene (Herbig and Sirocko, 2012; Bandowe et al., 2014). The first MIS 3 charcoal maxima should represent natural forest fires, because the strongest maxima occurred before anatomically modern humans moved into Central Europe.

Sample preparation for plant macrofossil analysis followed Jacomet and Kreuz (1999). The sediment was soaked in water for several hours and then wet-sieved with at 200 μm . Plant macrofossils were identified and counted at 12 to 40 times magnification under a stereo-microscope. For identification, guides (Jacomet et al., 1989; Mauquoy and van Geel, 2007; Cappers et al., 2006) as well as different reference collections in Kiel and Frankfurt were used.

The amount of plant macroremains was insufficient to calculate percentage values, so that they are presented as count numbers per kilogram, or presence/ absence of a respective

species, or as the sum of species belonging to a certain ecological group (e.g. crop weeds, littoral/ reed, submerge plants).

Dehner dry maar: core DE3

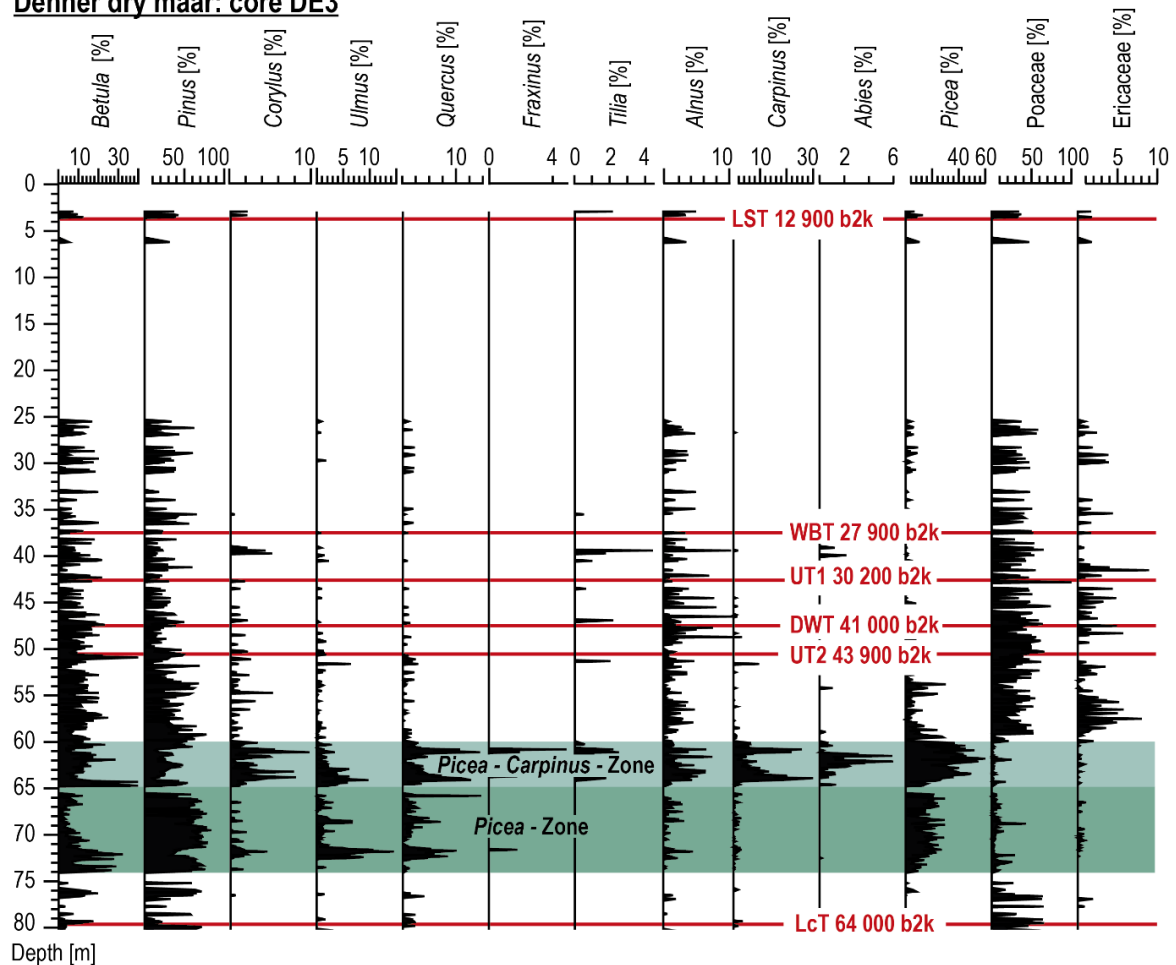


Fig. 2.6: Pollen percent concentrations and marker tephra layer of core DE3 from Dehner dry maar versus depth.

Other identifiable organic components frequently found in the sediments are mosses, oospores and ostracods. Photographs of selected macroremains are presented in Fig. 2.9; respective downcore plots for HM1, DE3 and AU2 are given in Figs. 2.10 to 2.12.

Palaeotemperature estimates (mean July temperature for LEZ 8) were carried out based on the climate indicator plant species method (Iversen, 1944). The indicator species method (Iversen, 1944) links the distribution of specific plant taxa to climate parameters (i.e. mean January and mean July temperature). Only the presence of selected indicator species with defined climate requirements were recorded and interpreted (e.g. *Typha* sp. *Ceratophyllum demersum*, *Schoenoplectus lacustris* and *Najas marina*).

Dehner dry maar: core DE3

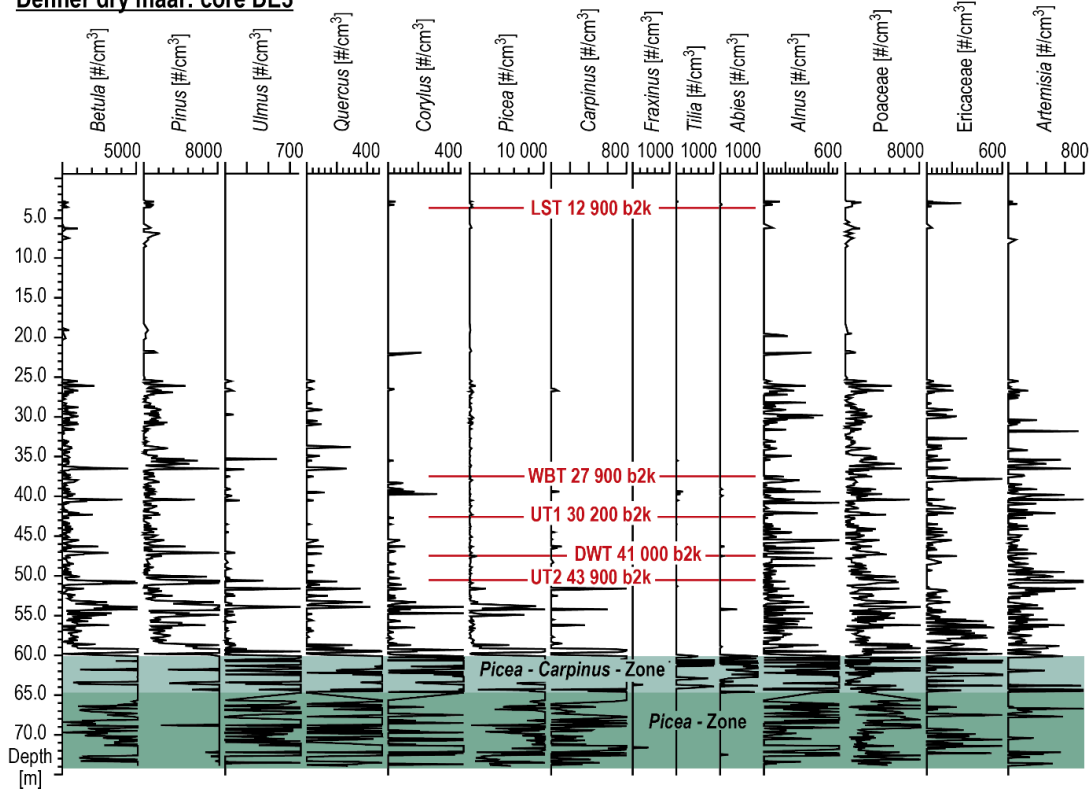


Fig. 2.7: Pollen counts [$\# / \text{cm}^3$] of sediment and marker tephra layer of core versus depth.

Auel dry maar: core AU2

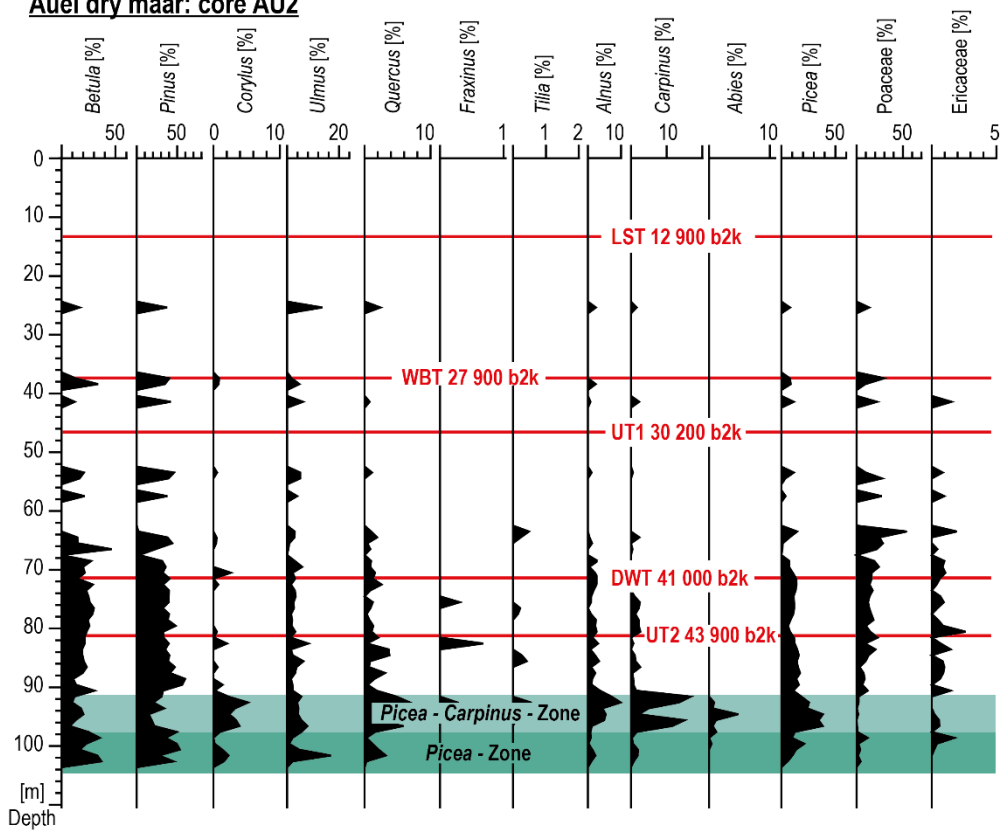


Fig. 2.8: Pollen concentrations of core AU2 from Auel dry maar versus depth.

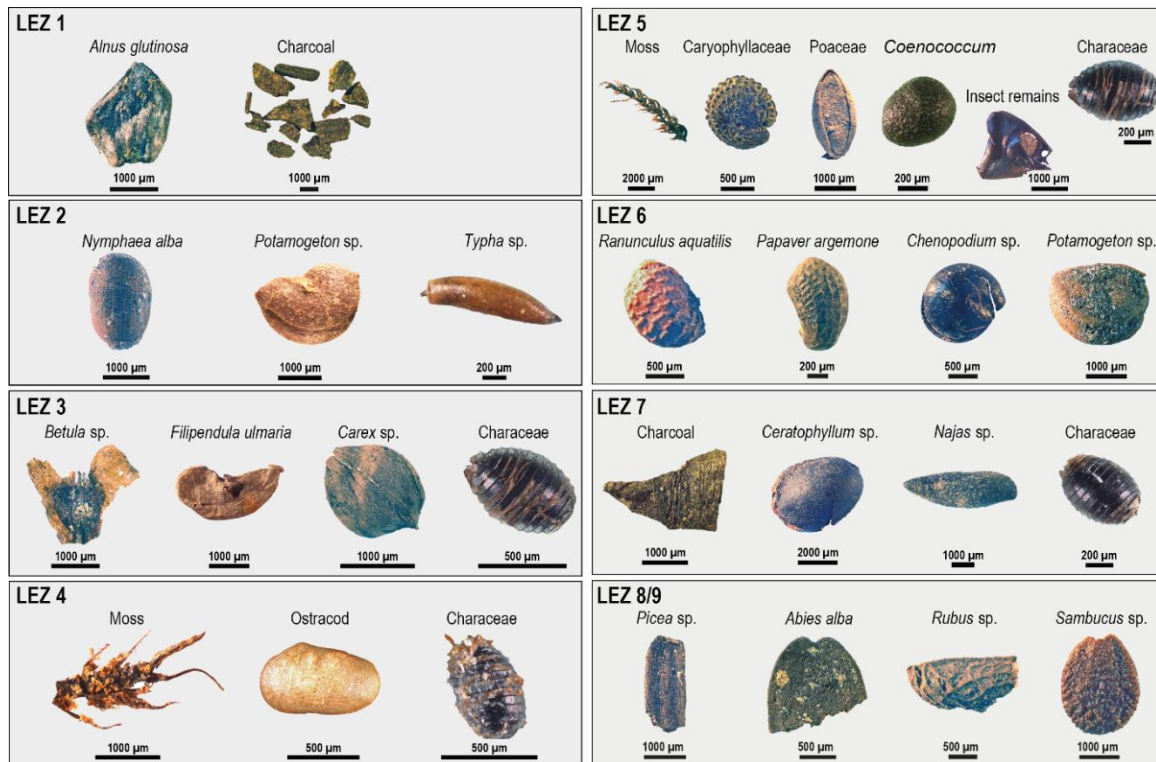


Fig. 2.9: Photos of selected macroremains typical for the LEZ.

2.4.6 Diatom Analysis

250 samples of about 50 mg collected from core DE3 were sieved and treated with concentrated HCl and H₂O₂ to remove the carbonates and the organic matter. The minerogenic fraction was then removed by decantation, and further sieving in order to concentrate the diatom tests. More than 235 different diatom species were identified and documented (Fig. 2.13). The taxa were grouped into planktonic and benthic species and presented as total sums. The benthic diatoms are further divided into species that live on the sediment and rocks (epilithic) and those that live on underwater vegetation (epiphytic). Maxima in the ratio of epiphytic to epilithic are thus an indicator of the abundance of underwater vegetation and of relatively high water temperature; minima in contrast indicate cold lakes with clastic bottom sediments – as today typical of alpine glacier lakes.

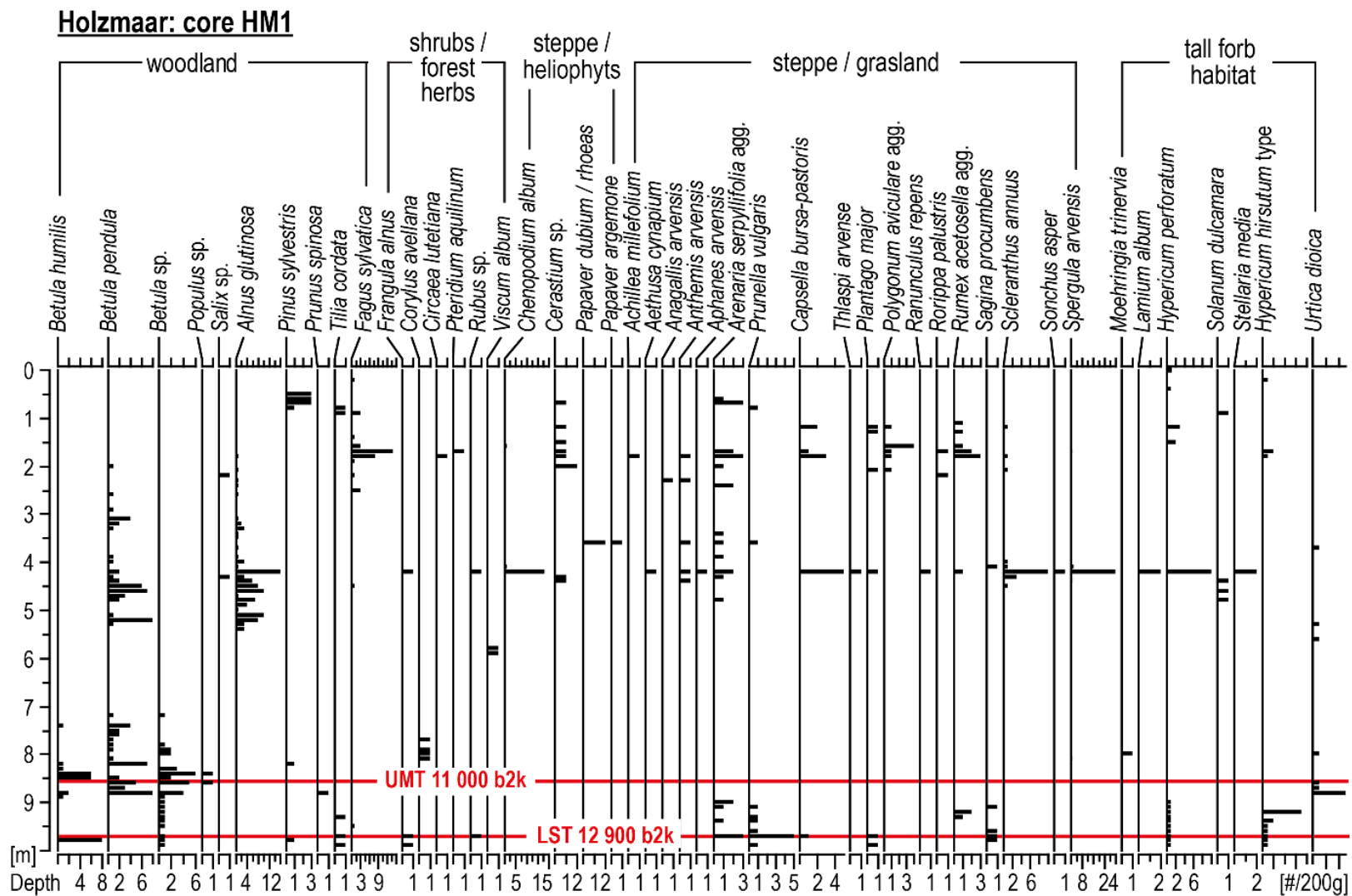


Fig. 2.10a: Macroremains (#/ 200 g) of core HM1 from Holzmaar versus depth.

Holzmaar: core HM1

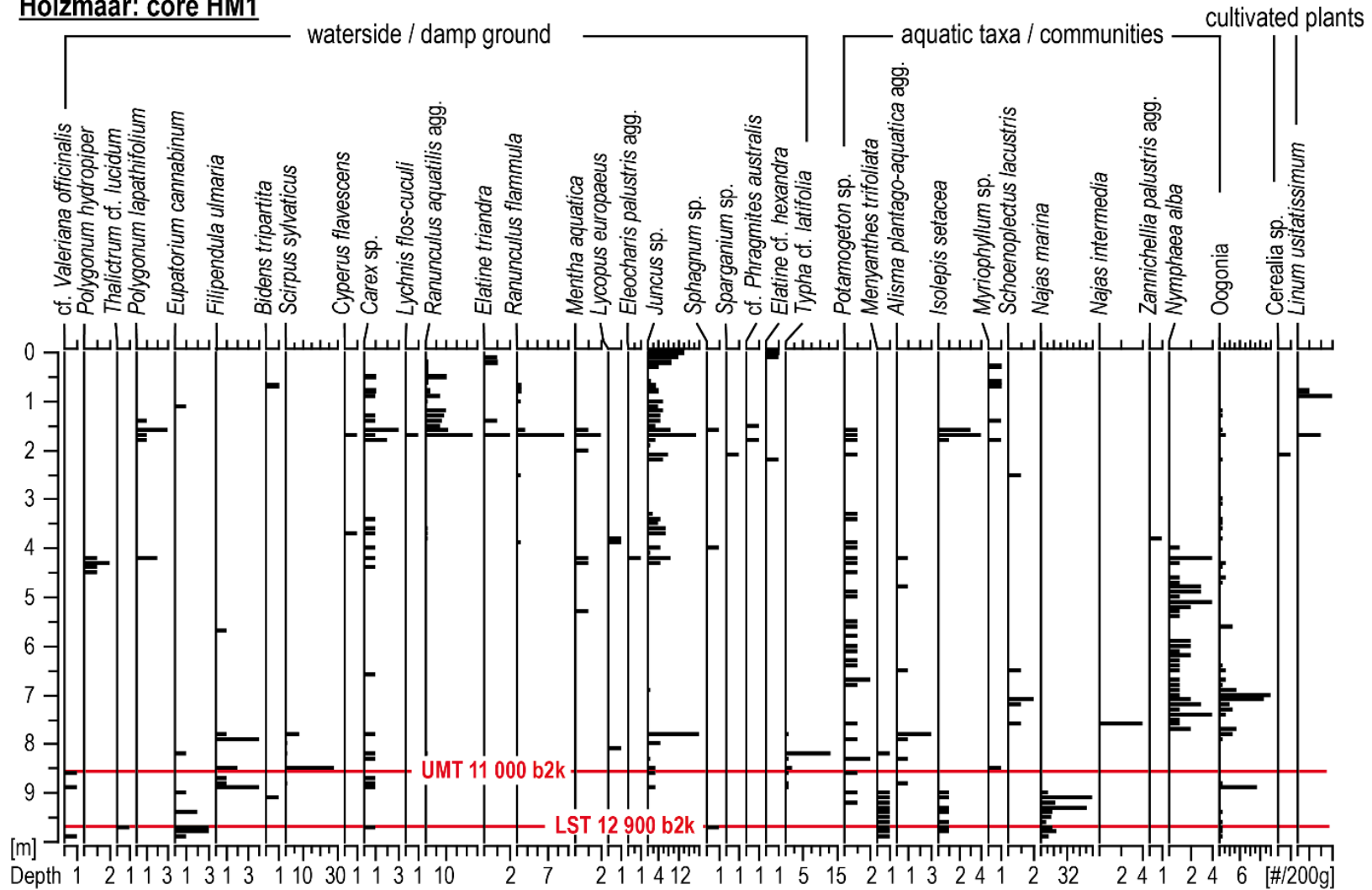


Fig. 2.10b: Macroremains (#/ 200 g) of core HM1 from Holzmaar versus depth.

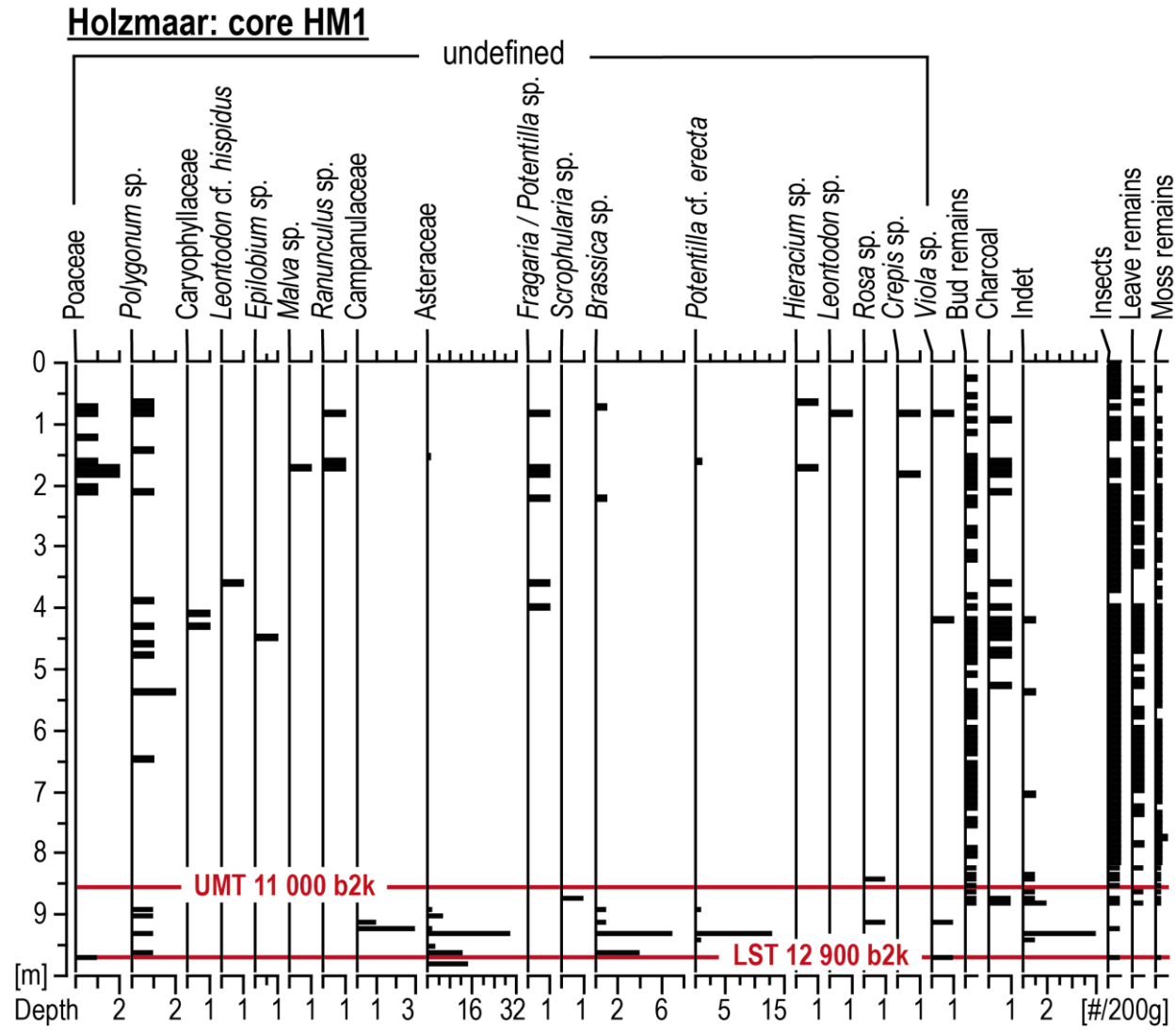


Fig. 2.10c: Macroremains (#/ 200 g) of core HM1 from Holzmaar versus depth.

Dehner dry maar: core DE3

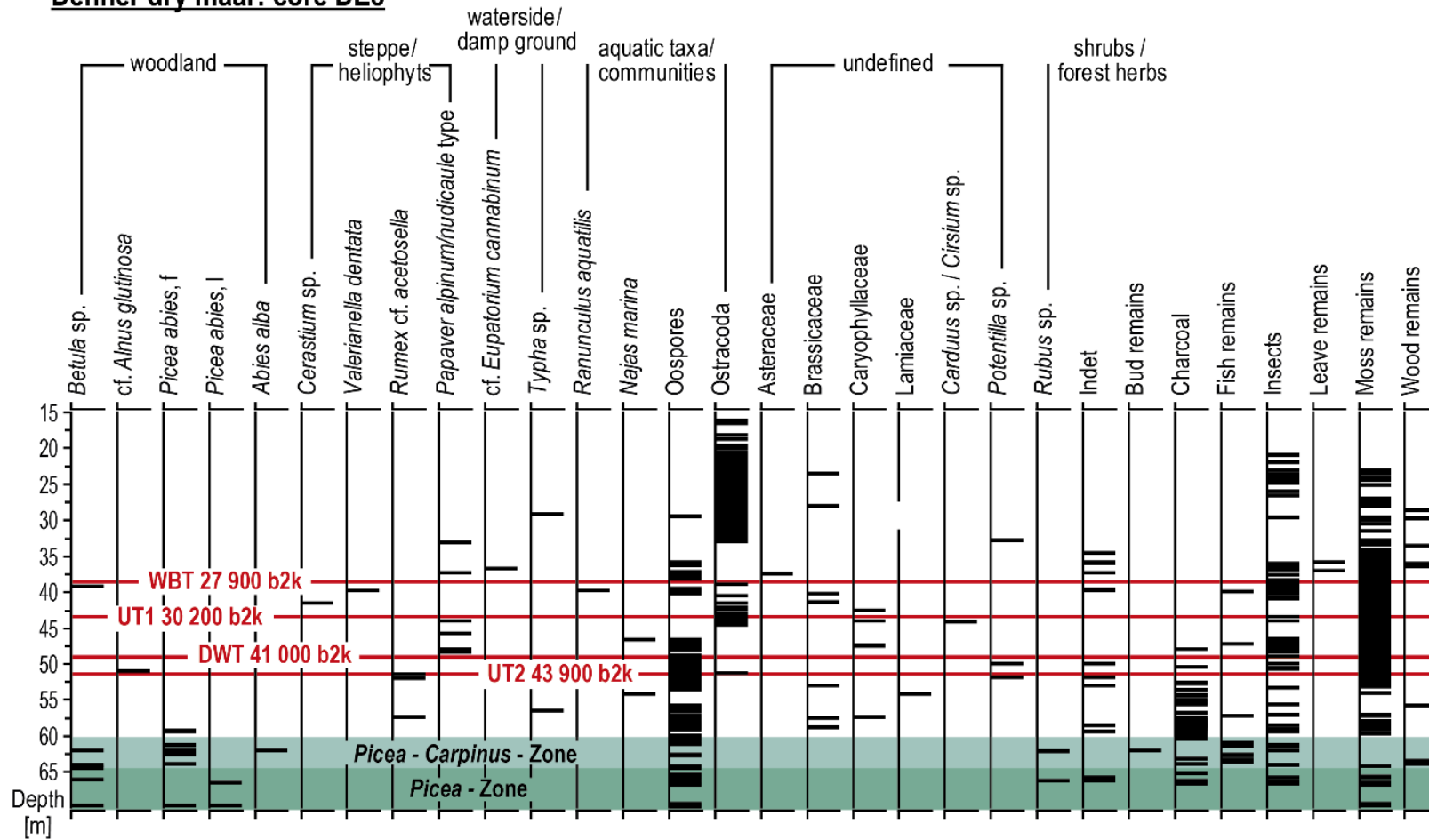


Fig. 2.11: Macroremains (presence/ absence) of core DE3 from Dehner dry maar versus depth.

Auel dry maar: core AU2

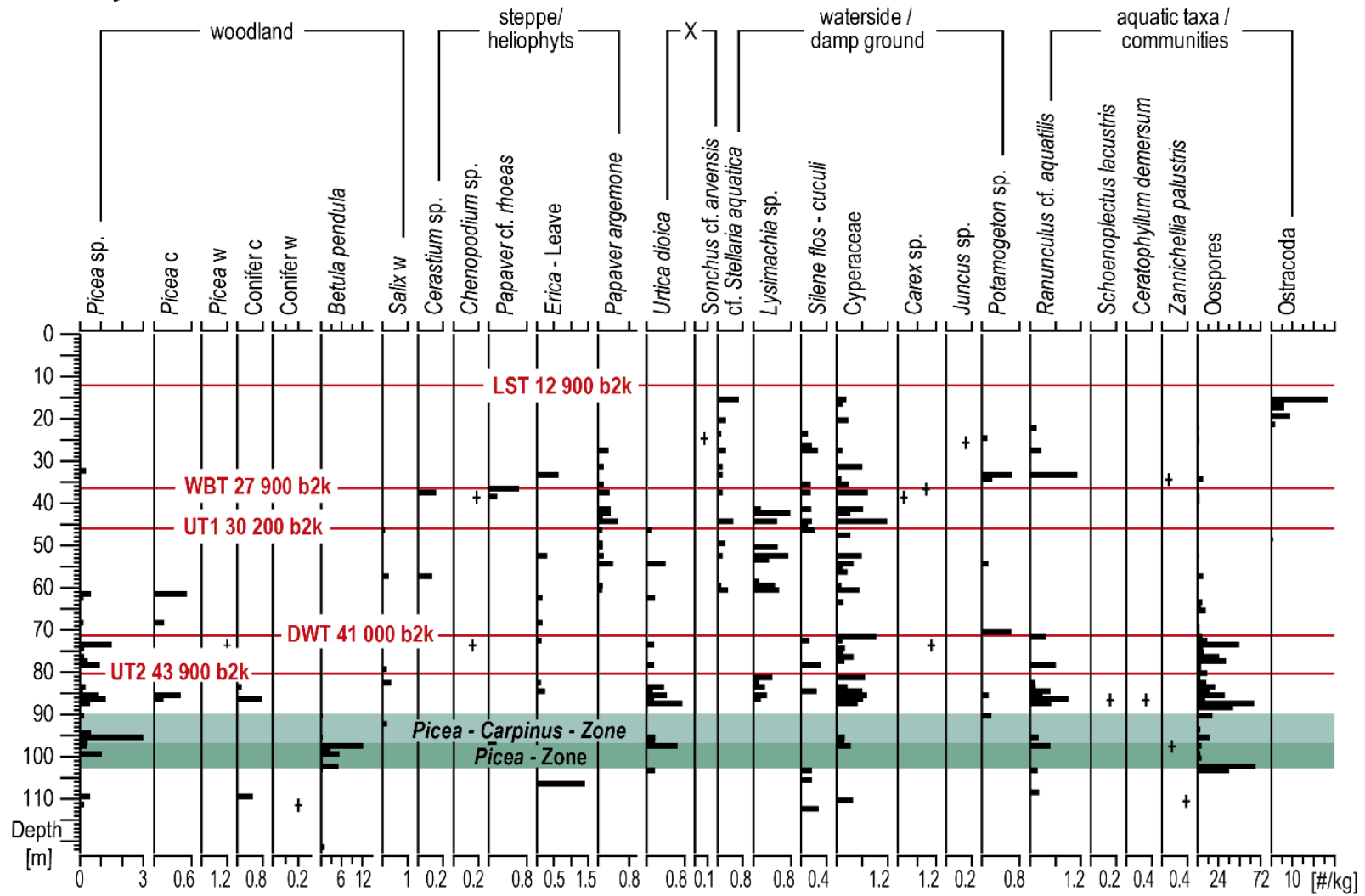


Fig. 2.12a: Macroremains (#/ kg) of core AU2 from Auel dry maar versus depth.

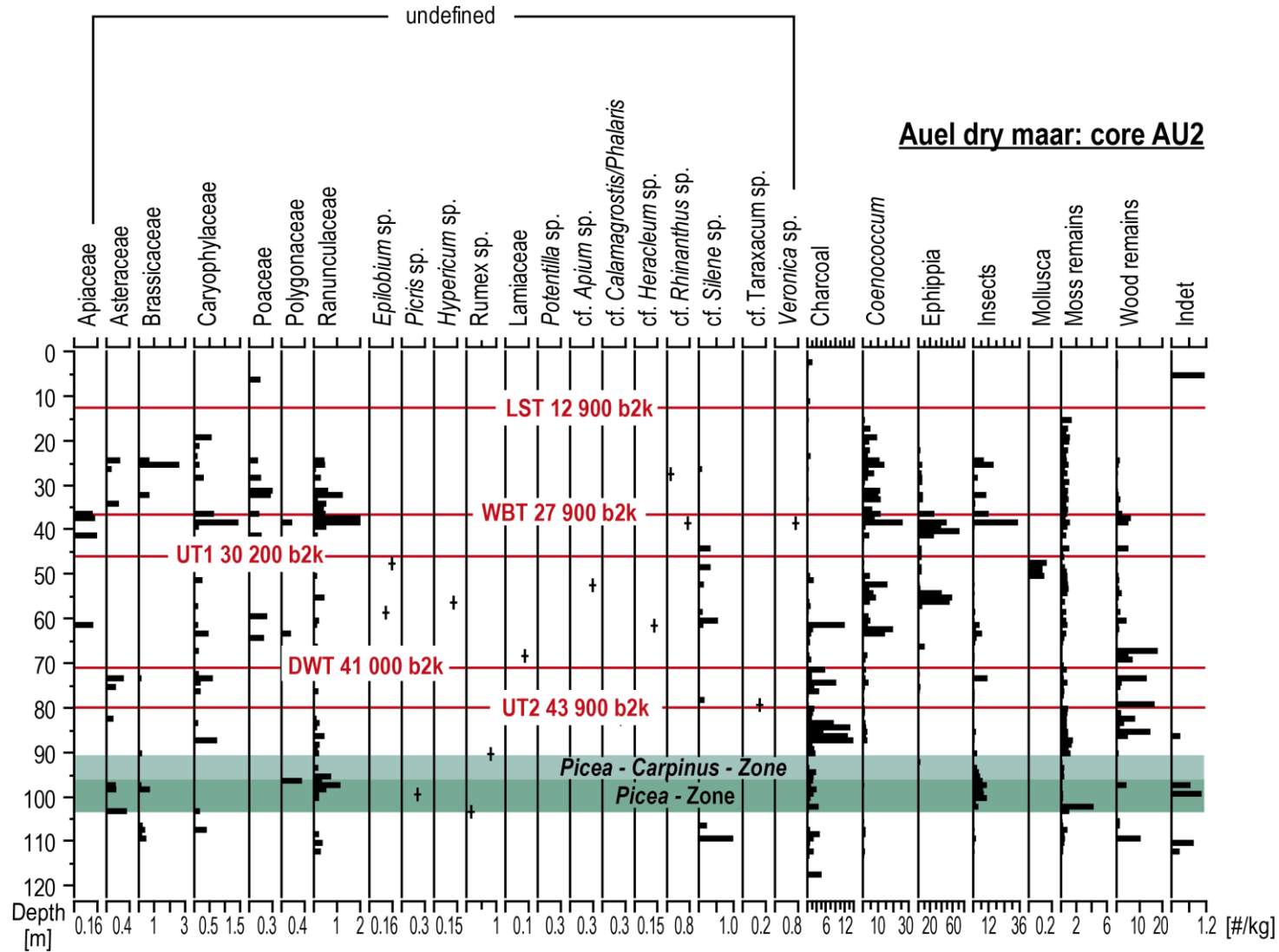


Fig. 2.12b: Macroremains (#/ kg) of core AU2 from Auel dry maar versus depth.

Dehner dry maar: core DE3

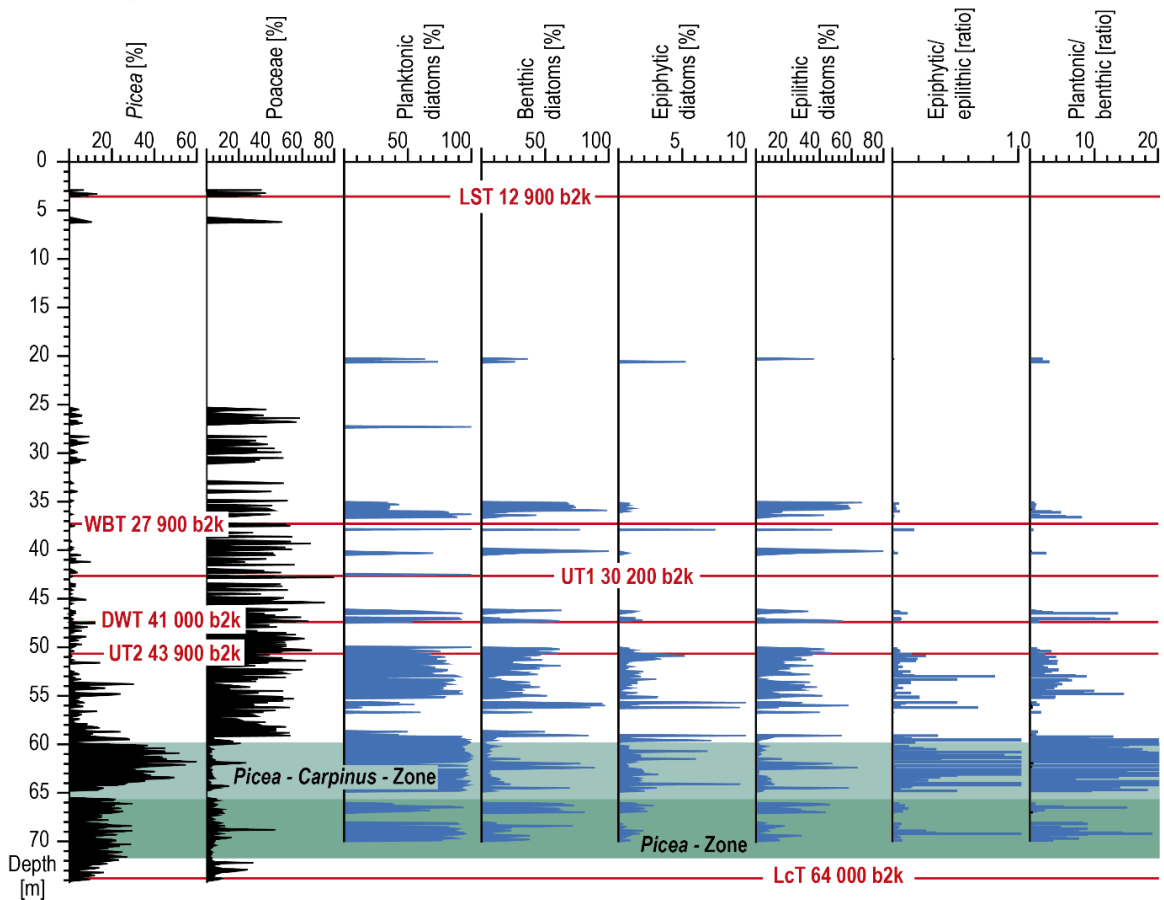


Fig. 2.13: Diatoms of core DE3 from Dehner dry maar versus depth.

2.4.7 Aeolian Dust

Aeolian dust can be best reconstructed from the Dehner dry maar records, because this maar has no fluvial inlet, but an outlet, which stabilizes the water level to some extent. The records from Dehner dry maar were used to construct the ELSA dust stack (Seelos et al., 2009; Dietrich and Seelos, 2010; Dietrich and Sirocko, 2011). The method of dust analysis is based on the sorting of the quartz silt fraction, detected from petrographic thin sections under a microscope with crossed nicols. The sorting is then used to approximate the percentage of the aeolian fraction in the bulk quartz fraction between 20 and 63 μm size.

The resolution of quartz grain size detection is in 0.5 mm steps, which allowed a seasonal resolution of the primary ELSA-Dust-Stack (Seelos et al., 2009). We include the DE3 part of the dust stack in this paper, however using the new stratigraphy. The offset of the new DE3 record from the MIS 2 stratigraphy of Seelos et al. (2009) is a maximum of 1000 years, because the record is now presented on the new varve time scale, not on the tuned time scale.

2.4.8 Flood events

Flood events can be best reconstructed from Auel maar because a large creek flows into the maar before leaving it on the opposite side. During the lake phase of this maar, all sediment influx must have settled in the deep basin. The fluvial inflow led to the generally very high sedimentation rate, as well as discrete flood layers emplaced following rainfall events.

10 cm-long thin sections were analysed by μ -XRF for elemental geochemistry at 100 μ m resolution and for grain size on a petrographic thin section in order to distinguish flood layers from distal turbidites. Turbidites have a continuous grain size gradation whereas the grain-size profile of flood events is in contrast characterized by several grain size maxima over the entire layer thickness, because a flood event over several days shows numerous plumes of intense discharge leading to a discontinuous grain size gradient (see Brunck et al., 2016). In addition, the thickness of each flood layer was measured for the classification of the event intensity. Accordingly, 88 flood layers over 7.5 mm thick were detected over the last 60 000 b2k (Brunck et al., 2016). The normalized flood index was calculated by the number of flood layers per millennium divided by the maximal number of flood layers per millennium in each core.

2.5 Results

2.5.1 Chronology

Tephrochronology

Ar/ Ar ages for the highly differentiated volcanic eruptions of the Laacher See Tephra, Dümpelmaar Tephra, Glees Tephra and Hüttenberg Tephra were established by van den Boogard et al. (1989). Sirocko et al. (2013) presented geochemical evidence that the ash from all of these classical Eifel tephra were indeed deposited in the Eifel maar lakes. Förster and Sirocko (2016) characterized these tephra by petrographic analysis of the coarse-grained mineral fraction and transferred the tephra Ar/ Ar ages of van den Boogard et al. (1989) to the ELSA sediment cores. Accordingly, the tephra from Laacher See (LST), Dümpelmaar (DMT), Glees (GT) and Hüttenberg (HT) have a characteristic mineral composition, which can be used to correlate cores on an absolutely dated age scale (Fig. 2.14).

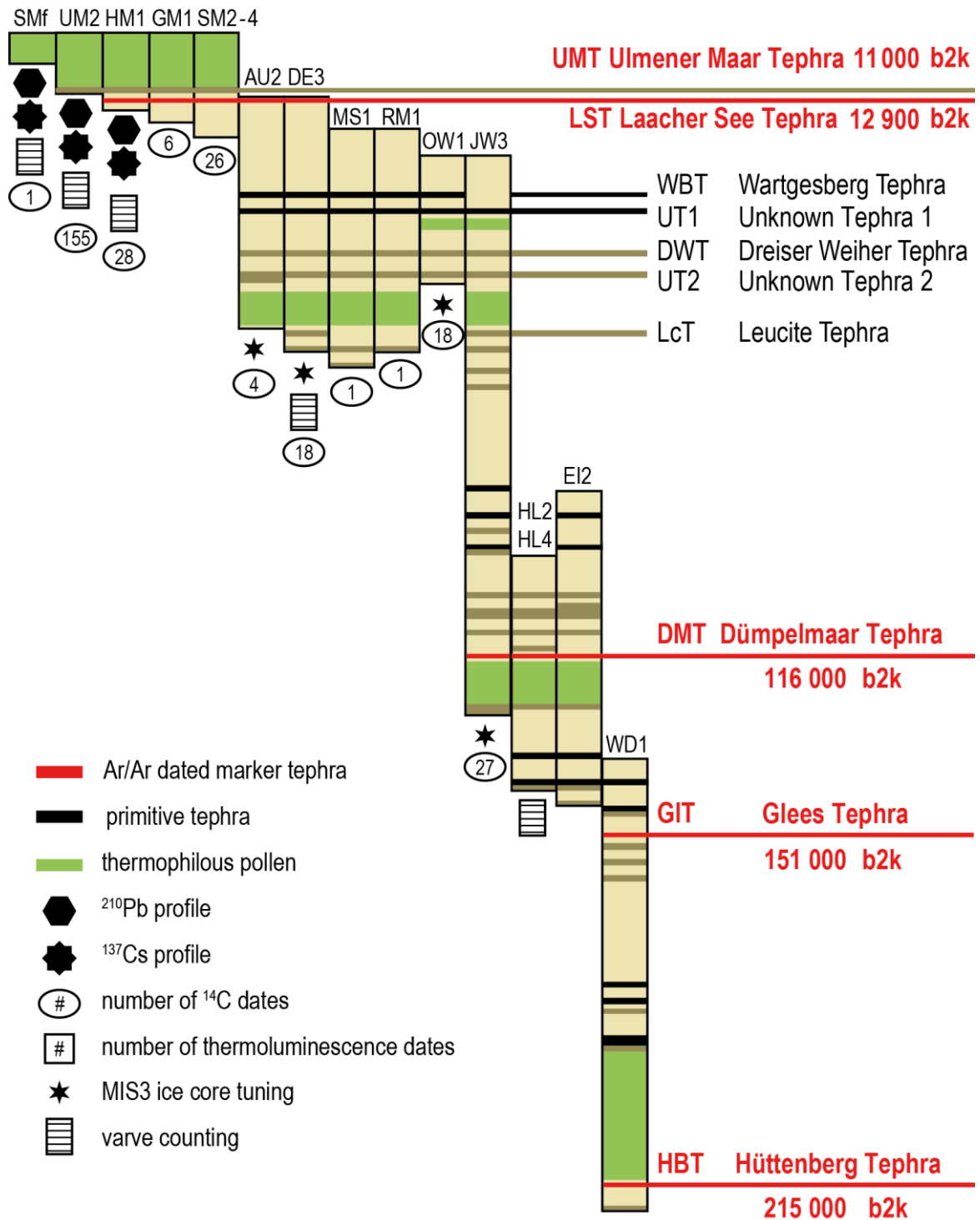


Fig. 2.14: Overview of main ELSA cores covering MIS 1 – 7. Marker layers from the ELSA-Tephra Stack are used to correlate the ^{14}C dated sediment cores and evolved marker tephra are highlighted in red with Ar/ Ar ages taken from van den Bogaard (1985) and van den Bogaard and Schmincke (1995).

The ELSA cores also revealed numerous other tephra, all of which were analyzed with the coarse-grained mineral method of Förster and Sirocko (2016). This increased the

number of correlation tie points significantly (Fig. 2.14). The ages for these non-Ar/ Ar dated tephra are taken from core AU2, and are thus on the Greenland ice core stratigraphy.

The same petrographic method was also applied to samples from the tuff walls of 30 maars in the West Eifel volcanic field (see also Förster and Sirocko, 2016). Apparently, the petrographic composition of the tephra from Wartgesberg (WBT) and Dreiser Weiher (DWT) were repeatedly found in numerous sediment cores (Figs. 2.3, 2.4, and 2.14). The Dreiser Weiher ash is most clearly distinguished, because this is the only very primitive tephra, which contains abundant pyroxene together with 10 % sanidine (a composition only explained if the sanidines are xenoliths, Förster and Sirocko, 2016). Accordingly, the Dreiser Weiher Tephra (DWT) at 41 000 b2k stands out as the best petrographically distinguishable stratigraphic markers of MIS 3 lake sediments in the Eifel.

All cores with WBT and DWT also contained two ash layers with a very distinct primitive composition for which the site of eruption location is unknown (UT1, UT2), but could still be used as marker tephra if WBT and DWT were present as well. The last tephra of importance for the time period studied in this paper is a unique leucite bearing tephra (Lc1), which is found below the early MIS 3 *Picea*-Zone and serves as the oldest marker tephra of the last 60 000 years.

Varve counting

Annually laminated lacustrine sediments are excellent archives for reconstruction of the climate and environmental changes of the past since the pioneering work of de Geer (1912) up to the most recent review of Zolitschka et al. (2015). The annually laminated sediments of the Eifel maar lakes in central Germany were one of the first to allow a reconstruction of a varve time series for the Holocene. The first ¹⁴C adjusted varve counts were completed for Holzmaar (Negendank et al., 1990; Zolitschka, 1991, 1998; Hajdas et al., 1995) followed by continuous varve counting of Meerfelder Maar (Brauer and Negendank, 1993; Brauer et al., 1999, 2001). Holzmaar covers the last 23 220 years, Meerfelder Maar the last 14 200 years. Varve counts in Eifel maar sediments below 23 000 b2k has not been reported yet, but varves have been counted for the last interglacial in the dry Maar westlich Hoher List (Sirocko et al., 2005; Rein et al., 2007).

All of the cores presented in this paper are laminated, but only few, or selected time intervals, allow the production of a varve chronology (Figs. 2.15 and 2.16). The freeze cores from Schalkenmehren (Fritz, 2011; Sirocko et al., 2013) and Holzmaar (HM1)

together provide a continuous varve counting during the entire Holocene from the present down to the Laacher See Tephra (LST: 12 880 b2k) (Fig. 2.2). Varve thickness during the Holocene mainly documents the erosion efficiency in the catchment and show a first spike up core at 6300 b2k (4300 BC) at Holzmaar when first Neolithic farmers began to clear the natural forest around the maar (Fig. 2.16). The second spike is centred after the introduction of the iron plough and the flood at 2800 b2k (800 BC). The third Holocene varve maximum was during the medieval period when mining and charcoal production increased strongly, leading again to extensive forest clearing (Fig. 2.16).

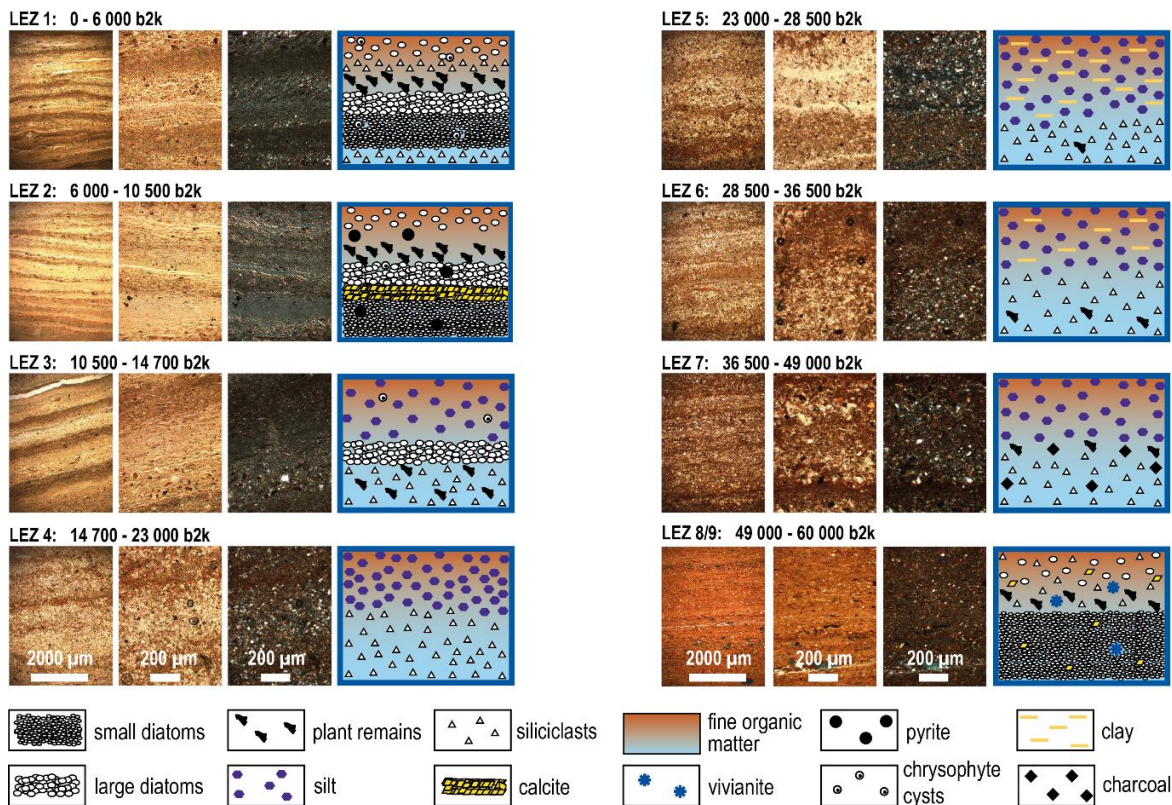


Fig. 2.15: Schematic diagrams of annual varve composition during the last 60 000 years as visible on petrographic thin sections.

The varve chronology below the LST was extended with core DE3, which is annually-laminated from the LST down to the Wartgesberg Tephra (WBT) at 27 900 b2k and further down to 30 200 b2k. The respective age/ depth relation is given in Figs. 2.17 and 2.18. Examples of the thin section itself are shown on the ELSA web page. The ELSA varve stack chronology is accordingly continuous from modern times back to 30 200 b2k. The major characteristic of the glacial section is a spike during the times of permafrost melt near 14 000 b2k, which must have led to strong erosion on the maar flanks. The second glacial feature is a pronounced increase in varve thickness at 23 000 b2k, marking the

onset of intense LGM dust activity. Finally, the varve counting corroborates independently the age of the ice core-tuned age of WBT at 27 900 b2k.

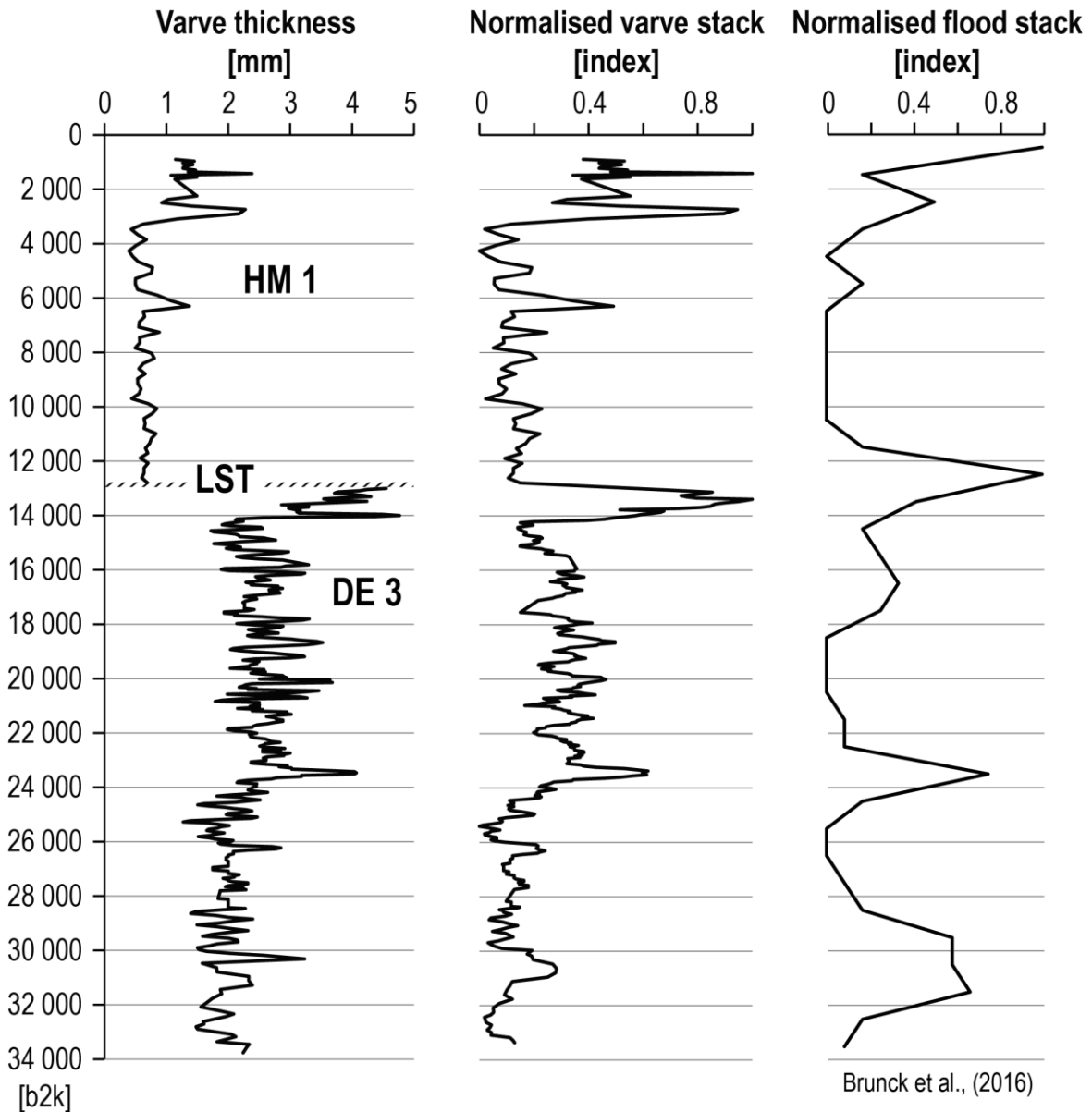


Fig. 2.16: Varve thickness and normalised varve stack in comparison with normalised flood stack (modified after Brunck et al., 2016).

Radiocarbon Dating

Schaber and Sirocko (2005), Sirocko et al. (2005, 2009), Dietrich (2011) and Dietrich and Sirocko (2011) developed a ^{14}C -based age model for cores DE2/ DE3 from the Dehner dry maar, which provided the backbone of the stratigraphy of all ELSA cores presented by Sirocko et al. (2013). This work included two ^{137}Cs and ^{210}Pb profiles, 270 ^{14}C -dates, two sediment records constrained with by a palaeomagnetism dataset, four luminescence dates

and two Ar/ Ar dates and shows that the sediment records used in this study (HM1, DE3, AU2) indeed document MIS 1 – 4.

Unfortunately, radiocarbon ages can usually not be used to date the Eifel maar core sections precisely. Sirocko et al. (2013) showed in a comparison of varve counting with the numerous ^{14}C ages obtained from the Ulmener Maar that the plant macrofossils in the Holocene sediments consists mainly of reworked pieces of wood, seeds and even small twigs. Twigs (one year old branches) proved to be the optimal material for dating the sediments because they decay fast if not rapidly buried in the sediment. The same observation was made for the Holzmaar (Fig. 2.17), where all Holocene ^{14}C ages were much too old for the varve counted age model, which is, however, consistent with the palynostratigraphy.

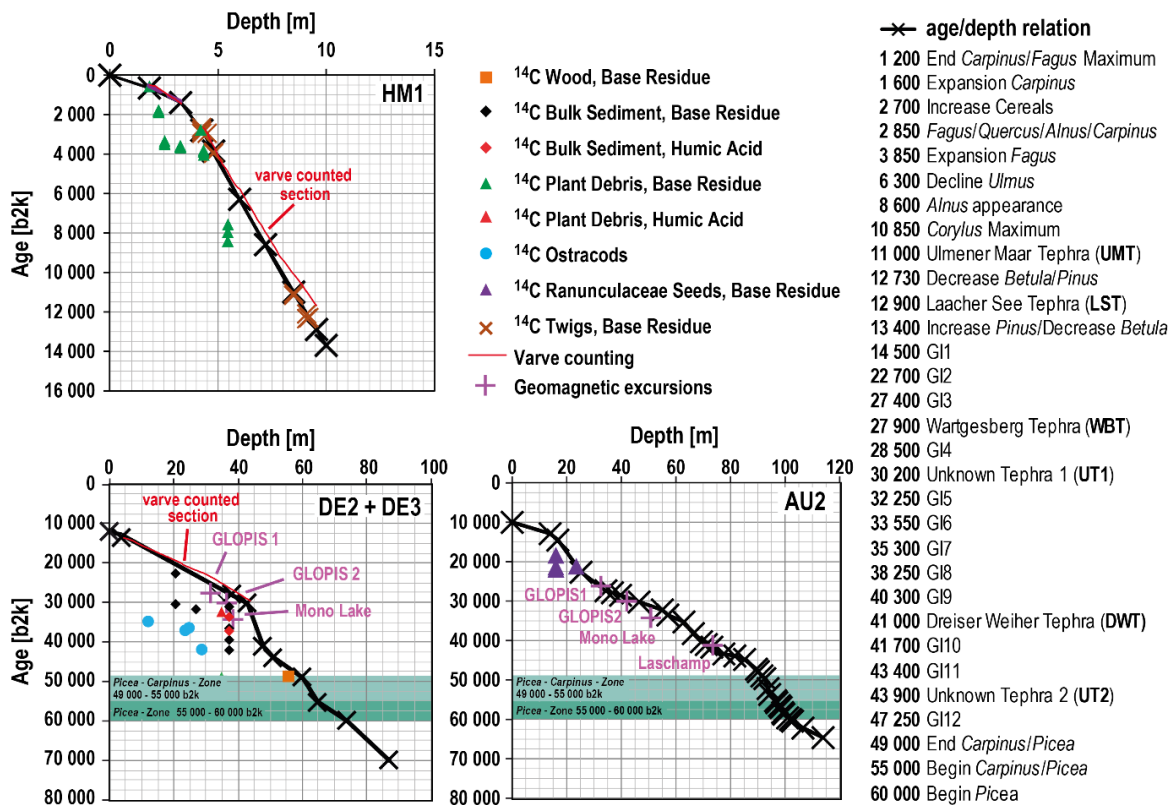


Fig. 2.17: Age/ depth relations for cores AU2 (Auel dry maar), DE2/ DE3 (Dehner dry maar) and HM1 (Holzmaar lake) with ^{14}C dates and the *Picea-Carpinus*-pollen-zones discussed in the main text.

Bulk sediment ^{14}C ages are even less reliable in the Eifel maar lakes because the anoxic bottom waters contain abundant old CO_2 from remineralisation of old organic matter in the sediments. In addition, outgassing of mantle CO_2 occurs even today at many

locations in the Eifel (May, 2002) and questions the applicability of ^{14}C dating for Eifel maar sediments in general.

The Holocene ^{14}C ages are thus problematic and the same is expected for the MIS 2/3 radiocarbon ages. Indeed, all ^{14}C ages presented in Fig. 2.17 are always older than the tephra-based age model. These ^{14}C ages thus only show that wood, seeds and bulk sediment must be younger than 55 000 b2k. Accordingly, we document the ^{14}C ages only to support other evidence for MIS 3 affinity for these sediments, and rely on ice core tuning and tephra correlation to date the entire ELSA sediments precisely.

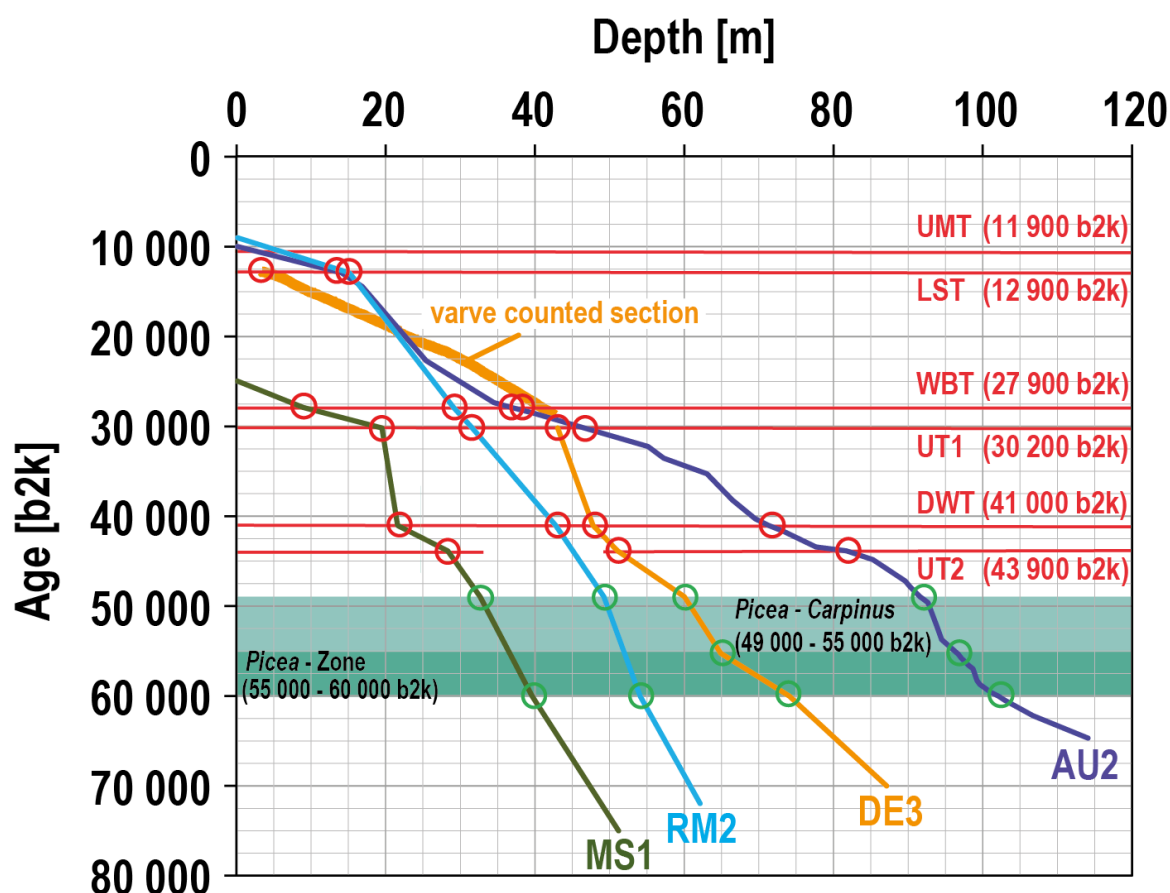


Fig. 2.18: Age/ depth relations for cores MS1 (Merscheid dry maar), RM2 (Roth dry maar), DE3 (Dehner dry maar) and AU2 (Auel dry maar) with detected tephra marker layers (after Förster and Sirocko, 2016) and the Picea dominated pollen zones. Cores RM2 and MS1 have only low resolution pollen profiles and are not included in the detailed palaeobotanic analysis discussed in this paper.

The main sediment record discussed here (AU2) was not included in Sirocko et al. (2013), because it was drilled in 2013. Core AU2 clearly archives the marker tephra horizons labelled as Laacher See Tephra (LST), unknown tephra 1 (UT1), Wartgesberg

Tephra (WBT), Dreiser Weiher Tephra (DWT) and unknown tephra 2 (UT2), as well as the dominance of *Picea* during early MIS 3 (Figs. 2.16 to 2.19). Several kilograms of sediment from core AU2 were sieved from the depths corresponding to the MIS 2 to obtain several mg of pure Ranunculaceae seeds for dating. This resulted in four new ^{14}C dates constraining a short phase of tundra environment during the GI 2, but seeds were apparently eroded and redeposited also in the LGM and late glacial sediments (Fig. 2.19).

Greenland ice core tuning

The most important record for the entire ELSA stratigraphy is AU2 with a length of 123 m (Fig. 2.4). The average sedimentation rate is $2 \frac{\text{mm}}{\text{a}}$ and, accordingly each core metre represents about 500 years in the pollen and plant macrofossil records. AU2 has the highest abundance of plant macroremains, because the dry maar at Auel is/ was fed by a stream. These specific conditions could explain why only AU2 closely resemble all Greenland interstadials as marked increases in the C_{total} record (Fig. 2.19). The total carbon content of AU2 was measured at 20 cm-intervals to obtain a record of approximately 100-year resolution, which was then compared to the NGRIP stadial – interstadial succession (Svensson et al., 2008). The similarity of the two records is so consistent that the late and middle MIS 3 record from AU2 allowed continuous direct tuning of AU2 to the Greenland ice core chronology (Fig. 2.19). The ages for all tephra in AU2 were then applied to all other ELSA cores. Accordingly, the results from all cores presented in this study directly can be compared to the Greenland climate history on the b2k time scale (Svensson et al., 2008).

Maxima in AU2 C_{total} curve match to some extent the diatom spikes in core DE3 (Figs. 2.13 and 2.19). The diatoms reflect apparently in-lake productivity (e.g. Veres et al., 2008, 2009) and must influence the C_{total} content during MIS 3 strongly. The MIS 3 diatom inferred interstadial succession is also visible in the DE3 tree pollen, but only in the absolute numbers of pollen counts (Fig. 2.7), not in the relative percentage values (Fig. 2.6).

The early MIS 3 linking is, however, still somewhat problematic because we observe a pronounced increase in total carbon of AU2 at 49 000 b2k (Fig. 2.19). Most likely, a dramatic change had occurred in the Eifel landscape at that time, but a respective signal in the Greenland ice is not apparent.

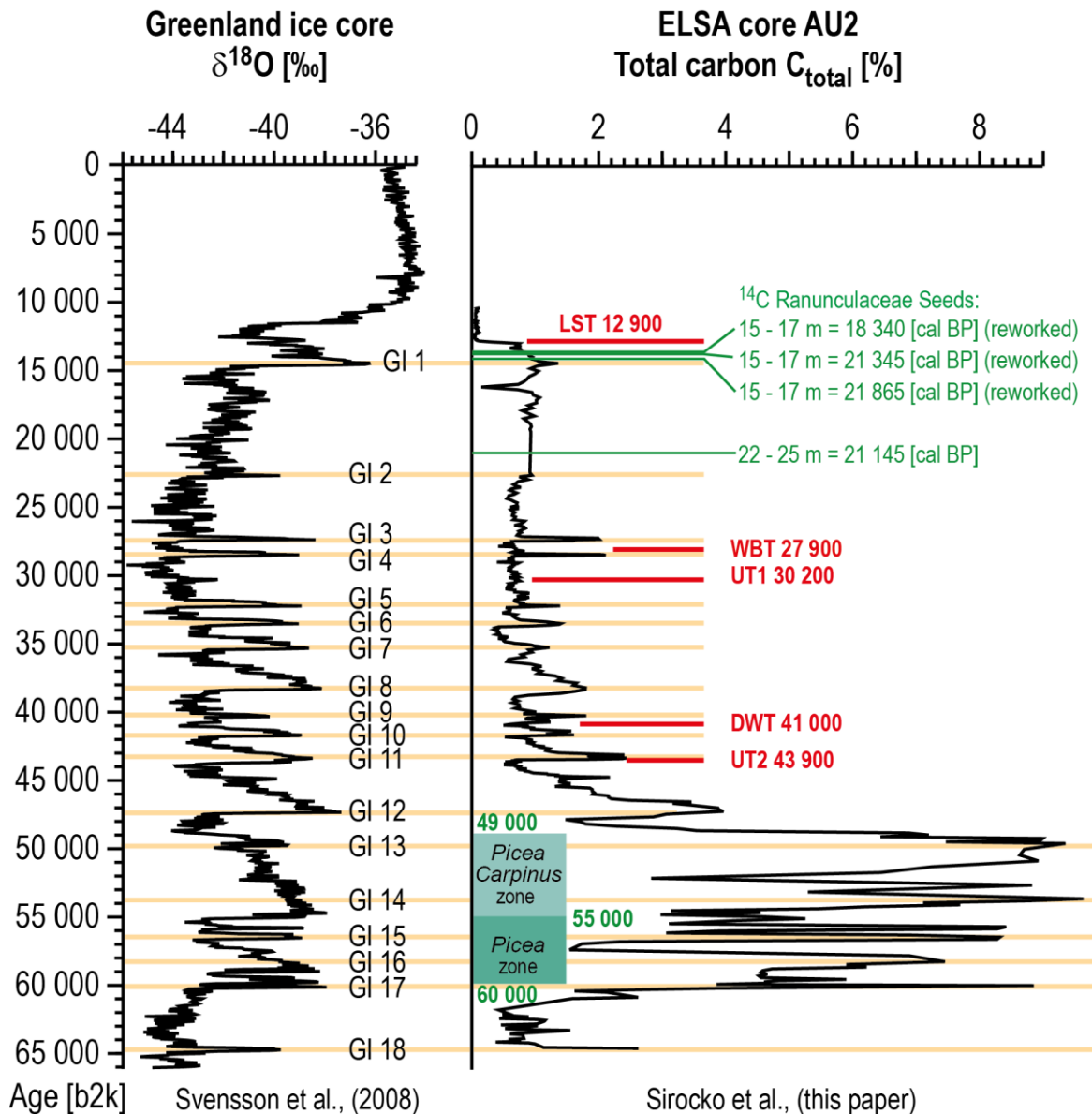


Fig. 2.19: AU2 ^{14}C dates on Ranunculaceae seeds and time series of total carbon concentrations tuned to the Greenland ice core stadial/ interstadial events as evidenced by variations in oxygen isotopes (Svensson et al., 2008).

Anchoring the tuned Auel time series to speleothem dates

High-resolution U/ Th dating of stalagmites in Europe (Moseley et al., 2014), and even nearby the Eifel (Bunkercave, D. Scholz, pers.comm.) indicate that stalagmites grew in Central Europe from 60 000 b2k to 46 000 b2k, which we use to anchor the last occurrence of *Picea* in the ice core tuned AU2 record. The section below with abundant *Picea* is then tuned to the GI 12 to GI 17 succession (Fig. 2.19). This tuning places the beginning of the *Picea* Zone at 60 000 b2k, almost exactly at the MIS 3 – 4 transition.

2.5.2 *The ELSA Vegetation Stack*

Based on the above stratigraphy and proxies the Pleistocene record of AU2 (Auel) and DE3 (Dehner) are stacked together with the Holocene records of SM₁₂ (Schalkenmehren) and HM1 (Holzmaar) in order to construct the ELSA vegetation stack spanning the entire last 60 000 years.

Late Holocene (0 – 6000 b2k)

The uppermost part of the Holocene pollen record shows the spruce maximum of the Prussian afforestation after AD 1820 (well visible in the plot of *Picea*) and the medieval forest clearings back to the early medieval dense hornbeam and beech forest that re-established after the retreat of the Romans (Fig. 2.5). The vegetation cover in the Eifel must have been similar during the Roman times and earlier Celtic times starting at the beginning of the Iron Age at 800 BC when a pronounced increase of cereals and grass pollen indicating further opening of the Bronze Age landscape. The Bronze Age landscape change had started in the Eifel at 1800 BC (Kubitz 2000) indicated by the spread of beech forests on used and abandoned farmland (Kalis et al., 2003).

The beginning of the Neolithic in the Eifel is marked by an increase in cereal pollen (Fig. 2.5), which are barely visible at Holzmaar, but clearly visible in the Ulmener Maar record, where farming had started already by 3700 BC (Gronenborn and Sirocko, 2009). Prior to the spread of cereals and other grasses, the HM1 record also shows the well-documented elm decline at 4300 to 4000 BC, synchronous with the spread of alder (Figs. 2.5 and 2.20). This feature is visible in both the pollen and the plant macroremain records and is also characteristic of many other parts of Europe (Kalis et al., 2003). This transition sees the introduction of cattle into the Eifel forest where elm, lime-tree, and ash-tree declined in abundance because the leaves of these trees were used for fodder production. Thus, from this time on forests were managed by humans for domestic purposes so that the mid-to-late Holocene vegetation is an anthropogenic-modified broadleaf forest within an open landscape dominated by cereal cultivation and cattle farming.

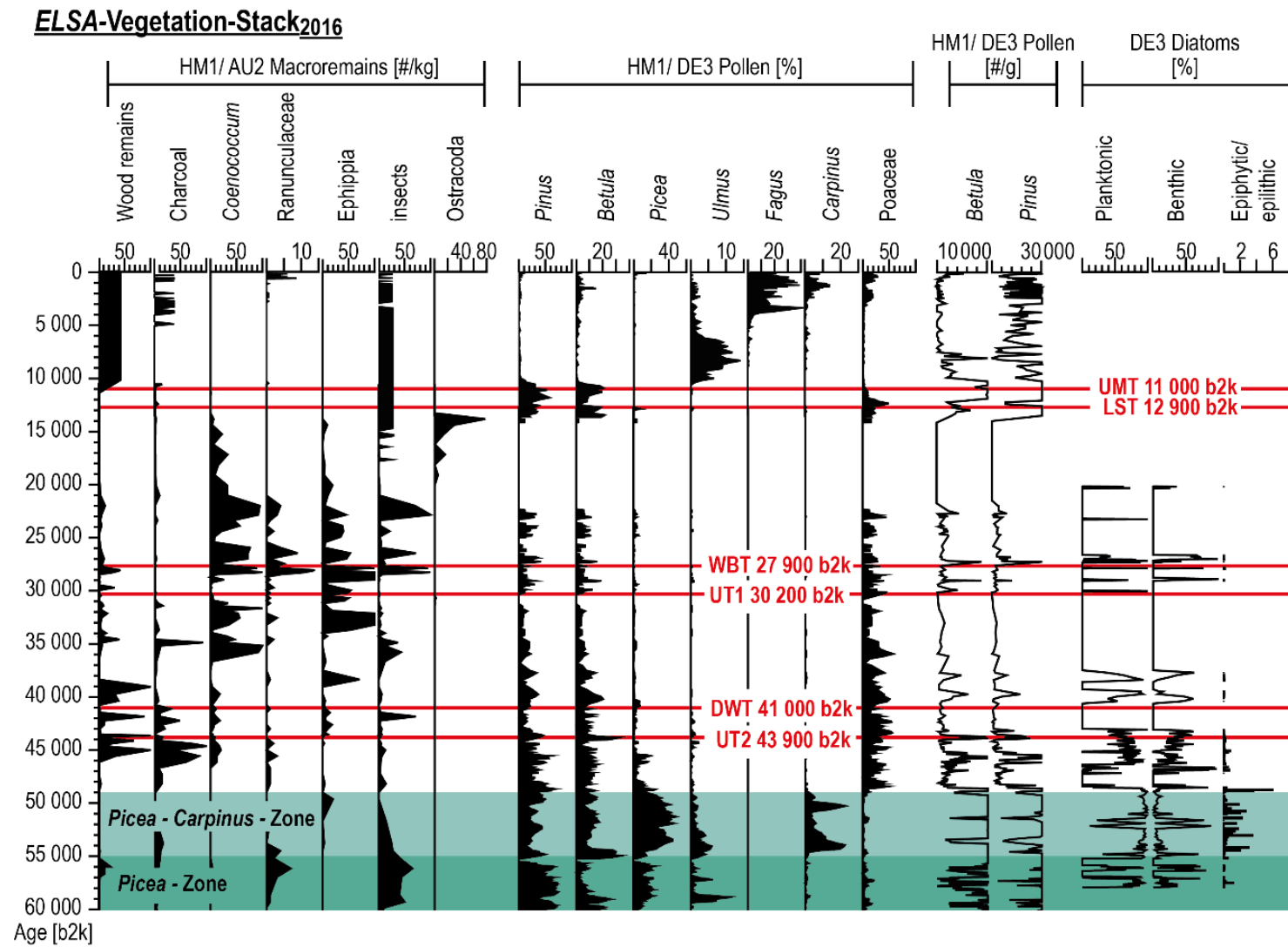


Fig. 2.20: The ELSA-Vegetation stack: Selected pollen concentrations and counts, macroremain counts.

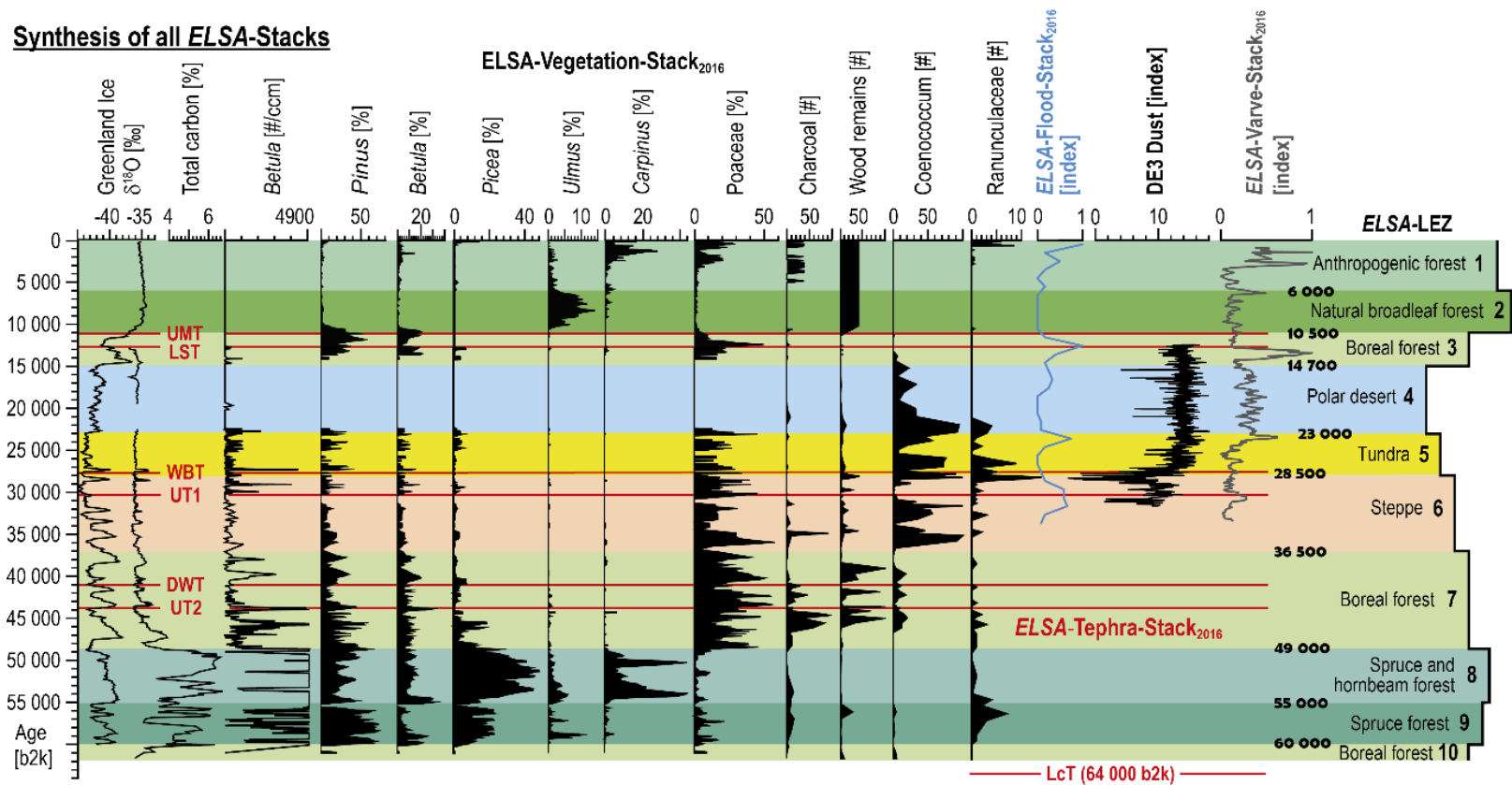


Fig. 2.21: Synthesis of all ELSA stacks: Total carbon of core AU2, selected pollen from core DE3, varve thickness stack for cores HM1 and DE3, updated part of the DE3 dust record (Seelos et al., 2009) and the ELSA-Tephra-Stack (Förster and Sirocko, 2016) together with Greenland ice isotope temperature index (Svensson et al., 2008) and with LEZ numbers.

	Age	HM1		SM3		AU2		RM2		DE3		MS1	
	[b2k]	Top [m]	Base [m]	Top [m]	Base [m]	Top [m]	Base [m]	Top [m]	Base [m]	Top [m]	Base [m]	Top [m]	Base [m]
LEZ 1		0.00	5.85	0.00	4.51								
LEZ 2	6 000		8.24		5.78	0.00	2.39	0.00	5.77				
LEZ 3	10 500					2.39	16.96	5.77	16.67	0.00	7.60		
LEZ 4	14 700					16.96	23.49	16.67	22.52	7.60	22.04		
LEZ 5	23 000					23.49	39.75	22.52	29.56	22.04	39.16	0.00	11.54
LEZ 6	28 500					39.75	64.33	29.56	37.97	39.16	45.65	11.54	20.61
LEZ 7	36 500					64.33	91.50	37.97	49.10	45.65	59.90	20.61	32.50
LEZ 8	49 000					91.50	96.30	49.10	51.80	59.90	64.65	32.50	36.50
LEZ 9	55 000					96.30	101.95	51.80	53.90	64.65	73.90	36.50	39.50
LEZ 10	60 000					101.95		53.90		73.90		39.50	

Tab. 2.1: Top and base for LEZ 1 – 10 in all ELSA cores.

Early Holocene (6000 – 10 500 b2k)

The lower elevations of the Eifel region prior to 4300 BC were covered with oak-lime woods, whilst higher altitudes were covered with oak-elm woods and hazel (Kalis et al., 2003). Neolithic settlers did not inhabit the Eifel at this time, and the plant macroremain assemblage is dominated by fruits and seeds of aquatic plants and taxa specific of flood-plain forests (Herbig and Sirocko 2012). The representative taxa from reed/ littoral vegetation are *Scirpus lacustris*, *Typha* sp., *Eupatorium cannabinum* and *Lycopus europaeus* (Fig. 2.10).

A cooling pulse from the latest meltwater discharge into the North Atlantic occurred at 6200 BC (8200 b2k). This cold anomaly lasted for about 100 years and is visible in the sediments of Lake Holzmaar and Meerfelder Maar (Prasad and Baier, 2014). Related changes in absolute temperature and precipitation cannot have been very large, because we do not see a corresponding change in the forest vegetation (Figs. 2.5 and 2.20), just a slight increase in grass and pine pollen. Accordingly, a mixed oak forest with significant hazel dominated the Eifel landscape during the first millennia of the Holocene.

Hazel was the first temperate tree to spread in the late glacial landscape and constituted up to 80 % of LEZ 2 pollen as well as found in the early Holocene plant macrofossil records (Fig. 2.10). The foliage of the birch and hazel trees must have been an important nutrient source for the brown earth soils that started to develop during this period. Increasing soil fertility and clay mineral content provided ideal conditions for the spread of oak, elm, and other deciduous trees during the millennia encompassed by LEZ 2.

Late Glacial/ Early Holocene Boreal Forest (10 500 – 14 700 b2k)

The vegetation after the end of the Younger Dryas at 11 700 b2k was still dominated by pine and birch (Fig. 2.20), but reveal a significant presence of aquatic plant macrofossils, in particular *Nymphaea alba*, *Najas marina* and *Potamogeton* sp. (Figs. 2.10, 2.11 and 2.12). The Younger Dryas cold spell is characterized by subarctic steppe tundra with heliophytes (*Artemisia*, *Helianthemum*), shrubs including *Juniperus*, *Betula nana* and sporadic tree birches. Birch and pine are present (Figs. 2.5 and 2.20), but most likely as dwarf forms and in patches on favorable stands such as south exposed slopes, river valleys etc. The occurrence of *Nymphaea alba* indicates a shift to more eutrophic condition in the Holzmaar during the late Glacial/ Holocene transition.

Remains of aquatic plants like *Ranunculus aquatilis* or *Najas marina*, as well as single diaspores from herbaceous plants and *Typha* sp., are typical around the time of Laacher See ash emplacement: a 10 cm thick tephra layer in core HM1/ DE3/ AU2 deposited during late Alleröd times (Figs. 2.2, 2.3 and 2.4). Steppic conditions with scattered birch and pine covered the landscape during the preceding Bölling (Fig. 2.20). Tundra dominated by grass was established in the very early Bölling when a few trees, i.e. *Salix* and *Populus*, grew in small stands around the maar. Macroremains of the Bölling reveal abundant oospores from Characeae (*Chara aspera*, *C. globularis*, *C. contraria*) as underwater vegetation in particular during the deglacial tundra (Figs. 2.10 to 2.12), when ostracods were most abundant in the Eifel maar lakes.

The plant macrofossil record points to birch trees scattered in grassland with abundant heliophytes (Figs. 2.10, 2.11, 2.12 and 2.20). The lake water must have been strongly oligotrophic with *Menyanthes trifoliata*, *Najas marina*, Potamogetaceae and Characeae, while the swamp vegetation in the vicinity comprise *Filipendula ulmaria*, *Isolepis secaceae*, *Juncus* sp., *Carex* sp. *Eupatorium cannabinum* and *Typha* cf. *latifolia* (Figs. 2.10 to 2.12). The drastic increase in ostracods and oospores from Characeae during a time of already existing shrubs and pine/ birch dwarf vegetation most likely parallels the abrupt warming at around 14 700 b2k when the Gulf Stream/ North Atlantic drift system jumped within several decades into an interglacial mode. Accordingly, the lake water was warm, but nutrients and biomass were still low. The development of vegetation during this part of Termination I was studied at high resolution by Stebich (1999), Litt and Stebich (1999) and Litt et al. (2001, 2003) and we refer the reader to these papers for a detailed description of the classical pollen zonation.

Seven *Chara* taxa have been identified in the ELSA maar lake records during the Termination I; *Chara aspera*, *C. globularis*, *C. contraria*, *C. vulgaris*, *Nitella capillaris*, *N. opaca* and *Tolypella glomerata* indicate a continuous warming of the lake, but without eutrophication.

The polar desert of the Last Glacial Maximum (23 000 – 14 700 b2k)

The maar lake sediments spanning 23 000 to 14 700 b2k are in general problematic for palaeoecological reconstructions because they show poor pollen preservation in all cores. The only core with glacial stage pollen preserved is from Schalkenmehrener Maar in which we observe a few grass pollen after ca. 16 000 b2k (Sirocko et al., 2013). Accordingly, we

have inferred for that time the existence of a landscape with permafrost, but some grassland. Characea oogones and ostracod give even further evidence for more biomass after 16 000 b2k, which might have been important for the late glacial megafauna like the mammoths and the first hunters moving from the glacial refuge areas in southern France back into Central Europe.

Pollen is completely absent during the LGM from 21 000 – 17 000 b2k but this might also be a result of poor pollen preservation. Oxic conditions must have reached the deepest part of the maar lake even on cold summer nights whereby only coarse plant macroremains would be capable of surviving the decay processes in the well-oxygenated glacial stage water columns (Veres et al., 2008, 2009). Accordingly, the LGM plant macroremains consist only of a few mosses, oogonia, ostracods, as well as some single seeds mainly from Ranunculaceae (Figs. 2.10 to 2.12). The LGM polar desert was thus likely not completely abiotic with at least some biomass present during the summer.

The occurrence of Ranunculaceae seeds and a diatoms spike at 21 000 b2k provides evidence that the LGM polar desert was punctuated with short-lived returns to tundra conditions (Figs. 2.20 and 2.21).

The tundra of the early MIS 2 (28 500 – 23 000 b2k)

Moss, fungi sclerotia (*Coenococcum geophilum*) and insect remains are typical for the millennia before the LGM (Fig. 2.20) and indicate a tundra vegetation. The ¹⁴C dating of this time is complicated because there is generally very little organic material, except for some Ranunculaceae, which reach from the steppe into the tundra phase.

The other typical plant macrofossils of the tundra reflect riparian and damp ground taxa i.e. *Stellaria aquatica*, *Silene flos-cuculi*, *Juncus* sp. and Cyperaceae as well as Caryophyllaceae, Poaceae, Brassicaceae and Asteraceae. Insects and sclerotia from *Coenococcum geophilum* (indicating the presence of fungi) (Figs. 2.20 and 2.21). The peak of *Coenococcum geophilum* might indicate higher sediment/ soil erosion and runoff into the lake (Drescher-Schneider, 2008).

The steppe of the middle and late MIS 3 (36 500 – 28 500 b2k)

Many sediment samples spanning the middle and late MIS 3 did not reach the minimum threshold of 50 pollen grains so that calculation of pollen percentage values was not possible and these data points were omitted from the pollen diagrams (Fig. 2.20). The

pollen concentration curves show no structure during all of MIS 3, but the interstadials of MIS 3 become clearly visible in the pollen count numbers (Figs. 2.7, 2.18, 2.20 and 2.21). The same taxa observed during the cold stadials were apparently also present during the warm interstadials, however with higher pollen numbers. This could be an effect from better pollen preservation in the carbon-rich interstadial sediments, but could alternatively be also explained by general higher plant numbers in the interstadial times (Fig. 2.21). In this case, the steppe persisted with the same taxa during all of the middle and late MIS 3, but the abundance of trees and diatoms increased significantly during the interstadials.

Plant macrofossils are generally scarce and can only be found in dry maar Auel where even the oospores of Characeae that are indicative of in-lake vegetation were often missing. Biomass was generally low – with the exception of *Coenococcum sclerotia*, especially during the late MIS 3 (Figs. 2.20 and 2.21). The sclerotia from *Coenococcum geophilum* coincide with occurrence of *Betula* seeds and may be indicative of *Alnus* and *Betula* peat along the banks of the lakes (Grosse-Brauckmann, 1974). Beside the remains of *Betula* several wetland taxa were found, including *Stellaria aquatica*, *Silene flos-cuculi*, *Lysimachia* sp., Cyperaceae, *Carex* sp., *Potamogeton* sp., *Typha* sp. (Fig. 2.11). It must be emphasized that *Coenococcum geophilum* is not a climate indicator as it is connected via mycorrhiza symbiosis with several plant taxa and thus not suitable for vegetation reconstruction (Tinner et al., 2005). However, during this time of low biomass we suppose that it indicates cold, moist conditions with abundant *Cristatella mucedo*. The landscape from 36 500 to 28 500 b2k is thus a steppe with scattered trees. Charcoal is almost absent suggesting that it was moist enough to prevent intensive burning of the grassland.

The dominant pollen are grass associated with abundant heliophyte macroremains such as *Papaver rhoeas*, *P. argemone*, *Cerastium* sp., *Chenopodium* sp. and *Erica* sp. (Figs. 2.6, 2.11 and 2.12). Alder must have been growing close to the maar lake because their macroremains were found in the sediments. Fish remains and water plants were recorded for the last time during GI 8.

The boreal forest of the middle MIS 3 (46 000 – 36 500 b2k)

The period from 46 000 to 40 000 b2k is marked by birch, pine and a strong increase in charcoal, which indicates that the boreal forest burned regularly, pointing to at least seasonal arid conditions during that interval (Figs. 2.20 and 2.22).

Three charcoal maxima (Fig. 2.20) are parallelized by synchronous rises in Characeae oogonia (indicative of shallow water) and Cyperaceae (shoreline vegetation) remains. In addition, several maxima in wood remains are visible, but not during the time of the charcoal maxima (Fig. 2.21). We cannot address these maxima of the forest remains to a specific climatic phase because the resolution of the macroremain sampling of AU2 is for entire core metres, containing about 500 years, whereas the C_{total} record is of 20 cm resolution, representing 100 years. It will have to wait for a future analysis of thin sections for this time interval to arrive at clear inferences on the nature and timing of the charcoal and wood remain maxima relative to the stadials and interstadials.

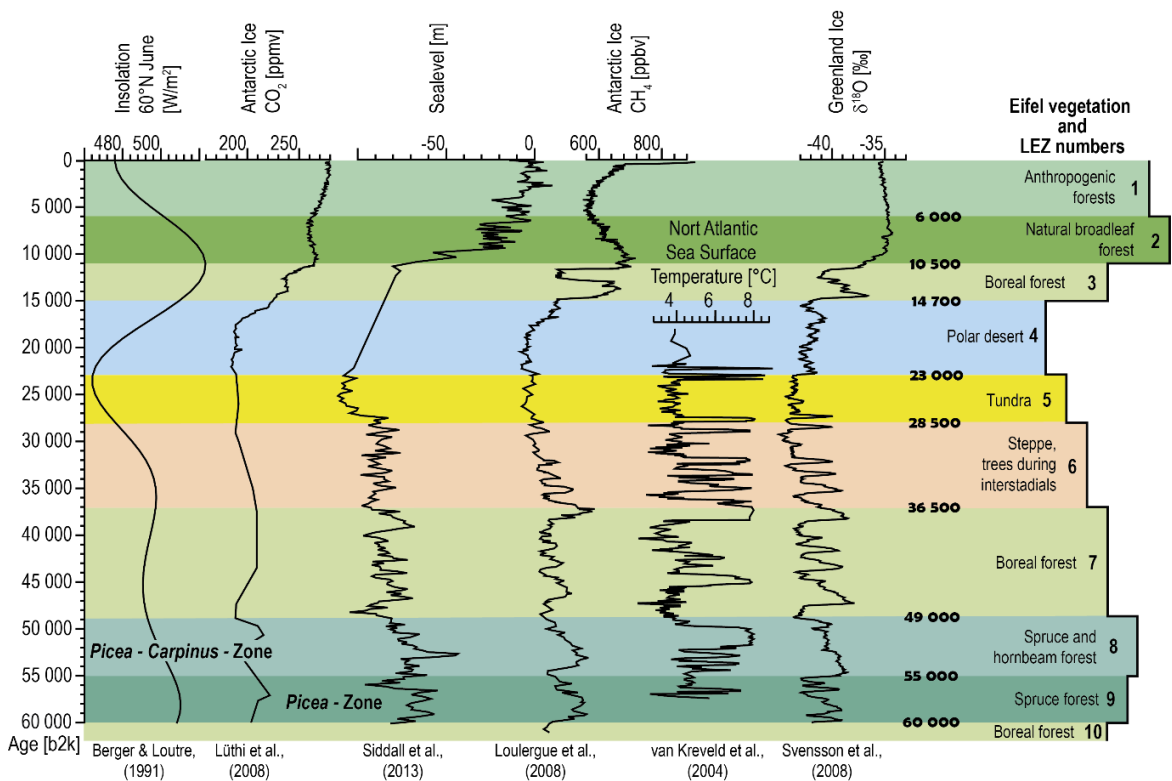


Fig. 2.22: Time series of the major forcings for the Central European climate during the last 60 000 years: summer insolation at 65 °N (Berger and Loutre, 1991), Greenland ice isotope temperature index (Svensson et al., 2008), the ice-core derived global records of CO₂ (Lüthi et al., 2008) and CH₄ (Loulergue et al., 2008) on the AICC₂₀₁₂ chronology (Veres et al., 2013), sea surface temperatures (van Kreveld et al., 2004) from the North Atlantic Drift.

The occurrence of *Ceratophyllum demersum*, *Schoenoplectus lacustris*, *Thypha* sp. and *Najas marina* in the time of the early charcoal maxima (Fig. 2.21) point to mean July temperature between 15 – 18 °C during late interstadial phase of GI 12 at

46 000 – 45 000 b2k (Fig. 2.21). Moreover, the presence of *Urtica dioica* indicates nutrient rich soil/ sediment conditions between 46 000 and 43 000 b2k.

The first traces of the subsequent steppic conditions become visible in the boreal forest accompanied by Cyperaceae, insects, Ranunculaceae, *Papaver argemone* and the first appearance of *Coenococcum sclerotia* (Figs. 2.20 and 2.21). Apparently, the landscape was much more open at this time than during the very early part of MIS 3.

The spruce forest of the early MIS 3 (60 000 – 49 000 b2k)

All maar records studied in this synthesis on the MIS 3 vegetation in the Eifel reveal a phase of several thousand years during the early MIS 3 with abundant tree pollen. Both pollen and plant macroremains show the omnipresent *Pinus* and *Betula* (Figs. 2.20 and 2.21), but with the dominance of a long-lasting peak of *Picea* that is just beyond the limit of ¹⁴C dating and thus assigned to GI 17 – GI 13 (60 000 – 49 000 b2k). Other thermophilous trees including *Ulmus*, *Quercus*, and *Tilia* are also represented in the pollen assemblages. Climatologically, these broadleaf taxa are indicative of summer temperatures slightly lower than modern temperatures, even if present only in small quantities. The warm phase had a duration of about 7000 years and favoured soil formation. The pronounced *Picea* pollen maximum is observed not only in AU2 and DE3 (Figs. 2.20 and 2.21), but in five other ELSA records not included in this study, but shown in the age/ depth relations of Fig. 2.18.

The macrofossil evidence corroborates the findings from the pollen record, because *Picea* sp. and *Abies alba* needles have been found at the same depth as the respective pollen maxima. The macroremain record is further supported by the presence of seeds and fruits of *Rubus idaeus*, *Rubus* sp., *Alnus* sp. and *Urtica dioica*, which may point to nutrient rich soil/ sediment.

Small amounts of lime tree pollen are present that might be explained by long distance transport from the Mosel-valley where average summer temperatures are today 2 degrees warmer than in the Eifel. We observed seeds of *Ceratophyllum demersum* at 86.5 m depth in core AU2 (Fig. 2.12). This plant needs summer temperatures of at least 17 °C so that it appears that the early MIS 3 growing season temperatures in the Eifel area were little lower than today. The occurrence of *Typha* sp. (13 – 15 °C) and several seeds of *Najas* support this palaeoclimatologic inference.

2.6 Discussion

2.6.1 Landscape Evolution Zones (LEZ) during the last 60 000 years

Here we present LEZ-based summaries of palaeoclimatic and -ecological evolution of the Eifel region during the last 60 000 years (Fig. 2.21). The ordering starts at the present with LEZ 1 and finishes at LEZ 10 in the very early MIS 3 (Tab. 2.1).

LEZ 1 0 – 6000 b2k

LEZ 1 is the time when humans altered the early Holocene forests containing elements from cereal and cattle farming. The timing of such environment changes is regionally very different depending on the timing of the introduction of foliage fodder production, soil dependent intensity of cereal farming, and urbanization.

Consequently, the varved lake sediment of the last 6000 years have very different character to that produced in earlier LEZs, mostly consisting of a dark minerogenic autumn and winter deposition and a bright spring and summer diatom influx layer (Fig. 2.15). Aeolian quartz particles are uncommon, but occurred sporadically during the last few centuries. The varves in the maar sediments revealed abundant spring and summer diatom blooms, sometimes with calcite, and plant leaves are common. The winter layers consist of minerogenic detritus with high proportions of chrysophyte cysts. LEZ 1 flood layers during are most common during Medieval and Roman times (Fig. 2.21), with the major events at AD 1342, 800 BC, and 2100 BC, respectively (Brunck et al., 2016). Volcanic activity was absent from the Eifel during LEZ 1.

LEZ 2 6000 – 10 500 b2k

The late glacial boreal forests transformed quickly into an early Holocene forest, which was soon dominated by hazel, oak, elm and lime (Fig. 2.20). The cause of this typical forest succession was not only the higher insolation during the early Holocene, but also the development of the soil profile. This can be attributed to the 6 °C inferred increase of North Atlantic sea surface temperatures when the Gulf Stream/ North Atlantic drift system warmed abruptly at 11 600 b2k (e.g. Alley et al., 1995; Knorr and Lohmann, 2007).

The temperature in Central Europe was high from 11 500 – 6000 b2k, which is best indicated by very high snowlines in the Alps (Nicolussi and Patzelt, 2006). The middle part of LEZ 2 displays a cold spell associated with the 8.2 ka event, a cool pulse from the final

meltwater discharges from the late North American ice sheet into the North Atlantic. This cold anomaly affected all of Central Europe (von Grafenstein et al., 1998; Hosek et al., 2014) and caused a 120-year long cool and dry signal in the sediments of the Holzmaar (Prasad and Baier, 2014). However, the 8.2 ka event did not change the Eifel landscape ecology in the long term (Fig. 2.5) as mixed oak forest with hazel covered the Eifel landscape continuously from ca. 10 500 to 6000 b2k.

The varves corresponding to the LEZ 2 sediments are composed of three layers. Spring layers consist mainly of calcite, followed by the summer layer of diatom frustules. The autumn/ winter layers consist mainly of detritus and chrysophyte cysts (Fig. 2.15). Flood layers are not as clearly visible in the Holzmaar or in the Schalkenmehrener Maar as during the later LEZ 1 (after initiation of crop cultivation), but visible flood layers are regularly observed in the LEZ 2 record from Ulmen (Sirocko 2009; Gronenborn et al., 2009). The eruption of the Ulmener Maar occurred at the LEZ 3 – 2 boundary, but we regard the youngest eruption of the Eifel volcanic fields as part of LEZ 3.

LEZ 3 Late Glacial/ Early Holocene Boreal Forest (15 000 – 10 500 b2k)

Summer insolation over the Northern Hemisphere increased at 17 000 b2k, when global sea level started to rise coeval with the initiation of post-LGM temperature increase around the Antarctic (Jouzel et al., 1994) (Fig. 2.22). The AU2 and DE3 cores reveal thick layers of laminated, but disturbed sediment from 16 000 – 14 000 b2k, which we associate with first melting of the LGM permafrost landscape. This initial summer warming resulted in the first deep thawing of the soils, which were soliflucted even on very gentle slopes at several centimetre/ metre per year. However, the summers were warm enough so that grasses spread, followed by birch and pine after 14 700 b2k.

Aeolian activity was significant well into the deglacial phase, but not as strong as during the preceding LGM (Fig. 2.21). The drastic increase in ostracods and oospores from Characeae during a time of dominant shrub and pine/ birch dwarf vegetation, most likely parallels the abrupt warming at around 14 700 b2k, when the Gulf Stream/ North Atlantic drift system jumped to an interglacial mode over a few decades. Accordingly, the lake water columns were warm, but nutrient availability and biomass was still low.

The subsequent Alleröd interval saw animals like red deer move into the expanding forest. This environmental change is also reflected in changing human behavior, because

the use of the bow and arrow are first documented during this period, thus indicating close range hunting of smaller animals in a closed/ open pine and birch forest.

The Netherlands and northern Germany were strongly affected by large-scale cover-sand deposition during the Younger Dryas (Vandenberghe, 1992a, 1992b; Kasse et al., 1995, 2003; van Huissteden et al., 2003). The end of the Younger Dryas came abruptly within several years at around 11 600 b2k and ended the dominance of grass, pine and birch in the late glacial landscape mantled with weakly developed soils (Fig. 2.21). Subsequently, loess and cover-sand deposits were transformed into fertile brown earth soils during the warmth of the subsequent LEZ 2.

The varves of the late glacial LEZ 3 are composed of three layers (Fig. 2.15): (1) spring layers consist of minerogenic components and plant residues; (2) diatom frustules form the summer layers, whereas (3) the autumn/ winter layer consists of detritus, chrysophyte cysts and diatoms. The plant residues deposited in spring are interpreted as inwash by intense late winter snowmelt in a climate when plant biomass was present, but no consistent leaf fall in autumn existed yet, as indicated by the absence of autumn layers from leaf fall.

LEZ 3 experienced an average of 4.8 flood events per 1000 years and the largest events were documented at ca. 11 700, 12 500 and 13 800 b2k respectively (Brunck et al., 2016). 12 strong flood events occurred in the time window 12 000 – 13 000 b2k (representing most of the Younger Dryas) and reveal the highest number of flood events per 1000 years in the whole of AU2, a situation likely caused by intense winter snow fall and early spring meltwater events.

The highly explosive eruption of the Laacher See occurred at 12 880 b2k in the middle of LEZ 3 followed by the Ulmener Maar eruption at 11 000 b2k. These are the only Eifel-derived tephra identified during the last 27 000 years.

LEZ 4 The polar desert of the Last Glacial Maximum (23 000 – 15 000 b2k)

Landscape Evolution Zone 4 denotes the coldest time of the last glaciation, equivalent to the Last Glacial Maximum (LGM). Pollen grains are completely absent and identifiable organic macroremains consist only of few mosses, oogonia and ostracods (Fig. 2.21). A few Ranunculaceae seeds were found in the sediment, but the ¹⁴C ages show that they are reworked from a Ranunculaceae maximum at 21 000 b2k (Fig. 2.19). Two short

warming intervals are apparent in the diatom record (Figs. 2.13 and 2.20) and by the occurrence of *Thypha* sp. (Figs. 2.10, 2.11 and 2.13), which today requires mean July temperatures above 13 – 15 °C. *Oogonia* are other indicators of submerged vegetation and reveal that Characeae were abundant even during the LGM, however, we cannot exclude that they are also reworked like the ¹⁴C dated Ranunculacea seeds (Fig. 2.19).

Dust activity was at a maximum during the LGM. The ELSA dust stack shows that silt deflation became strong near 28 000 b2k (Fig. 2.21) and dominated the sedimentation up to 14 000 b2k, when the vegetation cover slowly increased. The peak LGM dust deposition is even clearer in the varve thickness records, whereby they increase markedly at 23 000 b2k (Fig. 2.21).

The frontal margin of the Scandinavian ice sheet reached only up to the north of the river Elbe even during the maximum ice advance and thus the ice margin was about 500 km of the Eifel. The glacial maar lake sediments are laminated and yellowish, and consist of almost pure silt and fine sand (no clay or gravel). There is no indication of a permanent ice cover or drying of the lakes (Figs. 2.3 and 2.4). There are, however, subaqueous terraces at around 14 m below modern lake surface in Holzmaar and Schalkenmehrener Maar, indicating substantial lowering of the ground water and lake level during the LGM. The lakes were open during summer, however on a lower lake level, but we see no indication of strong weather anomalies. The climate of the LGM in the Eifel was apparently uniformly cold with clear air, with most active dust transport during late spring or summer.

The LGM section at Dehner dry maar is about 8 m-thick and consists of countable silt laminae. The number of aeolian laminae counts matches with a 4 % error the number of years for this section as derived from the ice core tuned age model. The nature of the layers are not fully understood yet and could represent continuous background dust activity in all summer months or just one dust storm in the spring of each LGM year. Presently, dust in desert storms often leave layers of 1 mm to 1 cm thickness on the ground (Sirocko and Raschke, 1993). Accordingly, one spring dust storm would be enough to explain the observed glacial stage aeolian lamination record.

Unexpectedly, the maar lake sediments do not document any clear response to North Atlantic Heinrich Event 1 (Fig. 2.21), which is thought to have caused extreme cold in Central Europe, because of the massive iceberg presence in the entire North Atlantic and

the resulting complete shutdown of the Meridional Overturning Circulation/ Gulf Stream system (Thornally et al., 2011). In contrast, the post-LGM conditions in the later part of LEZ 4 must have been quite stable until 14 700 b2k, when the Atlantic warmed abruptly. At this stage we cannot firmly assess whether the first grass pollen spread happened before or during that dramatic climatic change. This time interval is varve counted in DE3 but contains no pollen, whereas the core from Schalkenmehrener Maar clearly shows grass pollen in the glacial sediments, although the stratigraphy is problematic for this core. Archaeological evidence from the middle Rhine valley site of Gönnersdorf suggests that grasses grew even before 14 700 b2k (Terberger and Street, 2003; Street et al., 2012), which could place the first grass pollen in core SM3 from the Schalkenmehrener Maar (Sirocko et al., 2013) at 16 000 b2k in the polar desert landscape.

The laminations observed during LEZ 4 consist of only two clear components: bright coarse silt quartz layers and brown layers of fine silt (Fig. 2.15). Both layer types consist of well sorted quartz silt indicating that both layer types are of aeolian origin. Terrestrial plant remains are missing so that there is no clear seasonal variability apparent and these laminations cannot be regarded as classical varves, but still they will most certainly represent annual layers because the number of these dust layers match perfectly the time between the Laacher See Tephra and the GI 4. It is most likely that the fine dust layer presents continuous slow deflation during the snow-free summer season, and the coarser thick layer a large spring/ summer dust storm.

The late LEZ 4 revealed an average of 1.8 flood events per 1000 years and the biggest events were documented at about 15 300, 16 200 and 17 400 b2k, most probably associated with sporadic snow fall/ melt events during the Heinrich 1 interval (Brunck et al., 2016). The Last Glacial Maximum itself shows no flood events (Fig. 2.21) so that it must have been extremely dry during all seasons of peak glacial conditions.

LEZ 5 The tundra of the early MIS 2 (28 500 – 23 000 b2k)

LEZ 5 represents the transition from the steppe/ temperate environments of MIS 3 to the MIS 2 glacial conditions. Pine and birch pollen has occasionally been identified, but only sporadically and at low abundance (Fig. 2.21). In contrast, Ranunculaceae seeds, moss fragments, fungi sclerotia (*Coenococcum geophilum*) and insect remains are the typical organic macroremains (Fig. 2.9) and indicate a tundra environment persisted during LEZ 5 (Fig. 2.21).

The sediment in AU2 shows yellowish aeolian silt laminae (typical of the LGM, LEZ 4), but in LEZ 5 the silt is intercalated with grey clay layers (Fig. 2.15). Thus, compared to the LGM (LEZ 4), runoff was active during LEZ 5; either caused by summer rain, or spring snowmelt. A similar depositional environment with alternation of clay and silt layers is also visible in DE3, which has no river inlet so that runoff caused erosion of the poorly vegetated tuff ring and influx of clay into the maar. LEZ 5 is a time of tundra vegetation and spanned the transition from the forested LEZ 6 to the sparse vegetation cover that dominated LEZ 4. Archaeologically, this time interval corresponds to the later Gravettien, when humans hunted reindeer and mammoth, an observation in accordance with the reconstruction of a tundra environment over the Eifel region.

The sediment laminations produced during LEZ 5 consist of two main components (Fig. 2.15). Well sorted layers with sand sized minerogenic components are certainly of aeolian origin (spring or summer), but the occurrence of clay layers indicates strong snowmelt events. Apparently, winter snowfall was at a maximum during the millennia when the northern continental ice sheet grew larger, but the North Atlantic sea surface temperatures were still high during GI 3 and 4 (Fig. 2.22).

LEZ 5 contains an average of 1.8 flood events per 1000 years with the biggest events documented at 23 500, 23 600 and 24 000 b2k, i.e. around the time of the Heinrich Event 2 (Fig. 2.22). The massive tephra layers produced by the Wartgesberg eruption at 27 500 b2k characterizes the LEZ 5/ 6 boundary (Fig. 2.21).

LEZ 6 The steppe of the middle and late MIS 3 (36 500 – 28 500 b2k)

Aeolian dust deposition was active at least during the latter part of LEZ 6, but not at the level of the LGM. The beginning of LEZ 6 is clearly associated with the spread of *Coenococcum* at around 36 500 b2k at a time when wood remains became scarce in the cores (Fig. 2.21). Charcoal is almost absent suggesting that trees were very scattered in the landscape and it was moist enough to prevent the grassland from intensive burning. *Ephippa* and *Coenococcum* sclerotia are typical of the earlier part of LEZ 6, whereas *Ranunculaceae* and insects are characteristic for the later part of LEZ 6, when trees were almost absent. The landscape at this time must thus have been a steppe with scattered trees and the occasional dust storm during a dry season.

Early LEZ 6 following GI 8 (38 000 b2k) is when the early modern humans spread into Central Europe, even if the oldest artifact (Venus statuette from Hohle Stein) is now

dated to 43 000 b2k (Conard et al., 2006, 2008; Nigst et al., 2014). These early modern humans hunted horse, reindeer and mammoth with the former taxa indicative of steppe vegetation and mammoth/ reindeer of a tundra environment. This hunting practice, documented archaeologically, matches the landscape almost exactly as reconstructed from the ELSA pollen, plant macroremains, and dust activity.

An important marker of the late LEZ 6 is the onset of continuous aeolian activity after 30 000 b2k (Fig. 2.21), which corresponds to Heinrich Event 3. At this time, the Scandinavian ice sheet must have moved southward to an extent that it affected atmospheric circulation over Central Europe (Mangerud, 2011). Dietrich and Seelos (2010) presented scenarios of changing wind speed and direction over the Eifel, most probably associated with the position/ height of the ice sheet and sea surface temperatures over the North Atlantic.

The classical Dutch MIS 3 records call the GI 3 – 5 time as the Denekamp interstadial, which saw the last phase of soil formation before the LGM in Central Europe (Whittington and Hall, 2002). The GI 3 and 4 forest is best observed in core DE2 pollen count data at 33 m (Fig. 2.7), where pine and birch reach a short-lived maximum, indicating the last forest phase before the climate deterioration toward the tundra environment that dominated LEZ 5.

The LEZ 6 steppe environment has seen an average of 4 flood events per 1000 years and the biggest events are at 30 200, 30 800, 31 100 b2k, i.e. during the transition from GI 5 to GI 4 (Fig. 2.21). These may reflect intense winter snowmelt events, but also infrequent summer rains cannot be excluded. The large Wartgesberg eruption and another eruption from an unknown site also characterize the late LEZ 6. Thick tephra layers (20 cm) must have covered the sparse steppe vegetation and probably impacted on the development of the vegetation as it changed to a tundra environment after the Wartgesberg eruption (Fig. 2.21). The sediment laminations produced during LEZ 6 consist of two or three layers, including minerogenic spring layers of mainly quartz, and autumn/ winter layers of fine silt and clay. Some laminations are characterized by orange-brown silt layers, which probably reflect soil formation processes. This observation could match the evidence from the soil profile at Schwalbenberg in the Rhine valley, which revealed for the first time that loess-palaeosoils developed during all MIS 3 interstadials, especially during early MIS 3 (Schirmer et al., 2012).

LEZ 7 The boreal forest of the middle MIS 3 (49 000 – 36 500 b2k)

LEZ 7 is dominated by grass, but with presence of pine and birch (Fig. 2.21). Spikes of high charcoal abundance are prominent so that vegetation burning must have impacted on the landscape occasionally. The pine forest must have been still dense enough to burn during times of inferred severe drought. The laminations of LEZ 7 consist of two layers: spring/ summer layers of quartz and dark autumn/ winter layer of fine detritus (Fig. 2.15). Charcoal is found in both layers indicating that burning was a common process in the taiga forests.

LEZ 7 displays an average of 0.8 flood event per 1000 years with the biggest events at 44 100, 44 300 and 44 500 b2k (Fig. 2.21). The flood events are concentrated over a short period of time and must have occurred when the boreal forest deteriorated, i.e. during a time of vegetation and soil change during the first pronounced stadial/ interstadial changes.

LEZ 7 experienced the very large eruption of the Dreiser Weiher (DWT) and the deposition of an unknown tephra (UT2) (Figs. 2.16 and 2.21), both of which comprise of more than 10 cm-thickness in all ELSA cores. These eruptions occurred in a boreal forest environment and mark the end of wood remains in the maar records. Again, the volcanic activity probably had an impact into the vegetation and can be responsible also for the abundant charcoal in LEZ 7.

LEZ 8 The spruce-hornbeam forest of early MIS 3 (55 000 – 49 000 b2k)

The period from 60 000 – 49 000 b2k is characterized by abundant spruce (*Picea*) (Fig. 2.21), but this *Picea*-Zone is divided into two phases, the upper one with two maxima of *Carpinus* (*Picea-Carpinus*-Zone). *Corylus*, *Ulmus*, *Quercus*, *Fraxinus*, *Tilia*, *Abies* and *Alnus* were also present during this warmest interval of MIS 3. The ice core tuning has assigned the two maxima of *Carpinus* to GI 13 and GI 14 respectively, and indeed, GI 14 is the longest interstadial event of the early MIS 3.

Two pieces of *Picea* wood were ¹⁴C dated to ca. 46 000 BP (uncalibrated) (Sirocko et al., 2013) and mark the very end of the zone with abundant *Picea*. A reliable calibration for such an old ¹⁴C age is impossible; the ice core tuning suggests an age of 49 000 b2k. The lake level must have lowered significantly at the end of LEZ 8 leading to reworking of coarse-grained sediment with wood fragments and their influx into the maar lakes. This strong climatic change is marked by a marked decrease in the C_{total} (Fig. 2.19), which can

at least partly be explained by extremely low sedimentation rates during the entire spruce dominated interval. The very small layer thickness could be a climatic signal, but it could also be caused by a principle change in the drainage pattern, if the maar was not connected to a stream at that time, but a solitary deep crater with anoxic bottom water. The occurrence of the thermophilous pollen however, cannot be explained by the drainage processes, in particular because exactly the same pollen profile is observed in the Dehner dry maar, which has not fluvial inflow at all.

The tuning places the initial development of the hornbeam forest at 55 000 b2k, i.e. at the beginning of GI 14 (Fig. 2.21). The recovery of needle leaf fragments in the sediments of the *Picea* zone indicates that also *Abies alba* grew in the catchment of the maar. Consequently the occurrence of the thermophilous taxa cannot be explained only by long distance transport. However, we cannot exclude the possibility that some of the pollen was derived from the nearby Mosel and Rhone valley (Fig. 2.1), which are today about 2 – 3 °C warmer in summer than at the elevation of the Eifel. If the stands in the Mosel, where wine is cultivated today, acted as local refuge during the MIS 4 cold phase, it appears likely that the reappearance of such taxa could have occurred rapidly as soon as temperature and moisture were sufficiently high. Accordingly, the Eifel environment could have been different from other sites in northern and southern Germany where MIS 4 refuge were more distant. In addition, the Eifel is 400 km further south of Oerel in Northern Germany, where *Picea* obviously did not grow, but only *Betula* and *Pinus* (Behre and Lade, 1986). Accordingly, the Eifel region was probably beyond the periglacial rim surrounding the MIS 4 ice sheet and under the influence of warm and moist winds from the southwest (Seelos et al., 2009) – whereas the vegetation at Oerel must have been under the immediate influence of the nearby continental ice sheet.

LEZ 9 The spruce forest of the very early MIS 3 (60 000 – 55 000 b2k)

GI 18 to GI 15 period in the maar lake records are also dominated by *Picea* with some *Ulmus* and *Quercus*, but in lower abundance (Figs. 2.20 and 2.21). The vegetation is thus similar to LEZ 8, but the absence of *Carpinus* is significant enough to delimit this interval as an individual LEZ. The begin of LEZ 9 at 60 000 b2k matches when stalagmites started to grow again in the Spannagel cave in the Alps, indicating high mean annual air temperatures and significant precipitation and water availability during the very early MIS 3 warming (Moseley et al., 2014). Summer insolation was as high as today in the

Northern Hemisphere, and the North Atlantic warming comparable to today (van Krevelend et al., 2004), and CO₂ levels only 10 ppm lower than during interglacial times (Fig. 2.22). Consequently, it is not surprising that we see a rather warm climate distal of the northern ice sheets (see further discussion below).

The laminations produced during both LEZ 8 and 9 are all extremely thin, consisting mainly of diatoms and almost no coarse-grained detrital components. Flood events are absent from the entire early part of core AU2 with high C_{total} content (Figs. 2.19 and 2.21). The thin laminations of LEZ 9 and 8 could be related to climate if it was indeed almost as warm as today. However, we cannot exclude that a fundamental change in the landscape structure appeared near to the maar, for example if the creek that feeds the maar still today got in contact with the maar basin only at the end of Picea Zones.

LEZ 10 The MIS 4 – MIS 3 transition

Sediments below the Picea Zones have low organic carbon content and show only birch, pine and grass pollen, which indicate a boreal forest environment during the time when the Auel and Dehner maar structures erupted. Apparently, the Dehner maar structure is a little older than Auel, because it reveals the Leucite Tephra (LCT) in the lowermost lake sediments (Förster and Sirocko, 2016).

2.6.2 Evidence for a warm early MIS 3 (49 000 – 60 000 b2k)

Terrestrial records of climate and vegetation history in Central Europe during MIS 3 and MIS 2 are few because of a lack of suitable lakes to provide the necessary sedimentary basins (Helmens, 2014). Lakes in northern Europe and the Alps are generally formed by glacial processes either at the end of MIS 6 or MIS 2 and consequently mainly contain sediments deposited during the subsequent interglacials MIS 5e or MIS 1. Accordingly, Eemian and Holocene palaeoclimate records are numerous across Europe. In addition, such glacial lakes are mostly not very deep and rapidly infilled with sediments. Lakes of other origin that might have contained MIS 3 records were overridden by the maximum glacier extent during MIS 2 and therefore not preserved.

A few sedimentary basins survived the MIS 2 glacier advance in northern Germany, however only inside the area glaciated during MIS 6, but outside the glaciated area during MIS 2. Best known are the classical sites of Oerel (Behre and Lade, 1986), Rederstall (Menke and Tynni, 1984) or Gröbern (Litt et al., 1996). Gross Todtshorn may be the only

site in northern Germany to cover most of MIS 3 (Caspers and Freund, 2001), but the lake was situated in a colder environment than the Eifel.

In particular, the site at Oerel is known for the temperate Oerel interstadial with birch and pine trees at around 55 000 b2k (Behre and Lade, 1986). Even some pollen of *Quercus* were reported, but they are regarded as representing long distance transport from the south. A number of other dated MIS 3 records come from the Netherlands (e.g. Kasse et al., 1995; Vandenberghe 1992a, 1992b; Zagwijn, 1974, 1996) or East Germany (e.g. Mania and Stechemesser, 1970; Eissmann, 1981; Litt et al., 1996; Mol, 1997). Some of these are fluvial deposits, which contain sections of interstadials as peat deposits or in-fills of small local lakes (often oxbows) in the river alluvial plain.

The general palaeo-temperatures and overall climate dynamics of MIS 3 cold and warm phases have also already been reconstructed (Huijzer and Vandenberghe, 1998; Fletcher et al., 2010; van Meerbeek et al., 2011; Helmens, 2014). Profiles with several MIS 3 interstadials were reported for Aschersleben in the Harz area (Mania and Stechemesser, 1970), Nussloch east of the Upper Rhine (Antoine et al., 2001) and Schwalbenberg in the Middle Rhine area (Schirmer, 2012).

The correlation of these records from these different sites across central Europe is however difficult, because they all show pine and birch if they contain pollen, but there is no specific assemblage characteristic for a distinct interstadial (Fletcher et al., 2010). An interpretation for this observations becomes plausible when the pollen in the DE3 core are evaluated on the basis of pollen counts (Fig. 2.7). Spikes become visible, that could be interpreted in a way that the community of trees did not change between stadials and interstadials, but only the total abundance of trees. *Betula*, *Pinus*, and to some extent *Ulmus* and *Picea*, show maxima in their absolute numbers during the interstadials (Figs. 2.7 and 2.21). However, these maxima cannot be correlated to the classical Dutch interstadial succession, because the exact age and the succession of the interstadials Oerel, Glinde, Hengelo, Moorshöft and Denekamp are still not fully consistent between different authors. Some studies even shift the Brörup interstadial, which is in most papers attributed to MIS 5a/ GI 21 (Caspers and Freund, 2001; Reille and de Beaulieu, 1990; Woillard and Mook, 1982) or the Dürnten interstadial (mostly attributed to GI 20 or 19 (Welten, 1982; Müller, 2001) into early MIS 3 (e.g. Leroy et al., 1996). Fortunately, the order of interstadials is given in some French records, namely Grande Pile (Woillard, 1978) and

Velay (Kukla et al., 2002), but best resolved in the lake sediment records of Les Echets (de Beaulieu and Reille, 1989), which was reinvestigated following a multi-proxy approach with an updated chronology (Wohlfarth et al., 2008). For Les Echets, it has been shown that the lake responded sensitively to past environmental forcings, with both MIS 3 interstadial – stadial events clearly recognizable in the trends of organic content (Veres et al., 2008, 2009) that in turn matched the lake internal productivity and arboreal/ non-arboreal pollen trends (Wohlfarth et al., 2008). Moreover, two intervals of high organic content dated to early MIS 3 (Veres et al., 2008, 2009) also document the presence of spruce pollen (de Beaulieu and Reille, 1989), further supporting assertions that the early MIS 3 LEZ in the Eifel sensitively capture a regional signal of environmental change that also characterize the Alpine forelands (see also Heiri et al., 2014). Other high-resolution records of MIS 3 vegetation come from Italy, e.g., Lago Vico (Leroy et al., 1996) and Monticchio (Allen et al., 2000) but these sites near Rome and Naples respectively present the Mediterranean plant assemblages, which cannot be easily compared to the floral zones north of the Alps.

The general hemispheric boundary conditions during the early MIS 3 favour a warm summer climate in Central Europe. Summer insolation was higher than today, whilst atmospheric CO₂ and CH₄ were on the level of the early Holocene (Fig. 2.22). The Gulf Stream – North Atlantic drift reached to the southern tip of Norway (Kuipers et al., 1998) and sea surface temperatures in the North Atlantic were only 2 °C lower than today (van Kreveld et al., 2004). Ice sheet reconstructions for the middle MIS 3 show a small ice sheet covering only little parts of the Norwegian mountain ranges (Mangerud et al., 2011; Wohlfarth, 2008). Sea level was about 60 m lower than today and parts of the current North Sea and Baltic Sea were not submerged (Siddall et al., 2003).

Accordingly, the general climate forcing conditions during the early MIS 3 were not so very different from parts of the Holocene. The mean summer temperatures today in the Eifel are at 17 °C, and 19 °C in the Mosel and Rhine valleys. The plant macrofossils indicate that the early MIS 3 summer temperatures during LEZ 8 were near 15 – 16 °C, thus 2 – 3 °C lower than today.

Two grey forest soils in the loess around the Upper Rhine-Graben were described and named Gräselberger Boden 1 and 2 (Antoine et al., 2001; Bibus et al., 2007). Based on luminescence dating and relative palaeosol stratigraphy they were assigned to early MIS 3.

These soils are below the younger Lohne soil, which indicated a tundra environment with sparse trees, the only indicators of a pine-dominated forest in the loess landscape of Western Europe (Zech et al., 2012).

Consequently, it is possible that such conditions can allow the development of a *Picea* forest with abundant thermophile broadleaf taxa, in particular during the long interstadials GI 13 and GI 14, when temperatures in the Greenland NEEM record were up to 15 °C warmer than during the MIS 3 stadial phases (Rasmussen et al., 2014).

Other *Picea* forests have been dated to this time-interval on the Switzerland site of Gossau (Preusser et al., 2003). It appears that quite a number of records in France, Switzerland, the Eifel and even England show the environmental impact of a generally warm phase spanning GI 17 to GI 13, with duration of about 14 000 years.

The concept of a warm early MIS 3 in NW Europe is not new. Coope et al., (1998) investigated fossil beetle assemblages in English peat bogs and suggested that temperatures during this time-interval were only a few degrees below modern values, although there was no forest at this time in England. Quite likely, the forests from which the beetles spread were further to the east, most probably the Atlantic forests along the coast of France (Sanchez Goñi et al., 2013), where the forest community became increasingly dominated by *Picea* – similar to the forest in the Eifel during early MIS 3 (GI 17 to GI 12).

The ELSA core from the Oberwinkler Maar presents another line of evidence for a warm middle MIS 3. Here the sediments contain abundant chironomid remains, which included species that live in southern Scandinavia where summer temperatures are today ~ 14 °C (Engels et al., 2008).

The most compelling evidence for a warm early MIS 3 is the growth of speleothems in the Alps and in a cave of the Sauerland (D. Scholz, pers. comm.), just 150 km away from the Eifel. Speleothems grew from 56 000 to 47 000 b2k even at the elevation of the modern snowline in the Alps (Spötl and Mangini, 2007; Moseley et al., 2014). Accordingly, the early MIS 3, which we call LEZ 8 in the ELSA records, has a high summer insolation forcing at a time of high North Atlantic sea surface temperatures and small Skandinavian ice sheet extent; a climatic situation which favours the development of a spruce forest and allows even for thermophilous trees in well suited stands as the Moselle and Rhine from where the trees can spread fast into the nearby Eifel.

2.7 Summary and Conclusions

The ELSA core repository at Mainz now hosts 2700 m of laminated lake sediment, dated by 8 different methods, including 369 ^{14}C ages (Sirocko et al., 2013). The core HM1 from the Holzmaar (0 – 12 900 b2k) and core DE3 from the Dehner dry maar (12 900 – 32 000 b2k) have annual-resolution chronologies developed from varve counting. Core AU2 from the Auel dry maar is event-layer-laminated, because it is fed by a large stream and has the highest sedimentation rate of all extant and infilled Eifel maar lakes. It is tied tephrochronologically to the other MIS 3 ELSA cores by five tephra marker layers (Förster and Sirocko, 2016). Pollen and plant macrofossils from Dehner and Auel maar structures are used to build the ELSA palaeovegetation stack.

Core AU2 was sampled at 500 year intervals for pollen and macrofossils and at 100 year resolution for total carbon. The C_{total} record reveals the succession of all MIS 3 interstadials from the Laacher See Tephra back to 60 000 b2k allowing precise tuning to the Greenland ice core chronology. This age model was used to define the boundaries of Landscape Evolution Zone (LEZ) for the last 60 000 years in Central Europe.

LEZ 1 (0 – 6000 b2k): Forest with settlements and regional clearings for cattle and cereal farming.

LEZ 2 (6000 – 10 500 b2k): Natural broadleaf forest of the early Holocene climatic optimum with widespread thermophilous trees.

LEZ 3 (10 500 – 14 700 b2k): Boreal forest with cooler and warmer phases, volcanic activity.

LEZ 4 (14 700 – 23 000 b2k): Glacial desert with moss, some grass and submerged characea; annual dust activity, inter punctuated by short phases of tundra most likely during GI 2.

LEZ 5 (23 000 – 28 500 b2k): Tundra with abundant Ranunculaceae seeds, insect remains and fungal spores (Coenococcum). Dust activity almost every year.

LEZ 6 (28 500 – 36 500 b2k): Steppe with grass, pine, birch and fungal spores. Increases in the amount of pollen from pine and birch during interstadials, the last dense boreal forest around 30 000 b2k. Complete disappearance of all vegetation during stadials. Dust storms in 2 of 3 years. Volcanic activity during the final millennia of this LEZ. Spread of anatomically modern humans in the increasingly

open landscape, where horse, reindeer and mammoth, the favoured hunting preys, must have been abundant.

LEZ 7 (36 500 – 49 000 b2k): Boreal forest of pine, birch and few spruce, little dust activity. Charcoal indicates drought stress and frequent forest fires, volcanic activity.

LEZ 8 (49 000 – 55 000 b2k): Spruce and hornbeam forest with thermophilous trees.

LEZ 9 (55 000 – 60 000 b2k): Spruce forest.

LEZ 10 (older than 60 000 b2k): Intense volcanic activity at the end of MIS 4 in a fast changing environment of boreal forest.

2.8 Acknowledgements

We are very grateful to the “Stiftung Rheinland-Pfalz for Innovation”, who financed this study.

Chapter 3

Defining transport processes of the clastic sand fraction in lake sediments by rapid Camsizer[®] analysis

C. Adams¹, M. Röhner¹, H. Brunck¹, F. Sirocko¹

(1) Institute for Geosciences, Johannes Gutenberg-University, 55128 Mainz, Germany

A slightly modified version of this chapter has been submitted to “The Depositional Record”.

3.1 Abstract

Lake sediments are an important archive to understand and reconstruct the climate and environment of the past. A classical source of information is the grain size composition of the clastic fraction, which is controlled by fluvial and aeolian input. In addition, suspensions are generated by wave activity during ephemeral storms and redeposition occurs from the underwater slopes into the basin depth (turbidites and slumps). All these processes add to the mixture of clastic grains deposited in the lake basin. This background sedimentation is difficult to analyse, since its individual features lie mostly in the clay and silt fraction and form complex grain size mixtures.

All transport processes include at least some grains in the sand fraction, which are studied in detail for several maar lakes in the Eifel. These deep anoxic lakes with laminated sediments have the advantage that event layers can be analysed in discrete samples. This analysis has been done with a Retsch Camsizer[®] for the sand and gravel fraction. The coarse grain fractions have been photographed with the Extended Focal Imaging method to detect the texture of the rounded, frosted and pitted grain surfaces. The mode/ bimodality

of the sand fraction together with the grain symmetry and sphericity allows to detect organic particles and characterizes the aeolian, fluvial and limnic transport processes. The Camsizer[®] analyses are fast with low cost and provide a new tool to analyse lake sediments for palaeoclimatic and palaeoenvironmental reconstruction in high resolution – in combination with microscopic photos of the grain surface a very robust method to understand sedimentation processes in lakes.

3.2 Introduction

Grain size analysis can be performed by various techniques that differ in their applicability, technology and affordability. Settling devices are based on Stokes Law and are the standard procedure to analyse the clay and silt fraction. Wet or dry sieving is still the method of choice to analyse the sand and gravel fraction. Sieving can be performed manually or by machine shaking, usually in the particle range above 63 μm . Both procedures are sluggish, time-consuming and subject to many errors. Sieving according to the DIN is done in Phi Steps, which results in well reproducible grain size curves, but not with a high enough resolution for the discrimination of the transport processes in the sand fraction. For this reason, we examine the distribution of sediment particles as well as their shape parameters with the Retsch Camsizer[®] (Retsch Technology GmbH (Haan) and Jenoptik AG (Jena) in Germany; <http://www.retsch.com>). This tool allows the analysis of the sand fraction in $\frac{1}{5} \Phi$ steps, which is sufficient to study the coarse sand fraction in detail for conclusions about the transport processes. The $\frac{1}{5} \Phi$ grain size curve is combined with shape parameters and a photo analysis of the sand grain surface textures (rounding index, pitted, frosted surface) under the microscope. Finally, we define the key parameters for a distinct event allocation. Based on these approaches we present a new methodology to measure lake sediment grain size as a valuable tool in research of palaeoclimate and palaeoenvironment.

3.3 Material

We include in this study fluvial samples from the river Rhine and loess samples from the flanks of the Rhine, and compare them with lake sediments from the Eifel/ Germany (Sirocko et al., 2013; Sirocko et al., 2016), in particular flood layers (Brunck et al., 2016 and 2017) and Tephra layers (Förster and Sirocko, 2016).

Four sediment cores are used for the analysis with the Camsizer[®]: dry maar Auel (AU2), Dehner dry maar (DE3), dry maar Hoher List (HL2) and Holzmaar (HM1). Initially, several sediment samples from each core in zones with a normal sedimentation regime were analysed. The measured samples show very high clay and silt contents (98 – 99 %) and have a distinct peak in the fine grain size fraction with a steep and continuous decline. The median grain size lies between 0.09 and 0.25 mm. This so-called background sedimentation is omnipresent in maar lakes and always active. Every maar lake shows its own individual background sedimentation, depending on catchment area, maar depth and diameter. Representative for event layers is thus a combination of maar specific background sedimentation with superimposed event deposits. Subsequently, samples of different events and varying climatic conditions were analysed.

3.4 Methods

3.4.1 Retsch Camsizer[®]

The Camsizer[®] is a compact opto-electronic instrument for the simultaneous measurement of particle size distribution and particle shape of incoherent materials in the range of 30 µm to 30 mm, based on digital image processing. This technique provides a wide variety of information about the sample, from a general size measurement, to an evaluation of shape parameters, which can be closely correlated to specific performance characteristics. With this device, the possibility to define up to 50 grain size classes is given, which makes the measurements more suitable to identify narrow bi- or multimodal distributions, or slight coarsening or fining trends, than the sieving method. The greatest advance of this method lies in the reduced timespan, necessary for the analysis of each sample. The measuring time of sediments with the Camsizer[®] depends on particle number and size and totals to approximately 2 to 10 minutes per sample. The Camsizer[®] has been constructed for process and quality control over industrial processes and is used for example, to evaluate the fraction of broken specimen (e.g., glass spheres) during industrial production, as well as for scientific purposes. Scientifically, this device was previously applied in studies of various sediments, such as tsunami and storm surge washover deposits (e.g., Moore et al., 2007; Moore et al., 2011; Phantuwongraj et al., 2013), tephra material (Andronico et al., 2014; Andronico et al., 2015; Yu et al., 2013), in mineralogy (Dill et al., 2009), and even for the comparison with martian sediments (Cornwall et al., 2015). Although this instrument is becoming very common in industry for quality control,

research and production monitoring of very different kinds of materials, it was so far never been applied to analyse lake sediments. Here, we present a new methodology to characterise clastic sediment facies at lake sediments with the Camsizer[®]. The aim of this study is to determine, if and how the varying sedimentation conditions in a maar lake and fluvial environment can be distinguished and assigned to special climatic conditions as well as to different event types.



Fig. 3.1: Camsizer[®] device with sediment funnel and feeding channel on top left.

The Camsizer[®] measures the grain size range from 0.0625 – 3 mm; accordingly, the bulk sample has to be sieved at 63 μm . We used wet sieving to remove also small particles agglutinated to larger grains. This approach has the advantage to remove the entire clay fraction which otherwise would agglutinate the sand grains during the drying of the sample. The dry sample is then fed in from a vibrating feed channel that controls particles falling through the measurement field, where images of the particle flow are recorded by two digital cameras (basic and zoom) with different resolutions (Retsch Technology, 2010) (Fig. 3.1). As soon as the measuring process starts, the material passes a vibrating feeder and is conveyed into the detection-zone. Here, the single grains fall into the device and are

illuminated by strobe light (30 Hz). The projection of every grain on frosted glass is photographed by the two digital cameras, which leads to the fact that 60 images per second are taken. The feeder adjusts its vibration frequency automatically. This prevents the particles from falling too dense into the detection zone and to appear, by overlapping, as coarser, more deviant shaped particles, than really present.

The basic camera (Fig. 3.2) provides the analysis of the larger particles, while the zoom camera focuses on smaller particles furnishing high resolution images of the finer classes of the wide measuring range (Retsch Technology, 2010). Software created by Retsch Technology enables processing digital images and providing grain size and shape parameters. Although this instrument is becoming very common in industry for quality control, research and production monitoring of very different kinds of materials, it has, so far never been used for maar sediments. To obtain statistical relevance, the samples were taken to limit the measuring time to 2 – 10 minutes, which means around one million particles were measured. Dependent on the prevailing grain size, each sample size resulted in ca. 5 – 30 g of sediment. The fraction $< 63 \mu\text{m}$ of all samples was removed by wet-sieving, subsequently the samples, dried at $50 \text{ }^\circ\text{C}$, were measured with the Camsizer[®] to obtain grain size distributions, shape- and statistical parameters.

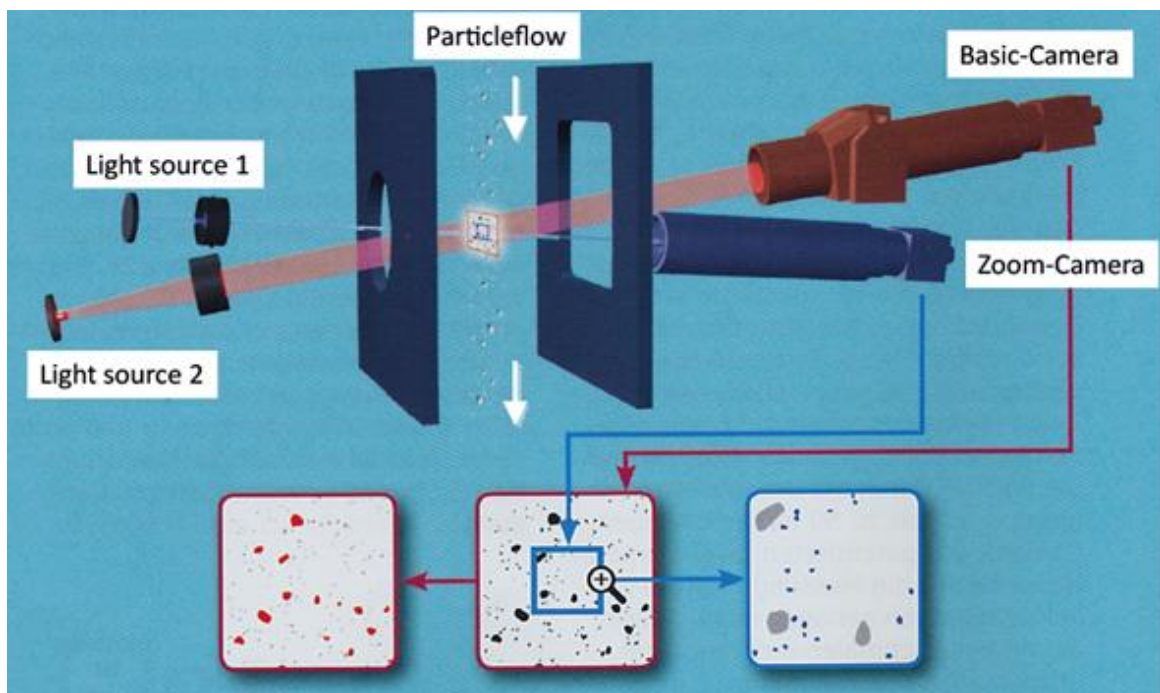


Fig. 3.2: Particle flow and detecting process in the Camsizer[®] with basic (red) and zoom camera (blue) (modified after Retsch Technology, 2011).

Finally, the coarse grain fraction of all samples were multifocal photographed with the imaging software cell^D. For the display of the histograms, the grain size classes were defined in $\frac{1}{5} \Phi$ width from 0.0625 to 32.0 mm. This leads to a broad possibility in the interpretation of grain size-distributions, since narrow bimodal distributions as well as sediment modes in long fine or coarse tails are better identifiable and distinguishable. The shape parameters sphericity, symmetry, breadth/ length-ratio and convexity were calculated by the Camsizer[®] software (version 4.4.19.418).

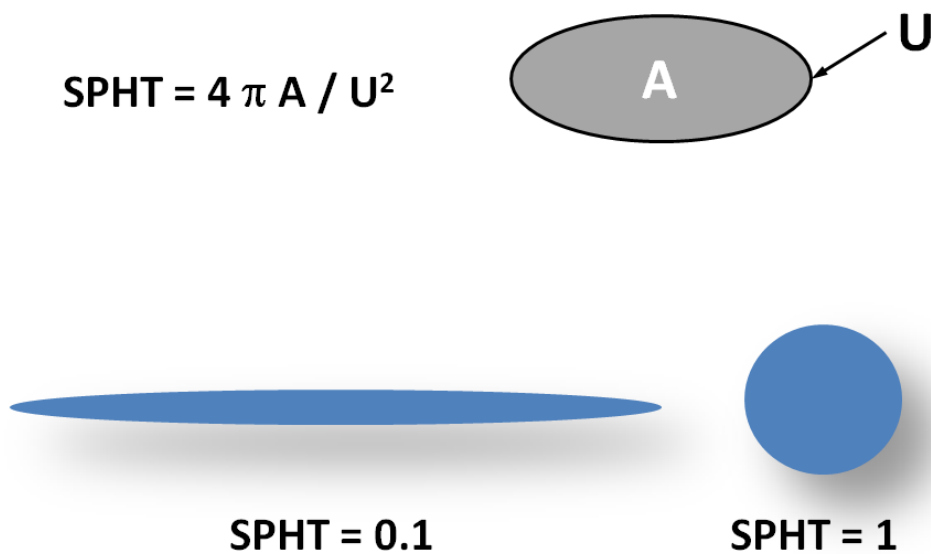


Fig. 3.3: Illustration of the shape parameter sphericity (SPHT).

The sphericity (SPHT) shows, to which extent the shape of a particle differs from the ideal sphere's shape (Fig. 3.3). It is calculated as shown in Fig. 3.3, whereby **A** represents the measured area of the particle projection and **U** the circumference of the particle projection (Retsch Technology, 2010). The symmetry (Symm) of the particles is being calculated as the minimal ratio of the distances of the barycentre to the fringe of the area in the given measuring direction (Fig. 3.4). For asymmetric particles symm is < 1 , is the barycentre of the area outside of the particle ($\frac{r_1}{r_2} < 0$), the symmetry is > 0.5 (Retsch Technology, 2010). The breadth/ length-ratio is being calculated as quotient of the smallest measured chord through the barycentre of the projection area ($x_{c \text{ min}}$) and the largest Feret-diameter ($x_{Fe \text{ max}}$, largest distance of parallel tangents) of a measured number of x_{c-} and x_{Fe-} values (Fig. 3.5). The convexity is the square root of the ratio of the real area

to the convex area of the particle (Fig. 3.6). The mean grain size, the median, the sorting, the skewness and the kurtosis of the grain size distribution is calculated after the equations from Folk and Ward (1957) and Tucker (1996) (Tab. 3.1).

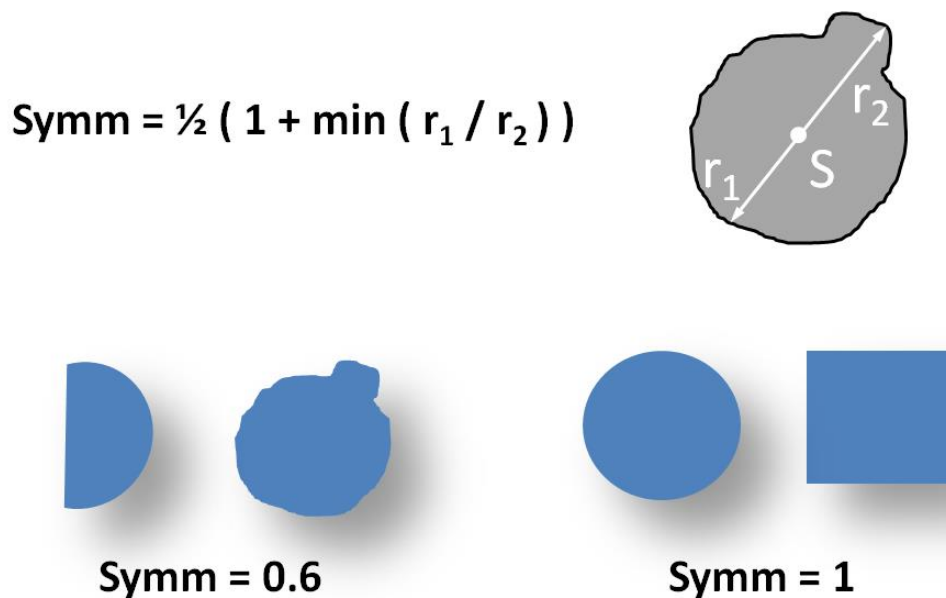


Fig. 3.4: Illustration of the shape parameter symmetry (Symm).

3.4.2 *Extended Focal Imaging microscopy*

Each sediment sample was photographed under the microscope (Olympus U-TTBI) with fourfold magnification and photographed with an Olympus Color View I camera. Since microscopes provide only a little depth of focus, objects should be as planar as possible to see most parts in the focal level and hence sharp. The Extended Focal Imaging method (EFI) enables to get images from three dimensional objects with virtually unlimited depth of sharpness, which highlights the surface of the single sediment grains. This leads to much better possibilities of any interpretation of the surface, mainly to detect frosted surfaces, which are typical for aeolian sand grains due to the saltation processes. To get such multifocal images, up to 48 photos of the object, each with a slightly different focus, were taken and blended together with the imaging software cell[^]D. In the resulting photograph every level is focused with a great depth of focus.

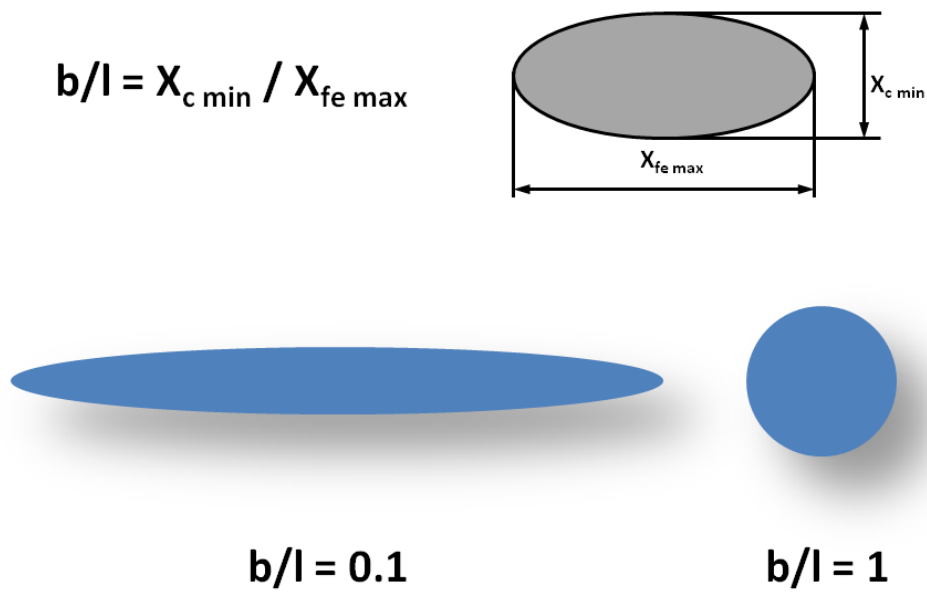


Fig. 3.5: Illustration of the shape parameter breadth/ length ratio ($\frac{b}{l}$).

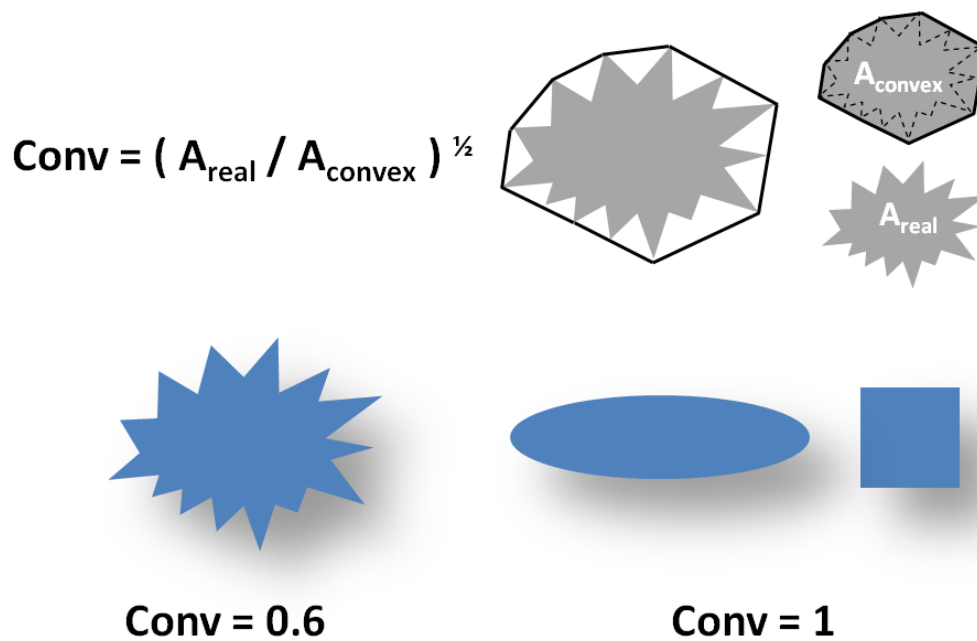


Fig. 3.6: Illustration of the shape parameter convexity (Conv).

$$\begin{aligned} \text{Median } M_d &= \Phi_{50} \\ \text{Mean } M_g &= (\Phi_{10} + \Phi_{20} + \Phi_{30} + \Phi_{40} + \Phi_{50} + \Phi_{60} + \Phi_{70} + \Phi_{80} + \Phi_{90}) / 9 \\ \text{Sorting } \sigma_1 &= ((\Phi_{16} - \Phi_{84}) / 4) + ((\Phi_5 - \Phi_{95}) / 6.6) \\ \text{Skewness } SK_1 &= (\Phi_{16} + \Phi_{84} - 2 \Phi_{50}) / (2 (\Phi_{84} - \Phi_{16})) + (\Phi_5 + \Phi_{95} - 2 \Phi_{50}) / (2 (\Phi_{95} - \Phi_5)) \\ \text{Kurtosis } K_G &= (\Phi_{95} - \Phi_5) / (2.44 (\Phi_{75} - \Phi_{25})) \end{aligned}$$

Tab. 3.1: Equations for mean grain size, the median, the sorting, the skewness and the kurtosis of the grain size distribution after Folk and Ward (1957) and Tucker (1996).

3.5 Results

3.5.1 Sample 1: HM1, depth 4.5 m/ Interglacial (Holocene at 3500 BP)

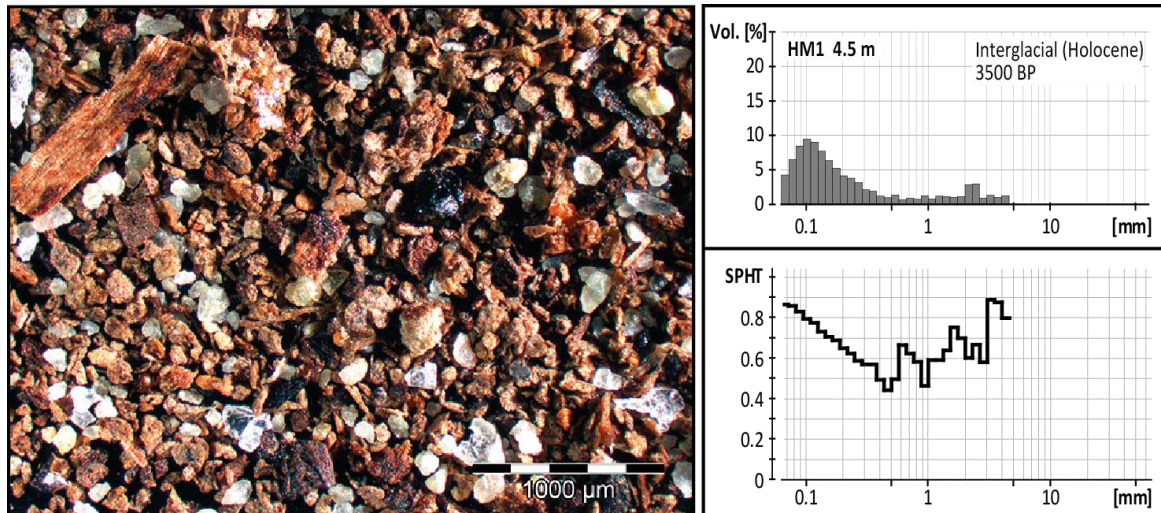


Fig. 3.7: Microscopic photo, grain size distribution and sphericity of Holocene interglacial sample from Holzmaar. The very high proportion of plant debris in the Holocene sample is conspicuous.

The sample HM1, depth 4.5 m from Holzmaar has an age of 3500 before present (BP) (Sirocko et al., 2013; Sirocko et al., 2016) and contains much plant detritus which adds to the clastic mode around 0.1 mm a coarse tail up to a grain size of approximately 4.5 mm (Fig. 3.7). The grain size distribution is defined by two processes: around the grain size of 0.1 mm the background sedimentation is dominant, while at larger grain sizes the discharge of organic particles completes the sample. The high sphericity values (Fig. 3.19, grey line) in the finest fractions can be interpreted as a result of aeolian and wave transport of the fine particles in an interglacial. Responsible for the broad coarse tail of this sample is a high content of plant detritus from the interglacial landscape. Due to the lower density

and the larger surface area compared against the volume of the plant detritus, as well as of the mica, they are transported farther into the centre of the maar lake and occur in this sample. The drastically decreasing sphericity with increasing grain size to a level below 0.4 at 0.4 mm can be interpreted as due to the high content of irregular shaped plant detritus. The increasing sphericity of particles with a larger grain size between 0.5 and 5 mm to values around 0.8 can be attributed to larger wood pieces that underwent abrasion and rounding during their transport, as well as plant seeds which often show naturally a spherical shape. For the interglacial and interstadial samples this pattern is relatively constant (Fig. 3.19). The shape parameter symmetry (Fig. 3.18) shows the same trend as the sphericity for this sample, only the variance is lower and the symmetry fluctuates between 0.9 and 0.7. The highest values were reached in the coarsest fractions above 2.5 mm.

3.5.2 Sample 2: HL2, depth 55.5 m/ Interglacial (Eemian at 120 000 BP)

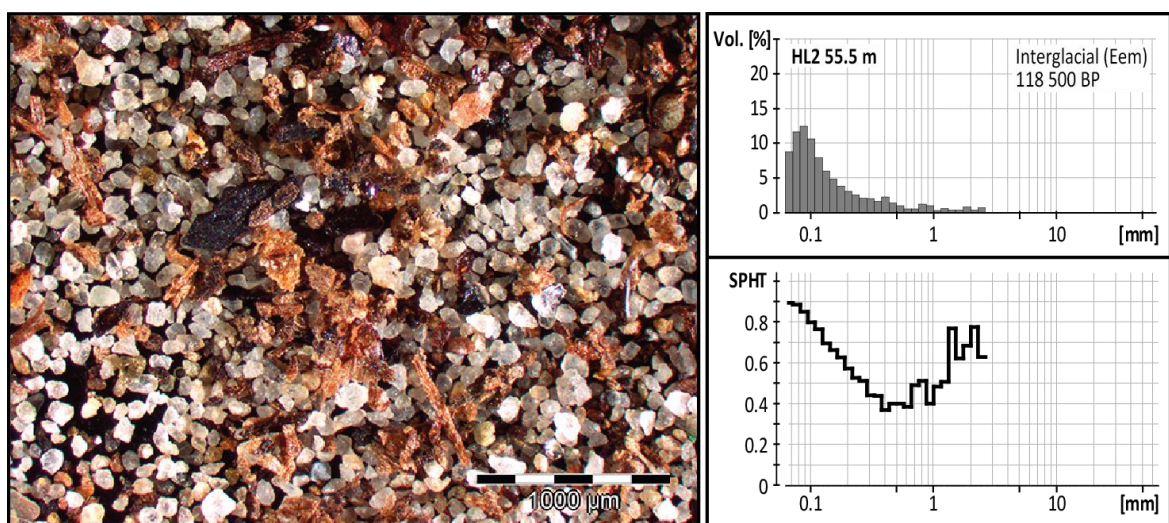


Fig. 3.8: Microscopic photo, grain size distribution and sphericity of Eemian interglacial sample from Maar westlich Hoher List. Once again, the Eemian sample is dominated by the high proportion of plant residues.

The sample is from Maar westlich Hoher List HL2, depth 55.5 m (120 000 BP – Sirocko et al., 2013) and shows very similar background sedimentation as sample 1; i.e., a mode of 0.09 mm and organic detritus with a grain size of around 2.5 mm (Fig. 3.8). As in sample 1 (Fig. 3.7), the background sedimentation is dominated by quartz grains and completed by a coarse tail rich in organic components. However, sample 2 contains less plant fragments compared to sample 1, which can be explained by the larger maar diameter

of westlich Hoher List. The shape parameters sphericity and symmetry (Figs. 3.19 and 3.18, grey and green line) are comparable to the Holocene sample 1 and show that the transport processes in the Eemian lake were similar to the Holocene lake. The pattern appears accordingly to be quite typical for interglacial samples in general – even in the centre of a lake with about 1 km diameter. Thus, interglacial sediments from the Holocene or the Eemian can be clearly detected with the Camsizer®.

3.5.3 *Sample 3: DE3, depth 23.15 m/ Glacial aeolian with coversand fraction (21 000 BP)*

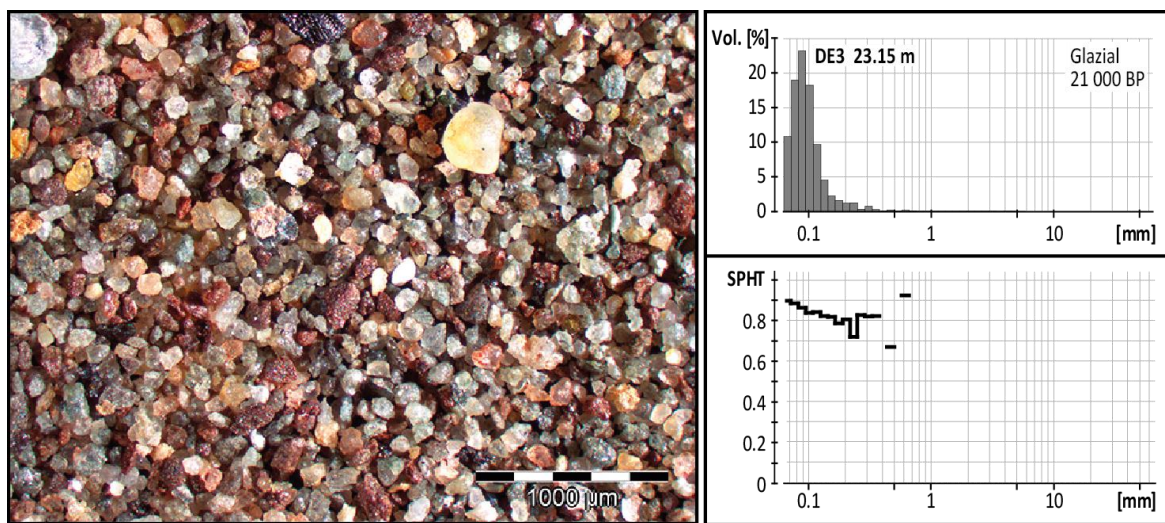


Fig. 3.9: Microscopic photo, grain size distribution and sphericity of glacial loess with an aeolian coversand fraction from Dehner dry maar.

Figure 3.9 shows a glacial sample from the Dehner dry maar. Grains larger than 0.7 mm are missing. Due to the absence of vegetation in a glacial, no organic particles can be deposited. This fact finds its expression in the lack of a coarse tail in the grain size distribution. The main mode of 0.09 mm appears well sorted (Sorting index: 0.42, Tab. 3.2). Only a small second mode in the medium sand fraction, which is detached from the finer mode, but also well sorted, is distinguishable. The composition of the sample is mainly quartz. Especially, larger quartz grains show a frosted surface indicating aeolian transport (Fig 3.10, top left). The deposits of the background sedimentation and the aeolian transport overlap in this sample, due to similar grain size ranges of the two processes. However, the background sedimentation quantity is comparably little, since the main sediment transport in a glacial period is of aeolian origin and the Dehner dry maar has no tributaries. The bimodality allows the determination of the coversand proportion

independently from the loess background deposition, which could also be partly washed into the lake by wave action. If this approach is done parallel in the two cores from Auel (fluvial inlet) and Dehner dry maar (no inlet – only dust) one can separate the different aeolian and fluvial proportions. The changes in the silt and sand mode are probably the most robust proxies of dust/ flood in the maar sediments, in particular, because the roundness of the grain and its surface texture (opaque Quartz grains) are an unambiguous attribute of the aeolian transport. The high sphericity values (Fig. 3.19, dark blue line) in the finest, aeolian fractions undergo a less steep decrease than interstadial and interglacial samples with a high organic content or clastic sediment with a relative short transport path. The high symmetry values (Fig. 3.18, dark blue line) in the grain size fractions larger than 0.2 mm and the high sphericity around 0.6 mm indicate a long sediment transport. According to the fact, that in a maar lake environment only short transport distances due to the small catchment areas of the lakes and absent or short tributaries, occur, a considerable particle rounding only can take place during sediment transport in a glacial environment with a strong dust and sand storm activity. Sample 3 shows a typical glacial grain size distribution of aeolian origin.

3.5.4 Sample 4: DE3, depth 21.05 m/ Glacial aeolian loess (20 000 BP)

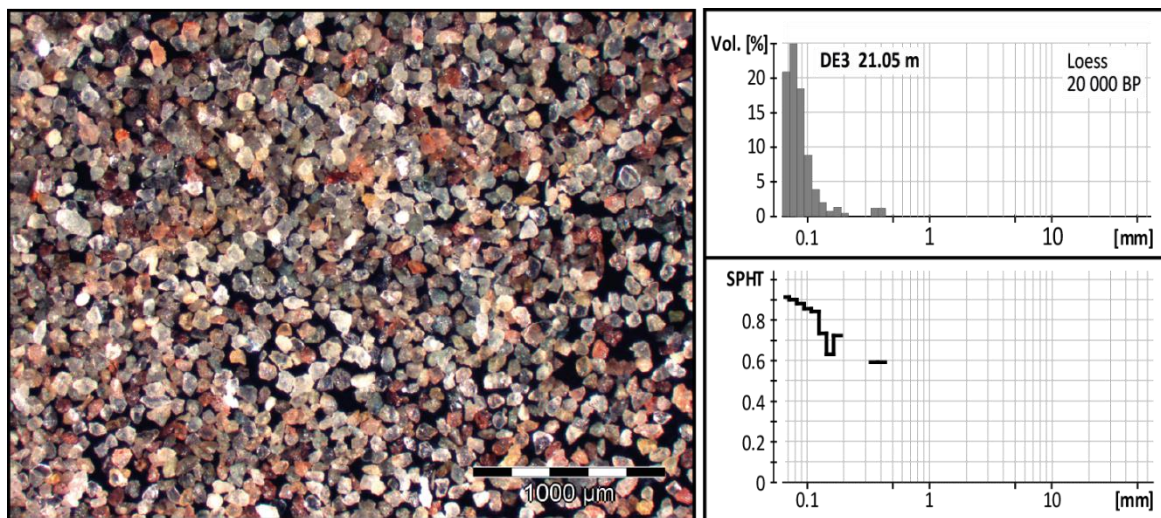


Fig. 3.10: Microscopic photo, grain size distribution and sphericity of glacial aeolian loess sample from Dehner dry maar.

Sample 4 consists mainly of very fine particles. Since the sediment has its mode in the silt fraction between 0.002 and 0.063 mm, which lies under the investigated size range, starting from 0.0625 mm upwards, in this sample only the coarse tail of the grain size

distribution is visible. The initial silt and clay content was very high and after wet sieving, the residue only makes ca. 0.5 wt.-% of the loess sample. The sample mainly consists of the fine, maar specific background sediment in combination with the coarse-grained loess particles in the finest fraction (Fig. 3.10). With a mode between 0.072 and 0.083 mm the sample shows the finest sediment as well as the highest sorting ($\sigma_1 = 0.37$, Tab. 3.1) of the maar lake samples. The sphericity of the finest two fractions is the highest of the samples (Fig. 3.20, pink line) and represents the pure aeolian transport. To a grain size of 1.25 mm the shape parameters sphericity and symmetry show a slight to moderate decline, above this size a stronger one. The low values can be attributed to the mica content in this grain size, which points to a constant background sedimentation caused by wave erosion in the littoral zone. Though both values show the same trend for the background sedimentation as sample 3 does. However, sample 4 shows no aeolian transported sand grains in the fraction. This leads to the conclusion that the loess event, leading to the deposition of this sediment, was of much lower wind strength, but with more constant wind speeds over a longer period.

3.5.5 Sample 5: AU2, depth 11.62 m/ Flood layer (Riparian zone at 12 400 BP)

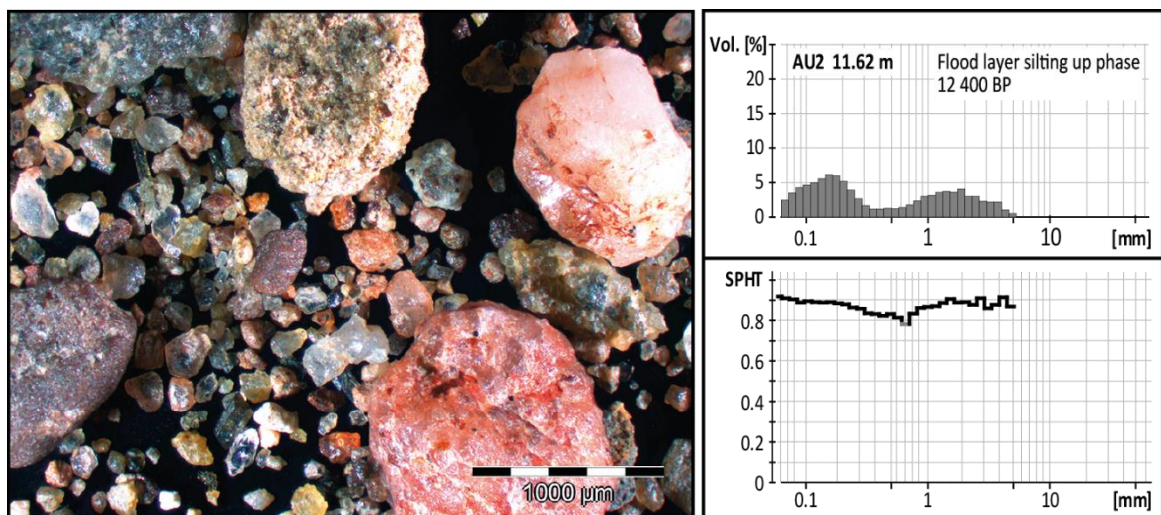


Fig. 3.11: Microscopic photo, grain size distribution and sphericity of a flood event from the riparian zone at Auel dry maar.

A flood event in the riparian zone with a bimodal distribution is represented by sample 5 (Brunck et al., 2016) (Fig. 3.11). In the silting up period the remaining maar centre lies closer to the zone where the material was transported into the lake. Additionally, the remaining depth of the lake is low. Hence, at strong discharge by a streamlet, a mixing of

rolling and suspensional transport is taking place. The main mode around 0.16 mm reflects a discharge at slower flow velocities of the streamlet. The maar specific background sedimentation around 0.07 and 0.08 mm only appears in a slight negative skewness of this mode. The second, coarser sediment mode around 2 mm contains mainly clastic material like sandstone and mineral grains (Fig. 3.11). This mode is generated by the main flood event with higher flow velocities and the large grain size confirms the small distance to the maar centre. The high sphericity values (Fig. 3.19, light blue line) in the finest fractions can be interpreted as caused by the background sedimentation, which is not clearly visible in the histogram. The sphericity values indicate that the background sedimentation mode still is in the same range around 0.09 mm. When viewing from fine to coarser sediment, the trend of the sphericity values clearly reflects the two sediment modes from the two sedimentation processes of the tributary streamlet, with increased sphericity values. The symmetry values (Fig. 3.18, light blue line) only show an increase with grain size up to 3 mm. This reflects the fact that larger particles are more prone to abrasion during transport and show a better rounding than the smaller ones.

3.5.6 Sample 6: AU2, depth 37.69 m/ Flood Layer (Deep maar at 28 000 BP)

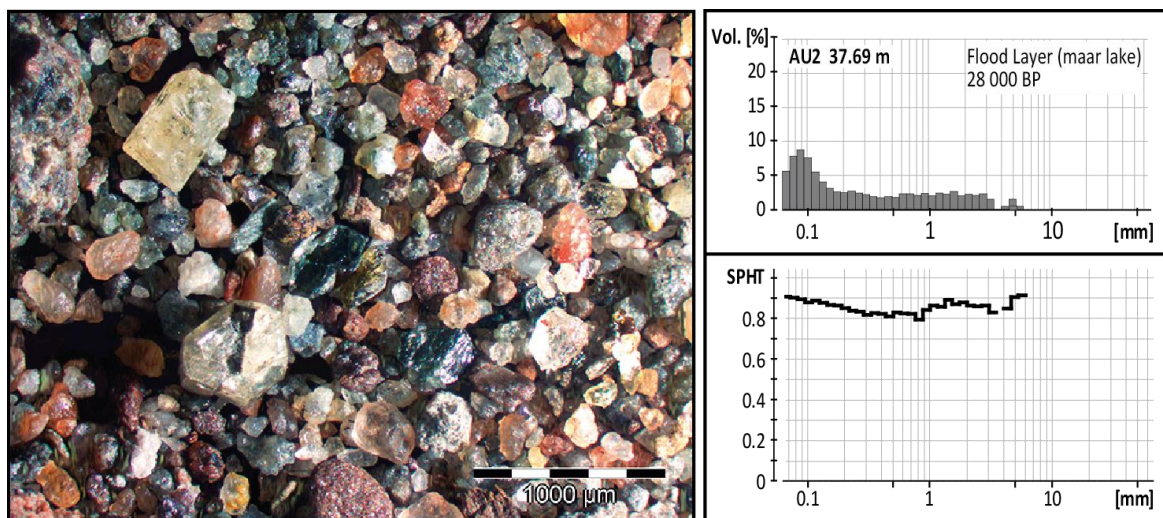


Fig. 3.12: Microscopic photo, grain size distribution and sphericity of interstadial flood sample from Auel dry maar.

Sample 6 from AU2, depth 37.69 m (Fig. 3.12) shows deposits of a prolonged flood-event over a couple of days (Brunck et al., 2016). The fine grain size classes are again marked by the regular background sedimentation, which shows a mode of around 0.09 mm. In contrast to the flood layers in the silting zone, the peak of the background

sedimentation seems to be shifted towards a lower grain size and is higher in percentage. This is explicable by the greater depth and the greater transport distance to the drilling point. In the maar centre the aeolian and wave transported background sedimentation dominates the transport from tributaries. The distribution of the coarser sediment with almost the same percentage (ca. 2.5 vol-%) in every grain size class is explainable by the repeated flood sedimentation over the time of a couple of days up to weeks. Every flood pulse shows a different maximum grain size due to the changing flow velocities, which interfere with each other. The closer the single peaks lie together and the more they are, the more similar the volume percentages of the different grain size classes are in the coarse part of the distribution. The sphericity (Fig. 3.19, yellow line) shows a similar pattern to the sphericity of the flood event from sample 4 (Fig. 3.19, light blue line). In the fractions between 0.13 and 0.8 mm the sphericity lies below the values of the sample from the maar margin. This indicates that not only the fluviually rounded particles from the tributary reached the maar centre, but due to precipitation larger particles from the maar vicinity were washed in. Figure 3.12 shows edgy crystals in this grain size range, which may have been washed out of the tuff ring around the maar lake.

3.5.7 Sample 7: HL2, depth 48.90 m/ Dümpelmaar Tephra (106 000 BP)

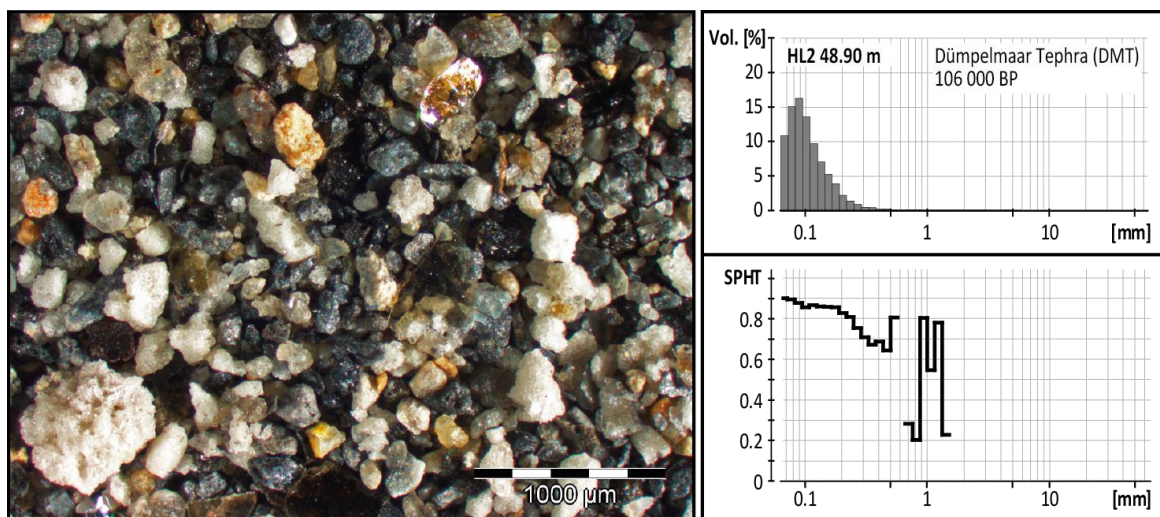


Fig. 3.13: Microscopic photo, grain size distribution and sphericity of tephra sample from Maar westlich Hoher List at 48.90 m depth.

Sample 7 was taken from the tephra layer of the Dümpelmaar Tephra (DMT) in the core of Maar westlich Hoher List. The histogram of the DMT (Fig. 3.13) shows the maar specific background sedimentation with a mode of 0.09 mm. There are no other sediment

modes and the sample appears quite similar to sample 3, a sample from the glacial. A distinction is only possible by taking the shape parameters or the volcanic mineral grains into account. The sample contains mineral grains like quartz, pyroxene, scoria, pumice and sanidine, as well as greyish sandstone from the substrate the diatreme erupted through. From the finest fraction with the highest sphericity value the same decrease (Fig. 3.19, brown line) as in the interglacial samples 1 and 2 is visible (Fig. 3.19, grey and green). The high sphericity values between 0.1 and 0.2 mm are a result of the aeolian transport of the tephra material and the rounding process in the eruption cloud or pyroclastic stream with a high sediment load, high flow velocities and relatively soft particles, and makes it clearly distinctive from similar looking distributions from temperate climates with only the maar specific background sedimentation peak and the coarser tail of decaying plant material. In this distribution the high sphericity values in the coarser fraction larger than 0.5 mm are not, like in samples from temperate climates, caused by well-rounded wood particles or plant seeds, but by larger pumice and scoria particles with a well-rounded shape. The tephra material is mixed with the maar specific background sedimentation. Nonetheless, the sample is dominated by aeolian transport. Single larger grains are attributed to density differences and their better transport properties, like exhibited by pumice and mica. In contrast to the glacial sample 3 with a likely grain size distribution (Fig. 3.9), the sphericity and symmetry values never reach the values of sample 3 (Fig. 3.19, dark blue line). This allows the distinction of local tephra material from the Eifel volcanoes from over long distance transported aeolian cover sand.

3.6 Discussion

Despite the same genetic origin each maar lake has an individual limnological character and sediment composition. This is caused by differences in size, depth, morphological setting, hydrological conditions and characteristics of the catchment area. For this reason, each maar structure or lake forms its own specific background sedimentation. The individual background sedimentation consists of the specific hydrological and aeolian input as well as the constantly present wave erosion in the littoral zone. Furthermore, differences between glacial and interglacial times are clearly visible in the sediment samples and attributed to the dominant transport processes. The analysis of the grain size in combination with the organic amount allows a clear climatic assignment. The grain size distribution of interglacial samples is mainly controlled by the presence of

biogenic remains, which can be easily detected by the symmetry and sphericity values of the coarse tail of the grain size distribution. Glacial sediment samples contain mainly clastic material and show a good sorting with high values in sphericity and especially symmetry due to the aeolian transport.

3.6.1 Rearrangement processes

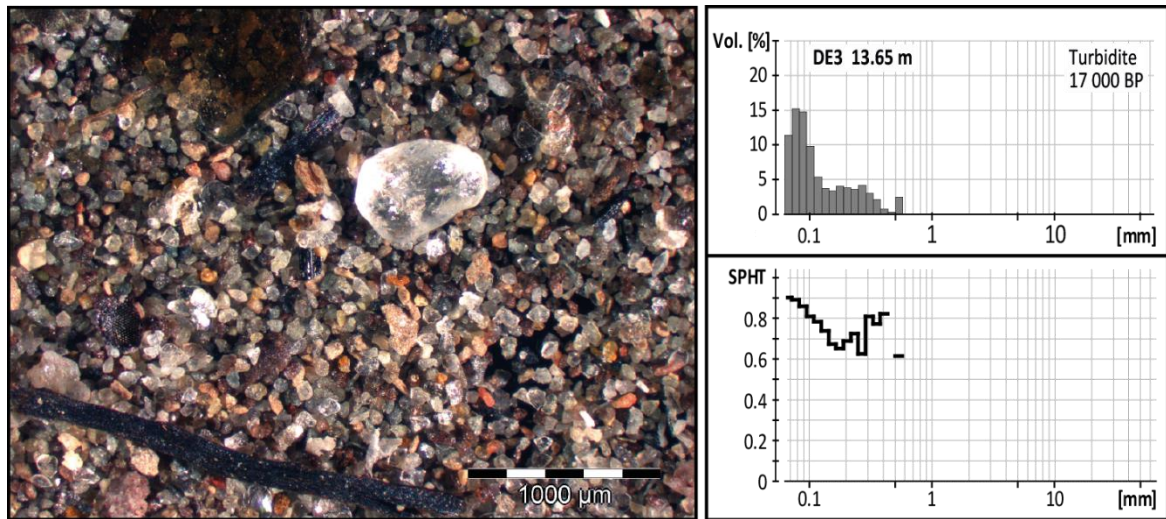


Fig. 3.14: Microscopic photo, grain size distribution and sphericity of turbidite sample from Dehner dry maar. The coarse fraction contains organic debris particles, as well as rounded quartz grains.

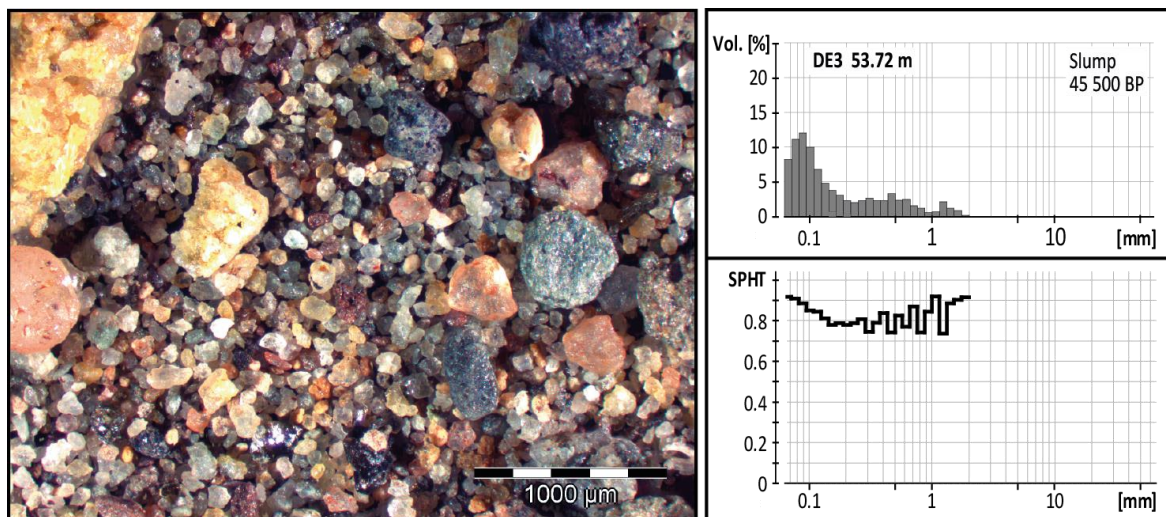


Fig. 3.15: Microscopic photo, grain size distribution and sphericity of slump sample from Dehner dry maar. Tephra particles combined with aeolian rounded quartz grains can be identified in the mineral composition.

Slumps and turbidites are lake-intern rearrangement events. Formerly deposited, unconsolidated material is transported by destabilization of the grains framework from the littoral zone as suspension flow or as slump gravitational to the lake bottom. The Camsizer[®] analysis of these sediments is problematic due to the fact that older sediment is reworked and deposited again elsewhere. Additionally, during the transport process other material can be embedded into the sediment. These factors lead to an unknown mixed sample, which, according to the initial material, shows divergent properties. Therefore, rearrangement processes allow only little conclusions about the climate and the transport processes and are to consider individually for each event. Figures 3.14 and 3.15 show exemplarily the grain size analysis of a turbidite and a slump event. The turbidite sample shows large organic debris particles, as well as rounded quartz grains. The former can be interpreted as a warm period tracer, the latter as a cold period one. Additionally, several insect and plant remains from the riparian zone are visible which were transported via rearrangement into the maar lake's centre. Both, the specific organic content and the conflicting indications of warm as well as cold period depositional conditions illustrate the alteration of the sediment during its transformational process. The sediments of the slump event show a wide grain size distribution with a moderate sorting. By accurate inspection of the mineral content, it appears that tephra particles (e.g., amphibole, pyroxene crystals) combined with aeolian components (rounded quartz grains) were deposited. This is another indication of the presence of a mixed sample from different depositional environments. Neither turbidite nor slump as rearrangement processes allow specific conclusions about the initial sediment including their transport processes. However, the rearrangement processes transport littoral zone material (e.g., insect and plant remains) into the maar center, wherefore these special particles are an indicator for slumps and turbidites.

3.6.2 *Riverine Sedimentation*

In contrast to the samples deposited in standing waters, river sediments contains a larger grain size spectrum due to the higher and more variable flow velocities. Figure 3.16 shows at first sight a striking reddish colour. This may be due to its age and the prevailing warmer and more humid climate (Cromerian) which leads to a different kind of weathering (lateritic/ saprolitic) as known from recent tropical and subtropical soils. The sample contains mainly quartz, showing red iron-rich crusts, rock fragments, chert, limestone and mineral grains like mica and feldspar due to the large and heterogeneous catchment area.

The single grains appear edgy and not well rounded, but rounded particles occur as well. The sphericity shows in the finest fractions a lower value of sphericity than the maar lake samples, due to the lack of the maar specific background sedimentation with a mode around 0.08 mm grain size. The sphericity shows its lowest values around 0.3 and 1 mm and two peaks appear at 1 – 2 mm and above 9 mm.

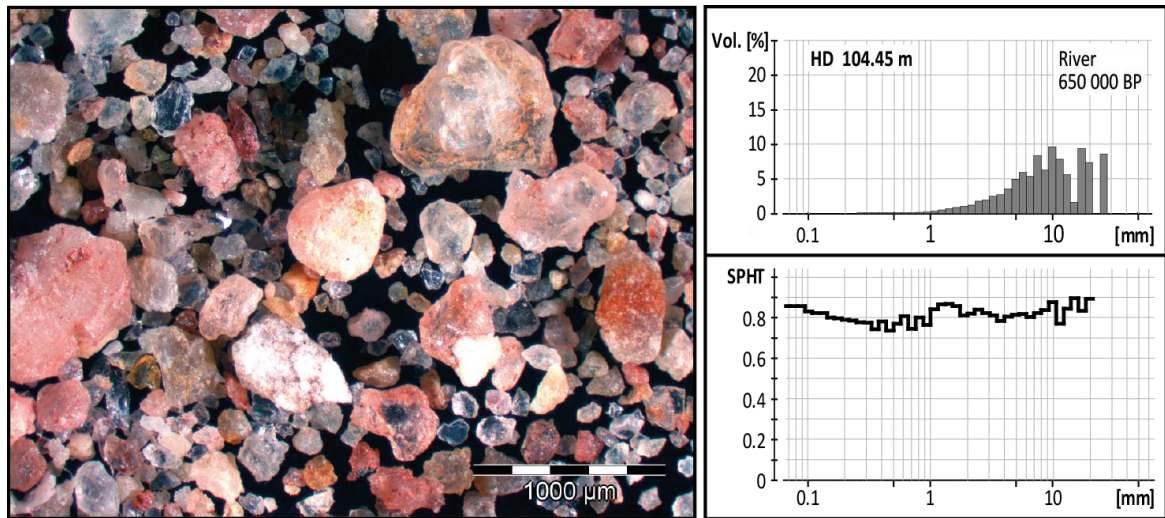


Fig. 3.16: Microscopic photo, grain size distribution and sphericity of a river sample from Heidelberg.

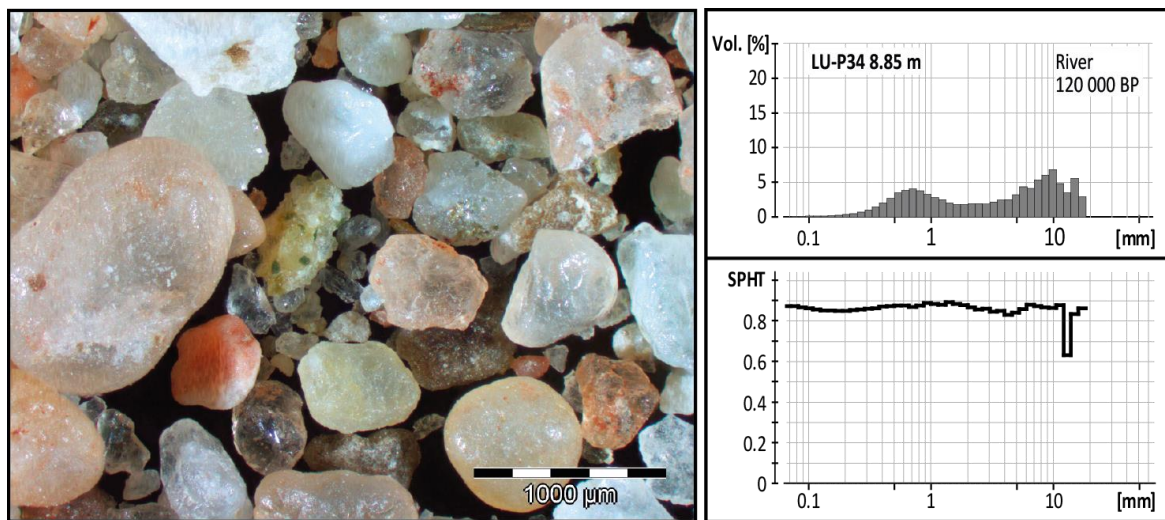


Fig. 3.17: Microscopic photo, grain size distribution and sphericity of a river sample from Ludwigshafen.

Figure 3.17 shows an edgy, chemically weathered appearance of many grains. The sample contains well-rounded quartz grains that were abraded during aeolian transport. A second mode at 0.7 mm represents aeolian sand being transported into the early river Rhine, forming bedforms like ripples and dunes, according to its grain size and the flow

velocity upon the coarse bedload sediment. Many of those formerly aeolian transported sand grains lost their matte surface during fluvial transport and appear now with a glossy surface, though still grains with a matte appearance occur. The sand fraction shows high values of sphericity (up to 0.9 as in sample 4 (Fig. 3.10) with sphericity values up to above 0.9), interpreted as the result of longer aeolian transport as coversand. The fact, that the loess sample 4 shows higher values in sphericity can be ascribed to the fact that a mixture of fresh aeolian particles, less spherical particles that underwent abrasion during their fluvial transport and the bedload sediment portion with a lower sphericity due to its only fluvial transport is present. In sample 3 and 4, the aeolian sand grains experienced no further fluvial transport and were deposited without changing shape parameters or surface texture in the low-energy environment of a stillwater maar lake. Both riverine samples are characterized by a negative skewed grain size distribution with a coarse sediment mode at 10 mm. The samples were deposited at the thalweg of a river with high flow velocities, thus fine sediment is washed out and only large particles, pebbles and cobbles were deposited.

In contrast to the fine maar lake sediments with comparable narrow modes, the sediments that passed through fluvial transport show, when sampled from the channel region, a much wider distribution. Whereas maar lake sediments have a mode of the maar specific background sedimentation in the very fine sand fraction, due to the low energy in this environment, fluvial sediments appear much coarser and the finest fraction is, according to the flow velocity, washed away.

3.6.3 *Descriptive statistics of sand fraction*

All samples show a strong positive skewness between 0.19 and 0.55 (Tab. 3.2). The sorting of the samples lies between 0.37 and 1.91. The glacial samples 3 and 4 are well sorted. The tephra sample 6 is moderately well sorted and the flood samples 4 and 5, as well as the interglacial samples 1 and 2 show a poor sorting. The kurtosis of the samples lies between 0.67 and 1.59. The flood samples 4 and 5 are of platykurtic appearance. The other samples show a leptokurtic distribution. The mean varies between 0.08 and 0.39 and the median between 0.08 and 0.25 (Tab. 3.2).

In Fig. 3.18 the symmetry is low in the two samples of interglacial climates (HM1 and HL2 (55.5 m), grey and light green line), especially in grain size classes between 0.09 and 0.5 mm. The fine fraction of sample HL2 (48.90 m, dark blue line) shows high symmetry

values in the fine fractions around to 0.3 mm. The samples AU2 (11.62 m, light blue line) and AU2 (37.69 m, yellow line) show over the whole distribution a relatively high value of the shape parameter sphericity. The highest values of symmetry show particles between 0.2 and 0.3 mm in sample DE3 (23 m, dark blue line). Sample DE3 (21.05 m, pink line) shows relatively high values in symmetry for the finest fractions up to 0.125 mm and a decline for coarser particles.

	HM1 4.5 m	HL2 55.5 m	DE3 23m	DE3 21.05 m	AU2 11.62 m	AU2 37.69 m	HL2 48.90 m
Skewness SK_1	0.55	0.46	0.21	0.20	0.35	0.45	0.19
Sorting (σ_1)	1.69	1.09	0.42	0.37	1.89	1.91	0.57
Kurtosis (K_G)	1.24	1.36	1.40	1.30	0.67	0.72	1.13
Mean M_0 [mm]	0.20	0.12	0.09	0.08	0.39	0.26	0.10
Median p_{50} [mm]	0.14	0.10	0.09	0.08	0.25	0.17	0.09

Tab. 3.2: Descriptive statistical parameters of the sand fraction in lake sediments.

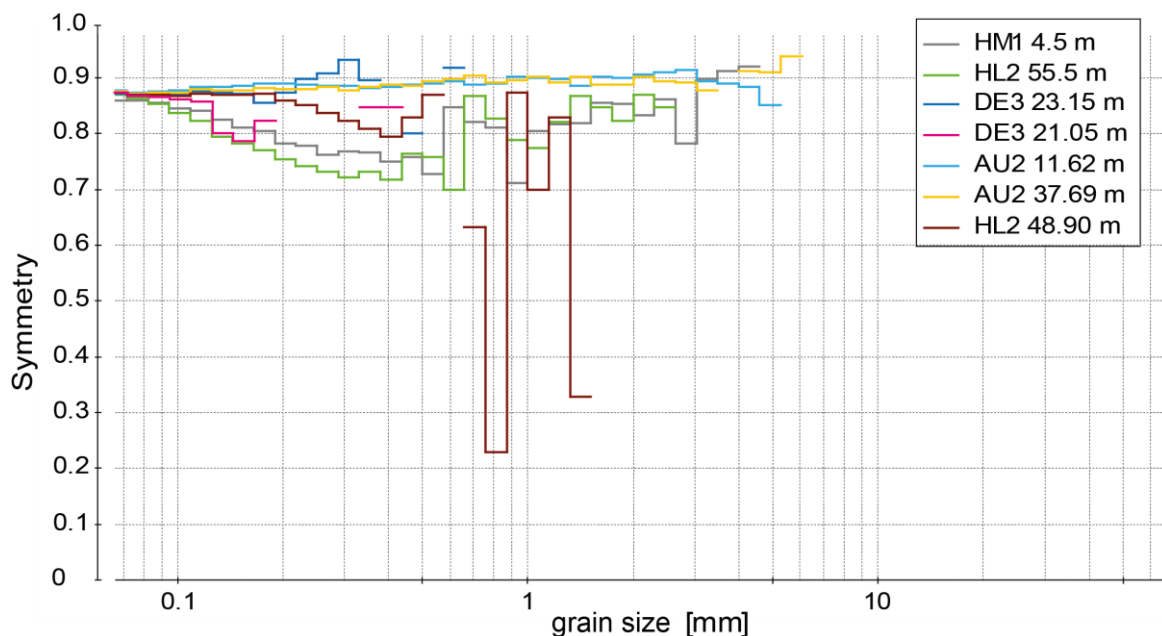


Fig. 3.18: Symmetry of the grain size classes for all studied samples.

The Samples HM1 and HL2 (55.5 m) (grey and light green) show very low sphericity values in the fractions coarser than the background sedimentation (Fig. 3.19). The

sphericity shows higher values in samples AU2 (11.62 m), AU2 (37.69 m), HL2 (48.90 m) and DE3 (light blue, yellow, brown and dark blue line). Sample DE3 (21.05 m, pink line) starts in the finest fraction with the highest value in sphericity for the finest fractions and a strong decline for coarser particles. The shape parameters breadth/ length ratio and convexity show in general the same trends, however less pronounced and weren't taken into account here.

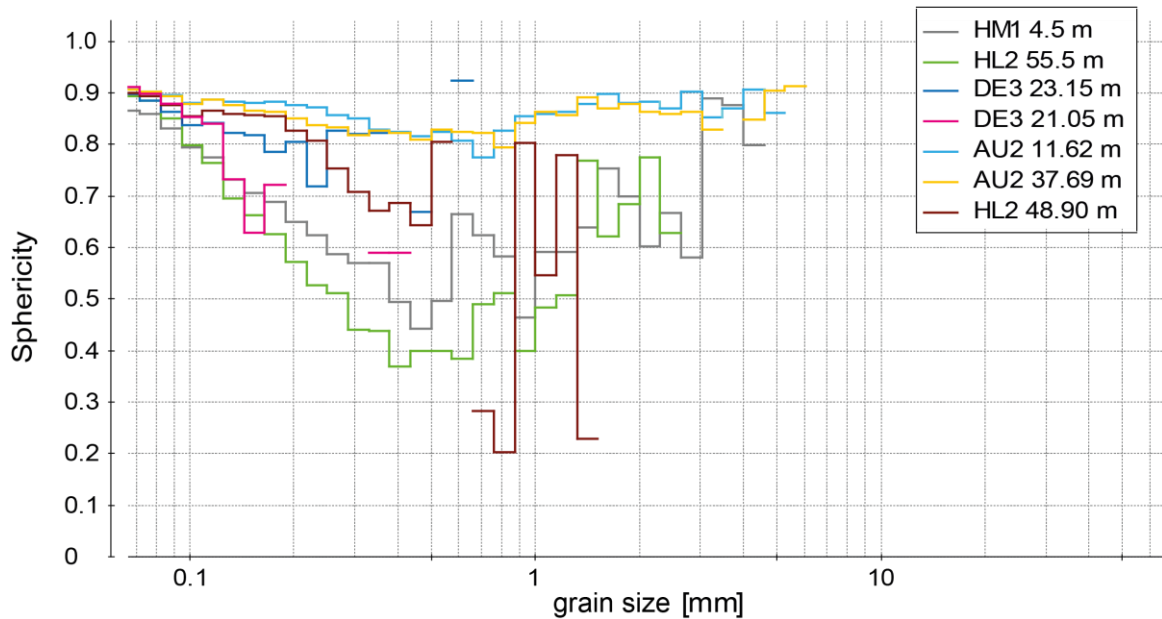


Fig. 3.19: Sphericity of the grain size classes for all studied samples.

3.7 Conclusions

Grain size distributions are influenced by many factors. The lake size, depth, morphological setting and hydrological conditions are the main factors to control the background sedimentation, which is mostly in the clay and silt fraction. However, the grain size distribution of the sand fraction changes with the prevailing climatic conditions and specific transport processes. The following statistical characteristics apply to lakes of about 1 km diameter:

Interglacial sediments

Interglacial samples can be identified by the shape and modes of the coarse tail of the size distribution. The samples are mainly controlled by the presence of biogenic remains, mainly plant and wood pieces, which can be easily detected by the symmetry and sphericity of the modes of the coarse tail of the grain size distribution. Interglacial and

interstadial samples show very low values of sphericity and symmetry due to a high amount of irregular shaped organic content.

Glacial sediments (coversand and loess)

Samples from glacial sediments are mainly of clastic origin and show good sorting with high values in sphericity and especially symmetry due to the aeolian transport of loess and cover sand grains. The high symmetry mode over 0.9 can be used as a proxy for the aeolian transport process and an unambiguous assignment to glacial samples is possible.

Tephra layer

Tephra sediments have a characteristic mineral composition with a grain size composition dependent on the transport distance, height and turbulence. They are, however, in general very well sorted. Extremely large grains of pumice (low density) settle together with small mineral grains (high density), because of the same equivalent grain size composition. The easiest way to detect tephra layers in lake sediments is to analyse the mineral grains and the mineral composition of the sample with the photo image.

Flood layer

Flood layers are characterised by a bimodal grain size distribution, because the pulsating rhythm of a flood phase produces an event layer of strong unconformity. The transported grains can be extremely large, in every case well above the size of the background sedimentation. Flood and tephra samples show in their sediment modes high values of the shape parameters sphericity and symmetry, due to the abrasion and rounding of the particles during their fluvial or aeolian transport. However, flood layers are clearly marked by a fluvial bimodal particle size distribution in combination with a mineral composition from the direct catchment area.

General Conclusion

The shape parameters allow estimation about the aeolian or fluvial transport processes in lake sediments and the statistics of the coarse tail of the grain size distribution allows even distinguishing between different climate conditions. Thus, the developed Camsizer method in combination with the photo evaluation of the coarse fraction enables a fast and accurate classification of lake sediments. This novel approach greatly facilitates and accelerates the analysis of lake sediments and replaces previous standard procedures.

Acknowledgments

The Camsizer[®] was financed by the German Science Foundation (DFG) under grant Si 594/27-1.

Nomenclature

A	= measured area of the particle projection
A_{real}	= real area of the particle projection
A_{convex}	= convex area of the particle projection
U	= circumference of the particle projection
r₁, r₂	= distances of the barycentre to the fringe of the area
x_c	= chord through the barycentre
x_{c min}	= smallest measured chord through the barycentre
x_{Fe}	= Feret-diameter, distance of parallel tangents
x_{Fe max}	= largest Feret-diameter
d	= particle diameter in mm
d₀	= unity diameter (1 mm)
Φ	= $-\log_2\left(\frac{d}{d_0}\right)$

Chapter 4

The ELSA-Flood-Stack: A reconstruction from the laminated sediments of Eifel maar structures during the last 60 000 years

H. Brunck¹, J. Albert¹, F. Sirocko¹

(1) Institute for Geosciences, Johannes Gutenberg-University, 55128 Mainz, Germany

A slightly modified version of this chapter has been published as Brunck et al. (2016) in the journal “Global and Planetary Change”.

4.1 Abstract

This study reconstructs the main flood phases in Central Europe from event layers in sediment cores from Holocene Eifel maar lakes and Pleistocene dry maar structures. These reconstructions are combined with recent gauge time-series to cover the entire precipitation extremes of the last 60 000 years. In general, Eifel maar sediments are perfectly suited for the preservation of event layers since the deep water in the maar lakes is seasonal anoxic and therefore, bioturbation is low. However, the preservation of annual lamination is only preserved in Holzmaar and Ulmener Maar. All other cores are dated by ¹⁴C, magnetostratigraphy, tephra markers and ice core tuning. The cores were drilled in the Eifel region of central western Germany, which represents a climatic homogenous region from Belgium to Poland and all across Central Europe. A total of 233 flood layers over 7.5 mm were detected in all analysed cores. The stratigraphic classification of the flood events follows the newly defined Landscape Evolution Zones (LEZ). The strongest events

in the Holocene have occurred during LEZ 1 (0 – 6000 b2k) in the years 658, 2800 and 4100 b2k. Flood layers in the LEZ 2 (6000 – 10 500 b2k) are not as frequent as during the LEZ 1, nevertheless, the floods cluster between 6000 and 6500 b2k. Twenty flood layers are found in the LEZ 3 (10 500 – 14 700 b2k), 11 in LEZ 4 (14 700 – 21 000 b2k), 15 in LEZ 5 (21 000 – 28 500 b2k), 34 in LEZ 6 (28 500 – 36 500 b2k), 8 in LEZ 7 (36 500 – 49 000 b2k), zero in LEZ 8 (49 000 – 55 000 b2k) and LEZ 9 (55 000 – 60 000 b2k). The maximum flood phases during the Pleistocene are at 11 500 – 17 500 (late glacial and Younger Dryas), 23 000 – 24 000 (before Greenland interstadial (GI) 2), 29 000 – 35 000 (especially between GI 5 and 4) and 44 000 – 44 500 b2k (transition from GI 12 to 11). The variations in flood dynamics are climatically driven and mainly associated with climate transitions and colder periods, combined with light vegetation. It turns out that low vegetation coverage related to both Greenland stadial phases and anthropogenic impacts since late Holocene is the main cause for the development of flood layers in maar sediments. The precipitation itself, plays only a secondary role. This interpretation is based on the current climate understanding of cold phases and several studies of fluvial erosion related to vegetation coverage.

4.2 Introduction

The weather of the next decades will most likely undergo an intensification of weather extremes. Prognostic models have highlighted an intensification of prolonged summer droughts and precipitation maxima combined with a higher risk of flash floods in creeks and rivers (IPCC report, 2014, 2007; Jacob et al., 2007). Lacustrine sediments are very sensitive to natural and anthropogenic environmental changes. Thus, lake sediments are excellent climate archives and have been used for reconstructions of vegetation, water temperature, environment, volcanic activity, climate and quite recently, for precipitation and flood events (e.g. Wessels, 1998; Macklin et al., 2006; Moreno et al., 2008; Zielhofer et al., 2008; Storen et al., 2010; Wilhelm et al., 2012a, 2012b; Swierczynski et al., 2013; Wirth et al., 2013; Kämpf et al., 2014).

Lakes that are used for the Holocene reconstructions are numerous in the landscape of Central Europe. However, lakes that have the potential to reconstruct the climate conditions between 10 000 and 60 000 b2k in central Germany are restricted to Eifel maar structures. The Eifel region is characterized by a climatic homogenous area from Belgium to Poland and all across Central Europe (Wernli and Pfahl, 2009). Other suitable locations

are in central France (Ampel et al., 2008; Wohlfahrt et al., 2008) or southern Italy (Brauer et al., 2000, 2001), and thus in regions with another climate forcing. River sediments are a complicated and incomplete archive, due to the fact that flood event layers are separated by erosion from the normal sedimentation (Brakenridge, 1988; Macklin, 1999; Thorndycraft et al., 2005). Small basins, like maars, with long water residence time and anoxic bottom water are better suited to preserve a complete flood archive, if they are fed by small creeks. The suspension layers can be distinguished from background sedimentation and seismites macroscopically or in thin sections (Marco et al., 1996; Moreno et al., 2008). Further sedimentological (e.g. grain size analysis) and geochemical (e.g. μ -XRF analysis) studies help to differentiate between flood layers, turbidites and slumps (Sturm et al., 1995; Mulder et al., 2003; Wirth et al., 2011). Accordingly, the Eifel maar lakes are the only location in Central Europe that allows one to generate a long time series with event resolution (Sirocko et al., 2013).

The maar lakes and the dry maar structures of the Eifel region have been systematically cored since 1998 by the ELSA Project (Eifel Laminated Sediment Archive; <http://www.elsa.geowissenschaften.uni-mainz.de>) of the Institute for Geoscience, Johannes Gutenberg University Mainz, Germany. In this study, the maar structures of Holzmaar, Ulmener Maar, Schalkenmehrener Maar and Auel dry maar are used to reconstruct the flood history of the last 60 000 years. In contrast, studies on the average precipitation are better done in the closed/ semiclosed basins of Gemündener Maar or Dehner dry maar, where terraces document past lake levels (Sirocko et al., 2013). So far, the flood history of the last 60 000 years is increasingly studied in the Holocene, the time before 10 000 years is still completely unknown.

The key objectives of this study are: (1) to develop a high resolution long time flood frequency record for Central Europe; (2) to analyse the relationship between flood activity and a) climate, b) precipitation and c) vegetation; and (3) to study the last 60 000 years with respect to the interlacing of flood layers and predominant climatic and anthropogenic development.

4.3 Coring sites

Four sediment cores (from three Holocene maar lakes and one Pleistocene dry maar structure) are used to reconstruct the flood activity in the Eifel for the last 60 000 years (Fig. 4.1).

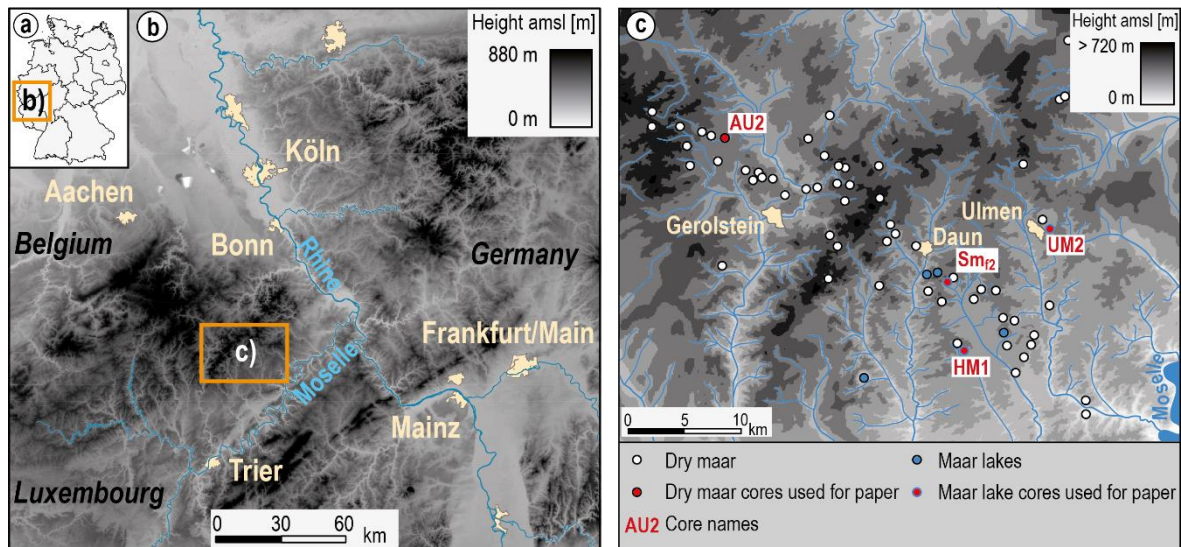


Fig. 4.1: a) Outline map of Germany. b) Digital terrain model West Germany with the drainage system c) Digital terrain model of the Eifel with the maar locations after Büchel (1993), the drainage system and the core positions: SM_{r2} (Gauß-Krüger-Koordinatensystem Zone 2 (GK-System) 2,561,310/ 5,559,585); HM1 (GK-System 2,562,900/ 5,554,030); UM2 (GK-System 2,570,165/ 5,564,270) and AU2 (GK-System 2,542,455/ 5,572,017).

4.3.1 Schalkenmehrener Maar

Lake Schalkenmehrener Maar is part of the Dauner Maare. It has a diameter of 528 m, an average depth of 14.5 m and a maximum depth of 21 m (Scharf and Oehms, 1992). With a lake surface of 219 000 m², it is one of the larger maar lakes of the Eifel. It has no large inflow or outflow stream. However, it is connected to a flanking dry maar, which is filled with sediment and peat since the middle Holocene (Straka, 1975) and drained since Roman times (Sirocko, 2009). Accordingly, Schalkenmehren is well suited to monitor the post-Roman landscape evolution. The freeze core SM_{r2} (Fig. 4.1) was used for the flood event reconstruction depicting the last 1000 years, in particular the medieval landscape history.

4.3.2 Holzmaar

The most investigated maar of the Eifel is the Holzmaar. The stratigraphy for this maar includes annual varve counting, which was constrained using ¹⁴C-dating (Brauer, 1994; Hajdas et al., 1995; Zolitschka, 1998; Brauer et al., 1999a, 1999b). Holzmaar has a diameter of 272 m and a maximum depth of 20 m (Scharf and Oehms, 1992). It also has the smallest water volume of all maar lakes in the Eifel. The Sammetbach flows from the

west into the maar. Just a few metres further south it flows out again. The small size of the maar and the direct inflow by the Sammetbach cause a relative high sedimentation rate (10 m Holocene). Persistent low deep water oxygenation led to the formation of countable varves throughout the entire Holocene (Sirocko et al., 2016).

4.3.3 *Ulmener Maar*

The Ulmener Maar is slightly smaller than the Holzmaar with a diameter of 265 m (Scharf and Oehms, 1992). It is the smallest and youngest maar in the Eifel (about 11 000 b2k). However, it is also one of the deepest with a maximum depth of 39 m (Scharf and Oehms, 1992). The Ulmener Maar has the largest catchment area of the three analysed Holocene maars. Up to the pre-Roman times flood sediments were flushed from the Dellbach into the maar. Nowadays, the Dellbach flows west of the maar and had no contact to it since the founding of the city Ulmen. Consequently, the Ulmener Maar can only be applied to reconstruct the pre-Roman flood history. Flood layers in the core UM2 have partly whitish colours, which correspond well to silt and clay sediments of Devonian age (Eckfeld and Reudelsterz layers) in the western catchment area of the maar. Pollen and botanical macroremains reveal that the region around the maar is anthropogenically modified since 5700 b2k (3700 BC) (Sirocko, 2009). Nevertheless, the Ulmener Maar is certainly the best suited for the early Holocene flood reconstruction and has a higher sedimentation rate than that of Holzmaar.

4.3.4 *Auel dry maar*

The silted up basin Auel is one of the largest dry maar structures of the Eifel with a diameter of 1325 m. The modern Tiefer Bach flows through the maar centre and leaves the dry maar again at the opposite side. This river has a large catchment area of 12.187 km² and a total length of 9.4 km (Water management administration Rhineland-Palatinate: German river code 266374). The core AU2 from the centre of the maar is 123 m long and covers the time from the Laacher See eruption (see also Förster and Sirocko, 2016) back to 60 000 b2k (Fig. 4.2). The average sedimentation rate of dry maar lake Auel is with $2 \frac{mm}{a}$ the highest of all Eifel maar structures, due to the abundant fluvial input. Therefore, the largest flood events and associated suspension injections are nicely visible in the sediment. Additionally, the fluvial inflow also leads to a high amount of botanical macroremains. Frequent Ranunculaceae seeds are used for four new ¹⁴C dates, which are

measured between 18 340 and 21 865 b2k (Sirocko et al., 2016). Carbon maxima are visible for all Greenland interstadials, which are used to fine-tune the ^{14}C stratigraphy to the established Greenland ice core chronology (Svensson et al., 2008).

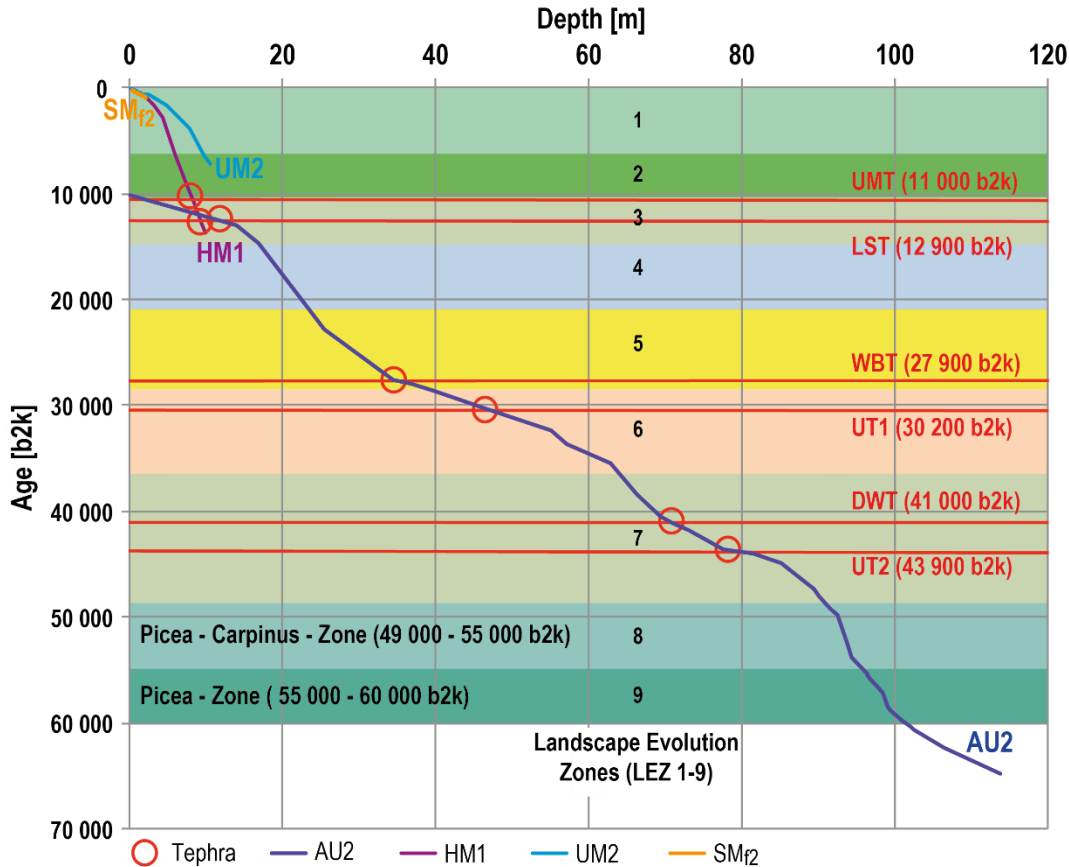


Fig. 4.2: Age/ depth model of the cores SM_{f2}, UM2, HM1 and AU2. The LEZ subdivisions 1 – 9 are colour-coded. Visible tephra layers are-represented by red lines and marked with red circles in each core.

4.4 Stratigraphy

An integrated age/ depth model for all ELSA cores was developed by using 9 different dating methods and sedimentological, palaeobotanical and geochemical data from 18 Eifel sediment cores (Sirocko et al., 2013). Based on this stratigraphical concept, tephra correlation and several new ^{14}C dates have improved the stratigraphy and leads to a classification of LEZ (Sirocko et al., 2016). The LEZ reconstruct the vegetation and the climate change mostly based on macroremains and pollen since 60 000 b2k (Sirocko et al., 2016). The stratigraphy and the LEZ classification are assumed on a one-to-one basis to discuss the flood event succession concerning environmental changes. The specific sedimentation conditions of Auel explain the unique possibility to detect all 17 GI in the

total carbon concentration of this dry maar. In a final step, the time series of C_{total} was tuned to the Greenland ice core chronology GICC05 (Svensson et al., 2008) to link the Central European landscape evolution directly to the Greenland climate curve. The allocation of the core material to all Greenland interstadials and stadials (defined after Andersen et al., 2006) enables the exact climatic interpretation of the flood frequency.

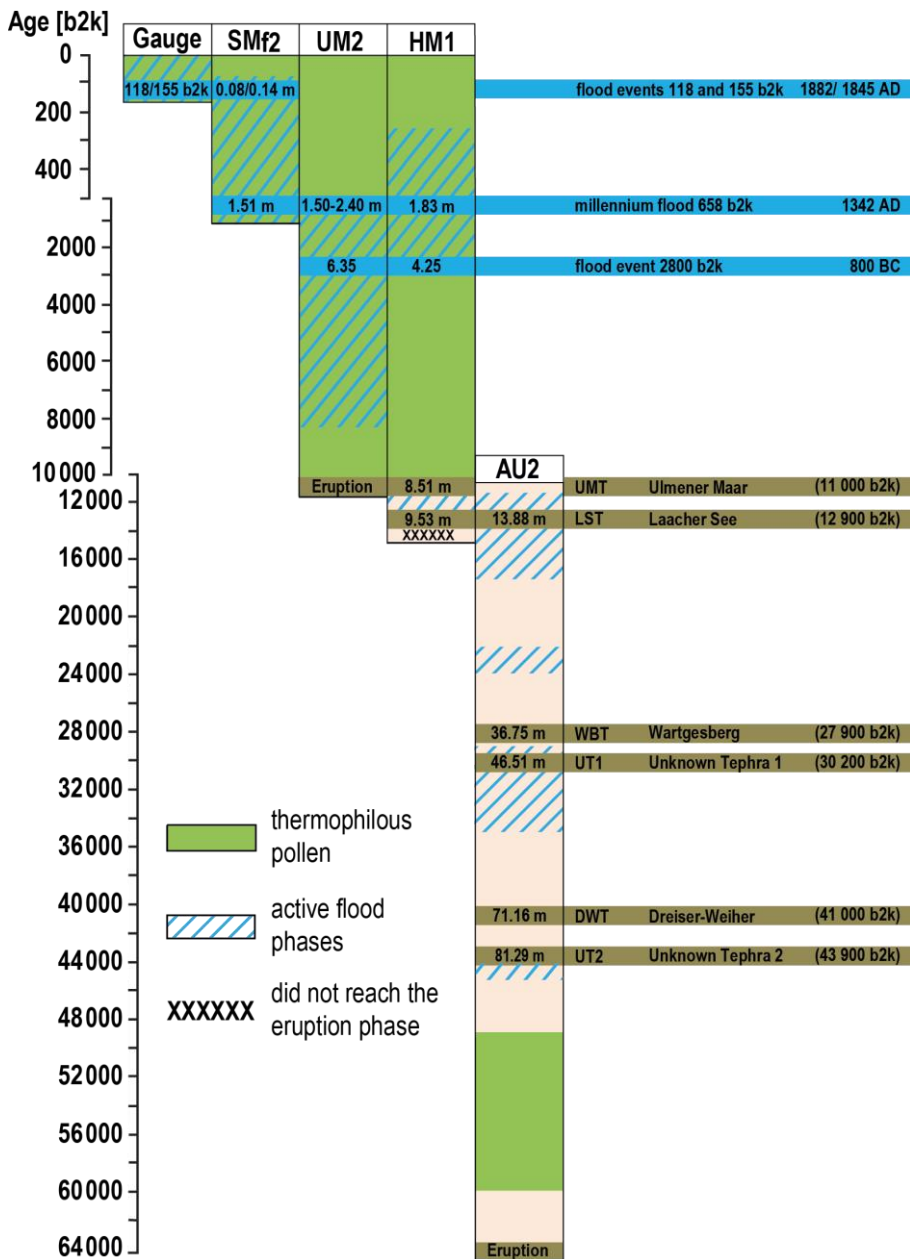


Fig. 4.3: Time series with transition points between the gauge analysis and the cores SM_{f2}, UM2, HM1 and AU2. In each core the transition points and all tephra layers are marked with their exact depth. The green highlighted parts of the cores represent time periods with thermophilous pollen (Sirocko et al., 2016) and the hatched blue parts stands for active flood phases (Fig. 4.8).

In order to extend the flood record to the present, daily gauge values from the Rhine, Moselle and several Eifel rivers (Ahr, Kyll and Prüm) were analysed. Due to the fact that sediment cores are disturbed from human impact in all maar sites of the Eifel for the last decades, the strongest flood events since 195 b2k (AD 1820) were identified from the historical values. The correlation between the gauge analysis and the freeze core SM_{f2} is carried out with the flood events 118 and 155 b2k (AD 1882 and AD 1845) (Fig. 4.3). The millennium flood 658 b2k (AD 1342) was used for the transition from the freeze core SM_{f2} to the two Holocene cores (Bork et al., 1998). Additionally, the flood event 2800 b2k (800 BC/ Sirocko et al., 2013) and the Ulmener Maar Tephra (11 000 b2k/ Zolitschka et al., 1995) are applied as time markers between the cores HM1 and UM2. The Holocene core HM1 is correlated to the core AU2 through the Laacher See Tephra (LST) (12 900 b2k; Brauer et al., 1999b) (Figs. 4.2 and 4.3).

4.5 Material and method

Four sediment cores were visually and lithologically examined to identify flood layers over 7.5 mm thickness. Some flood layers are several cm thick and clearly visible by the eye (Figs. 4.6 and 4.7). Others are mm thick and were petrographically studied in 10 cm long thin sections under an Olympus U-TTBI microscope to distinguish them from distal turbidites and distal slumps. The event intensity was classified through the thickness of each flood layer (Mulder et al., 2003).

The reconstructed time series was aligned with meteorological precipitation data and historically documented flood events. The historical record from Cologne (Municipal Drainage Operations of Cologne, Flood Protection Centre. www.steb-koeln.de) was used as reference system since 195 b2k (AD 1820). An extreme value analysis was applied to combine the daily gauge values from the Rhine and Eifel rivers to the core SM_{f2} (Dyck and Peschke, 1995). Thus, it was possible to extend the flood time series to recent years.

The core event sections were scanned for selected elements at 1 mm resolution using the X-ray fluorescence scanner Eagle III (Röntgenanalytik Meßtechnik GmbH, Germany) of the University of Mainz (Germany). The major elements (Na, Mg, Al, Si, P, S, K, Ca, Ti, Mn, and Fe) as well as trace elements (Ni, Cu, Zn and Sr) were measured on 10 cm long resin impregnated samples with the μ -XRF (Fig. 4.4).

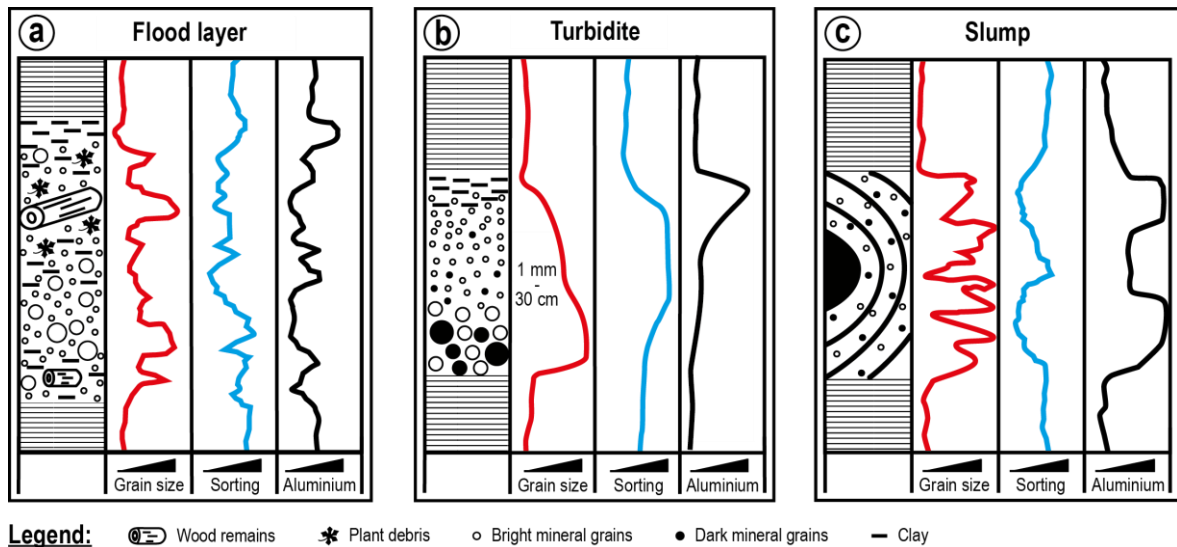


Fig. 4.4: a) Pattern of an idealized flood layer for the grain size, the sorting and the aluminium content. At the end of the flood layer the “clay cap” is visible. b) Pattern of an idealized turbidite for the grain size, the sorting and the aluminium content. c) Pattern of an idealized slump for the grain size, the sorting and the aluminium content.

The particle analysis method RADIUS — Rapid Particle Analysis of digital Images by ultra-high-resolution scanning of thin sections (for details see Seelos and Sirocko, 2005), was used to analyse and identify the different sediment structures and events in the drilling cores of the ELSA archive (Sirocko et al., 2005) (Figs. 4.4 and 4.5).

4.6 Flood Layer — a definition

Flood Layers indicate fluvial inflow due to singular or repeating heavy rain events. The intensified sediment input is on one hand attributable to increased rainfall in the catchment area of the maar and on the other hand a combination of wind and wave erosion along the lakeside (Sturm et al., 1995; Mulder et al., 2003). During this process, mostly detrital minerogenic particles and terrestrial organic material are transported into the lake (Mulder et al., 2003; Wirth et al., 2011). Coarse-grained material deposits gravitationally on the slope and does not reach the position in the central maar basin where the ELSA cores are taken. During and immediately after heavy rain events, material stored in creeks and slopes are eroded and transported into the maar. Our field observations during three rain events and collected water samples in Schalkenmehren showed two major points: 1) increased fluvial transport of plant debris, wood remains and sand into the maar. 2) fine clastic and biogenic particles are transported within 2 h after the suspension event into the

maar centre and settle to the ground. The final deposition of the finest particles occurs several days after the event (Moschen, 2004). Thus, the mm to cm thick flood events are usually completed by a clay layer, or “clay cap” (Schlölaut et al., 2014). The strongest flood events last over several days and result in a complex pattern of particle size and density as a consequence of variable sink rates of the particles. This causes a discontinuous grain size gradient within the flood layer. Therefore, the occurrence of several grain size maxima over the entire flood layer thickness is a key characteristic against turbidites and slumps (Sturm et al., 1995; Anselmetti et al., 2009) (Figs. 4.4 and 4.5).

A turbidite is a singular event that leads to segregation and rearrangement of the entire carried sediment package (Bouma, 1987; Sturm et al., 1995). Such an event remobilizes unconsolidated and water-saturated particles, by the destabilization of the grain structure or pore water overpressure (Sirocko and Dietrich, 2009). The particles then segregate and flow to the maar bottom in a turbulent suspension layer. The fine-grained components remain in a suspension cloud, while denser and heavier material accumulates quickly on the ground or slide down the slope (Mulder and Alexander, 2001; Sirocko and Dietrich, 2009). The deposits extend over the entire ground and due to decreasing transport energy of the turbidity current, large and heavy particles settle first. The lighter and smaller particles remain essentially longer in suspension, therefore, deposited sediments are continuously graded (Walker and Mutti, 1973; Bouma, 1987; Schnellmann et al., 2005). Thus, turbidite sediments have a widespread grain size distribution and moderate sorting. In contrast to flood events, coarse particles are restricted to the base layer (Figs. 4.4 and 4.5).

Slumps are characterized by missing segregation of the sediment packages (Nardin, 1979). These packages move as a whole block down the slope and can be folded in a large scale from dm to m. Slumps are expressed by bent and tilted layers in the core; completely mixed slumps can be identified by the typical mottled appearance. Since slumps are triggered at the slope near the lakefront, all particle sizes and sediment colorations are present. Furthermore, slumps can also be detected in the particle size analysis by a very poor sorting and extreme changes of grain sizes (Fig. 4.4).

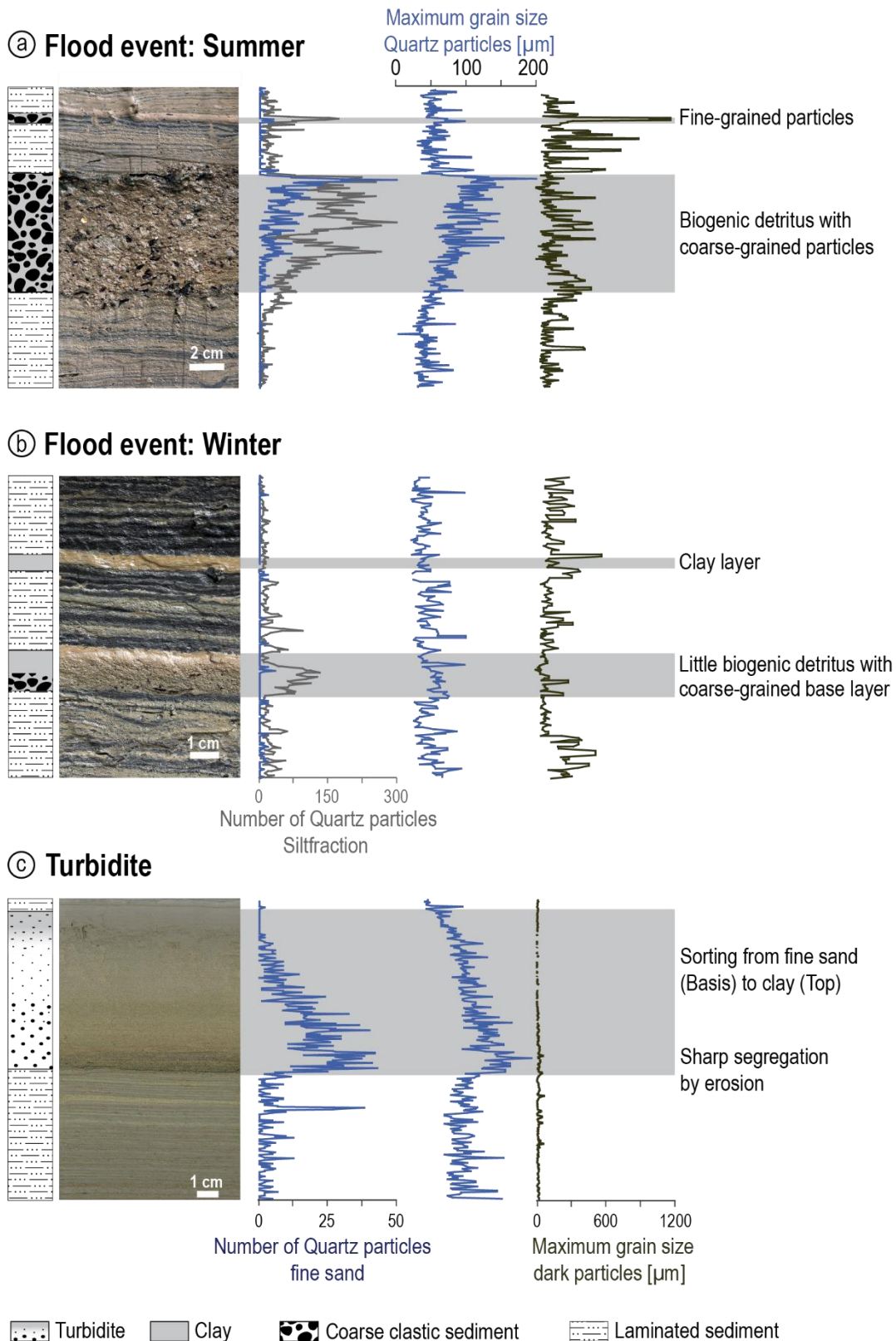


Fig. 4.5: a) Summer suspension layer. b) Winter suspension layer. c) Turbidite. Summer and winter suspension layers differ mainly in the content of biogenic detritus. In contrast, a turbidite is characterized by continuous grading of particle sizes. Modified after Sirocko and Dietrich (2009).

4.7 Results: The ELSA-Flood-Stack

Flood events recorded by the gauge extreme value analysis identify the years 5 b2k (AD 1995), 7 b2k (AD 1993), 12 b2k (AD 1988), 52 b2k (AD 1948), 74 b2k (AD 1926), 80 b2k (AD 1920), 118 b2k (AD 1882) and 155 b2k (AD 1845) as the strongest floods since 195 b2k (AD 1820) (Tab. 4.1 and Fig. 4.8) (Federal Waterways and Shipping Administration, 2015). This is consistent with historical documents from Cologne (Municipal Drainage Operations of Cologne, Flood Protection Centre). The flood events 118 b2k (AD 1882) and 155 b2k (AD 1845) are observed in the gauge analysis and can be correlated to the core SM_{f2} (Fig. 4.3). The varve counting of core SM_{f2} assigns these two flood layers to the years 119 b2k (AD 1881) and 154 b2k (AD 1846) (Tab. 4.1). Accordingly, the correlation error between varve counting and historical dates is within the normal $\pm 2\%$ range for the last 1000 years (Brauer et al., 1999a; Sirocko et al., 2016).

A combination of the cores SM_{f2}, HM1 and UM2 represents the Holocene. A total of 109 flood layers were detected in the LEZ 1 (0 – 6000 b2k; anthropogenic forest), with a clear maximum in the medieval and Roman sections of the cores. The strongest flood events are reconstructed for the years 658, 2800 and 4100 b2k (AD 1342, 800 BC and 2100 BC) (Tab. 4.1 and Fig. 4.8). The most pronounced flood was the St. Mary Magdalene's millennium flood in July 658 b2k (AD 1342) (Bork et al., 1998). This flood layer is unusually thick and contains a large amount of plant remains, which indicate the tremendous event strength. The millennium flood is visible in all maars and is therefore a distinct time and correlation marker. Another major hydrological event is dated to approximately 2800 b2k (800 BC) in the cores HM1 and UM2. The layers include a large amount of reworked sediment and are thus difficult to date. Nevertheless, the flood layer is recognizable in all Holocene cores and can be used as a second time marker.

Flood events in LEZ 2 (6000 – 10 500 b2k; natural broadleaf forest) are not clearly visible in Holzmaar or Schalkenmehrener Maar. They become visible only in LEZ 1, when humans cultivated the landscape. However, 34 flood events are recognizable in the Ulmener Maar from 8500 to 6000 b2k (Gronenborn and Sirocko, 2009) (Tab. 4.1 and Fig. 4.8). They seem to cluster slightly between 6000 and 6500 b2k.

The Holocene core HM1 is correlated through the LST with the core AU2, which represents the time interval from the LST up to 60 000 b2k (Fig. 4.3). Generally, 88 flood layers over 7.5 mm occur in AU2 (Tab. 4.1 and Fig. 4.7). The LEZ 3

(10 500 – 14 700 b2k; boreal forest) has 20 flood layers and an average of 4.8 events per 1000 years. 12 strong flood events from 12 000 to 13 000 b2k represent the highest number of flood events per 1000 years in the whole time series of AU2 (Tab. 4.1) and is comparable to the Younger Dryas (McManus et al., 2004).

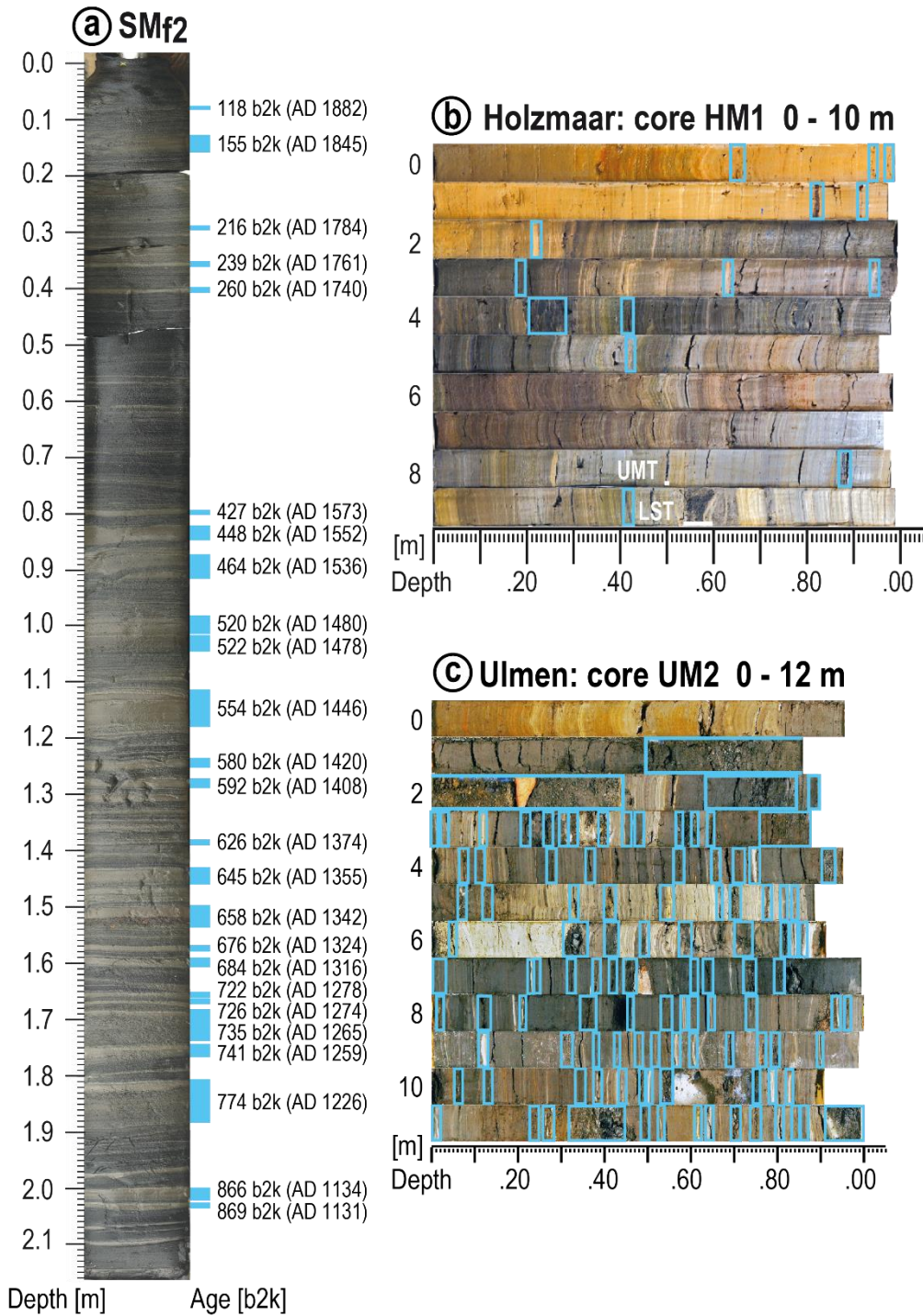
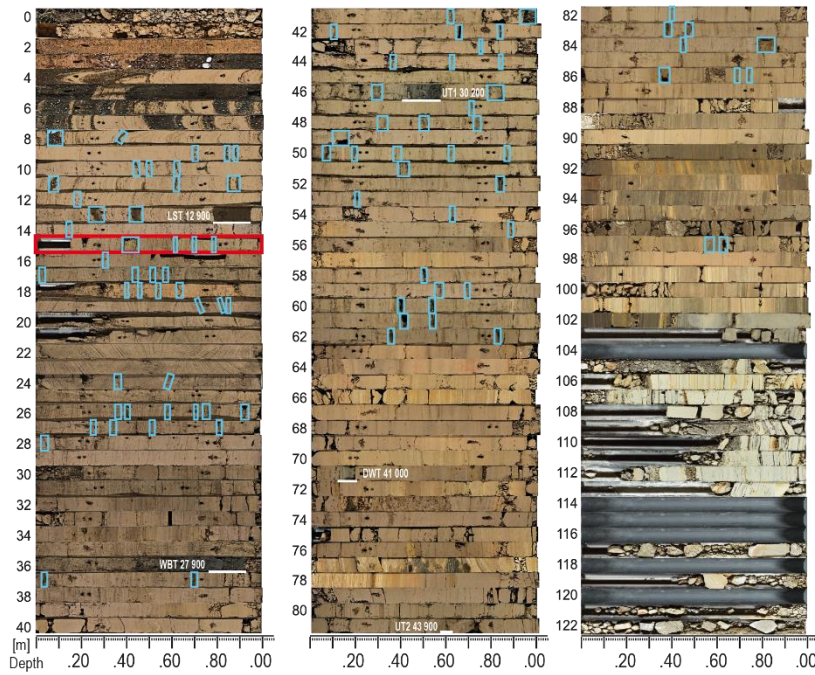


Fig. 4.6: a) Core SM_{f2} with all detected flood events (blue squares) and varve counted years. b) Core HM1 with all detected flood events (blue boxes) and tephra (white lines). c) Core UM2 with all detected flood events (blue boxes).

a) **AUEL: core AU2 0 - 123 m**



b)

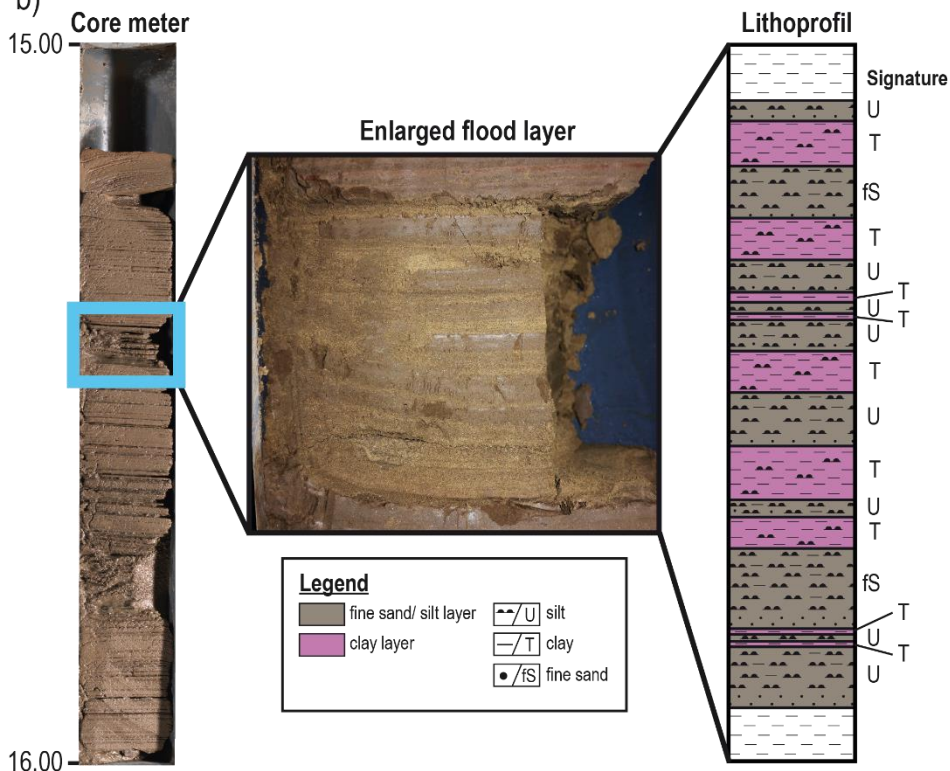


Fig. 4.7: a) Core AU2 with all detected flood events (blue boxes) and tephra (white lines). The red core metre is the sample metre for part b. b) Exemplary flood layer from the depth of 15.41 m. The enlarged flood layer and the lithoprofil show multiple water discharge peaks. Within the same flood event sand and silt layers, which represent water discharge peaks, alternate with clay sections.

The late LEZ 4 (14 700 – 21 000 b2k, polar desert) reveals an average of 1.8 flood events per 1000 years and has 11 events in total. The Last Glacial Maximum (LGM) from 17 500 to 22 000 b2k shows no flood events at all; apparently it was so dry, that there was no spring snow melt during the peak glacial permafrost conditions. However, the summer temperatures each year were high enough to break up the winter ice. There is no indication of event layers that could document perennial frozen ice on the maar lake. The succession of laminae appears to be almost continuous throughout the entire glaciation maximum (Sirocko et al., 2016). The first suspension layers arise again at the time around 17 500 b2k (Tab. 4.1 and Fig. 4.8) and show, that the final phase of the Weichselian glaciation must have been already more humid than the LGM. Most probably, the precipitation fell as winter snow, leading to spring meltwater runoff into the maar lakes.

The LEZ 5 (21 000 – 28 500 b2k; tundra) has 15 flood layers with an average of 1.8 flood events per 1000 years. Almost all flood events are restricted to the time period from 23 000 to 24 000 b2k, representing the end of Greenland stadial 3 (Tab. 4.1 and Fig. 4.8).

The LEZ 6 (28 500 – 36 500 b2k; steppe) was a steppe environment and has seen an average of 4 flood events per 1000 years. The period shows a total of 34 flood events and thus, the highest number in the whole time series of AU2 (Tab. 4.1). The maximum flood cluster appears during the Greenland stadial 5, particular during the transition from GI 5 to GI 4 (Tab. 4.1 and Fig. 4.8). The late winter snow melt events still seem to be the main causes for these flood events, indeed the occurrence of summer rains in a landscape with little vegetation cover might have lead to erosion even at moderate rainfall intensity. The occurrence of large amounts of Ranunculaceae seeds point towards quite humid conditions during summer (Sirocko et al., 2016).

The LEZ 7 (36 500 – 49 000 b2k; boreal forest) has an average of 0.6 flood events per 1000 years and 8 events in total. Once again the flood events are concentrated in a short period of time from 44 000 to 44 500 b2k (Tab. 4.1 and Fig. 4.8). They occurred in a time when the boreal forest deteriorated into the subsequent steppe, (i.e. during a time of vegetation and soil change). This represents the Greenland stadial 12 between GI 12 and GI 11.

Flood events are absent in LEZ8 (49 000 – 55 000 b2k; spruce and hornbeam forest) and LEZ 9 (55 000 – 60 000 b2k; spruce forest), most probably since dense forests with roots stabilized the ground and no extreme precipitation events occurred (Tab. 4.1 and

Fig. 4.8). On the other hand, it is very unlikely that flood events lacking in the entire warmer phase of the LEZ 8 and 9. It can be also explained by a missing connection between the young maar and the local river. Therefore, the sensitivity for flood events at this time was not given.

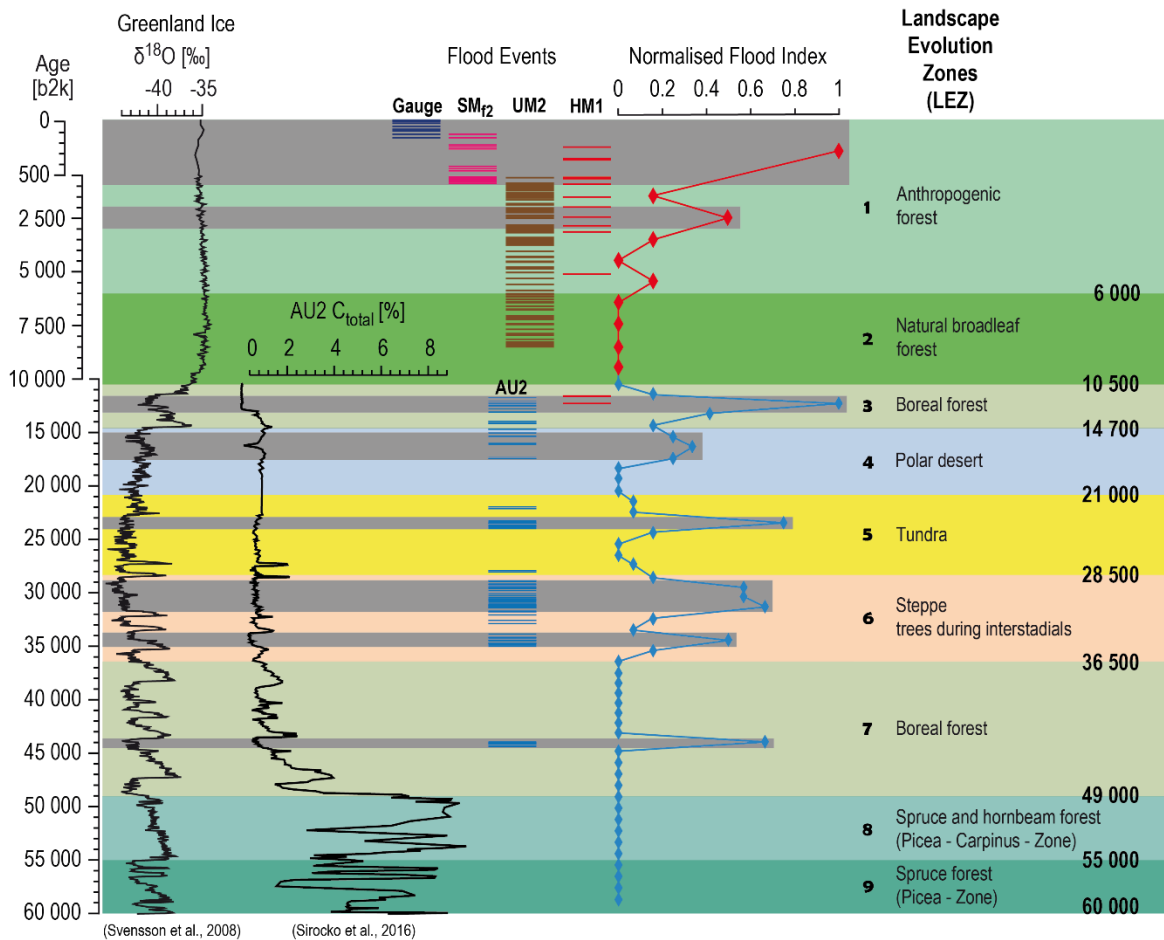


Fig. 4.8: The ELSA-Flood-Stack. Interaction between flood events (purple, pink, brown, red and blue lines), normalized flood events per millennium in percent of maximum (red line represents HM1; blue line AU2) and LEZ subdivisions (Sirocko et al., 2016). Due to the distinct catchment areas and time relations of the two maars (HM1 and AU2), the floods per millennium are given by the percentage related to the maximum of detectable flood layers in each core. Additionally, the Greenland ice core isotopes time series (Svensson et al., 2008) and the C_{total} time series from Auel (Sirocko et al., 2016) are shown.

Summarized the main flood stages for AU2 are from 11 500 to 17 500, 23 000 to 24 000, 29 000 to 35 000 and 44 000 to 44 500 b2k (Tab. 4.1). However, the section from 11 500 to 17 500 b2k is the only one, which is spread over two LEZ zones. The period

begins with the first snow melt events at the end of the polar desert phase, although the stage reaches the flood peak intensity around the Younger Dryas (Tab. 4.1 and Fig. 4.8). All three other flood stages are limited to one LEZ, whereby the phase from 29 000 to 35 000 b2k has a special position. Although it is with 6000 years the longest continuous phase with flood layers in the core AU2, there is a flood maximum from 29 000 to 32 000 b2k representing the Greenland stadial 5 between the GI 5 and 4 (Fig. 4.8).

4.8 Discussion

The aim of this study is to analyse the variances of the flood frequency in Central Europe and not to provide an absolute count of flood layers. The flood events are reconstructed from three Holocene maar lakes and one Pleistocene dry maar structure and thus, the data are not fully comparable. Therefore, the ELSA-Flood-Stack is a summary, which cannot be used as a direct precipitation curve. It can be understood as a reliable record of periods with extreme weather events or local to the Eifel. It is obvious that the particles in flood layers are not solely associated to ephemeral precipitation and seasonal runoff. They are certainly affected by permafrost conditions, soil development and especially vegetation. A seasonal subdivision in summer and winter flood layers is currently not possible. Further analyses of pollen and diatoms are prime candidates to solve this problem. Nevertheless, the flood frequency of the Eifel indicates a trans-regional pattern and represents a climatic homogenous region from Belgium to Poland across Central Europe (Wernli and Pfahl, 2009). Varying offsets between flood events of rivers both in Germany and Europe have been described by Glaser (2008) and can be explained by the complex regional weather situation. In this context, a detailed comparison with the flood time series from Macklin et al., 2006; Zielhofer et al., 2008; Storen et al., 2010; Swierczynski et al., 2013; Wilhelm et al., 2013 and Wirth et al., 2013 will be subject of a future publication. Despite the complexity of the flood stack, it is possible to draw several conclusions about precipitation, flood frequency and related topics (Fig. 4.8).

The Picea-Zone (LEZ 9) and the Picea-Carpinus-Zone (LEZ 8) include the GI 17 up to GI 13 (see Fig. 4.8). Warm temperatures and sufficient rainfall were necessary for the spread of the relatively thermophilous forest. The soil stabilization as a result of increasing vegetation is mainly responsible for the reduction of fluvial sediment erosion. Nevertheless, a missing connection between the river and the young maar cannot be

excluded at this time. Both possibilities explain the lack of flood layers in the LEZ 9 and 8 (Fig. 4.8).

During the climate change from GI 12 to GI 11, the vegetation passes into an open boreal coniferous forest with high proportions of grasses (Sirocko et al., 2016). Through the withdrawal of forests and the increasing desertification of the landscape, the root penetration of the soil declines. The soil loses stability, so that heavy rain events could erode and easier rearrange the sediments. This process is confirmed by several flood layers in the period from 44 500 to 44 000 b2k (Fig. 4.8).

The evolution from a boreal forest to an almost treeless steppe took place at the end of the LEZ 7 (GI 8). Thus, occasional rain and snow melt events could easily erode the soil. Therefore, this steppe phase is characterized by continuous flood events with a maximum during the climate change after the GI 5 (Fig. 4.8).

The LEZ 5 is characterized by a vegetation decrease as a result of reduced temperatures and low precipitation rates. However, a bigger cluster of flood events could be identified at the time interval from 24 000 to 23 000 b2k and display the end of Greenland stadial 3 (Fig. 4.8).

After 21 000 b2k, the landscape in the Eifel turned into an ice desert and represents the last glacial maximum (22 000 – 17 500 b2k). The first flood layers appear again at the time around 17 500 b2k when the first snow melt events start. Due to the lack of vegetation, the high potential of soil erosion leads to several flood layers. The slightly moister climate combined with only gradually increasing vegetation density induces a large number of flood layers in the LEZ 3 (Fig. 4.8). Especially the Younger Dryas cold event stands out with a high number of flood events. A detailed consideration of the short transitional period from the cores HM1 and AU2 allows further conclusions. Due to the fact that the river just touches lake Holzmaar, only extreme flood events are preserved. In contrast, the Auel dry maar is very sensitive for flood deposits, since the river flows directly through the maar center. While in Auel 14 flood layers have been identified only two flood layers are classified in Holzmaar. Thus, the Younger Dryas cold event is characterized by a large amount of flood events, where only a few have the potential for a millennium flood.

Gauge	Gauge	SMf ₂	SMf ₂		Time interval	HM1	UM2	AU2
[b2k]	[AD]	[b2k]	[AD]		[b2k]	[n per 1000 a]	[n per 1000 a]	[n per 1000 a]
5	1995	118	1882		1 - 1000	6	10	
7	1993	155	1845		1001 - 2000	1	20	
12	1988	216	1784		2001 - 3000	3	13	
52	1948	239	1761		3001 - 4000	1	15	
74	1926	260	1740		4001 - 5000	0	8	
80	1920	427	1573		5001 - 6000	1	5	
118	1882	448	1552		6001 - 7000	0	13	
155	1845	464	1536		7001 - 8000	0	11	
		520	1480		8001 - 9000	0	10	
		522	1478		9001 - 10 000	0		
		554	1446		10 001 - 11 000	0		
		580	1420		11 001 - 12 000	1		2
		592	1408		12 001 - 13 000	1		12
		626	1374		13 001 - 14 000			5
		645	1355		14 001 - 15 000			2
		658	1342		15 001 - 16 000			3
		676	1324		16 001 - 17 000			4
		684	1316		17 001 - 18 000			3
		722	1278		18 001 - 19 000			0
		726	1274		19 001 - 20 000			0
		735	1265		20 001 - 21 000			0
		741	1259		21 001 - 22 000			1
		774	1226		22 001 - 23 000			1
		866	1134		23 001 - 24 000			9
		869	1131		24 001 - 25 000			2
					25 001 - 26 000			0
					26 001 - 27 000			0
					27 001 - 28 000			1
					28 001 - 29 000			2
					29 001 - 30 000			7
					30 001 - 31 000			7
					31 001 - 32 000			8
					32 001 - 33 000			2
					33 001 - 34 000			1
					34 001 - 35 000			6
					35 001 - 36 000			2
					36 001 - 37 000			0
					37 001 - 38 000			0
					38 001 - 39 000			0
					39 001 - 40 000			0
					40 001 - 41 000			0
					41 001 - 42 000			0
					42 001 - 43 000			0
					43 001 - 44 000			0
					44 001 - 45 000			8
					45 001 - 46 000			0
					46 001 - 47 000			0
					47 001 - 48 000			0
					48 001 - 49 000			0
					49 001 - 50 000			0
					50 001 - 51 000			0
					51 001 - 52 000			0
					52 001 - 53 000			0
					53 001 - 54 000			0
					54 001 - 55 000			0
					55 001 - 56 000			0
					56 001 - 57 000			0
					57 001 - 58 000			0
					58 001 - 59 000			0
					59 001 - 60 000			0

Tab. 4.1: Time overview of all flood events from the gauge analysis and the core SM_{f2}, as well as the number of flood events per 1000 years from the cores HM1, UM2 and AU2.

After the Younger Dryas, the late glacial boreal forest transforms quickly into a thermophilic forest. The early Holocene forests reduce the building of flood layers despite high rainfall, thus, flood layers occur not as pronounced as during LEZ 3 (Fig. 4.8). Nevertheless, a slight flood cluster arises between 6500 and 6000 b2k. This period confirms new evidences on a mid-Holocene climatic depression with elevated flood activity (Macklin et al., 2006; Magny et al., 2007; Zielhofer et al., 2008).

The beginning of the LEZ 1 was described as a shift to a more humid and cooler climate (Firbas, 1949; Overbeck, 1975). Especially after 4000 b2k the number of flood layers increase rapidly in all cores (Fig. 4.8). The pollen analysis indicates a strong anthropogenic influence, as a result of forest clearing and agricultural activities. The growing population of the Bronze Age results in rising soil erosion, which is reflected in the Holocene river activity from Germany (Hoffmann et al., 2008). The period after 4000 b2k shows the highest flood activity at all, although it is the only flood stage which belongs to a warm phase. The increase of the flood frequency is therefore a combination between higher amounts of precipitation and in particular the human impact.

4.9 Conclusions

The understanding of magnitudes and frequencies of flood events are still limited, although they are one of the most important natural hazards in the world. Flood layers in maar sediments represent an environmental history based on individual events. Consequently, flood layers provide a proxy archive with unique environmental information, depending on local conditions like vegetation and permafrost. Our time-series from the Eifel represents the first highly-resolved flood frequency record for the last 60 000 years and indicates variable periodicities of flood activity linked to predominant climatic and anthropogenic development. The maximum flood phases in the Eifel reflect regional and global climate fluctuations. They are clustered in the periods from 11 500 to 17 500 (late glacial and Younger Dryas), 23 000 to 24 000 (before GI 2), 29 000 to 35 000 (especially between GI 5 and 4) and 44 000 to 44 500 b2k (transition from GI 12 to 11). Summarized, episodes with high frequencies of extreme flood events were found to be associated with periods of cool and wet climate, whereas episodes with low frequencies of extreme floods were related to periods of warm and constant climate. However, during the late Holocene land use related to the human impact has been the main trigger for the increase of flood events. It turns out that low vegetation coverage related to Greenland

stadial phases or anthropogenic impact are the main causes for the development of flood layers in maar sediments, while precipitation plays only a secondary role. This interpretation of our data is consistent with several studies of fluvial erosion related to vegetation coverage (Mol, 1997; Macklin et al., 2002; Vandenberghe, 2003).

Acknowledgments

This work is financed by the German Science Foundation (DFG; project number: SI 594/32-1).

Chapter 5

Reconstruction of the Stadial – Interstadial flood frequency from dry maar structure Auel and laminated Eifel maar sediments

H. Brunck¹, P. Fischer², T. Wunderlich³, A. Vött², F. Sirocko¹

(1) Institute for Geosciences, Johannes Gutenberg-University, 55128 Mainz, Germany

(2) Institute of Geography, Johannes Gutenberg-University Mainz, 55128 Mainz, Germany

(3) Institute of Geosciences, Christian-Albrechts-University of Kiel, 24118 Kiel, Germany

A slightly modified version of this chapter has been submitted to “Journal of Limnology”.

Note:

Based on recent analyses and results from dry maar Auel, the existing stratigraphy of Auel had to be slightly updated. These changes have been made only in the range of centuries. However, this leads to minor differences in the absolute age of the tephra marker layers and the number of flood layers per millennium between Chapter 4 and Chapter 5.

5.1 Abstract

Lake sediments can record past floods in the form of coarser-grained laminations that reflect the capacity for river flows with greater hydrodynamic energy to transport larger particles into the lake. This study reconstructs the main flood phases in Central Europe from event layers in sediment cores from three Pleistocene maar structures. The cores were drilled in the Eifel region of western Germany and were dated by ¹⁴C, luminescence, tephra markers and ice core tuning.

From 10 000 to 70 000 b2k a total of 152 flood layers over 7.5 mm were detected in the sediment cores from Auel, Roth and Merscheid. The 6 main flood stages in the glacial – interglacial cycle are from 10 000 to 17 500 b2k, from 21 500 to 24 000 b2k, from 26 000 to 35 000 b2k, from 39 000 to 47 000 b2k, from 51 500 to 54 500 b2k and from 60 500 to 64 000 b2k. The analyses confirm the fact that several Eifel maar structures are suitable for creating a flood time series, although the most precise and highly resolved flood record is only preserved in Auel. The maximum flood phases in the Eifel reflect regional and global climate changes. The flood system is controlled by a combination of the local to regional factors vegetation, precipitation and sediment transport. Consequently, the flood events most likely document the erodibility of the soils to the first order, and climate events only to the second order.

5.2 Introduction

The west Eifel region in Germany has 7 maar lakes and a total of 61 silted up maar structures (Büchel, 1993). Coring in the maar lakes produced the first palaeoclimate records from Central Europe based on varve chronologies for the Holocene and late glacial (Brauer, 1994; Litt and Stebich, 1999; Negendank et al., 1990; Zolitschka, 1998). Most of the maar lakes and dry maar structures have been systematically drilled since 1998 from the Institute for Geoscience, Johannes Gutenberg-University Mainz, Germany as part of the ELSA Project (Eifel Laminated Sediment Archive) to extend the Holocene chronologies to the Pleistocene. First results of the stratigraphy were published in Schaber and Sirocko (2005) and Sirocko et al. (2005). The latest scientific publication combined the recent stratigraphy with the history of climate, environment and vegetation in Central Europe during the last 60 000 years (Sirocko et al., 2016).

Records of the flood frequency are needed on centennial or millennial timescales to place the occurrence and the intensity into a larger scale as possible by historical records and gauge data. Lakes that are used for the Holocene climate reconstructions are numerous in the landscape of Central Europe (Brauer et al., 1999; Litt et al., 2001; Mayewski et al., 2004; Magny et al., 2007; Zolitschka, 1992). However, lakes that have the potential to reconstruct the climate conditions between 10 000 and 60 000 b2k in Germany are restricted to the Eifel. Other suitable locations for this time interval were found in France (Ampel et al., 2008; Wilhelm et al., 2013; Wohlfahrt et al., 2008) and southern Italy (Brauer et al., 2001), and thus in regions with another climate forcing. Small basins, like

maars, with long water residence time and anoxic bottom water are perfect climate archives. If these lakes are fed by small creeks they are also suitable as flood archive. The suspension layers can be distinguished from background sedimentation and other event layers (seismites, turbidites and slumps) macroscopically or in thin sections (Adams et al., 2016; Brunck et al., 2016; Gilli et al., 2003; Marco et al., 1996; Moreno et al., 2008; Mulder et al., 2003; Sturm et al., 1995; Wirth et al., 2011). So far, the ELSA-Flood-Stack₂₀₁₆ (Brunck et al., 2016) is the first high resolution European dataset of flood frequency for the entire last 60 000 years. The flood events from dry maar Auel are sourced from a creek flowing into the maar lake and thus representing the local precipitation extremes. A comparison of modern gauge data shows that the small flood events in the Eifel creeks, correlate on a statistical basis, with events of the river Rhine (Pfahl et al., 2009). Thus, the local flood event history recorded in Auel is likely representative for the Central European flood history.

In this study, the flood frequencies of the Merscheid maar and the Roth maar are added to the flood record of the Auel maar to reconstruct the glacial – interglacial flood frequency for the last 70 000 years. The key objectives are: (1) to present new stratigraphical results of the unique maar structure of Auel; (2) to subdivide all maar structures of the west Eifel region into hydrological groups according to the best study tracers; and (3) to compare the flood history of Auel with the new flood results from the maar structures of Merscheid and Roth to define the main glacial – interglacial flood phases.

5.3 Regional setting

Sediment cores from three different Pleistocene dry maar structures are used to reconstruct the flood activity in the Eifel region for the last 70 000 years (Fig. 5.1). Additionally, Fig. 5.2 provides an independently developed geological map of the region with the maar structures Auel, Merscheid and Roth. The morphology of the maar structures is described below.

5.3.1 Auel dry maar

The silted up basin of Auel is one of the largest dry maar structures of the Eifel with a diameter of 1325 m (Seib et al., 2013). The modern Tiefer Bach flows through the maar centre from west to east. This river has a catchment area of 12.187 km² and a total length

of 9.4 km (Water management administration Rhineland-Palatinate: German river code 266374). The core AU2 from the centre of the maar is 123 m long and covers the time from the Laacher See eruption (Förster and Sirocko, 2016) back to 60 000 b2k. The short core AU8 is used for the generation of the transition zone in Auel (Figs. 5.4 and 5.6). The average sedimentation rate of dry maar Auel of $2 \frac{mm}{a}$ is the highest ever measured of all Eifel maar structures, due to the abundant fluvial input. Therefore, flood events and associated suspension injections are seasonally resolved and clearly visible in the sedimentary record.

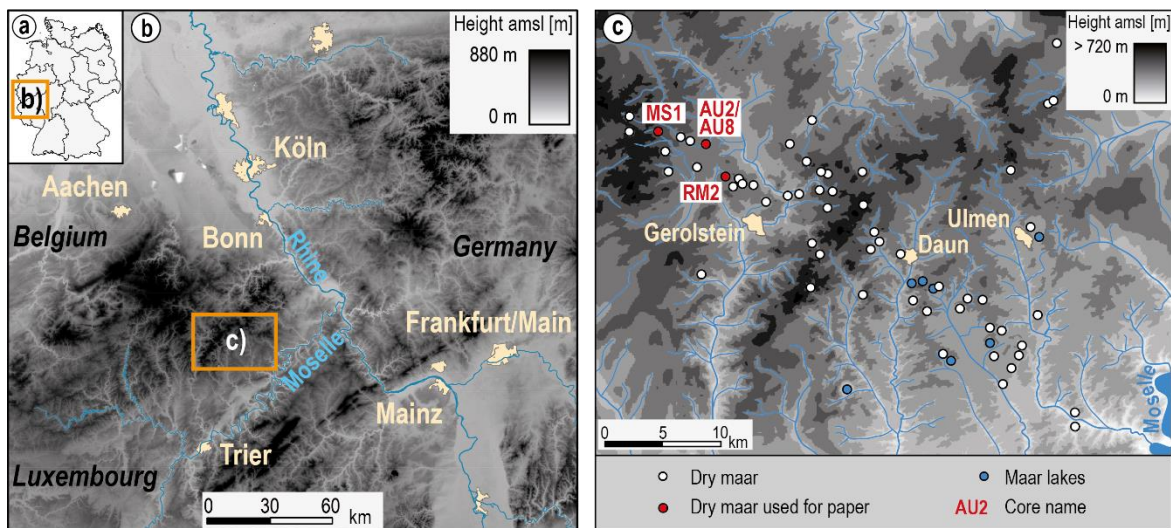


Fig. 5.1: a) Outline map of Germany. b) Digital terrain model of central western Germany and surroundings including the drainage system. c) Digital terrain model of the Eifel showing maar locations after Büchel (1993), drainage system and core positions: AU2 (German Grid Zone 2 (GK-System) 2542455/ 5572017), AU8 (GK-System 2542509/ 5572020), MS1 (GK-System 2538562/ 5573162) and RM2 (GK-System 2543958/ 5569786).

5.3.2 Merscheid dry maar

The Merscheid dry maar is located approximately 4.5 km west of the Auel dry maar. The maar is slightly smaller than the Roth dry maar with a diameter of 771 m (Seib et al., 2013) and a sediment thickness of 50 m. The sedimentary record contains the time window between 24 000 and 70 000 b2k. The Mannebacher creek flows from west into the maar and turns to the south in the centre of the maar. The creek has only a regional catchment area of 1.78 km² and a length of 1 km before it reaches the maar. Nevertheless bigger flood events are clearly visible in the core material.

5.3.3 Roth dry maar

The Roth dry maar has a diameter of 823 m (Seib et al., 2013) and is located 5 km southeast from Auel. Thus, the maar counts to the larger maar structures of the Eifel region. The core RM2 from the middle of the maar is 65 m long and covers the time from 10 000 back to 65 000 b2k. The Rother creek flows through the maar centre and leaves the dry maar at the opposite side, similar to the dry maar structure of Auel. However, the catchment area of the creek is with 2.33 km² significantly smaller than Auel (Water management administration Rhineland-Palatinate: German river code 266462).

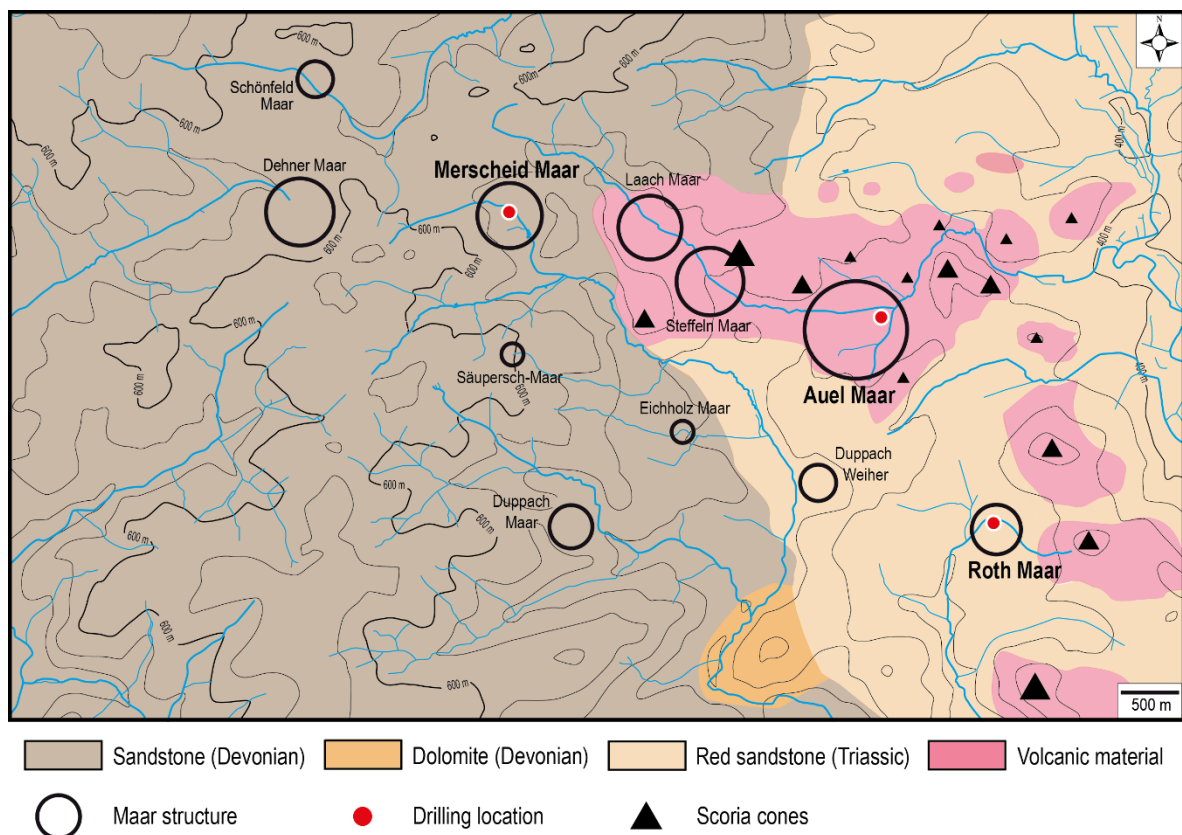


Fig. 5.2: Geological overview map of the maar structures Auel, Merscheid and Roth with the exact core position.

5.4 Material and methods

All cores from the ELSA project have been drilled either from open maar lakes with freeze core and Niederreiter technology, or from silted up dry maar structures with the Wireline coring technology (Sirocko et al., 2013). At the dry maar structure Auel geophysical measurements were combined with sediment coring and Direct Push Electrical Conductivity (DP-EC) logging in order to decipher the local stratigraphy of the shallow

subsurface along one transect (Figs. 5.4 and 5.5). Electrical resistivity tomography (ERT) measurements were conducted using a multi-electrode device (type Syscal R1 Plus Switch 48, Iris Instruments) and a Wenner-Schlumberger electrode array with 48 electrodes and 5 m spacing. ERT inversion was carried out using BERT (Boundless Electrical Resistivity Tomography, Günther et al., 2006). The subsurface model consists of triangular cells that become larger towards greater depths. The increase of cell size corresponds to the decrease of structural resolution of ERT with depth (Fischer et al., 2016). To calibrate ERT results, we conducted five DP-EC logs using a Geoprobe SC520 soil conductivity probe. Electrical conductivity in unconsolidated sediments is mainly controlled by sediment mineralogical characteristics, moisture content and the chemical composition of the pore water (Schön, 2004). In general, higher electrical conductivities typically represent finer sediments, such as silt and clay, while sand and gravel have distinctively lower conductivities (e.g. Fischer et al., 2016; Wunderlich et al., 2013). Ionic contaminants possibly increase the conductivity of the soil (or sediment) (Direct Image, 2008). The EC probe is composed of 4 electrodes in linear arrangement and was operated in a Wenner electrode array enabling a vertical resolution of 0.02 m (www.geoprobe.com; for further details see Fischer et al., 2016). Inverse values of electrical conductivity are defined as electrical resistivity (Fig. 5.5). Coring was conducted using a drill rig (type Nordmeyer RS 0/2.3) and closed steel auger with core diameters of 50 mm of inlying plastic liner. Sediment cores were splitted, cleaned and photo-documented in the laboratory. Position and elevation of coring sites and ERT measurements were measured using a DGPS (type TOPCON HiPerPRO).

The hydrological classification of the entire Eifel maar structures in different groups was carried out by evaluation of aerial photographs and a detailed analysis in the destination area over the last 3 years. Pleistocene sediments of infilling Eifel maar lakes are normally yellowish to brown, and have abundant quartz and clay minerals. Discrete volcanic ash layers are easy to recognize, because of their grayish to black colour and the formation of usually well-defined layers of coarser grained material in the silt to fine sand fraction (Sirocko et al., 2013). Every succession of a tephra were petrographically studied in 10 cm long thin sections and sampled equidistantly over its exposure in the core, achieving an average mineral composition of each event.

The tephra layers were sieved to extract the 250 – 125 µm fraction. This fraction was analysed for characteristic grains of reddish and grayish sandstone, quartz, amphibole, pyroxene, scoria, pumice, sanidine, leucite and mica by using a picking tray and a

binocular microscope with 20 – 40 x magnification. The particular grain selection was chosen due to its high abundance in the tephra, ease recognition, as well as physical and chemical stability. To characterize the individual tephra layers, a minimum of 100 grains were counted and sorted into their groups. The grain counts are presented as the % abundances of each group and were plotted as bar graphs (for more details see Förster and Sirocko, 2016).

Three sediment cores (AU2, MS1 and RM2) were visually and lithologically examined to identify flood layers over 7.5 mm thickness. Some flood layers are several cm thick and visible macroscopically (Figs. 5.9 to 5.11). Others are mm thick and were petrographically studied in 10 cm long thin sections under an Olympus U-TTBI microscope to distinguish them from distal turbidites and distal slumps. A detailed description for the preparation of thin sections can be found in Seelos and Sirocko (2005). The time series of the flood events is not presented as a table of dated flood events. Instead, the number of flood events is given per millennia to show only the times of maximum flood activity. This method improved the identification of phases with increased flood frequency and has already been applied for the ELSA-Flood-Stack₂₀₁₆ (Brunck et al., 2016).

5.5 Results

5.5.1 Stratigraphy

22 Wireline drill cores of a length between 10 and 160 m were dated by 320 ¹⁴C dates (Sirocko et al., 2013) and Greenland ice-core tuning (Sirocko et al., 2016). The most important core of the ELSA Project was retrieved from the dry maar of Auel in the drilling phase of 2013. The 123 m long AU2 core contained the Laacher See Tephra (12 880 +/- 30 b2k; Brauer et al., 1999) at 13.8 m depth and an organic carbon time-series of 100 year resolution was measured.

The specific sedimentation conditions of Auel with $2 \frac{mm}{a}$ explain the unique possibility to detect all 17 Greenland interstadial (GI) in the organic carbon concentration of this dry maar (Sirocko et al., 2016). Finally, the time series of C_{total} was tuned to the Greenland ice core chronology GICC05 (Svensson et al., 2008) to link the Central European landscape evolution directly to the Greenland climate curve (Sirocko et al., 2016) (Fig. 5.3). The allocation of the core material to all Greenland interstadials and

stadials enables the exact climatic interpretation of the flood records. Thus, the ELSA age depth model has the same error as the Greenland ice core chronology after Svensson (2008) at the tuning points (Fig. 5.3). Between the tuning points, the age depth model was verified by tephra layers, ^{14}C data and pollen analyses (Sirocko et al., 2016).

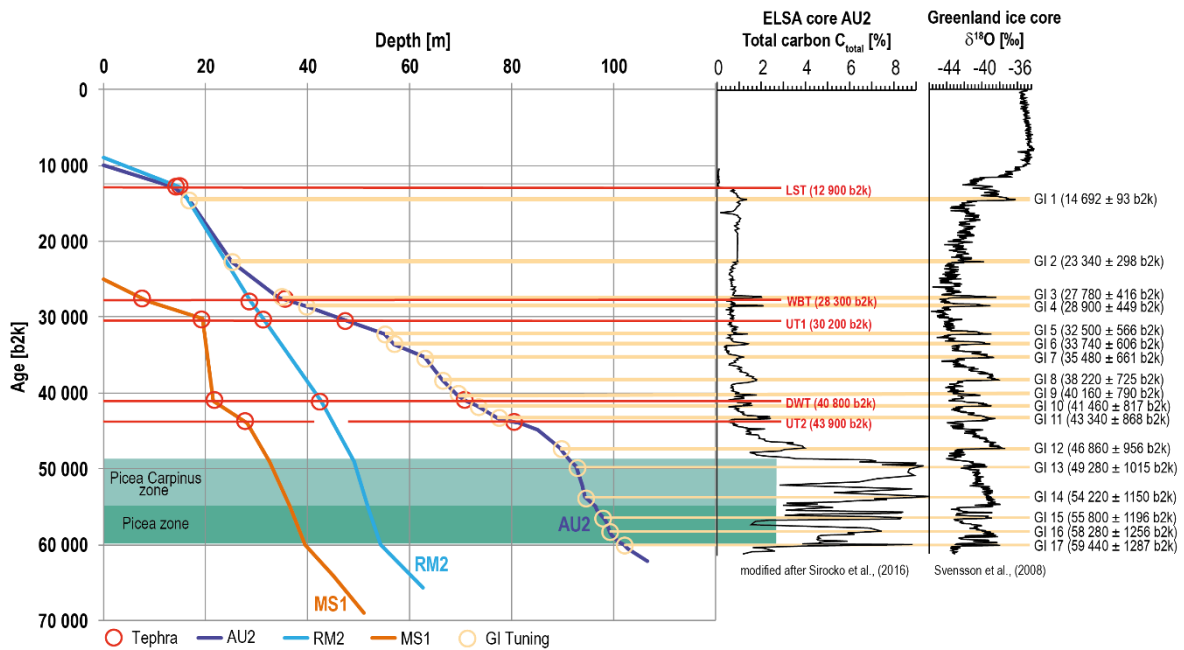


Fig. 5.3: Age/ depth model for cores AU2, MS1 and RM2. In addition, the C_{total} from Auel is directly tuned to the GI 1 – 17. All tuning points are directly projected onto the age model. The Picea-Carpinus zone and the Picea zone are colour-coded (Sirocko et al., 2016). Visible tephra layers are represent by red lines and marked with red circles in each core (Förster and Sirocko, 2016).

The local stratigraphical composition of Auel was analysed with ERT 1 for a geoelectrical classification of the upper 20 m of the infill (Figs. 5.4 and 5.5). Due to the fact that this section contains only the Laacher See Tephra and no GI assignments, the investigation of upper 20 m improves the stratigraphical information for the silting up area of the maar structure. The transect clearly shows high resistivity values close to the surface from the start in the southwest up to approx. 150 m distance that significantly decrease with depth. From 150 m to the end in the northeast, the unit of high resistivities disappear. In this part relatively low resistivity values reach to the top of the transect. The general structure is well reflected by the DP-EC logs 1 – 4 that show highest resistivities in the upper parts and decreasing values towards their base. In contrast, DP 5 also shows high resistivities closed to surface which are not resolved by the surface based ERT measurements.

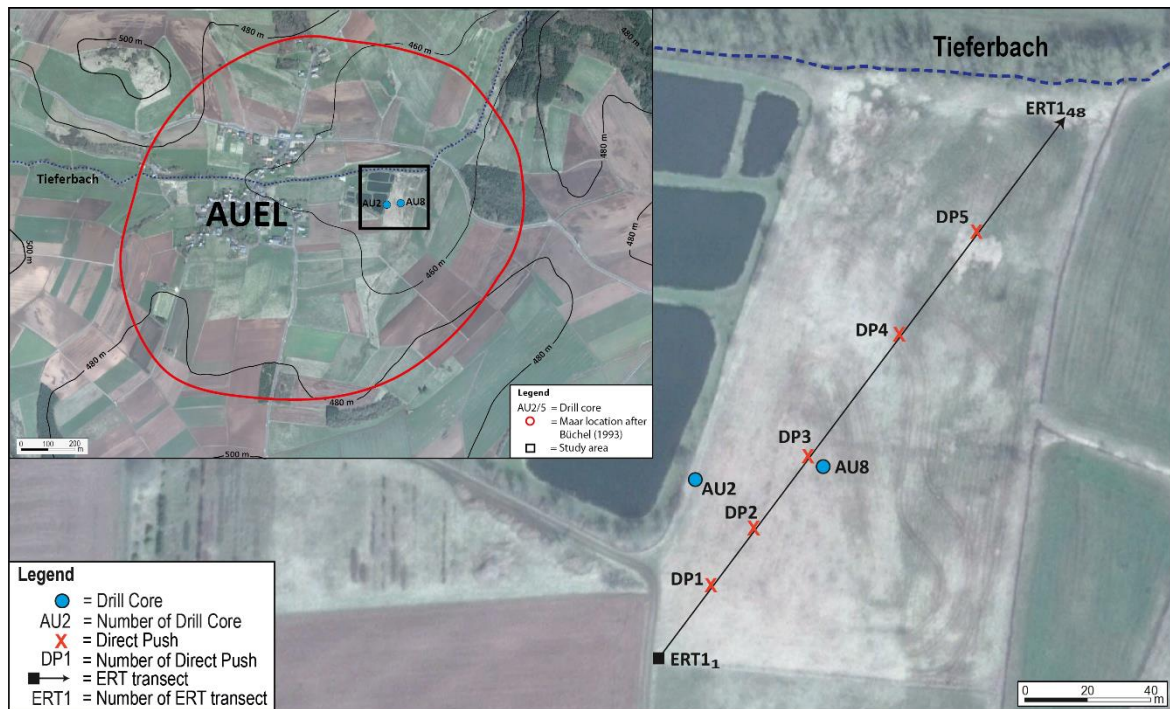


Fig. 5.4: Overview of the study area and field work location of Auel. ERT transect, coring sites and DP-EC sites were measured using a Topcon HiPer Pro DGPS device (type FC-250).

The DP logs show that the higher-resistant layer continuously thins out towards the end of the ERT transect being too thin to be resolved by ERT data alone (see discussion in Fischer et al., 2016). Greatest discrepancies between the ERT measurement and EC logging can be observed for DP 3. Here, a layer of high resistivities occurs in a depth of 9.7 – 10.8 m below surface which is not visible in the inversion results of ERT 1. Comparing the EC log with core AU5 (Fig. 5.6), which was drilled only a few metres to the southeast it can be stated that the EC log well reflects the stratigraphical units as described for the sediment core. The upper 3.6 m of the sequence are generally characterized by relatively low conductivity (= high resistivity) values intersected by thin layers of higher conductivity. The reddish coarse grained layer between 3.35 and 3.66 m as detected in the sediment core is clearly depicted within the log in greater thickness showing constantly low conductivity values. Below this coarser layer, conductivities significantly increase indicating finer material which was also observed within the sediment core. The coarse grained layer between 9.7 – 10.8 m as described above is again characterized by low conductivity values.

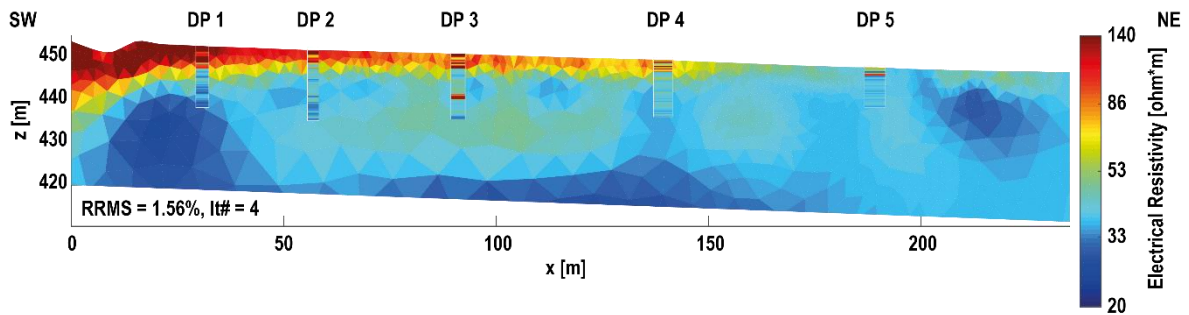


Fig. 5.5: Unconstrained inversion model of ERT 1 and DP EC logs 1 – 5 that were converted to electrical resistivities using the identical colour scale.

Towards the base of the log (Fig. 5.6) conductivity values increase again indicating reduced input of coarse grained material and dominating quiescent depositional conditions. Overall, results show that the stratigraphical composition of the shallow subsurface in this case is well reflected by the surface based ERT measurements. In addition, ERT results are in good agreement with the EC logs, apart from coarser layers which are too thin to be resolved by the ERT inversion (Fischer et al., 2016).

The combination of ERT data, DP EC logs and core data significantly enhance the existing stratigraphy of Auel in the upper 20 m and provide for the first time helpful insights into the local structure of the maar compared to point data from single drill cores. Therefore, it is now possible to classify the 31 flood layers in the upper 20 m of Auel more precisely. The complete sequence from Auel contains five distinct tephra layers, up to several cm-thick. These tephra layers can also be found in the ELSA cores MS1 and RM2 and allow a secure inter-maar core to core correlation with ages from the Greenland ice core chronology (Figs. 5.3 and 5.7). The resulting multiproxy age model is used to date tephra layers of the last 100 000 years (Förster and Sirocko, 2016) (Figs. 5.3 and 5.7). Tephrochronology is a well-established method for the geochemical fingerprinting and dating of volcanic particles.

During the last decades tephrochronology has been developed into a powerful correlation tool with large applicability in stratigraphic, chronologic and palaeoclimatic studies by providing unique non-climatic marker horizons (Lowe, 2011). Tephra layers of individual volcanic eruptions are traced in several cores from Eifel maar lakes and were characterized by the petrographic composition of basement rock fragments, glass particles and volcanic minerals (Förster and Sirocko, 2016).

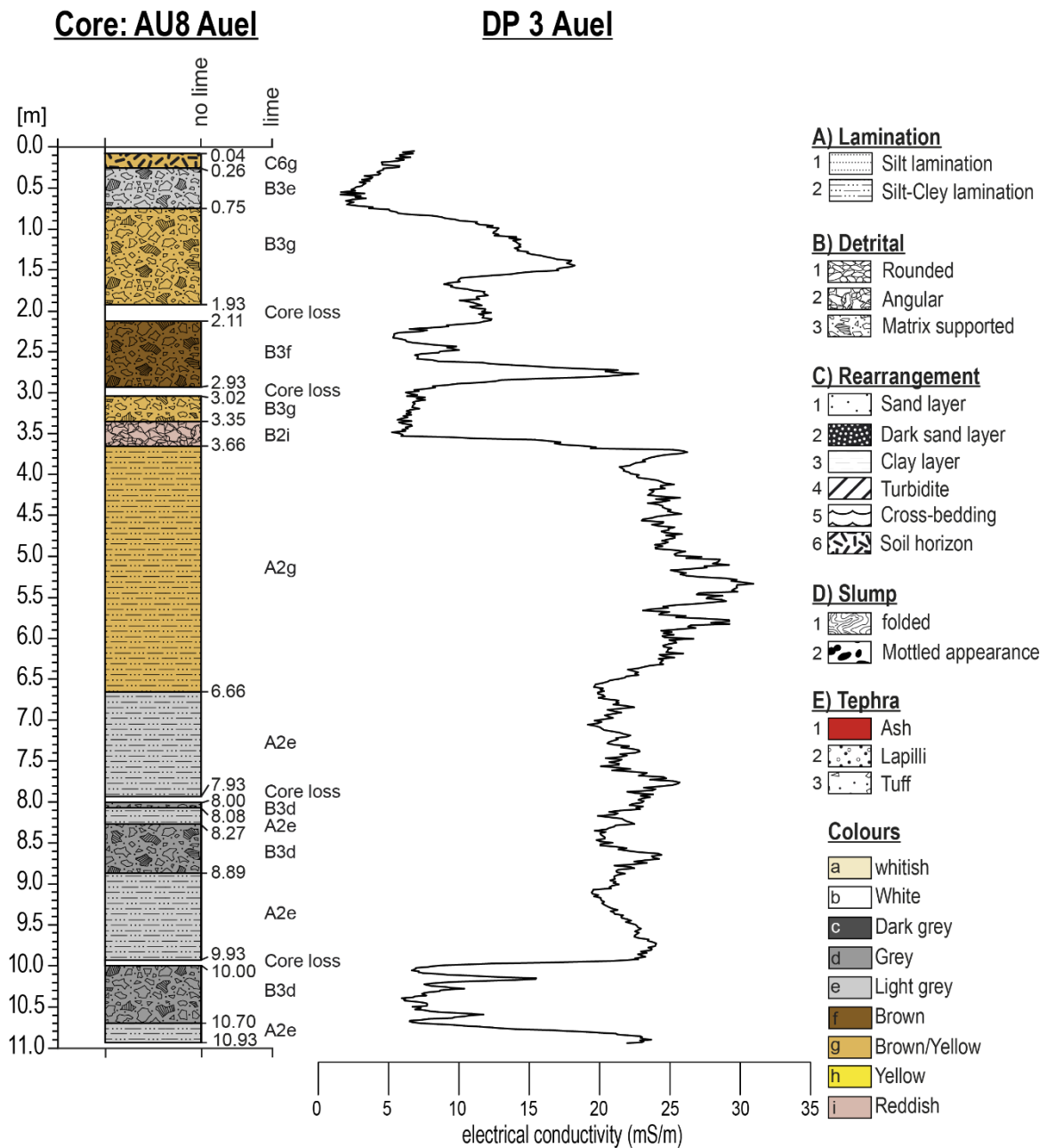


Fig. 5.6: Stratigraphical log of core AU8 and electrical conductivity values of DP 3 depicted in $\frac{mS}{m}$. Note that the resolution of the EC log exceeds the accuracy of layer boundaries as detected in the sediment core.

Figure 5.7 shows the grain count ratios of the marker layers from the Laacher See, Wartgesberg, Dreiser-Weiher, unknown origin UT1 and unknown origin UT2. In addition, images of the respective tephra layers from the cores AU2, MS1 and RM2 are also presented in Fig. 5.7. Based on this stratigraphical concept, a classification of landscape evolution zones, shortly LEZ, were developed (Sirocko et al., 2016). The LEZ reconstruct the vegetation and the climate change mostly based on macroremains and pollen since

60 000 b2k. The detailed results from the stratigraphy are presented in the paper from Sirocko et al. (2016).

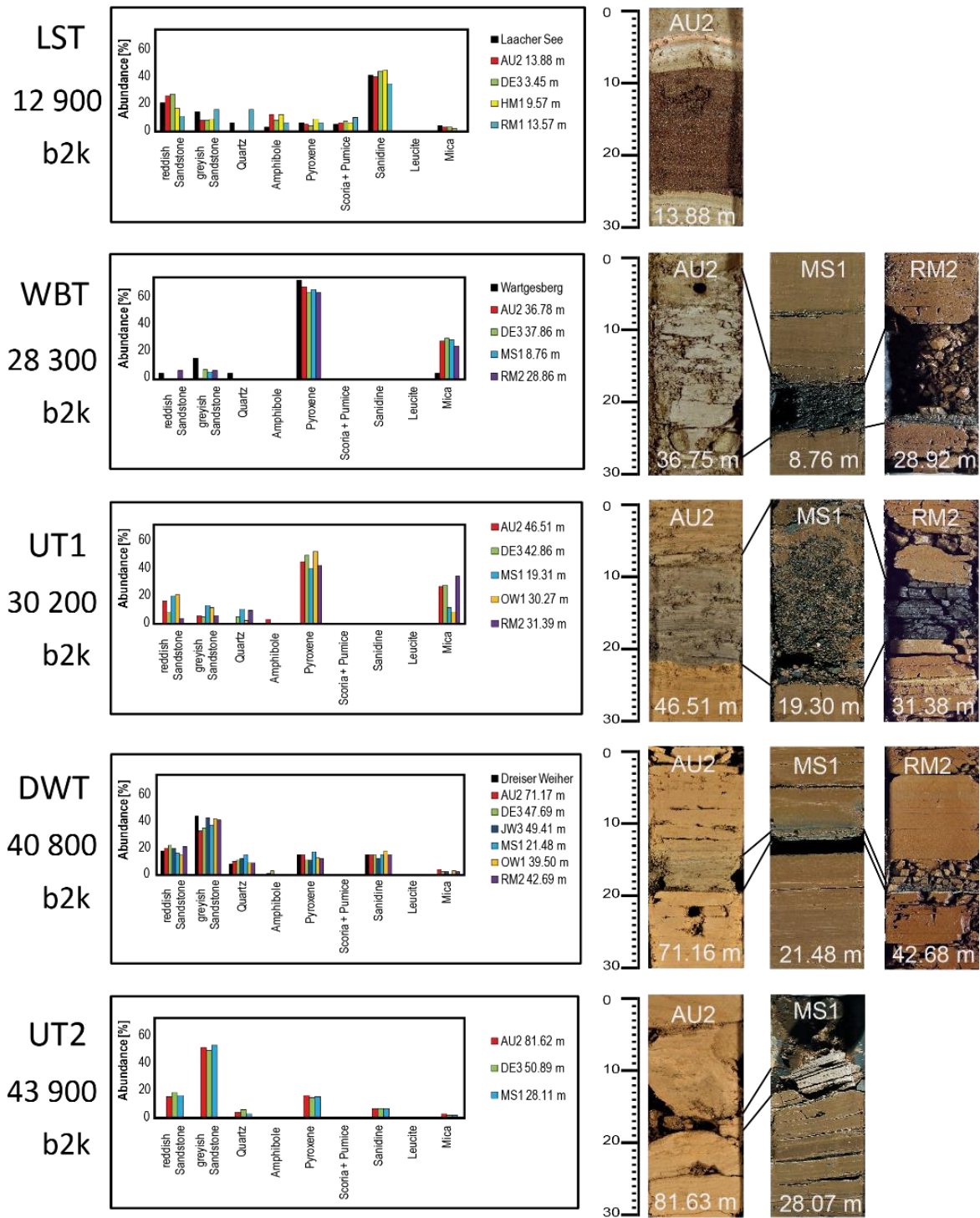


Fig. 5.7: Grain count ratios of the marker layers from Laacher See, Wartgesberg, Dreiser-Weiher, unknown origin UT1 and unknown origin UT2. The ages for the marker layers are from ^{14}C dates and ice core tuning (Sirocko et al., 2016; Förster and Sirocko, 2016).

5.5.2 *Reconstruction of the glacial – interglacial flood frequency*

Extreme meteorological events such as heavy rains and the resulting flash floods had a major impact on the environment and society. A comparison of modern gauge data shows that the small flood events in the Eifel creeks correlate on a statistical basis with the events described for the river Rhine (Pfahl et al., 2009). Thus, the record of flood layers in a maar system, fed by local rivers, could be directly linked with floods in the Rhine valley for the last 200 years (Brunck et al, 2016), which are historically well documented (Bork et al., 1998; Stolz and Grunert, 2008). The Eifel maar lakes are the only location that allows generating long time series with event resolution in Central Europe (Sirocko et al., 2016).

Despite the same genetic origin each maar lake has an individual limnological character and sediment composition. This is caused by differences in size, depth, morphological setting and hydrological conditions. For this reason, the numerous maar structures of the Eifel region are particularly suitable for various research questions.

The intensive analysis of aerial photographs combined with regional spot investigations over 3 years for each Eifel maar structure led to an accurate classification of the hydrological environment (Fig. 5.8). The maar structures were divided into 4 classes with the following features:

- Group 1: Closed Basin, no inflow or outflow; well suited for lake level changes and precipitation analysis.
- Group 2: Bypass, a creek flows in close vicinity to the maar lake; well suited for extreme flood events.
- Group 3: Throughflow, a creek runs right through the maar lake; well suited for all flood events.
- Group 4: Outflow, no real inflow (only the precipitate from the slope) in combination with an outflow; well suited for dust reconstruction or lake level analysis.

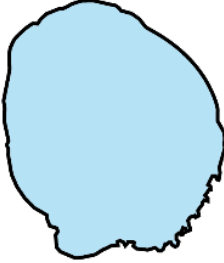
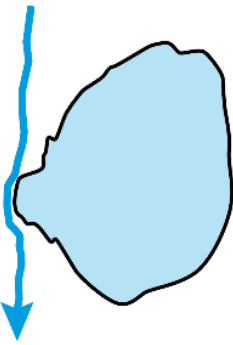
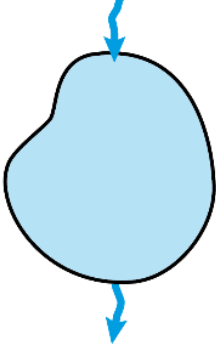
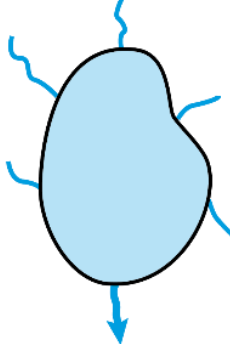
Maar structure			
Closed basin	Bypass	Throughflow	Outflow
			
Well suited for: • lake level change • precipitation	• only extreme flood events	• all flood events	• dust • constant lake level
Maar type A: Pulvermaar Weinfelder Maar Lierwiesen Maar Gemündener Maar Maar am Hohen List Dürres Maar Strohner Maar Trautzberger Maar Hardt Maar	Maar type B: Holzmaar Ulmener Maar Duppacher Maar Duppacher Weiher Oberstadtfelder Maar Sprinker Maar	Maar type C: Auler Maar Merscheider Maar Rother Maar Schönfelder Maar Laach Maar Kerpener Maar Hohenfelser Maar Kirchweiler Maar Seiderather Maar Geeser Maar Steinborner Maar Meerfelder Maar Dreiser Weiher Hengstweiler Maar Wallenborner Maar Döttinger Maar Schalkenmehrener Maar	Maar type D: Dehner Maar Eigelbach Maar Jungferweiher Wollmerather Maar Walsdorfer Maar Essinger Maar Immerather Maar Immerather Risch Maar western Hohen List Gerolsteiner Maar Oberwinkeler Maar Steineberger Maar Mürmes Moosbrucher Maar Ellscheider Maar In der Boos Mehrener Maar Säupersch Maar

Fig. 5.8: Subdivision of the maar structures from the west Eifel region into groups according to their hydrological background. Maar type C includes the investigated maar structures and represents best conditions for possible flood layers recorded in the sediments.

For the reconstruction of the glacial – interglacial flood frequency, three maar structures from group 3 (Auel, Merscheid and Roth) were compared with the Greenland ice core chronology, regarding the number and the timing of flood layers. The selected maar

structures are all fed by local creeks, which transport coarser-grained suspended sediment into the lake where it is deposited and preserved. The cores AU2, MS1 and RM2 represent the time interval from the LST up to 70 000 b2k (Fig. 5.7).

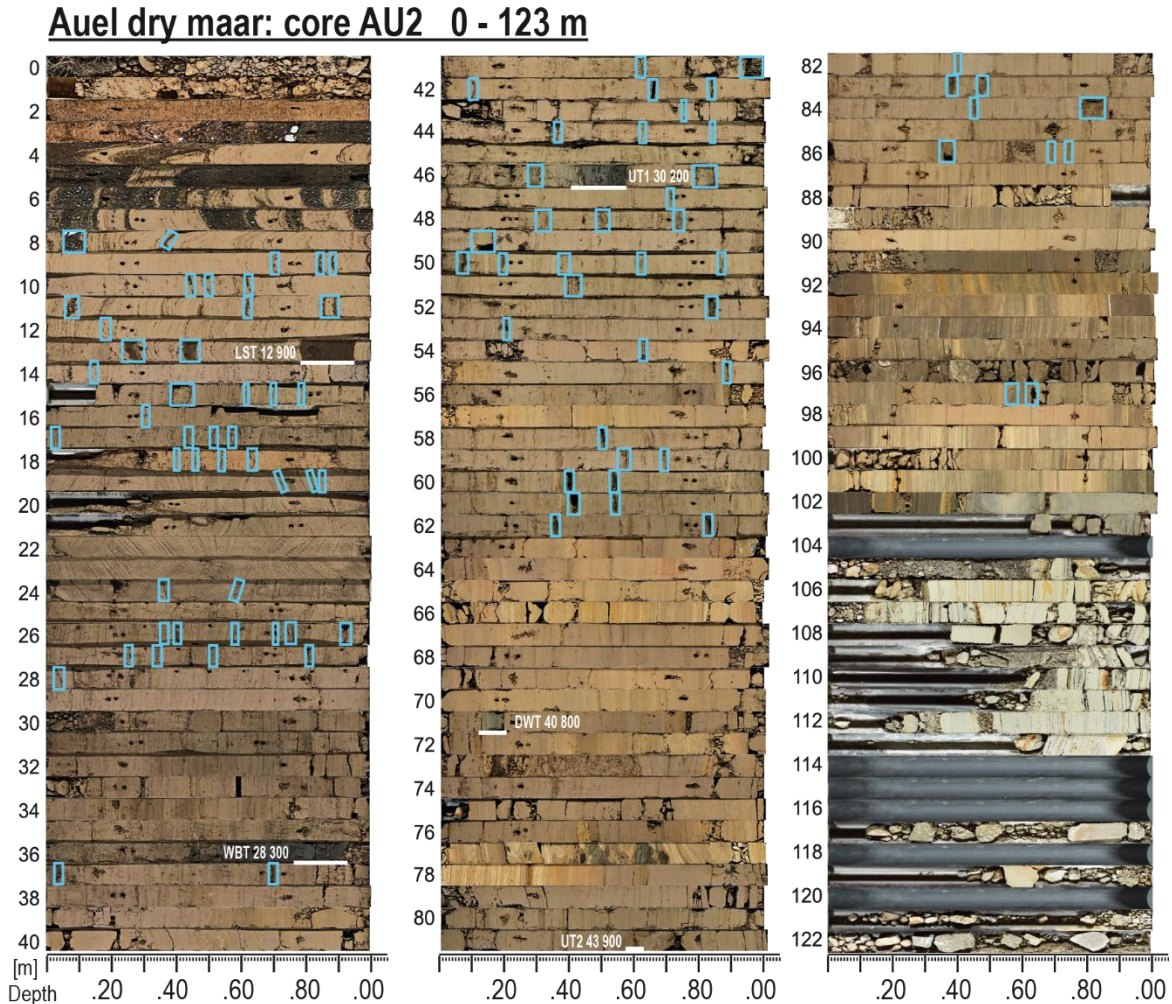


Fig. 5.9: Core AU2 with all detected flood events (blue boxes) and tephra layers (white lines). The first 7 metres cannot be analysed due to the coarse natural infill and strong anthropogenic impact. Core metres from 103 onwards count to the eruption phase.

A total of 152 flood layer over 7.5 mm were observed in all three sediment cores. Due to the distinct catchment areas and time relations of the maar structures, the flood events were classified in millennium steps (Tab. 5.1). Generally, 88 flood layers over 7.5 mm occur in AU2 (Fig. 5.9), 24 flood layers over 7.5 mm in MS1 (Fig. 5.10) and 40 flood layers over 7.5 mm in RM2 (Fig. 5.11).

In summary, the main flood stages for AU2 are from 11 000 to 17 500, 23 000 to 24 000, 27 500 to 35 000 and 44 000 to 45 500 b2k (Tab. 5.1 and Fig. 5.9) (Brunck et al., 2016). 12 strong flood events from 12 000 to 13 000 b2k represent the highest number of

flood events per 1000 years in the whole time series of AU2 (Tab. 5.1) and is comparable to the Younger Dryas (McManus et al., 2004).

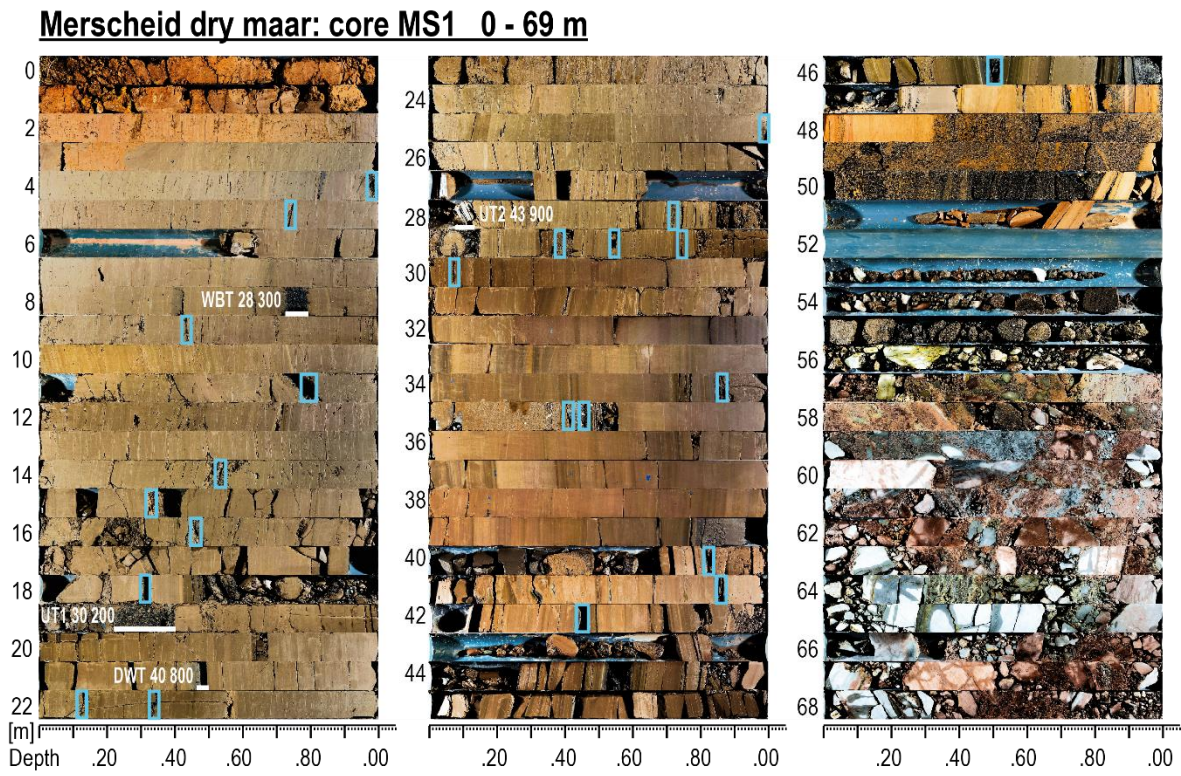


Fig. 5.10: Core MS1 with all detected flood events (blue boxes) and tephra layers (white lines). Core metres from 52 onwards belong to the eruption phase.

Core MS1 from Merscheid contains 24 flood layers and covers the time interval from 25 000 up to 69 000 b2k (Fig. 5.10). The flood layers occur in clusters and are primarily observed in the time period between 26 500 – 30 000, 41 000 – 46 000, 52 500 – 54 000 and 60 500 – 64 000 b2k (Tab. 5.1). The majority of the flood layers are focused in the millennium 29 000 – 30 000 and 45 000 – 46 000 b2k.

The Roth dry maar was investigated using core RM2 and covers the time period from 10 000 back to 65 000 b2k (Fig. 5.11). Core RM2 contains 40 flood events over 7.5 mm. Again, the detailed analysis of the flood layer showed several flood phases. These time intervals are from 10 000 – 15 000, 26 000 – 30 000, 42 000 – 47 000, 53 000 – 54 000 and 61 000 – 63 500 b2k (Tab. 5.1). The flood frequency reaches its peak during the Younger Dryas, from 29 000 – 30 000 and from 62 000 – 63 000 b2k.

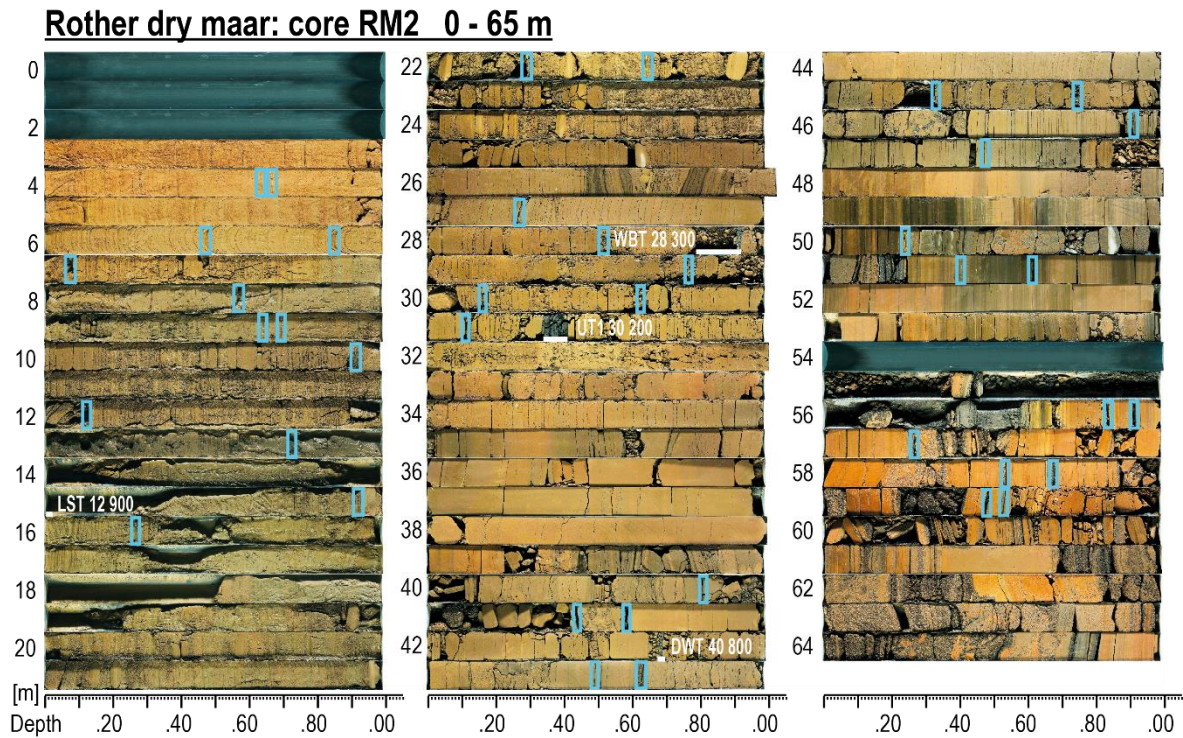


Fig. 5.11: Core RM2 with all detected flood events (blue boxes) and tephra layers (white lines). The core does not reach into the erupted material.

The comparison between the flood records of the three maar structures is provided in Fig. 5.12. The flood records clearly correlate with each other and forms 6 main flood stages in the period from 10 000 to 70 000 b2k. These are from 10 000 to 17 500 b2k (Phase 1), from 21 500 to 24 000 b2k (Phase 2), from 26 000 to 35 000 b2k (Phase 3), from 39 000 to 47 000 b2k (Phase 4), from 51 500 to 54 500 b2k (Phase 5) and from 60 500 to 64 000 b2k (Phase 6). However, there are also differences in the main flood phases; phases 1 and 3 are most pronounced and represent the Younger Dryas and the Greenland stadial 5, respectively, in particular the transition from GI 5 to GI 4 (Rasmussen et al., 2014). The analysis of the largest precipitation events in different maar structures does not indicate a local occurrence of flood events; instead it shows a trans-regional pattern suitable for Central Europe.

The maximum flood phases in the Eifel reflect regional and global climate changes. The regional driving factors such as vegetation, precipitation and erosion potential seem to overlap the global factors like Heinrich events (Hemming, 2004), Greenland stadial and interstadial (Rasmussen et al., 2014), Dust (Seelos et al., 2009) and Insolation (Berger and Loutre, 1991) (Fig. 5.12). Therefore, the regional driving factors are mainly responsible for the formation of flood layers in the Eifel maar structures.

Time interval	AU2	MS1	RM2
[b2k]	[n per 1000 a]	[n per 1000 a]	[n per 1000 a]
10 001 - 11 000	0		5
11 001 - 12 000	2		4
12 001 - 13 000	12		2
13 001 - 14 000	3		1
14 001 - 15 000	4		1
15 001 - 16 000	3		0
16 001 - 17 000	4		0
17 001 - 18 000	3		0
18 001 - 19 000	0		0
19 001 - 20 000	0		0
20 001 - 21 000	0		0
21 001 - 22 000	0		1
22 001 - 23 000	2		1
23 001 - 24 000	3		0
24 001 - 25 000	8		0
25 001 - 26 000	0	0	0
26 001 - 27 000	0	2	1
27 001 - 28 000	0	0	1
28 001 - 29 000	2	2	1
29 001 - 30 000	8	4	3
30 001 - 31 000	7	0	0
31 001 - 32 000	7	0	0
32 001 - 33 000	2	0	0
33 001 - 34 000	1	0	0
34 001 - 35 000	5	0	0
35 001 - 36 000	4	0	0
36 001 - 37 000	0	0	0
37 001 - 38 000	0	0	0
38 001 - 39 000	0	0	0
39 001 - 40 000	0	0	3
40 001 - 41 000	0	0	0
41 001 - 42 000	0	2	0
42 001 - 43 000	0	1	2
43 001 - 44 000	0	0	0
44 001 - 45 000	5	1	2
45 001 - 46 000	3	3	0
46 001 - 47 000	0	1	2
47 001 - 48 000	0	0	0
48 001 - 49 000	0	0	0
49 001 - 50 000	0	0	0
50 001 - 51 000	0	0	0
51 001 - 52 000	0	0	1
52 001 - 53 000	0	1	0
53 001 - 54 000	0	2	0
54 001 - 55 000	0	0	2
55 001 - 56 000	0	0	0
56 001 - 57 000	0	0	0
57 001 - 58 000	0	0	0
58 001 - 59 000	0	0	0
59 001 - 60 000	0	0	0
60 001 - 61 000		1	0
61 001 - 62 000		2	2
62 001 - 63 000		1	3
63 001 - 64 000		1	2
64 001 - 65 000		0	0
65 001 - 66 000		0	
66 001 - 67 000		0	
67 001 - 68 000		0	
68 001 - 69 000		0	
69 001 - 70 000			

Tab. 5.1: Number of flood events per 1000 years for the cores AU2, MS1 and RM2.

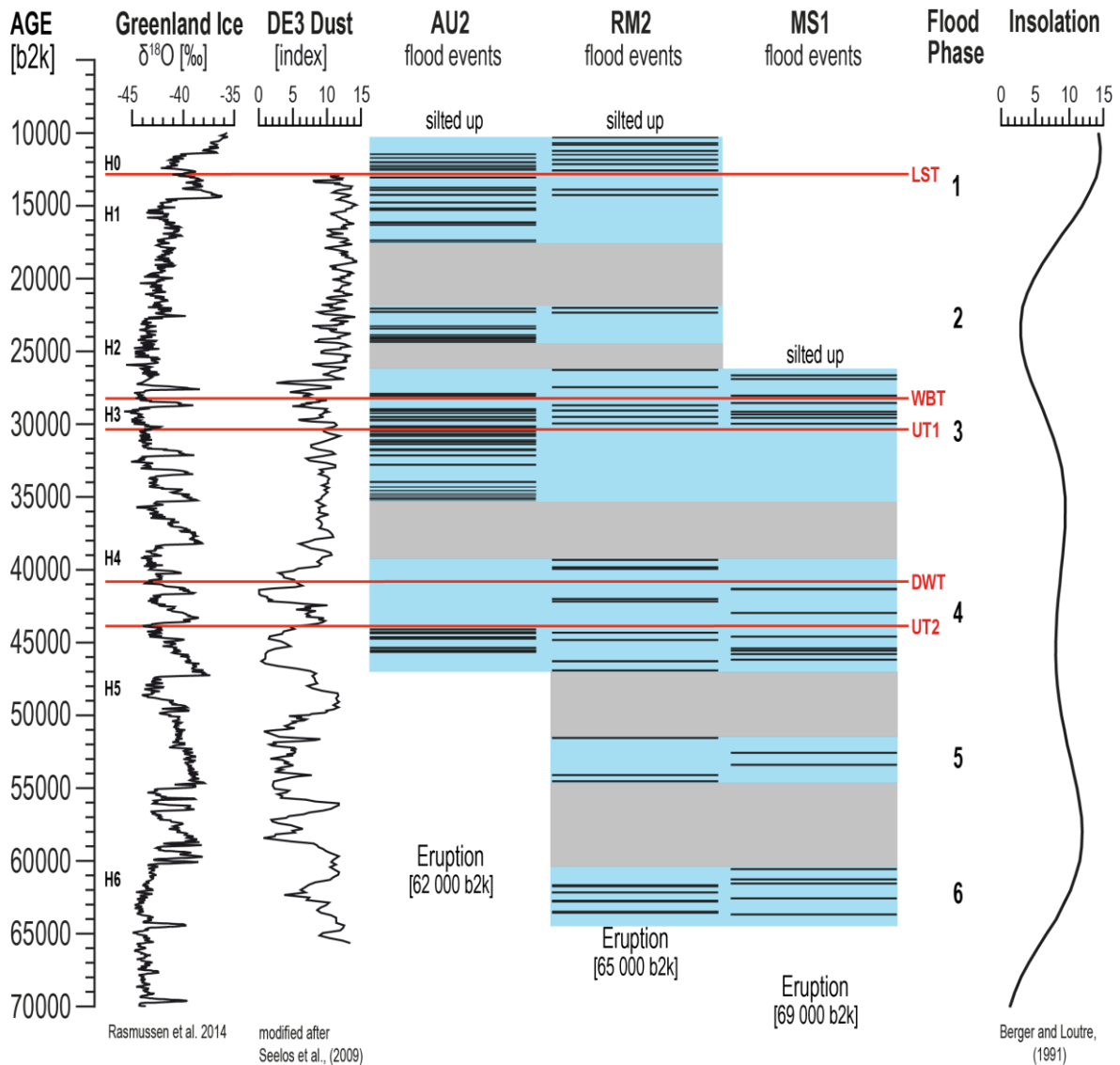


Fig. 5.12: Comparison of the flood records from Auel (Brunck et al., 2016) with the new results from the cores MS1 and RM2. The studied maar structures show related main flood phases, which are marked with the numbers 1 to 6. Additionally, the Greenland ice core isotopes time series (Rasmussen et al., 2014), the dust time series from DE3 (Seelos et al., 2009), visible tephra layers (red lines) and the insolation (Berger and Loutre, 1991) are shown.

5.6 Discussion

The aim of this study is to analyse the variances of the glacial – interglacial flood frequency in Central Europe and not to provide an absolute count of flood layers. The comparison between the flood histories of the three analysed maar structures clarifies the main flood phases of the last 70 000 b2k. However, there are also regional differences in

the frequency and temporal occurrence of flood layers. In this project, only the largest floods with layers thicker than 7.5 mm were investigated. Therefore, it is most likely that the magnitude of the inflow provides the main explanation for the regional differences. The dry maar structure of Auel has both the greatest inflow and the highest sedimentation rate of approximately $2 \frac{mm}{a}$. The combination of the highest sedimentation rate with the direct allocation of the organic measurement to the Greenland ice core demonstrates that only Auel yields the most precise and best resolved flood chronology. The Merscheid maar and the Roth maar have minor inflows and a lower sedimentation rate of $0.8 \frac{mm}{a}$ and $1.0 \frac{mm}{a}$, respectively. The described regional factors (e.g. sedimentation rate and greatest inflow) result in a greater sensitivity to floods in Auel and thus explain the faster reach of the lower analysis limit from 7.5 mm. This assumption is also confirmed by the correlation from the lowest sedimentation rate to the lowest amount of flood layers in dry maar Merscheid with only 24 flood layers. Cores MS1 and RM2 contain several minor disturbances thinner than 7.5 mm, especially in the time between 35 000 and 30 000 b2k. However, future analyses must show whether or not these layers are possible flood events or rearrangements.

A further chronological problem is probably associated with the tuning of the individual cores. If the sedimentation rate between two anchor points is not linear, the inaccuracy leads to temporal deviations of the flood events. The stratigraphy of the cores is precise and microscopic analysis of thin sections from the cores confirmed a constant sedimentation rate, so this error can be excluded.

Inevitably, the question arises why there are phases with increased flood activity and phases without flood activity. A distinct correlation of the flood phases to the Greenland glacial and interglacial conditions is not possible. Brunck et al. (2016) establish a relationship between low vegetation coverage, precipitation and the development of flood layers in maar sediments. This linkage can be confirmed by the extended analysis of the new data and explain also the absence of the flood layers in the times from 17 500 – 22 000 b2k, 24 500 – 26 500 b2k, 35 500 – 39 500 b2k and 47 000 – 60 500 b2k. The phases without flood events in the time interval from 17 500 to 22 000 b2k and from 24 500 to 26 500 b2k can be correlated with very cold climate sections. Both the Last Glacial Maximum and the Greenland stadial 3 turned the Eifel into an ice desert without vegetation (Anderson et al., 2006). Due to the lack of precipitation combined with the frozen soil, the erosion potential is very low and flood layers could not be formed. Flood

layers are absent in the time from 35 000 to 39 000 b2k which coincides exactly with the warm GI 8 (Rasmussen et al., 2014). This interstadial is the most pronounced of the past 40 000 years, with a strong vegetation increase and a corresponding decrease of the erosion potential. Thus, the dense vegetation stabilized the ground and prevented the occurrence of large flood layers in the Eifel maar lakes. Similar interpretations can be made for the time between 47 000 to 60 000 b2k, which exactly coincides with the Picea-Zone (LEZ 9) and the Picea-Carpinus-Zone (LEZ 8) (Sirocko et al., 2016) and represents a warm period (Sarala et al., 2016). A forested environment can be confirmed by pollen data from the Eifel region (Sirocko et al., 2016). The diverse vegetation reduces the erosion potential and prevents the formation of flood layers. Thus, the occurrence of few flood events in flood phase 5 represent extreme warm-season precipitation events, whereby a very strong suspension input into the maar became possible. These floods are comparable with the strength of the millennium flood 658 b2k (AD 1342) (Bork et al., 1998).

The dry maar structure of Auel contains no flood events in phase 5, although the maar is most sensitive to such events. In addition, a significantly higher proportion of organic content characterised the sediment of this period. This can be explained by the diminished oxygen in the water column and a much longer dwell time of the water in the maar lake. This supports the assumption that the maar system of Auel did not have any connection with the local creek in the development phase and thus, no flood layers were formed before 46 000 b2k.

The intensive analysis of the flood phases in comparison with various global climate forcings result in an irrelevant connection. The primary climate factors such as CO₂, Heinrich events and Insolation show no significant correlation with the flood phases in maar sediments (Fig. 5.12). The variations in flood dynamics are climatically driven and mainly associated with vegetation changes, thus reflecting climate response within the catchment areas. The complex flood system of the maar structures in the Eifel is highly correlated with the vegetation and precipitation in combination with the size of the inflow. Extremely cold, warm or stable climate phases minimize the formation of the flood layers in the maar structures, while phases of climate change and subsequent changes in vegetation are the ideal prerequisites for the formation of flood layers. Thus, the overall consideration of all factors leads to the conclusion that the flood layers reflect the predominant erosion potential and denudation processes of Central Europe for the last 70 000 years and not the precipitation in the first place.

5.7 Conclusion

Lake sediments can record past floods in the form of coarser-grained laminations that reflect the capacity for river flows with greater hydrodynamic energy to transport larger particles into the lake. Flood layers over 7.5 mm thickness show an inhomogeneous grain size gradient with several maxima representing the discharge pulses during the days or weeks of a flood event and not a grading. New geophysical results of the maar structure of Auel lead to a better understanding of the internal processes and improve the stratigraphy of the silting up period. The subdivision of the Eifel maar structures into hydrological groups according to the best study tracers makes the correct selection of the maar systems considerably easier. Now, it is possible to preselect the relevant maar structures according to the initial question.

The comparison between the flood frequencies of the three investigated dry maars show the same main flood phases in the analysed cores. The 6 main flood stages are from 10 000 to 17 500 b2k (Phase 1), from 21 500 to 24 000 b2k (Phase 2), from 26 000 to 35 000 b2k (Phase 3), from 39 000 to 47 000 b2k (Phase 4), from 51 500 to 54 500 b2k (Phase 5) and from 60 500 to 64 000 b2k (Phase 6). The analyses confirm the fact that several Eifel maar structures are suitable for creating a flood time series, although the most precise and highly resolved flood record was found in the Auel maar.

The variation in flood frequency is climatically driven and mainly associated with climate transitions. The maximum flood phases in the Eifel reflect regional and global climate fluctuations. Important is the independence of the main flood phases from the global climate forcings such as CO₂, Greenland stadial and interstadial and insolation. The flood system is controlled by a combination of the regional factors vegetation, precipitation and sediment transport. In summary, extremely cold, warm or stable climate phases minimize the formation of the flood layers in the maar structures, whereas climate change episodes and subsequent changes in the vegetation cover cause ideal conditions for the evolution of flood layers. Consequently, flood events most likely document the erodibility of the soils to the first order, and climate events only to the second order.

Acknowledgments

This study is financed by the German Science Foundation (DFG; project number: SI 594/32-1).

Chapter 6

Conclusion and Outlook

The understanding of magnitudes and frequencies of flood events are still limited, although they are one of the most important natural hazards in the world. For a comprehensive understanding of flood-generating climate mechanisms, long-term periods and regional patterns must be analysed. Palaeoflood hydrology opens up the possibility to extend existing flood chronologies into the past. Lake sediments can record past floods in the form of coarser-grained laminations that reflect the capacity for river flows with greater hydrodynamic energy to transport larger particles into the lake. The Eifel maar structures provide an ideal climate and sediment archive with precise chronologies and seasonal resolution. Flood layers in maar sediments represent the environmental history based on individual events.

The present study reconstructs the main flood phases in Central Europe from event layers in sediment cores from Holocene Eifel maar lakes and Pleistocene dry maar structures. For a better understanding of the sedimentation history, the focus of the “Palaeoflood project” was on the detection of event layers and the correlation of these layers between several maar structures. The frequency of flood deposits in the Eifel maar sediments allows a detailed reconstruction of the flood history in the context of climate development. The period of interest in this work includes, for the first time, a climate-related flood chronology based on recent gauge data combined with palaeoflood events from the Holocene and the late Pleistocene. A summary of the most important data is shown in the graphic 6.1. All three overarching objectives could be successfully implemented. The aim of developing a high resolution long time flood frequency record for the last 60 000 years as well as the proving of the natural and anthropogenic influence on the flood frequency were fully realized.

For the first time, the new age model allows the direct comparison between the Eifel maar structures and the Greenland ice core chronology. Thus, the determination of the Landscape Evolution Zone could be realized. It is clear that the new results could only be achieved through the analysis of sediments from Auel. For this reason, new funds have now been granted for further researches in Auel. At the end of October 2016, two new overlapping cores were drilled in dry maar structure Auel, which are now being processed in the laboratory. As part of the new high-resolution analysis, the creation of a Bayesian age model is planned for the year 2017.

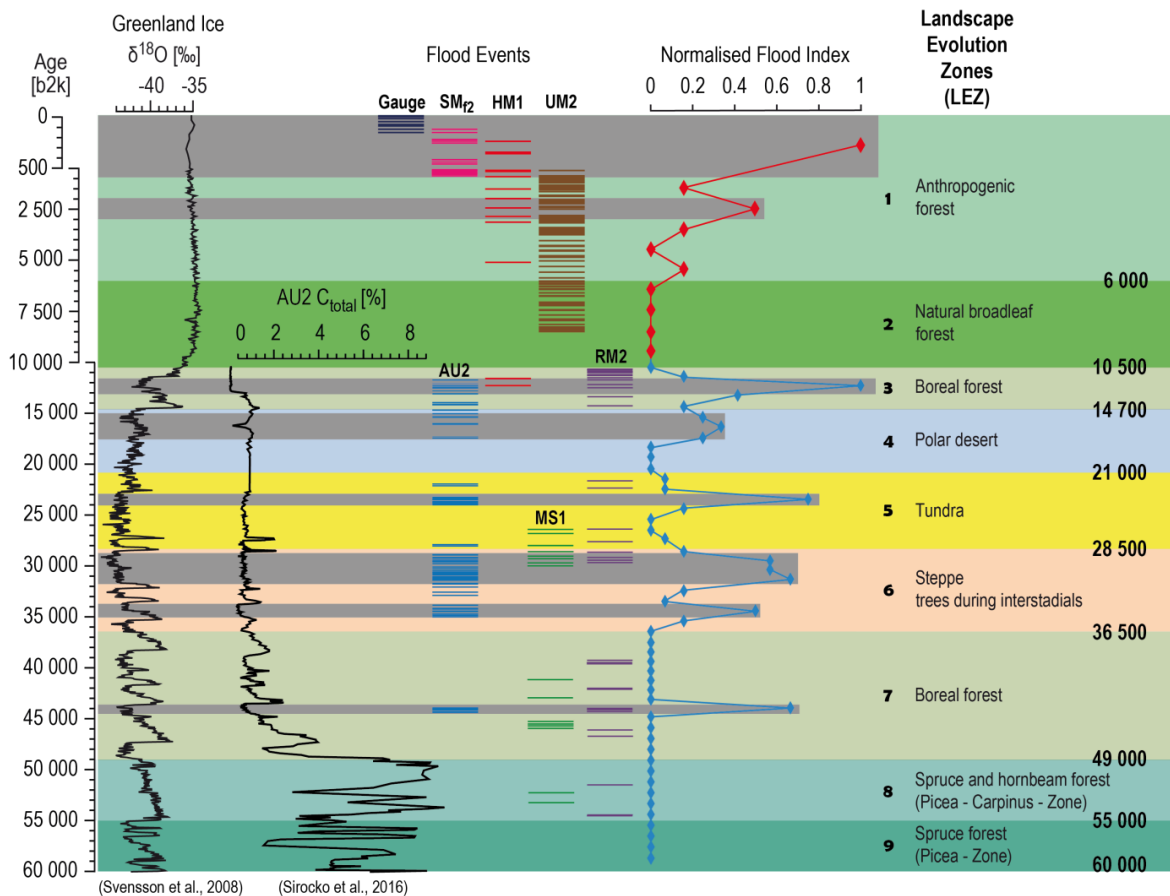


Fig. 6.1: The Elsa-Flood-Stack with the new results from dry maar structures of Merscheid and Roth in comparison with the defined LEZ and the Greenland ice core chronology.

Due to the high-resolution geochemical, petrological and macroscopic analysis of the different event types, general distinction criteria between flood layers, turbidites, and slumps could be developed. Flood layers over 7.5 mm thickness show an inhomogeneous grain size gradient with several maxima representing the discharge pulses during the days or weeks of a flood event and not a grading. The lower analysis limit of the flood layers was set to 7.5 mm in order to ensure an unambiguous assignment. This limitation was

necessary, since it was not always possible to trace all the elaborated criteria in smaller suspension layers.

Overall, 297 flood layers were detected in the analysed sediment cores from Schalkenmehren, Ulmen, Holzmaar, Roth, Merscheid und Auel. The strongest flood events in the Holocene have occurred during LEZ 1 (0 – 6000 b2k) in the years 658, 2800 and 4100 b2k (AD 1342, 800 BC and 2100 BC). Suspension layers in the LEZ 2 (6000 – 10 500 b2k) are not as frequent as during the LEZ 1, nevertheless, the floods cluster between 6000 and 6500 b2k. For the Pleistocene 33 flood layers are detected in the LEZ 3 (10 500 – 14 700 b2k), 11 in LEZ 4 (14 700 – 21 000 b2k), 20 in LEZ 5 (21 000 – 28 500 b2k), 45 in LEZ 6 (28 500 – 36 500 b2k), 25 in LEZ 7 (36 500 – 49 000 b2k), 6 in LEZ 8 (49 000 – 55 000 b2k), zero in LEZ 9 (55 000 – 60 000 b2k) and 10 older than 60 000 b2k. The analysis of the sediment cores showed 6 distinct flood phases in the glacial – interglacial cycle, which clusters in the time from 10 000 to 17 500 b2k, from 21 500 to 24 000 b2k, from 26 000 to 35 000 b2k, from 39 000 to 47 000 b2k, from 51 500 to 54 500 b2k and from 60 500 to 64 000 b2k.

As a result of the differentiated flood analysis it is conspicuous that several maar structures are suitable for the reconstruction of flood phases, while the highest resolution and accuracy are only possible in the sediments of Auel. The variation of the flood dynamics is primarily climatically controlled and predominantly associated with moister and colder periods in combination with vegetation changes. It turned out that low vegetation cover, which is related to Greenland stadials or anthropogenic influence, is mainly responsible for the formation of flood layers in the sediments of the maar structures. On the other hand, the main flood phases are independent of global climate factors such as CO₂ or solar insolation. Consequently, flood events most likely document the erodibility of the soils to the first order, and climate events only to the second order.

Our results confirm the large unexploited potential to improve the instrumental data sets with records from laminated lake sediments to develop long time series. However, many further applications of the results are still possible. For example, modelling results from the fields of climate and hydrology can be significantly improved by incorporating palaeohistorical analogies. Detailed studies about the anthropogenic impact on the Eifel region are also possible. Both recent and historical changes can be examined using maar sediments. In this context, an interesting approach would be the investigation of the flood

frequency change in the late Holocene. Further questions that could not be solved in this work are, on the one hand, the seasonal resolution of the flood layers and, on the other hand, the origin of each flood layer. Currently, it is not possible to distinguish between rain- and snow-generated flood layers. The analysis of seasonal occurring diatoms was not effective for the annual subdivision of the flood layers, and thus both issues remain as key topics for future studies. Finally, it must be noted that the research field of palaeohydrology provides essential foundations for understanding current and future environmental questions and will therefore play an increasingly role in the future.

Bibliography

- Adams, C., Röhner, M., Brunck, H., Sirocko, F., 2016. Defining transport processes of the clastic sand fraction in lake sediments by rapid Camsizer® analysis. Submitted to “The Depositional Record”.
- Allen, J.R.M., Huntley, B., 2000. Weichselian palynological records from southern Europe: correlation and chronology. *Quaternary International*, 73, 111-125.
- Allen, J.R.M., Watts, W.A., Huntley, B., 2000. Weichselian palynostratigraphy, palaeovegetation and palaeoenvironment, the record from lago Grande di Monticchio, southern Italy. *Quaternary International*, 73, 91-110.
- Alley, R.B., Finkel, R.C., Nishizumi, K., Anandakrishnan, A., Shuman, C.A., Mershon, G., Zielinski, G.A., Mayewski, P.A., 1995. Changes in continental and sea-salt atmospheric loadings in central Greenland during the most recent deglaciation: Model-based estimates. *Journal of Glaciology*, 41, 503-514.
- Ampel, L., Wohlfarth, B., Risberg, J., Veres, D., 2008. Paleolimnological response to millennial and centennial scale climate variability during MIS 3 and 2 as suggested by the diatom record in Les Echets. *Quaternary Science Reviews*, 27, 1493-1504.
- Andersen, K.K., Azuma, N., Barnola, J.M., Bigler, M., Biscaye, P., Caillon, N., Chappellaz, J., Clausen, H.B., Dahl-Jensen, D., Fischer, H., Flückiger, J., Fritzsche, D., Fujii, Y., Goto-Azuma, K., Grønvold, K., Gundestrup, N.S., Hansson, M., Huber, C., Hvidberg, C.S., Johnsen, S.J., Jonsell, U., Jouzel, J., Kipfstuhl, S., Landais, A., Leuenberger, M., Lorrain, R., Masson-Delmotte, V., Miller, H., Motoyama, H., Narita, H., Popp, T., Rasmussen, S.O., Raynaud, D., Rothlisberger, R., Ruth, U., Samyn, D., Schwander, J., Shoji, H., Siggard-Andersen, M.-L., Steffensen, J.P., Stocker, T., Sveinbjörnsdottir, A.E., Svensson, A., Takata, M., Tison, J.-L., Thorsteinsson, T., Watanabe, O., Wilhelms, F., White, J.W.C., 2004. High-resolution record of Northern Hemisphere climate extending into the last interglacial period. *Nature*, 431, 147-151.

- Andersen, K.K., Svensson, A., Johnsen, S.J., Rasmussen, S.O., Bigler, M., Röthlisberger, R., Ruth, U., Siggaard-Andersen, M.-L., Steffensen, M.B., Dahl-Jensen, D., Vinther, B.M., Clausen, H.B., 2006. The Greenland ice core chronology 2005, 15 – 42 ka. Part 1: constructing the time scale. *Quaternary Science Reviews*, 25, 3246-3257.
- Andronico, D., Scollo, S., Castro, M.D.L., Cristaldi, A., Lodato, L., Taddeucci, J., 2014. Eruption dynamics and tephra dispersal from the 24 November 2006 paroxysm at South-East Crater, Mt Etna, Italy. *Journal of Volcanology and Geothermal Research*, 274, 78-91.
- Andronico, D., Scollo, S., Cristaldi, A., 2015. Unexpected hazards from tephra fallouts at Mt Etna: The 23 November 2013 lava fountain. *Journal of Volcanology and Geothermal Research*, 304, 118-125.
- Anselmetti, F.S., Artiztegui, D., De Batist, M., Gebhardt, A.C., Haberzettl, T., Niessen, F., Ohlendorf, C., Zolitschka, B., 2009. Environmental history of southern Patagonia unravelled by the seismic stratigraphy of Laguna Potrok Aike. *Sedimentology*, 56, 873-892.
- Antoine, P., Rousseau, D.D., Zöller, L., Lang, A., Munaut, A.V., Hatté, C., Fontugne, M., 2001. High-resolution record of the last interglacial – glacial cycle in the Nussloch loess – palaeosol sequences, Upper Rhine Area, Germany. *Quaternary International*, 76, 211-229.

- Augustin, L., Barbante, C., Barnes, P.R., Barnola, J.M., Bigler, M., Castellano, E., Cattani, O., Chappellaz, J., Dahl-Jensen, D., Delmonte, B., Dreyfus, G., Durand, G., Falourd, S., Fischer, H., Flückiger, J., Hansson, M.E., Huybrechts, P., Jugie, G., Johnsen, S.J., Jouzel, J., Kaufmann, P., Kipfstuhl, J., Lambert, F., Lipenkov, V.Y., Littot, G.C., Longinelli, A., Lorrain, R., Maggi, V., Masson-Delmotte, V., Miller, H., Mulvaney, R., Oerlemans, J., Oerter, H., Orombelli, G., Parrenin, F., Peel, D.A., Petit, J.-R., Raynaud, D., Ritz, C., Ruth, U., Schwander, J., Siegenthaler, U., Souchez, R., Stauffer, B., Steffensen, J.P., Stenni, B., Stocker, T.F., Tabacco, I.E., Udisti, R. van de Wal, R.S.W., van den Broeke, M., Weiss, J., Wilhelms, F., Winther, J.-G., Wolff, E.W., Zucchelli, M., 2004. Eight glacial cycles from an Antarctic ice core. *Nature*, 429, 623-628.
- Baker, V.R., Pickup, G., 1987. Flood geomorphology of the Katherine Gorge, northern territory, Australia. *Geological Society of America Bulletin*, 98, 635-646.
- Bandowe, B.M., Srinivasan, P., Seelge, M., Sirocko, F., Wilcke, W., 2014. A 2600-year record of past polycyclic aromatic hydrocarbon (PAH) deposition at Holzmaar (Eifel, Germany). *Palaeogeography, Palaeoclimatology, Palaeoecology*, 401, 111-121.
- Behl, R.J., Kennett, J.P., 1996. Oceanographic and ecologic manifestations of brief interstadials (Dansgaard-Oeschger events) in Santa Barbara basin, NE Pacific. *Nature*, 379, 243-246.
- Behre, K.-E., Lade, U., 1986. Eine Folge von Eem und 4 Weichsel – Interstadialen. Orel/Niedersachsen und ihr Vegetationsablauf. *Eiszeitalter und Gegenwart*, 36, 11-36.
- Bell, B., 1970. The oldest records of the Nile floods. *The Geographical Journal*, 136, 569-573.
- Berger, A., Loutre, M.F., 1991. Insolation values for the climate of the last 10 million years. *Quaternary Science Reviews*, 10, 297-317.
- Berglund, B.E., Ralska-Jasiewiczowa, M., 1986. Pollen analysis and pollen diagrams. *Handbook of Holocene Palaeoecology and Palaeohydrology*, 455, 484-486.

- Bibus, E., Frechen, M., Kösel, M., Rähle, W., 2007. Das jungpleistozäne Lößprofil von Nußloch (SW-Wand) im Aufschluss der Heidelberger Zement AG. *Eiszeitalter und Gegenwart*, 56, 227-255.
- Bork, H.R., Bork, H., Dalchow, C., Faust, B., Piorr, H.P., Schatz, T., 1998. *Landschaftsentwicklung in Mitteleuropa*. Klett-Perthes, Gotha/ Stuttgart.
- Bouma, A.H., 1987. Megaturbidite: an acceptable term? *Geo-Marine Letters*, 7, 63-67.
- Brauer, A., Negendank, J.F.W., 1993. Palaeoenvironmental reconstruction of the late- and postglacial sedimentary record of Lake Weinfelder Maar. In: *European maar lakes. Lecture Notes in Earth Sciences*, 49, 223-235.
- Brauer, A., 1994. Weichselzeitliche Sedimente des Holzmaares – Warvenchronologie des Hochglazials und Nachweis von Klimaschwankungen. *Documenta Natura*, 85, 1-210.
- Brauer, A., Endres, C., Negendank, J.F.W., 1999a. Lateglacial calendar year chronology based on annually laminated sediments from Lake Meerfelder Maar, Germany. *Quaternary International*, 61, 17-25.
- Brauer, A., Endres, C., Günter, C., Litt, T., Stebich, M., Negendank, J.F., 1999b. High resolution sediment and vegetation responses to Younger Dryas climate change in varved lake sediments from Meerfelder Maar, Germany. *Quaternary Science Reviews*, 18, 321-329.
- Brauer, A., Mingram, J., Frank, U., Günter, C., Schettler, G., Wulf, S., Zolitschka, B., Negendank, J.F.W., 2000. Abrupt environmental oscillations during the Early Weichselian recorded at Lago Grande di Monticchio, southern Italy. *Quaternary International*, 73, 79-90.
- Brauer, A., Litt, T., Negendank, J.F., Zolitschka, B., 2001. Lateglacial varve chronology and biostratigraphy of lakes Holzmaar and Meerfelder Maar, Germany. *Boreas*, 30, 83-88.

- Brakenridge, G.R., Thomas, P.A., Conkey, L.E., Schiferle, J.C., 1988. Fluvial sedimentation in response to postglacial uplift and environmental change, Missisquoi River, Vermont. *Quaternary Research*, 30, 190-220.
- Bretz, J.H., Smith, H.U., Neff, G.E., 1956. Channeled Scabland of Washington: New data and interpretations. *Geological Society of America Bulletin*, 67, 957-1049.
- Brunck, H., Albert, J., Sirocko, F., 2016. The ELSA-Flood-Stack: A reconstruction from the laminated sediments of Eifel maar structures during the last 60 000 years. *Global and Planetary Change*, 142, 136-146.
- Brunck, H., Fischer, P., Wunderlich, T., Vött, A., Sirocko, F., 2017. Reconstruction of the Stadial – Interstadial flood frequency from dry maar structure Auel and laminated Eifel maar sediments. Submitted to “*Journal of Limnology*”.
- Büchel, G., Lorenz, V., 1982. Zum Alter des Maarvulkanismus der Westeifel. *Neues Jahrbuch für Geologie, Paleontologie, Mineralogie*, 163, 1-22.
- Büchel G., 1993. Maars of the Westeifel, Germany, p. 1-13. In: *Paleolimnology of European maar lakes*. Springer, Berlin/ Heidelberg.
- Büchel, G., 1994. *Volcanological map West- and Hocheifel*. Ed. By: Institute of Geosciences. Johannes Gutenberg University. Printed by: Landesvermessungsamt Rheinland-Pfalz, Koblenz, Germany.
- Cappers, R.T.J., Bekker, R.M, Jans, J.E.A., 2006. *Digitale Zadenatlas van Nederland*. Groningen Archaeological Studies 4. Barkhuis, Groningen.
- Caspers, G., Freund, H., 2001. Vegetation and Climate in the Early- and Pleni-Weichselian in Northern Central Europe. *Journal of Quaternary Science*, 16, 31-48.
- CLIMAP Project, 1981. Seasonal reconstructions of the Earth's surface at the last glacial maximum. Geological Society of America. Map and Chart Series, MC-36.
- Conard, N. J., Bolus, M., 2008. Radiocarbon dating the late Middle Paleolithic and the Aurignacian of the Swabian Jura. *Journal of Human Evolution*, 55, 886-897.

- Conard, N. J., Bolus, M., Goldberg, P., Münzel, S., 2006. The last Neanderthals and first modern humans in the Swabian Jura. When Neanderthals and Modern Human met. Tübingen Publications in Prehistory. Kerns Verlag, Tübingen, 305-342.
- Coope, G.R., Lemdahl, G., Lowe, J.J., Walking, A., 1998. Temperature gradients in northern Europe during the last glacial-Holocene transition (14 – 9 ¹⁴C kyr B.P.) interpreted from coleopteran assemblages. *Journal of Quaternary Science*, 13, 419-433.
- Cornwall, C., Bandfield, J.L., Titus, T.N., Schreiber, B.C., Montgomery, D.R., 2015. Physical abrasion of mafic minerals and basalt grains: Application to martian aeolian deposits. *Icarus*, 256, 13-21.
- De Beaulieu, J.-L., Reille, M., 1989. The transition from temperate phases to stadials in the long Upper Pleistocene sequence from Les Echets (France). *Palaeogeography, Palaeoclimatology, Palaeoecology*, 72, 147-159.
- De Geer, G., 1912. A geochronology of the last 12,000 years. 11th International Geological Congress, *Compte Rendu*, Stockholm, 1, 241-258.
- Diehl, M., Sirocko, F., 2006. A new Holsteinian pollen record from the dry maar at Döttingen (Eifel). *The Climate of Past Interglacials*, 7, 397.
- Dietrich, S., Seelos, K., 2010. The reconstruction of easterly wind directions for the Eifel region (Central Europe) during the period 40.3 – 12.9 ka b2k. *Climate of the Past*, 6, 145-154.
- Dietrich, S., 2011. Paleo wind system reconstruction of the last glacial period over Europe, using high-resolution proxy data and model-data-comparison. PhD Thesis, Johannes Gutenberg University Mainz, Germany.
- Dietrich, S., Sirocko, F., 2011. The potential for dust detection by means of μ -XRF scanning in Eifel maar lake sediments. *E&G – Quaternary Science Journal*, 60, 90-104.

- Dill, H.G., Klosa, D., Steyer, G., 2009. The "Donauplatin": source rock analysis and origin of a distal fluvial Au-PGE placer in Central Europe. *Mineralogy and Petrology*, 96, 141-161.
- Direct Image, 2008. Electrical Conductivity (EC) Logging. Standard Operating Procedure. Kansas.
- Drescher-Schneider, R., 2008. Das Kohltratten-Moor im Süden von Schloss Lind. Neue pollen- und großrestanalytische Ergebnisse zur spät- und postglazialen Vegetations- und Klimaentwicklung im Gebiet Neumarkt (Steiermark, Österreich). *Naturwissenschaftlicher Verein für Steiermark*, 137, 63-84.
- Dyck, S., Peschke, G., 1995. *Grundlagen der Hydrologie*. Verlag Bauwesen.
- Ehlers, J., Gibbard, P.L., 2003. Extent and chronology of glaciations. *Quaternary Science Reviews*, 22, 1561-1568.
- Ehlers, J., Gibbard, P.L., 2004. *Quaternary Glaciations-Extent and Chronology: Part I: Europe. Vol. 2*. Elsevier, Netherlands.
- Eissmann, L., 1981. Periglaziäre Prozesse und Permafroststrukturen aus sechs Kaltzeiten des Quartärs. Ein Beitrag zur Periglazialgeologie aus der Sicht des Saale-Elbe-Gebietes. In: "Altenburger Naturwissenschaftliche Forschungen, Band 1". Naturkundliches Museum, Altenburg.
- Ely, L.L., Baker, V.R., 1985. Reconstructing paleoflood hydrology with slackwater deposits: Verde River, Arizona. *Physical Geography*, 6, 103-126.
- Engels, S., Bohnke, S.J., Heiri, O., Schaber, K., Sirocko, F., 2008. The lacustrine sediment record of Oberwinkler Maar (Eifel, Germany): Chironomid and macroremain based inferences of environmental changes during Oxygen Isotope Stage 3. *Boreas*, 37, 414-425.
- Faegri, K., Iversen, J., 1989. *Textbook of Pollen Analysis*. John Wiley & Sons, New York.

- Federal Waterways and Shipping Administration, 2015. (WSV) provided by the German Federal Institute of Hydrology (BfG): Daily Gauge Values, Moselle, Cochem 1963 – 2013; Daily Gauge Values, Moselle, Trier 1966 – 2013; Daily Gauge Values, Rhine, Koblenz 1955 – 2013; Daily Gauge Values, Rhine, Bonn 1920 – 2013; Daily Gauge Values, Rhine, Cologne 1900-2013.
- Feurdean, A., Perşoiu, A., Tantău, I., Stevens, T., Magyari, E.K., Onac, B.P., Markovič, S., Andriči, M., Connorj, S., Fărcaş, S., Gaikal, M., Gaudenym, T., Hoekn, W., Kolaczekl, P., Kunešo, P., Lamentowiczl, M., Marinovap, E., Michczyńskaq, D.J., Perşoiur, I., Plócienniks, M., Slowińskit, M., Stancikaitev, M., Sumegiw, P., Svenssonx, A., Tămaşb, T., Timary, A., Tonkovz, S., Tothaa, M., Veskiab, S., Willisac, K.J., Zernitskaya, V., 2014. Climate variability and associated vegetation response throughout Central and Eastern Europe (CEE) between 60 and 8 ka. *Quaternary Science Reviews*, 106, 206-224.
- Firbas, F., 1949. Spät- und nacheiszeitliche Waldgeschichte Mitteleuropas nördlich der Alpen. Band 1 und 2. Gustav Fischer Verlag, Jena.
- Fischer, P., Wunderlich, T., Rabbel, W., Vött, A., Willershäuser, T., Baika, K., Rigakou, D., Metallinou, G., 2016. Combined Electrical Resistivity Tomography (ERT), Direct-Push Electrical Conductivity (DP-EC) Logging and Coring – A New Methodological Approach in Geoarchaeological Research. *Archaeological Prospection*, 23, 213-228.
- Fletcher, W.J., Sanchez Goni, M.F., Allen, J.R.M., Cheddadi, R., Combourieu-Nebout, N., Huntley, B., Lawson, I., Londeix, L., Magri, D., Margari, V., Muller, U.C., Naughton, F., Novenko, E., Roucoux, K., Tzedakis, P.C., 2010. Millennial-scale variability during the last glacial in vegetation records from Europe. *Quaternary Science Reviews*, 29, 2839-2864.
- Folk, R.L., Ward, W., 1957. Brazos River Bar: a study in the significance of grain size parameters. *Journal of Sedimentary Petrology*, 27, 3-26.
- Förster, M.W., Sirocko, F., 2016. Episodic activity of the Eifel Volcanic Fields: Insights from tephrochronology and thermobarometry. *Global and Planetary Change*, 142, 100-107.

- Frechen, M., van Vliet-Lanoe, B., van den Haute, P., 2001. The Upper Pleistocene loess record at Harmignies/ Belgium – high-resolution terrestrial archive of climate forcing. *Palaeogeography, Palaeoclimatology, Palaeoecology*, 173, 175-195.
- Fritz, T., 2011. Warvenchronologie der letzten 1000 Jahre anhand ausgewählter Eifelmaare (Holzmaar, Schalkenmehrener Maar, Ulmener Maar). Diploma thesis, Johannes Gutenberg-Universität Mainz.
- Fuchs, K., Gehlen, K., Mälzer, H., Murawski, H., Semmel, A., 2013. Plateau uplift: The Rhenish Shield – a case history. Springer Science and Business Media.
- Gilli, A., Anselmetti, F.S., Ariztegui, D., McKenzie, J.A., 2003. A 600-year sedimentary record of flood events from two sub-alpine lakes (Schwendiseen, Northeastern Switzerland). In: *Lake Systems from the Ice Age to Industrial Time*. Birkhäuser, Basel.
- Gilli, A., Anselmetti, F.S., Glur, L., Wirth, S.B., 2013. Lake sediments as archives of recurrence rates and intensities of past flood events. In: *Dating torrential processes on fans and cones*. Springer, Netherlands.
- Glaser, R., 2008. *Klimageschichte Mitteleuropas. 1200 Jahre Wetter, Klima, Katastrophen. Mit Prognosen für das 21. Jahrhundert*. Wissenschaftliche Buchgesellschaft, Darmstadt.
- Glaser, R., Riemann, D., Schönbein, J., Barriendos, M., Brázdil, R., Bertolin, C., Camuffo, D., Deutsch, M., Dobrovolný, P., van Engelen, A., Enzi, S., Halíčková, M., Koenig, S.J., Kotyza, O., Limanówka, D., Macková, J., Sghedoni, M., Martin, B., and Himmelsbach, I., 2010. The variability of European floods since AD 1500. *Climatic Change*, 101, 235-256.
- Gronenborn, D., Sirocko, F., 2009. 4400 – 3400 BC Viehwirtschaft und Ausbreitung der Michelsberger Kultur. In: *Wetter – Klima – Menschheitsentwicklung. Von der Eiszeit bis ins 21. Jahrhundert*. Theiss, Stuttgart.
- Grosse-Brauckmann, G., 1974. Über pflanzliche Makrofossilien mitteleuropäischer Torfe. II: Weitere Reste (Früchte und Samen, Moose u. a.) und Ihre Bestimmungsmöglichkeiten. *Telma*, 4, 51-117.

- Grootes, P.M., Stuiver, M., White, J.W.C., Johnsen, S., Jouzel, J., 1993. Comparison of oxygen isotope records from the GISP2 and GRIP Greenland ice cores. *Nature*, 366, 552-554.
- Güiter, F., Andrieu-Ponel, V., de Beaulieu, L.J., Cheddadi, R., Calvez, M., Ponel, P., Reille, M., Keller, T., Goeury, C., 2003. The last climatic cycles in Western Europe: a comparison between long continuous lacustrine sequences from France and other terrestrial records. *Quaternary International*, 111, 59-74.
- Güiter, F., Andrieu-Ponel, V., Digerfeldt, G., Reille, M., de Beaulieu, L.-J., Ponel, P., 2005. Vegetation history and lake-level changes from the Younger Dryas to the present in Eastern Pyrenees (France): pollen, plant macrofossils and lithostratigraphy from Lake Racou (2000 m a.s.l.). *Vegetation History and Archaeobotany*, 14, 99-118.
- Günther, T., Rücker, C., Spitzer, K., 2006. Three-dimensional modelling and inversion of DC resistivity data incorporating topography – II. Inversion. *Geophysical Journal International*, 166, 506-517.
- Haesaerts, P., Borziac, I., Chekha, V.P., Chirica, V., Drozdov, N.I., Koulakovska, L., Orlova, L.A., van der Plicht, J., Damblon, F., 2010. Charcoal and wood remains for radiocarbon dating Upper Pleistocene loess sequences in Eastern Europe and Central Siberia. *Palaeogeography, Palaeoclimatology, Palaeoecology*, 291, 106-127.
- Hajdas, I., Zolitschka, B., Ivy-Ochs, S.D., Beer, J., Bonani, G., Leroy, S.A.G., Negendank, J.W., Ramrath, M., Suter, M., 1995. AMS radiocarbon dating of annually laminated sediments from Lake Holzmaar, Germany. *Quaternary Science Reviews*, 14, 137-143.
- Heiri, O., Koinig, K.A., Spötl, C., Barrett, S., Brauer, A., Drescher-Schneider, R., Gaar, D., Ivy-Ochs, S., Kerschner, H., Luetscher, M., Moran, A., Nicolussi, K., Preusser, F., Schmidt, R., Schoeneich, P., Schwörer, C., Sprafke, T., Terhorst, B., Tinner, W., 2014. Palaeoclimate records 60 – 8 ka in the Austrian and Swiss Alps and their forelands. *Quaternary Science Reviews*, 106, 186-205.

- Helmens, K., 2014. The Last Interglacial – Glacial cycle (MIS 5 – 2) re-examined based on long proxy records from central and northern Europe. *Quaternary Science Reviews*, 86, 115-143.
- Hemming, S.R., 2004. Heinrich events: Massive late Pleistocene detritus layers of the North Atlantic and their global climate imprint. *Reviews of Geophysics*, 42.
- Herbig, C., Sirocko, F., 2012. Palaeobotanical evidence for agricultural activities in the Eifel region during the Holocene: plant macroremain and pollen analysis from three maar lake sediments in the Quaternary Westeifel Volcanic Field (Germany, Rheinland-Pfalz). *Vegetation history and archaeobotany*, 22, 447-462.
- Hoffmann, T., Lang, A., Dikau, R., 2008. Holocene river activity: analysing ¹⁴C-dated fluvial and colluvial sediments from Germany. *Quaternary Science Reviews*, 27, 2031-2040.
- Hošek, J., Pokorný, P., Kubovčík, V., Horáček, I., Žáčková, P., Kadlec, J., Rojic, F., Lenka, L., Bučkuliaková, S., 2014. Late glacial climatic and environmental changes in eastern-central Europe: Correlation of multiple biotic and abiotic proxies from the Lake Švarcenberk, Czech Republic. *Palaeogeography, Palaeoclimatology, Palaeoecology*, 396, 155-172.
- Huijzer, B., Vandenberghe, J., 1998. Climate reconstruction of the Weichselian Pleniglacial in northwestern and Central Europe. *Journal of Quaternary Science*, 13, 391-418.
- Imbrie, J., Shackleton, N.J., Pisias, N.G., Morley, J.J., Prell, W.L., Martinson, D.G., Hays, J.D., McIntyre, A., Mix, A.C., 1984. The orbital theory of Pleistocene climate: support from a revised chronology of the marine $\delta^{18}\text{O}$ record. In: *Milankovitch and climate: Understanding the response to astronomical forcing*. Springer Science and Business Media, Netherlands.
- IPCC, 2007. *Climate Change 2007: Synthesis Report. Contribution of Working Groups I, II and III to the Fourth Assessment Report of the Intergovernmental Panel on Climate Change*.

- IPCC, 2014. Climate Change 2014: Synthesis Report. Contribution of Working Groups I, II and III to the Fifth Assessment Report of the Intergovernmental Panel on Climate Change.
- Iversen, J., 1944. *Viscum, Hedera and Ilex as climate indicators, a contribution to the study of the postglacial temperature climate.* Geological Society of Sweden, 66, 463-483.
- Jacob, D., Bärring, L., Christensen, O.B., Christensen, J.H., Hagemann, S., Hirschi, M., Kjellström, E., Lenderink, G., Rockel, B., Schär, C., Seneviratne, S.I., Somot, S., van Ulden, A., van den Hurk, B., 2007. An inter-comparison of regional climate models for Europe: Design of the experiments and model performance. *Climatic Change*, 81, 31-52.
- Jacomet, S., Kreuz, A., 1999. *Archäobotanik.* Ulmer Verlag, Stuttgart.
- Jacomet, S., Brombacher, C., Dick, M., 1989. *Archäobotanik am Zürichsee. Ackerbau, Sammelwirtschaft und Umwelt von neolithischen und bronzezeitlichen Seeufersiedlungen im Raum Zürich. Ergebnisse von Untersuchungen pflanzlicher Makroreste der Jahre 1979-1988.* Züricher Denkmalpflege, Monographien 7, Orell Füssli, Zürich.
- Johnsen, S.J., Dahl-Jensen, D., Gundestrup, N., Steffensen, J.P. Clausen, H.B. Miller, H., Masson-Delmotte, V., Sveinbjörnsdottir A.E., White, J., 2001. Oxygen isotope and palaeotemperature records from six Greenland ice-core stations: Camp Century, Dye-3, GRIP, GISP2, Renland and NorthGRIP. *Journal of Quaternary Science*, 16, 299-307.
- Jouzel, J., Vaikmae, R., Petit, J.R., Martin, M., Duclos, Y., Stievenard, M., Lorius, C., Toots, M., Mélières, M.A., Burckle, L.H., Barkov, N.I., Kotlyakov, V.M., 1994. The two-step shape and timing of the last deglaciation in Antarctica. *Climate Dynamics*, 11, 151-161.
- Kadereit, A., Kind, C.J., Wagner, G.A., 2013. The chronological position of the Lohne Soil in the Nussloch loess section – re-evaluation for a European loess-marker horizon. *Quaternary Science Reviews*, 59, 67-86.

- Kale, V.S., Singhvi, A.K., Mishra, P.K., Banerjee, D., 2000. Sedimentary records and luminescence chronology of Late Holocene palaeofloods in the Luni River, Thar Desert, northwest India. *Catena*, 40, 337-358.
- Kalis, A.J., Merkt, J., Wunderlich, J., 2003. Environmental changes during the Holocene climatic optimum in Central Europe – human impact and natural causes. *Quaternary Science Reviews*, 22, 33-79.
- Kämpf, L., Brauer, A., Swierczynski, T., Czymzik, M., Müller, P., Dulski, P., 2014. Processes of flood-triggered detrital layer deposition in the varved Lake Mondsee sediment record revealed by a dual calibration approach. *Journal of Quaternary Science*, 29, 475-486.
- Kasse, C., Bohncke, S.J.P., Vandenberghe, J., 1995. Fluvial periglacial environments, climate and vegetation during the middle Weichselian in the northern Netherlands with special reference to the Hengelo Interstadial. *Mededelingen Rijks Geologische Dienst*, 52, 387-414.
- Kasse, C., Vandenberghe, J., Van Huissteden, J., Bohncke, S.J.P., Bos, J.A.A., 2003. Sensitivity of Weichselian fluvial systems to climate change (Nochten mine, eastern Germany). *Quaternary Science Reviews*, 22, 2141-2156.
- Knorr, G., Lohmann, G., 2007. Rapid transitions in the Atlantic thermohaline circulation triggered by global warming and meltwater during the last deglaciation. *Geochemistry, Geophysics, Geosystems*, 8, Q12006.
- Kochel, R.C., Baker, V.R., 1982. Paleoflood hydrology. *Science*, 215, 353-361.
- Kuijpers, A., Troelstra, S.R., Wisse M., Heier Nielsen, S., van Weering, T.C.E., 1998. Norwegian Sea overflow variability and NE Atlantic surface hydrography during the past 150,000 years. *Marine Geology*, 152, 75-99.
- Kubitz, B., 2000. Die holozäne Vegetations- und Siedlungsgeschichte in der Westeifel am Beispiel eines hochauflösenden Pollendiagrammes aus dem Meerfelder Maar. *Dissertationes Botanicae*, 339, 1-106

- Kukla, G.J., Bender, M.L., de Beaulieu, J.L., Bond, G., Broecker, W.S., Cleveringa, P., Gavin, J.E., Herbert, T.D., Imbrie, J., Jouzel, J., Keigwin, L.D., Knudsen, K.-L., McManus, J.F., Merkt, J., Muhs, D.R., Müller, H., Poore, R.Z., Porter, S.C., Seret, G., Shackleton, N.J., Turner, C., Tzedakis, P.C., Winograd, I.J., 2002. Last interglacial climates. *Quaternary Research*, 58, 2-13.
- Lang, A., Hatté, C., Rousseau, D.D., Antoine, P., Fontugne, M., Zöller, L., Hambach, U., 2003. High-resolution chronologies for loess: comparing AMS ^{14}C and optical dating results. *Quaternary Science Reviews*, 22, 953-959.
- Leroy, S.A.G., Giralt, S., Francus, P., Seret, G., 1996. The High Sensitivity of the Palynological Record in the Vico maar Lacustrine Sequence (Latium, Italy) Highlights the Climatic Gradient through Europe for the Last 90 ka. *Quaternary Science Reviews*, 15, 189-201.
- Lisiecki, L.E., Raymo, M.E., 2005. A Pliocene – Pleistocene stack of 57 globally distributed benthic $\delta^{18}\text{O}$ records. *Paleoceanography*, 20, PA1003.
- Litt, T., Junge, F.W., Böttger, T., 1996. Climate during the Eemian in north-central Europe – a critical review of the palaeobotanical and stable isotope data from central Germany. *Vegetation History and Archaeobotany*, 5, 247-256.
- Litt, T., Stebich, M., 1999. Bio-and chronostratigraphy of the lateglacial in the Eifel region, Germany. *Quaternary International*, 61, 5-16.
- Litt, T., Brauer, A., Goslar, T., Merkt, J., Bałaga, K., Müller, H., Ralska-Jasiewiczowa, M., Stebich, M., Negendank, J.F., 2001. Correlation and synchronisation of Lateglacial continental sequences in northern Central Europe based on annually laminated lacustrine sediments. *Quaternary Science Reviews*, 20, 1233-1249.
- Litt, T., Schmincke, H.-U., Kromer, B., 2003. Environmental Response to Climatic and Volcanic Events in Central Europe during the Weichselian Lateglacial. *Quaternary Science Reviews*, 22, 7-32.

- Loulergue, L., Schilt, A. Spahni, R. Masson-Delmotte, V. Blunier, T., Lemieux, B., Barnola, J.-M. Raynaud, D. Stocker, T.F., Chappellaz, J.J., 2008. Orbital and millennial-scale features of atmospheric CH₄ over the past 800,000 years. *Nature*, 453, 383-386.
- Lowe, D.J., 2011. Tephrochronology and its application: a review. *Quaternary Geochronology*, 6, 107-153.
- Lüthi, D., Le Floch, M., Bereiter, B., Blunier, T., Barnola, J.M., Siegenthaler, U., Raynaud, D., Jouzel, J., Fischer, H., Kawamura, K., Stocker, T.F., 2008. High-resolution carbon dioxide concentration record 650,000 – 800,000 years before present. *Nature*, 453, 379-382.
- Macklin, M.G., 1999. Holocene river environments in prehistoric Britain: human interaction and impact. *Journal of Quaternary Science*, 14, 521-530.
- Macklin, M.G., Fuller, I.C., Lewin, J., Maas, G.S., Passmore, D.G., Rose, J., Woodward, J.C., Black, S., Hamlin, R.H.B., Rowan, J.S., 2002. Correlation of fluvial sequences in the Mediterranean basin over the last 200 ka and their relationship to climate change. *Quaternary Science Reviews*, 21, 1633-1641.
- Macklin, M.G., Benito, G., Gregory, K.J., Johnstone, E., Lewin, J., Michczyńska, D.J., Soja, R., Starkel, L., Thorndycraft, V.R., 2006. Past hydrological events reflected in the Holocene fluvial record of Europe. *Catena*, 66, 145-154.
- Magny, M., Aalbersberg, G., Bégeot, C., Benoit-Ruffaldi, P., Bossuet, G., Disnar, R.-J., Heiri, O., Laggoun-Defarge, F., Mazier, F., Millet, L., Peyron, O., Vannière, B., Walter-Simonnet, V.-A., 2006. Environmental and climatic changes in the Jura mountain (eastern France) during the Lateglacial – Holocene transition: a multi-proxy record from Lake Lautrey. *Quaternary Science Reviews*, 25, 414-445.
- Magny, M., de Beaulieu, J.L., Drescher-Schneider, R., Vanniere, B., Walter-Simonnet, A.V., Miras, Y., Millet, L., Bossuet, G., Peyron, O., Brugiapaglia, E., Leroux, A., 2007. Holocene climate changes in the central Mediterranean as recorded by lake-level fluctuations at Lake Accesa (Tuscany, Italy). *Quaternary Science Reviews*, 26, 1736-1758.

- Mangerud, J., Gyllencreutz, R., Lohne, Ö., Svendsen, J.I., 2011. Glacial history of Norway. In: Quaternary glaciations – extent and chronology. *Developments in Quaternary Science*, 15, 279-298.
- Mangili, C., Brauer, A., Moscariello, A., Naumann, R., 2005. Microfacies of detrital event layers deposited in Quaternary varved lake sediments of the Piànico-Sèllere Basin (northern Italy). *Sedimentology*, 52, 927-943.
- Mania, D., Stechemesser, H., 1970. Jungpleistozäne Klimazyklen im Harzvorland. *Petermanns Geographische Mitteilungen, Ergänzungsheft*, 274, 39-55.
- Marco, S., Stein, M., Agnon, A., Ron, H., 1996. Long-term earthquake clustering: A 50,000-year paleoseismic record in the Dead Sea Graben. *Journal of Geophysical Research: Solid Earth*, 101, 6179-6191.
- Marković, S.B., Bokhorst, M.P., Vandenberghe, J., McCoy, W.D., Oches, E.A., Hambach, U., Gaudenyi, T., Jovanović, M., Stevens, T., Zöller, L., Machalett, B., 2008. Late Pleistocene loess – paleosol sequences in the Vojvodina region, North Serbia. *Journal of Quaternary Science*, 23, 73-84.
- Marković, S.B., Stevens, T., Kukla, G.J., Hambach, U., Fitzsimmons, K.E., Gibbard, P., Buggle, B., Zech, M., Guo, Z.T., Hao, QZ., Wu, H.B., Dhand, K.O., Smalley, I.J., Ujvari, G., Sumegi, P., Timar-Gabor, A., Veres, D., Sirocko, F., Vasiljevic, D.A., Jary, Z., Svensson, A., Jovic, V., Lehmkuhl, F., Kovacs, J., Svircev, Z., 2015. Danube loess stratigraphy – Towards a pan-European loess stratigraphic model. *Earth-Science Reviews*, 148, 228-258.
- Martin-Puertas, C., Brauer, A., Dulski, P., Brademann, B., 2012. Testing climate-proxy stationarity throughout the Holocene: an example from the varved sediments of Lake Meerfelder Maar (Germany). *Quaternary Science Reviews*, 58, 56-65.
- Mauquoy, D., van Geel, B., 2007. *Plant Macrofossil Methods and Studies. Mire and Peat Macros*. Elsevier, Netherlands.
- May, F., 2002. Quantifizierung des CO₂-Flusses zur Abbildung magmatischer Prozesse im Untergrund der Westeifel. Shaker Verlag, Aachen.

- Mayewski, P.A., Rohling, E.E., Stager, J.C., Karlen, W., Maasch, K.A., Meeker, L.D., Meyerson, E.A., Gasse, F., van Kreveld, S., Holmgren, K., Lee-Thorp, J., Rosqvist, G., Rack, F., Staubwasser, M., Schneider, R.R., Steig, E.J., 2004. Holocene climate variability. *Quaternary Research*, 62, 243-255.
- McManus, J.F., Bond, G.C., Broecker, W.S., Johnsen, S., Labeyrie, L., Higgins, S., 1994. High-resolution climate records from the North Atlantic during the last interglacial. *Nature*, 371, 326-329.
- McManus, J.F., Francois, R., Gherardi, J.M., Keigwin, L.D., Brown-Leger, S., 2004. Collapse and rapid resumption of Atlantic meridional circulation linked to deglacial climate changes. *Nature*, 428, 834-837.
- Menke, B., Tynni, R., 1984. Das Eem Interglazial und das Weichselfrühglazial von Rederstall/Dithmarschen und ihre Bedeutung für die mitteleuropäische Jungpleistozän-Gliederung. *Geologisches Jahrbuch A76*, 3-120.
- Mol, J., 1997. Fluvial response to Weichselian climate changes in the Niederlausitz (Germany). *Journal of Quaternary Science*, 12, 43-60.
- Moore, A.L., McAdoo, B.G., Ruffman, A., 2007. Landward fining from multiple sources in a sand sheet deposited by the 1929 Grand Banks tsunami, Newfoundland. *Sedimentary Geology*, 200, 336-346.
- Moore, A., Goff, J., McAdoo, B.G., Fritz, H.M., Gusman, A., Kalligeris, N., Kalsum, K., Susanto, A., Suteja, D., Synolakis, C.E., 2011. Sedimentary Deposits from the 17 July 2006 Western Java Tsunami, Indonesia: Use of Grain Size Analyses to Assess Tsunami Flow Depth, Speed, and Traction Carpet Characteristics. *Pure and Applied Geophysics*, 168, 1951-1961.
- Moseley, G.E., Spötl, C., Svensson, A., Cheng, H., Brandstätter, S., Edwards, R.L., 2014. Multi-speleothem record reveals tightly coupled climate between Central Europe and Greenland during Marine Isotope Stage 3. *Geology*, 42, 1043-1046.
- Moreno, A., Valero-Garces, B., Gonzales-Samperiz, P., Rico, M., 2008. Flood response to rainfall variability during the last 2000 years inferred from the Taravilla Lake record (Central Iberian Range, Spain). *Journal of Paleolimnology*, 40, 943-961.

- Moreno, A., Svensson, A., Brooks, S.J., Connor, S., Engels, S., Fletcher, W., Genty, D., Heiri, O., Labuhn, I., Persoiu, A., Peyron, O., Sadori, L., Valero-Garcés, B., Wulf, S., Zanchetta, G., 2014. A compilation of Western European terrestrial records 60 – 8 ka BP: towards an understanding of latitudinal climatic gradients. *Quaternary Science Reviews*, 16, 167-185.
- Moschen, R., 2004. Die Sauerstoffisotopenverhältnisse des biogenen Opals lakustriner Sedimente als mögliches Paläothermometer. PhD Thesis, Universität Köln, Germany.
- Mudelsee, M., Börngen, M., Tetzlaff, G., Grünewald, U., 2003. No upward trends in the occurrence of extreme floods in Central Europe. *Nature*, 425, 166-169.
- Mulder, T., Alexander, J., 2001. The physical character of subaqueous sedimentary density flows and their deposits. *Sedimentology*, 48, 269-299.
- Mulder, T., Syvitski, J.P.M., Migeon, S., Faugères, J.-C., Savoye, B., 2003. Marine hyperpycnal flows: initiation, behavior and related deposits. A review. *Marine and Petroleum Geology*, 20, 861-882.
- Müller, U., 2001. Die Vegetations- und Klimageschichte im jüngeren Quartär anhand ausgewählter Profile aus dem südwestlichen Alpenvorland. *Tübinger Geowissenschaftliche Arbeiten D7*, 118-125.
- Müller, U.C., Pross, J., Tzedakis, P.C., Gamble, C., Kotthoff, U., Schmiedl, G., Wulf, S., Christanis, K., 2011. The role of climate in the spread of modern humans into Europe. *Quaternary Science Reviews*, 30, 273-279.
- Municipal drainage operations of Cologne, Flood Protection Centre. www.steb-koeln.de (20.01.2016).
- Nardin, T.R., 1979. A review of mass movement processes sediment and acoustic characteristics, and contrasts in slope and base-of-slope systems versus canyon-fan-basin floor systems. *The Society of Economic Paleontologists and Mineralogists*, 27, 61-73.

- Negendank, J.F.W., Brauer, A., Zolitschka, B., 1990. Die Eifelmaare als erdgeschichtliche Fallen und Quellen zur Rekonstruktion des Paläoenvironments. Mainzer geowissenschaftliche Mitteilungen, 19, 235-262.
- Nicolussi, K., Patzelt, G., 2006. Klimawandel und Veränderungen an der alpinen Waldgrenze – aktuelle Entwicklungen im Vergleich zur Nacheiszeit. In: BFW-Praxisinformation, 10, 3-5.
- Nigst, P.R., Haesaerts, P., Damblon, F., Frank-Fellner, C., Mallol, C., Viola, B., Göttinger, M., Niven, L., Trnka, G., Hublin, J.J., 2014. Early modern human settlement of Europe north of the Alps occurred 43,500 years ago in a cold steppe-type environment. Proceedings of the National Academy of Sciences, 111, 14394-14399.
- Overbeck, F., 1975. Botanisch-Geologische Moorkunde: unter besonderer Berücksichtigung der Moore Nordwestdeutschlands als Quelle zur Vegetations-, Klima- und Siedlungsgeschichte. Karl Wachholtz Verlag, Neumünster, 145-154.
- Parrenin, F., Jouzel, J., Waelbroeck, C., Ritz, C., Barnola, J.-M., 2001. Dating the Vostok ice core by an inverse method, Journal of Geophysical Research, 106, 837-851.
- Petit, J.R., Jouzel, J., Raynaud, D., Barkov, N. I., Barnola, J.-M., Basile, I., Bender, M., Chappellaz, J., Davis, M., Delaygue, G., Delmotte, M., Kotlyakov, V. M., Legrand, M., Lipenkov, V. Y., Lorius, C., Pépin, L., Ritz, C., Saltzman, E., Stievenard, M., 2004. Climate and atmospheric history of the past 420,000 years from the Vostok ice core, Antarctica. Nature, 399, 429-436.
- Peyron, O., Bégeot, C., Brewer, S., Heiri, O., Magny, M., Millet, L., Ruffaldi, P., Van Campo, E., Yu, G., 2005. Late-Glacial climatic changes in Eastern France (Lake Lautrey) from pollen, lake-levels, and chironomids. Quaternary Research, 64, 197-211.
- Pfahl, S., Sirocko, F., Seelos, K., Dietrich, S., Walter, A., Wernli, H., 2009. A new windstorm proxy from lake sediments: a comparison of geological and meteorological data from western Germany for the period 1965 – 2001. Journal of Geophysical Research: Atmospheres, 114, D18106.

- Phantuwongraj, S., Choowong, M., Nanayama, F., Hisada, K.-I., Charusiri, P., Chutakositkanon, V., Pailoplee, S., Chabangbon, A., 2013. Coastal geomorphic conditions and styles of storm surge washover deposits from Southern Thailand. *Geomorphology*, 192, 43-58.
- Piao, S., Ciais, P., Huang, Y., Shen, Z., Peng, S., Li, J., Zhou, L., Liu, H., Ma, Y., Ding, Y., Friedlingstein, P., Liu, C., Tan, K., Yu, Y., Zhang, T., Fang, J., 2010. The impacts of climate change on water resources and agriculture in China. *Nature*, 467, 43-51.
- Preusser, F., 2004. Towards a chronology of the Late Pleistocene in the northern Alpine Foreland. *Boreas*, 33, 195-210.
- Prasad, S., Baier, J., 2014. Tracking the impact of mid-to late Holocene climate change and anthropogenic activities on Lake Holzmaar using an updated Holocene chronology. *Global and Planetary Change*, 122, 251-264.
- Rasmussen, S.O., Bigler, M., Blockley, S.P., Blunier, T., Buchardt, S.L., Clausen, H.B., Cvijanovic, I., Dahl-Jensen, D., Johnsen, S.J., Fischer, H., Gkinis, V., Guillevic, M., Hoek, W.Z., Lowe, J.J., Pedro, J.B., Popp, T., Seierstad, I.K., Steffensen, J.P., Svensson, A.M., Vallelonga, P., Vinther, B.M., Walker, M.J.C., Wheatley, J.J., Winstrup, M., 2014. A stratigraphic framework for abrupt climatic changes during the Last Glacial period based on three synchronized Greenland ice-core records: refining and extending the INTIMATE event stratigraphy. *Quaternary Science Reviews*, 106, 14-28.
- Reille, M., de Beaulieu, J.-L., 1990. Pollen analysis of a long upper Pleistocene continental sequence in a Velay maar (Massif Central, France). *Palaeogeography, Palaeoclimatology, Palaeoecology*, 80, 35-48.
- Rein, B., Jäger, K., Kocot, Y., Grimm, K., Sirocko, F., 2007. Holocene and Eemian varve types of Eifel maar sediments. In: *The climate of past interglacials. Developments in Quaternary Science*, 7, 141-156.
- Retsch Technology GmbH, 2010. Operating Manual: Particle Size Analysis System Camsizer®.

- Retsch Technology GmbH, 2011. Die Probe: Partikelmesstechnik. ISSN 0949-6025.
- Sanchez Goñi, M.F., Bard, E., Landais, A., Rossignol, L., d'Errico, F., 2013. Air-sea temperature decoupling in Western Europe during the last interglacial-glacial transition. *Nature Geoscience*, 6, 837-841.
- Sarala, P., Väiliranta, M., Eskola, T., Vaikutienė, G., 2016. First physical evidence for forested environment in the Arctic during MIS 3. *Scientific Reports*, 6, 29054.
- Schaber, K., Sirocko, F., 2005. Lithologie und Stratigraphie der spätpleistozänen Trockenmaare der Eifel. *Mainzer geowissenschaftliche Mitteilungen*, 33, 295-340.
- Scharf, B.W., Oehms, M., 1992. Physical and chemical characteristics. *Limnology of Eifel Maar Lakes. Ergebnisse der Limnologie*, 38, 63-83.
- Schirmer, W., 2012. Rhine loess at Schwalbenberg II – MIS 4 and 3. *Eiszeitalter und Gegenwart*, 61, 32-47.
- Schlolaut, G., Brauer, A., Marshall, M.H., Nakagawa, T., Staff, R.A., Bronk Ramsey, C., Lamb, H.F., Bryant, C.L., Naumann, R., Dulski, P., Brock, F., Yokoyama, Y., Tada, R., Haraguchi, T., Suigetsu 2006 Project members, 2014. Event layers in the Japanese Lake Suigetsu 'SG06' sediment core: description, interpretation and climatic implications. *Quaternary Science Reviews*, 83, 157-170.
- Schmincke, H.-U., 2007. The Quaternary volcanic fields of the east and west Eifel (Germany). In: *Mantle Plumes*. Springer, Berlin/ Heidelberg.
- Schnellmann, M., Anselmetti, F.S., Giardini, D., McKenzie, J.A., 2005. Mass movement induced fold-and-thrust belt structures in unconsolidated sediments in Lake Lucerne (Switzerland). *Sedimentology*, 52, 271-289.
- Schön, J.H., 2004. Physical properties of rocks: Fundamentals and principles of petrophysics. In: *Handbook of Geophysical Exploration 18*. Elsevier, Netherlands.
- Schulz, M., Berger, W.H., Sarnthein, M., Grootes, P.M., 1999. Amplitude variations of 1,470-year climate oscillations during the last 100,000 years linked to fluctuations of continental ice mass. *Geophysical Research Letters*, 26, 3385-3388.

- Seelos, K., Sirocko, F., 2005. RADIUS – rapid particle analysis of digital images by ultra high resolution scanning of thin sections. *Sedimentology*, 52, 669-681.
- Seelos, K., Sirocko, F., Dietrich, S., 2009. A continuous high-resolution dust record for the reconstruction of wind systems in Central Europe (Eifel, Western Germany) over the past 133 ka. *Geophysical Research Letters*, 36, L20712.
- Seib, N., Kley, J., Büchel, G., 2013. Identification of maars and similar volcanic landforms in the West Eifel Volcanic Field through image processing of DTM data: efficiency of different methods depending on preservation state. *International Journal of Earth Sciences*, 102, 875-901.
- Sheffer, N.A., Rico, M., Enzel, Y., Benito, G., Grodek, T., 2008. The palaeoflood record of the Gardon river, France: a comparison with the extreme 2002 flood event. *Geomorphology*, 98, 71-83.
- Siddall, M., Rohling, E.J., Almogi-Labin, A., Hemleben, C. Meischner, D. Schmelzer, I., Smeed, D.A., 2003. Sea-level fluctuations during the last glacial cycle. *Nature*, 423, 853-858.
- Siegenthaler, C., Sturm, M., 1991. Die Häufigkeit von Ablagerungen extremer Reuss-Hochwasser: Die Sedimentationsgeschichte im Urnersee seit dem Mittelalter. *Mitteilung Landeshydrologie und Geologie*, 14, 127-139.
- Sirocko, F., Raschke, E., 1993. Present means to define and estimate atmospheric "turbidity" and its effects on radiation fields at ground level: possible projections into the past. In: *Global Changes in the Perspective of the Past* (pp. 121-131). John Wiley & Sons Ltd., Chichester.
- Sirocko, F., Seelos, K., Schaber, K., Rein, B., Dreher, F., Diehl, M., Lehne, R., Jäger, K., Krbetschek, M., Degering, D., 2005. A late Eemian aridity pulse in Central Europe during the last glacial inception. *Nature*, 436, 833-836.
- Sirocko, F., 2009. *Wetter – Klima – Menschheitsentwicklung. Von der Eiszeit bis ins 21. Jahrhundert*. Theiss Verlag, Stuttgart.

- Sirocko, F., Dietrich, S., 2009. Wetter – Klima – Menschheitsentwicklung. Von der Eiszeit bis ins 21. Jahrhundert (Chapter 4). Theiss Verlag, Stuttgart.
- Sirocko, F., Dietrich, S., Veres, D., Grootes, P., Schaber-Mohr, K., Seelos, K., Nadeau, M.-J., Kromer, B., Rothacker, L., Röhner, M., Krbetschek, M., Appleby, P., Hambach, U., Rolf, C., Sudo, M., Grim, S., 2013. Multi-Proxy-Dating of Holocene maar lakes and Pleistocene dry maar sediments in the Eifel, Germany. *Quaternary Science Reviews*, 62, 56-72.
- Sirocko, F., Knapp, H., Dreher, F., Förster, M.W., Albert, J., Brunck, H., Veres, D., Dietrich, S., Zech, M., Hambach, U., Röhner, M., Rudert, S., Schwibus, K., Adams, C., Sigl, P., 2016. The ELSA-Vegetation-Stack: Reconstruction of Landscape Evolution Zones (LEZ) from laminated Eifel maar sediments of the last 60,000 years. *Global and Planetary Change*, 142, 108-135.
- SPECMAP Project, 1994 update. Paleoclimate Data, NOAA/ NCDC/ WDC Paleoclimatology, <http://gcmd.gsfc.nasa.gov/index.html>.
- Spötl, C., Mangini, A., 2007. Speleothems and paleoglaciars. *Earth and Planetary Science Letters*, 2554, 323-331.
- Starkel, L., 2002. Change in the frequency of extreme events as the indicator of climatic change in the Holocene (in fluvial systems). *Quaternary International*, 91, 25-32.
- State Office for Environment, Water Management and Trade Control Rhineland-Palatinate, 2015. (LUWG): Daily Gauge Values, Ahr, Altenahr 1945 – 2014; Daily Gauge Values, Kyll, Densborn 1972 – 2014; Daily Gauge Values, Prüm, Prümzurlay 1972-2014.
- Stebich, M., 1999. Palynologische Untersuchungen zur Vegetationsgeschichte des Weichsel-Spätglazial und Frühholozän an jährlich geschichteten Sedimenten des Meerfelder Maars (Eifel). *Dissertationes Botanicae*, 320, 1-127.
- Stolz, C., Grunert, J., 2008. Floodplain sediments of some streams in the Taunus and Westerwald Mts., western Germany, as evidence of historical land use. *Zeitschrift für Geomorphologie*, 52, 349-373.

- Storen, E.N., Dahl, S.O., Nesje, A., Paasche, O., 2010. Identifying the sedimentary imprint of high-frequency Holocene river floods in lake sediments: development and application of a new method. *Quaternary Science Reviews*, 29, 3021-3033.
- Straka, H., 1975. Die spätquartäre Vegetationsgeschichte der Vulkaneifel. *Beiträge zur Landespflege in Rheinland-Pfalz*, 3, 1-163.
- Street, M., Jöris, O., Turner, E., 2012. Magdalenian settlement in the German Rhineland – An update. *Quaternary International*, 272, 231-250.
- Sturm, M., Siegenthaler, C., Pickrill, R. A., 1995. Turbidites and homogenites – a conceptual model of flood and slide deposits. In: *Publication of IAS – 16th regional meeting sedimentology*. Paris.
- Svensson, A., Andersen, K.K., Bigler, M., Clausen, H.B., Dahl-Jensen, D., Davies, S.M., Johnsen, S.J., Muscheler, R., Parrenin, F., Rasmussen, S.O., Röthlisberger, R., Seierstad, I., Steffensen, J.P., Vinther, B.M., 2008. A 60 000 year Greenland stratigraphic ice core chronology. *Climate of the Past*, 4, 47-57.
- Swierczynski, T., Lauterbach, S., Dulski, P., Delgado, J., Merz, B., Brauer, A., 2013. Mid-to late Holocene flood frequency changes in the northeastern Alps as recorded in varved sediments of Lake Mondsee (Upper Austria). *Quaternary Science Reviews*, 80, 78-90.
- Tantau, I., Reille, M., de Beaulieu, L.-J., Farcas, S., 2005. Late Glacial and Holocene vegetation history in the southern part of Transylvania (Romania): pollen analysis of two sequences from Avrig. *Journal of Quaternary Science*, 21, 49-61.
- Terberger, T., Street, M., 2003. New evidence for the chronology of the Aurignacian and the question of Pleniglacial settlement in western Central Europe. *The Chronology of the Aurignacian and of the Transitional Technocomplexes: Dating, Stratigraphies, Cultural Implications*, *Trabalhos de Arqueologia*, 33, 213-221.
- Thornalley, D.J., Barker, S., Broecker, W.S., Elderfield, H., McCave, I.N., 2011. The deglacial evolution of North Atlantic deep convection. *Science*, 331, 202-205.

- Thorndycraft, V.R., Benito, G., Rico, M., Sopeña, A., Sánchez-Moya, Y., Casas, A., 2005. A long-term flood discharge record derived from slackwater flood deposits of the Llobregat River, NE Spain. *Journal of Hydrology*, 313, 16-31.
- Timar-Gabor, A., Vandenberghe, D.A.G., Vasiliniuc, S., Panaitu, C.E., Panaiotu, C.G., Dimofte, D., Cosma, C., 2011. Optical dating of Romanian loess: a comparison between silt-sized and sand-sized quartz. *Quaternary International*, 240, 62-70.
- Tinner, W., Lotter, A.F., 2006. Holocene expansion of *Fagus silvatica* and *Abies alba* in Central Europe: where are we after eight decades of debate? *Quaternary Science Reviews*, 25, 526-549.
- Tucker, M., 1996. *Methoden der Sedimentologie*. Ferdinand Enke-Verlag, Stuttgart.
- Usinger, H., 1982. Pollenanalytische Untersuchungen an spätglazialen und präborealen Sedimenten aus dem Meerfelder Maar (Eifel). *Flora*, 172, 373-409.
- Vandenberghe, J., 1992a. Periglacial Phenomena and Pleistocene Environmental Conditions in the Netherlands-An Overview. *Permafrost and Periglacial Processes*, 3, 363-374.
- Vandenberghe, J., 1992b. Geomorphology and climate of the cool oxygen isotope stage 3 in comparison with the cold stages 2 and 4 in The Netherlands. *Zeitschrift der Geomorphologie*, 86, 65-75.
- Vandenberghe, J., 1995. Timescales, climate and river development. *Quaternary Science Reviews*, 14, 631-638.
- Vandenberghe, J., 2003. Climate forcing of fluvial system development: an evolution of ideas. *Quaternary Science Reviews*, 22, 2053-2060.
- van den Bogaard, P., 1995. $^{40}\text{Ar}/^{39}\text{Ar}$ ages of sanidine phenocrysts from Laacher See Tephra (12 900 b2k): Chronostratigraphic and petrological significance. *Earth Planet. Science Letters*, 133, 163-174.
- van den Bogaard, P., Schmincke, H.-U., 1990. Die Entwicklungsgeschichte des Mittelrheinraumes und die Eruptionsgeschichte des Osteifel-Vulkanfeldes. *Rheingeschichte zwischen Mosel und Maas. deuqua-Führer*, 1, 166-190.

- van den Bogaard, P., Schmincke, H.-U., 1985. Laacher See Tephra – a Widespread Isochronous Late Quaternary Tephra Layer in Central and Northern Europe. *Geological Society of America Bulletin*, 96, 1554-1571.
- van den Bogaard, P., Hall, C.M., Schmincke H.-U., York, D., 1989. Precise single-grain $^{40}\text{Ar}/^{39}\text{Ar}$ dating of a cold to warm climate transition in Central Europe. *Nature*, 342, 523-525.
- van Kreveld, S., Sarnthein, M., Erlenkeuser, H., Grootes, P., Jung, S., Nadeau, M.J., Pflaumann, U., Voelker, A., 2004. Potential links between surging ice sheets, circulation changes, and the Dansgaard-Oeschger cycles in the Irminger Sea, 60-18 kyr. *Paleoceanography*, 15, 425-442.
- van Huissteden, K., Vandenberghe, J., Pollard, D., 2003. Paleotemperature reconstructions of the European permafrost zone during marine oxygen isotope Stage 3 compared with climate model results. *Journal of Quaternary Science*, 18, 453-464.
- van Meerbeek, C.J., Renssen, H., Roche, D.M., Wohlfarth, B., Bohncke, S.J.P., Bos, J.A.A., Engels, S., Helmens, K.F., Sanchez-Goni, M.F., Svensson, A., Vandenberghe, J., 2011. The nature of MIS 3 stadial-interstadial transitions in Europe: New insights from model-data comparisons. *Quaternary Science Reviews*, 30, 3618-3637.
- Veres, D., Bazin, L., Landais, A., Toyé Mahamadou Kele, H., Lemieux-Dudon, B., Parrenin, F., Martinerie, P., Blayo, E., Blunier, T., Capron, E., Chappellaz, J., Rasmussen, S.O., Severi, M., Svensson, A., Vinther, B., Wolff, E., 2013. The Antarctic ice core chronology (AICC2012): an optimized multi-parameter and multi-site dating approach for the last 120 thousand years. *Climate of the Past*, 9, 1733-1748.
- Veres, D., Lallier-Vergès, E., Wohlfarth, B., Lacourse, T., Kéravis, D., Björck, S., Preusser, F., Andrieu-Ponel, V., Ampel, L., 2009. Climate-driven changes in lake conditions during MIS 3 and 2: a high-resolution geochemical record from Les Echets, France. *Boreas*, 38, 230-243.

- Veres, D., Davies, S.M., Wohlfarth, B., Preusser, F., Wastegard, S., Ampel, L., Hormes, A., Possnert, G., Raynal, J.-P., Vernet, G., 2008. Age, origin and significance of a new middle MIS 3 tephra horizon identified within a long-core sequence from Les Echets, France. *Boreas*, 37, 434-443.
- von Grafenstein, U., Erlenkeuser, H., Müller, J., Jouzel, J., Johnsen, S., 1998. The cold event 8200 years ago documented in oxygen isotope records of precipitation in Europe and Greenland. *Climate dynamics*, 14, 73-81.
- Walker, R.G., Mutti, E., 1973. Part IV. Turbidite Facies and Facies Associations. *Turbidites and Deep Water Sedimentation*, 119-158.
- Water management administration Rhineland-Palatinate: German river code.
- Welten, M., 1982. Pollenanalytische Untersuchungen im Jüngeren Quartär des nördlichen Alpenvorlandes der Schweiz. Beiträge zur Geologischen Karte der Schweiz N.F. In: Beiträge zur Geologischen Karte der Schweiz. Stämpfli + Cie.
- Wernli, H., Pfahl, S., 2009. Grundlage des Klimas und extremer Wettersituationen. In: *Wetter, Klima, Menschheitsentwicklung. Von der Eiszeit bis ins 21. Jahrhundert*. Theiss, Stuttgart.
- Wessels, M., 1998. Natural environmental changes indicated by Late Glacial and Holocene sediments from Lake Constance, Germany. Wessels, M. (1998). Natural environmental changes indicated by Late Glacial and Holocene sediments from Lake Constance, Germany. *Palaeogeography, Palaeoclimatology, Palaeoecology*, 140, 421-432.
- Whittington, G., Hall, A.M., 2002. The Tolsta Interstadial, Scotland: correlation with D-O cycles GI-8 to GI-5? *Quaternary Science Reviews*, 21, 901-915.
- Wilhelm, B., Arnaud, F., Enters, D., Allignol, F., Legaz, A., Magand, O., Revillon, S., Giguet-Covex, C., Malet, E., 2012a. Does global warming favour the occurrence of extreme floods in European Alps? First evidences from a NW Alps proglacial lake sediment record. *Climatic Change*, 113, 563-581.

- Wilhelm, B., Arnaud, F., Sabatier, P., Crouzet, C., Brisset, E., Chaumillon, E., Disnar, J.-R., Guiter, F., Malet, E., Reyss, J.-L., Tachikawa, K., Bard, E., Delannoy, J.-J., 2012b. 1400 years of extreme precipitation patterns over the Mediterranean French Alps and possible forcing mechanisms. *Quaternary Research*, 78, 1-12.
- Wilhelm, B., Arnaud, F., Sabatier, P., Magand, O., Chapron, E., Courp, T., Tachikawa, K., Fanget, B., Malet, E., Pignol, C., Bard, E., Delannoy, J.-J., 2013. Palaeoflood activity and climate change over the last 1400 years recorded by lake sediments in the north-west European Alps. *Journal of Quaternary Science*, 28, 189-199.
- Wirth, S.B., Girardclos, S., Rellstab, C., Anselmetti, F.S., 2011. The sedimentary response to a pioneer geo-engineering project: Tracking the Kander River deviation in the sediments of Lake Thun (Switzerland). *Sedimentology*, 58, 1737-1761.
- Wirth, S.B., Glur, L., Gilli, A., Anselmetti, F.S., 2013. Holocene flood frequency across the Central Alps—solar forcing and evidence for variations in North Atlantic atmospheric circulation. *Quaternary Science Reviews*, 80, 112-128.
- Wohlfahrt, B., Veres, D., Ampel, L., Lacourse, T., Blaauw, M., Preusser, F., Andrieu-Ponel, V., Kéravis, D., Lallier-Vergés, E., Björck, S., Davies, S.M., de Beaulieu, J.-L., Risberg, J., Hormes, A., Kasper, H.U., Possnert, G., Reille, M., Thouveny, N., Zander, A., 2008. Rapid ecosystem response to abrupt climate changes during the last glacial period in Western Europe, 40 – 16 ka. *Geology* 36, 407-410.
- Woillard, G.M., 1978. Grand Pile peat bog: a continuous pollen record for the last 140,000 years. *Quaternary Research*, 9, 1-21.
- Woillard, G.M., Mook, W.G., 1982. Carbon-14 Dates at Grande Pile: Correlation of Land and Sea Chronologies. *Science*, 215, 159-161.
- Wolff, E.W., Chappellaz, J., Blunier, T., Rasmussen, S.O., Svensson, A., 2010. Millennial-scale variability during the last glacial: The ice core record. *Quaternary Science Reviews*, 29, 2828-2838.
- Wunderlich, T., Petersen, H., Attia al Hagrey, S., Rabbel, W., 2013. Pedophysical models for resistivity and permittivity of partially water-saturated soils. *Vadose Zone Journal*, 12.

- Yang, D., Yu, G., Xie, Y., Zhan, D., Li, Z., 2000. Sedimentary records of large Holocene floods from the middle reaches of the Yellow River, China. *Geomorphology*, 33, 73-88.
- Yu, H., Xu, J., Luan, P., Zhao, B., Pan, B., 2013. Probabilistic assessment of tephra fallout hazard at Changbaishan volcano, Northeast China. *Natural Hazards*, 69, 1369-1388.
- Zagwijn, H.W., 1996. An analysis of the Eemian climate in western and Central Europe. *Quaternary Science Reviews*, 15, 451-469.
- Zagwijn, W.H., 1974. Vegetation, Climate and Radiocarbon Datings in the Late Pleistocene of the Netherlands: Middle Weichselian, 25, 101-111.
- Zech, M., 2012. Reconstructing Quaternary vegetation history in the Carpathian Basin, SE Europe, using n-alkane biomarkers as molecular fossils: problems and possible solutions, potential and limitations. *Quaternary International*, 279, 555.
- Zielhofer, C., Faust, D., Linstädter, J., 2008. Late Pleistocene and Holocene alluvial archives in the Southwestern Mediterranean: Changes in fluvial dynamics and past human response. *Quaternary International*, 181, 39-54.
- Zolitschka, B., 1991. Absolute dating of late Quaternary lacustrine sediments by high-resolution varve chronology. *Hydrobiologia*, 214, 59-61.
- Zolitschka, B., 1992. Climatic change evidence and lacustrine varves from maar lakes, Germany. *Climate Dynamics*, 6, 229-232.
- Zolitschka, B., Negendank, J.F.W., Lottermoser, B.G., 1995. Sedimentological proof and dating of the Early Holocene volcanic eruption of Ulmener Maar. *Geologische Rundschau*, 84, 213-219.
- Zolitschka, B., 1998. "Paläoklimatische Bedeutung laminiertes Sedimente." Gebrüder Bornträger, Berlin/ Stuttgart.
- Zolitschka, B., Francus, P., Ojala, A.E., Schimmelmann, A., 2015. Varves in lake sediments – a review. *Quaternary Science Reviews*, 117, 1-41.

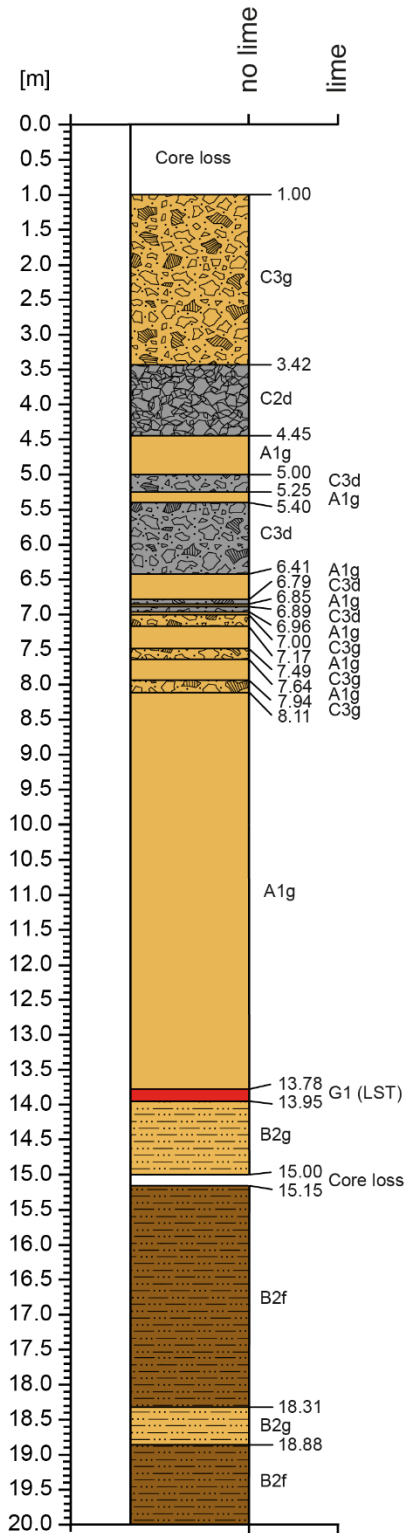
Zöller, L., Richter, D., Blanchard, H., Einwögerer, T., Händel, M., Neugebauer-Maresch, C., 2014. Our oldest children: Age constraints for the Krems-Wachtberg site obtained from various thermoluminescence dating approaches. *Quaternary International*, 351, 83-87.

Appendix A Core data table

Maar structure	core	GK Zone 2 Rechtswert	GK Zone 2 Hochwert	core depth (m)	hight above sealevel (m)	UTM coordinates
Auel dry Maar	AU1	2542210	5572160	44,50	455	32 N 328427 5572977
Auel dry Maar	AU2	2542458	5572044	123,00	453	32 N 328668 5572850
Auel dry Maar	AU6	2542475	5572054	9,20	452	32 N 328686 5572859
Auel dry Maar	AU7	2542516	5572174	3,00	452	32 N 328732 5572977
Auel dry Maar	AU8	2542509	5572020	11,00	452	32 N 328718 5572824
Auel dry Maar	AU9	2542458	5572018	5,00	454	32 N 328667 5572824
Auel dry Maar	AU10	2542524	5571996	11,00	452	32 N 328732 5572799
Holzmaar (lake)	HM1	2562900	5554030	10,00	425	32 N 348369 5554031
Immerather Risch	IM1	2568735	5555520	6,00	376	32 N 354256 5555284
Mehren dry Maar	MEH1	2564347	5559481	9,00	417	32 N 350032 5559418
Merscheid dry Maar	MS1	2538562	5573162	69,00	534	32 N 324823 5574125
Merscheid dry Maar	MS2	2538294	5573218	15,00	545	32 N 324555 5574191
Merscheid dry Maar	MS3	2538400	5573137	19,00	546	32 N 324658 5574105
Oberstadtfeld dry Maar	OS1	2555156	5560041	5,00	413	32 N 340872 5560347
Roth dry Maar	RM2	2543958	5569786	65,00	453	32 N 330076 5570533
Schalkenmehrener Maar West (lake)	SM3	2561375	5559668	12,00	420	32 N 347072 5559725
Schalkenmehrener Maar West (lake)	SMf2	2561310	5559615	2,06	420	32 N 347005 5559674
Ulmener Maar (lake)	UM2	2570165	5564270	12,00	410	32 N 356038 5563969
Wollmerath dry Maar	Woll1	2570079	5557919	12,00	355	32 N 355695 5557627

Appendix B High resolution lithology

Core: AU2 Auel



A) Interglacial/Interstadial

- 1 Gyttja
- 2 Sapropel
- 3 Diatom gyttja

B) Glacial

- 1 Silt lamination
- 2 Silt-Cley lamination

C) Detrital

- 1 Rounded
- 2 Angular
- 3 Matrix supported

D) Rearrangement

- 1 Sand layer
- 2 Dark sand layer
- 3 Clay layer
- 4 Turbidite
- 5 Cross-bedding
- 6 Soil horizon

E) Slump

- 1 folded
- 2 Mottled appearance

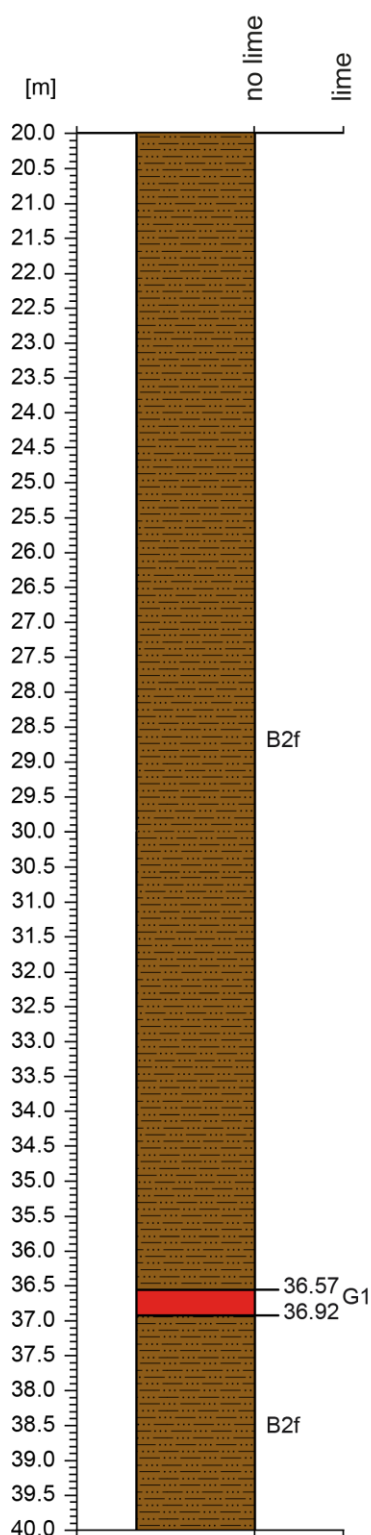
F) Tephra

- 1 Ash
- 2 Lapilli
- 3 Tuff

Colours

- | | |
|--|--------------|
| | whitish |
| | White |
| | Dark grey |
| | Grey |
| | Light grey |
| | Brown |
| | Brown/Yellow |
| | Yellow |
| | Reddish |

Core: AU2 Auel



A) Interglacial/Interstadial

- 1 Gyttja
- 2 Sapropel
- 3 Diatom gyttja

B) Glacial

- 1 Silt lamination
- 2 Silt-Cley lamination

C) Detrital

- 1 Rounded
- 2 Angular
- 3 Matrix supported

D) Rearrangement

- 1 Sand layer
- 2 Dark sand layer
- 3 Clay layer
- 4 Turbidite
- 5 Cross-bedding
- 6 Soil horizon

E) Slump

- 1 folded
- 2 Mottled appearance

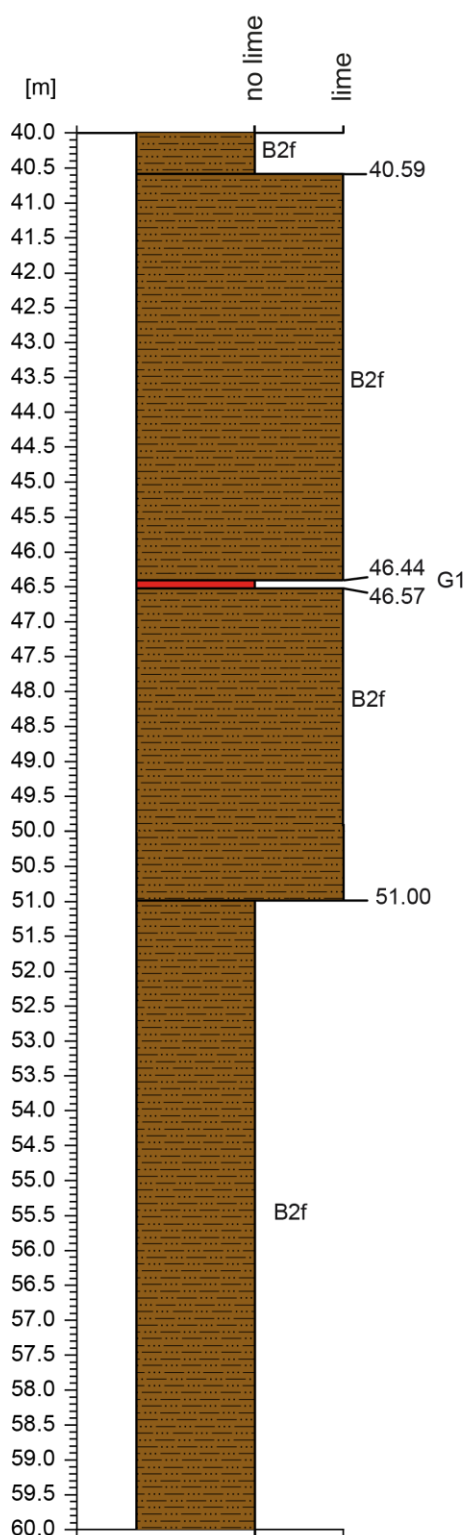
F) Tephra

- 1 Ash
- 2 Lapilli
- 3 Tuff

Colours

- a** whitish
- b** White
- c** Dark grey
- d** Grey
- e** Light grey
- f** Brown
- g** Brown/Yellow
- h** Yellow
- i** Reddish

Core: AU2 Auel



A) Interglacial/Interstadial

- 1 Gyttja
- 2 Sapropel
- 3 Diatom gyttja

B) Glacial

- 1 Silt lamination
- 2 Silt-Cley lamination

C) Detrital

- 1 Rounded
- 2 Angular
- 3 Matrix supported

D) Rearrangement

- 1 Sand layer
- 2 Dark sand layer
- 3 Clay layer
- 4 Turbidite
- 5 Cross-bedding
- 6 Soil horizon

E) Slump

- 1 folded
- 2 Mottled appearance

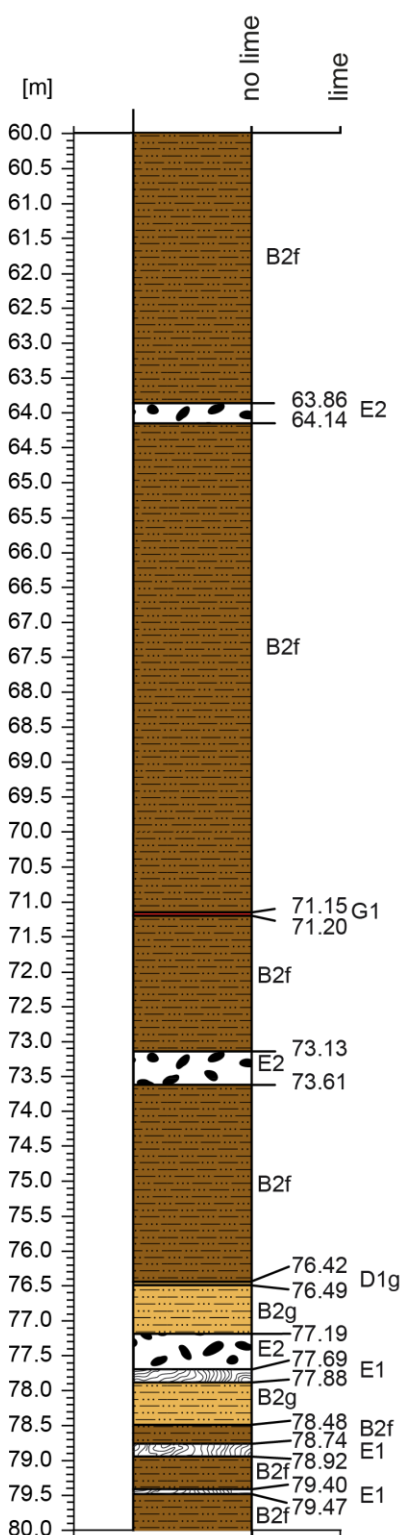
F) Tephra

- 1 Ash
- 2 Lapilli
- 3 Tuff

Colours

- a whitish
- b White
- c Dark grey
- d Grey
- e Light grey
- f Brown
- g Brown/Yellow
- h Yellow
- i Reddish

Core: AU2 Auel



A) Interglacial/Interstadial

- 1 Gyttja
- 2 Sapropel
- 3 Diatom gyttja

B) Glacial

- 1 Silt lamination
- 2 Silt-Cley lamination

C) Detrital

- 1 Rounded
- 2 Angular
- 3 Matrix supported

D) Rearrangement

- 1 Sand layer
- 2 Dark sand layer
- 3 Clay layer
- 4 Turbidite
- 5 Cross-bedding
- 6 Soil horizon

E) Slump

- 1 folded
- 2 Mottled appearance

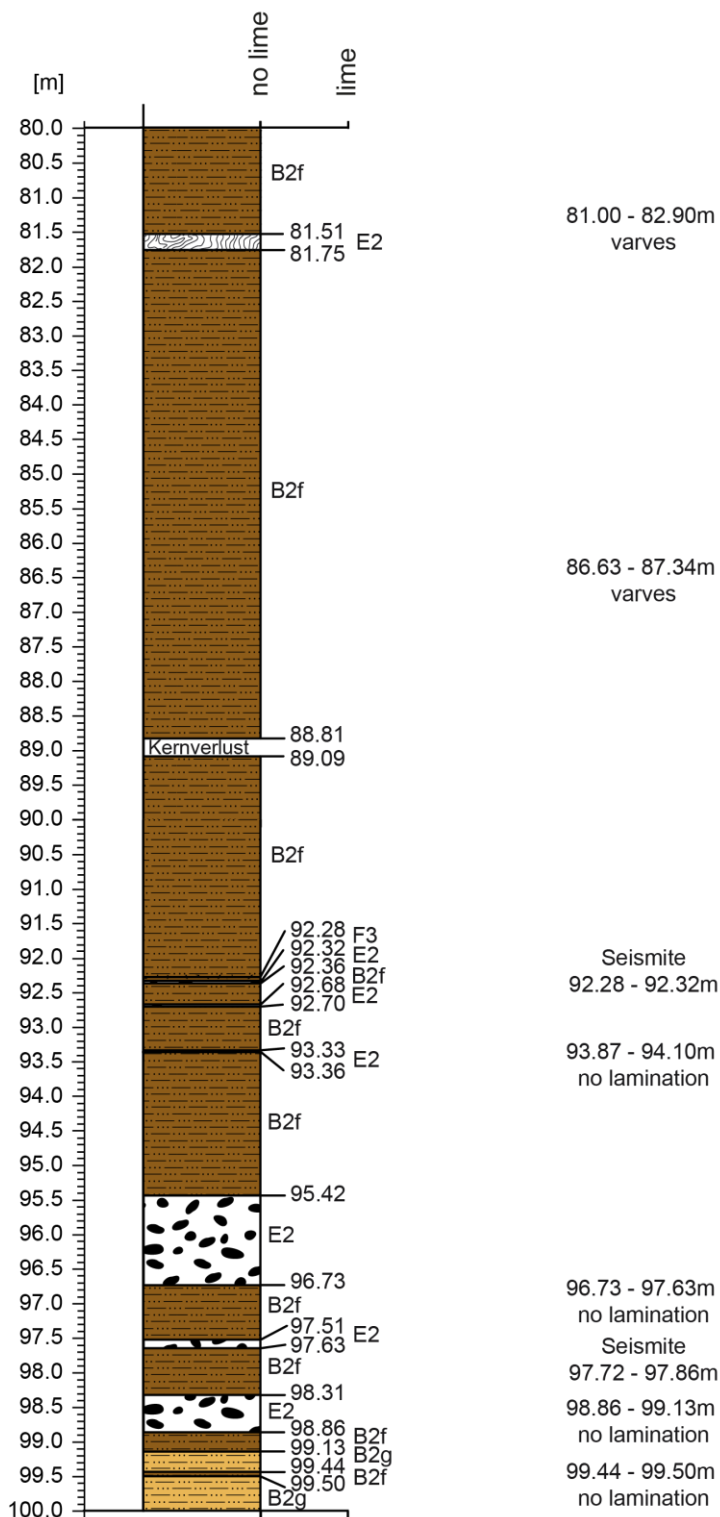
F) Tephra

- 1 Ash
- 2 Lapilli
- 3 Tuff

Colours

- a** whitish
- b** White
- c** Dark grey
- d** Grey
- e** Light grey
- f** Brown
- g** Brown/Yellow
- h** Yellow
- i** Reddish

Core: AU2 Auel



A) Interglacial/Interstadial

- 1 Gyttja
- 2 Sapropel
- 3 Diatom gyttja

B) Glacial

- 1 Silt lamination
- 2 Silt-Cley lamination

C) Detrital

- 1 Rounded
- 2 Angular
- 3 Matrix supported

D) Rearrangement

- 1 Sand layer
- 2 Dark sand layer
- 3 Clay layer
- 4 Turbidite
- 5 Cross-bedding
- 6 Soil horizon

E) Slump

- 1 folded
- 2 Mottled appearance

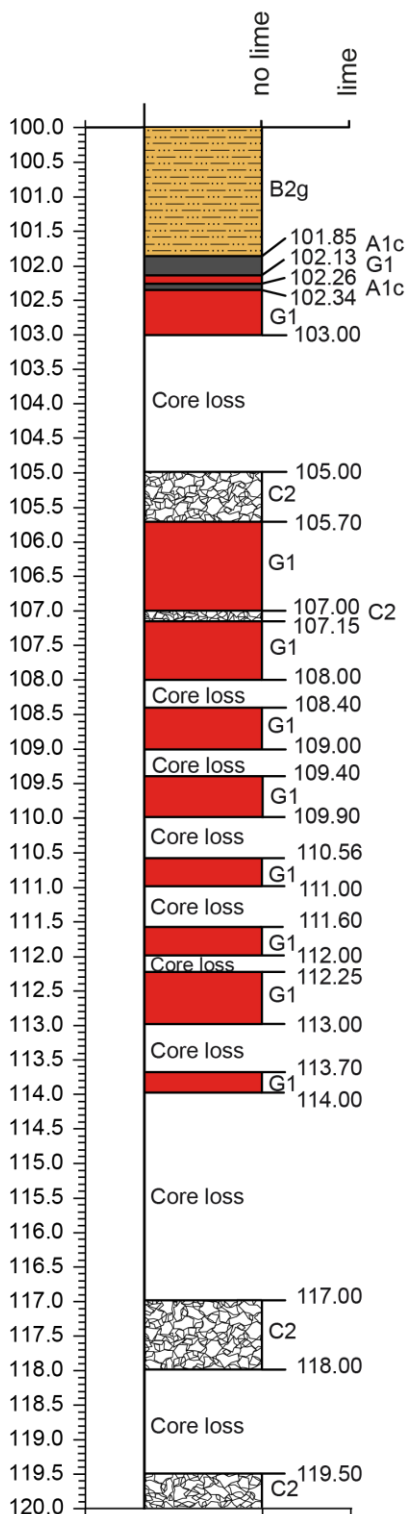
F) Tephra

- 1 Ash
- 2 Lapilli
- 3 Tuff

Colours

- a whitish
- b White
- c Dark grey
- d Grey
- e Light grey
- f Brown
- g Brown/Yellow
- h Yellow
- i Reddish

Core: AU2 Auel



A) Interglacial/Interstadial

- 1 Gyttja
- 2 Sapropel
- 3 Diatom gyttja

B) Glacial

- 1 Silt lamination
- 2 Silt-Cley lamination

C) Detrital

- 1 Rounded
- 2 Angular
- 3 Matrix supported

D) Rearrangement

- 1 Sand layer
- 2 Dark sand layer
- 3 Clay layer
- 4 Turbidite
- 5 Cross-bedding
- 6 Soil horizon

E) Slump

- 1 folded
- 2 Mottled appearance

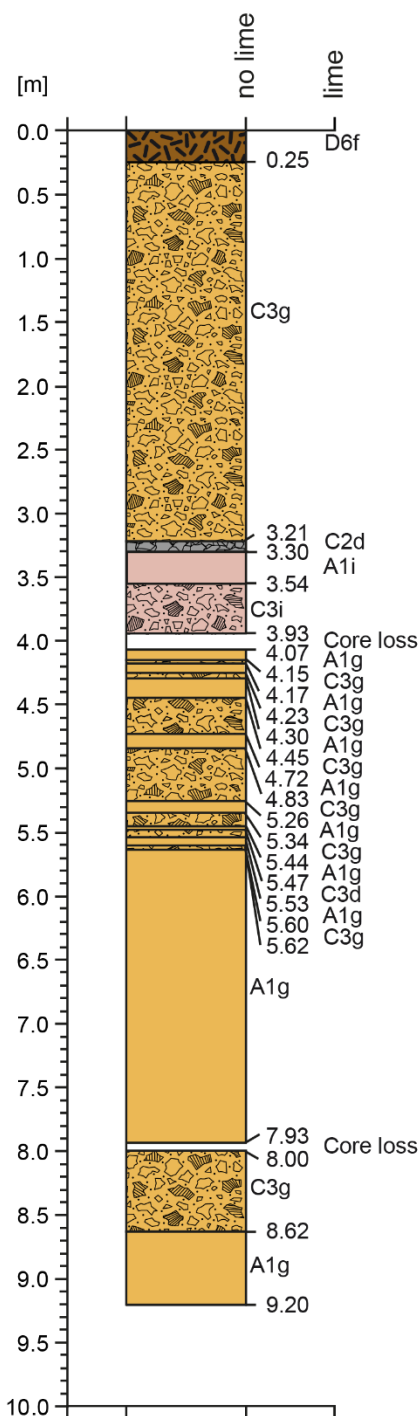
F) Tephra

- 1 Ash
- 2 Lapilli
- 3 Tuff

Colours

- a whitish
- b White
- c Dark grey
- d Grey
- e Light grey
- f Brown
- g Brown/Yellow
- h Yellow
- i Reddish

Core: AU6 Auel



A) Interglacial/Interstadial

- 1 Gyttja
- 2 Sapropel
- 3 Diatom gyttja

B) Glacial

- 1 Silt lamination
- 2 Silt-Cley lamination

C) Detrital

- 1 Rounded
- 2 Angular
- 3 Matrix supported

D) Rearrangement

- 1 Sand layer
- 2 Dark sand layer
- 3 Clay layer
- 4 Turbidite
- 5 Cross-bedding
- 6 Soil horizon

E) Slump

- 1 folded
- 2 Mottled appearance

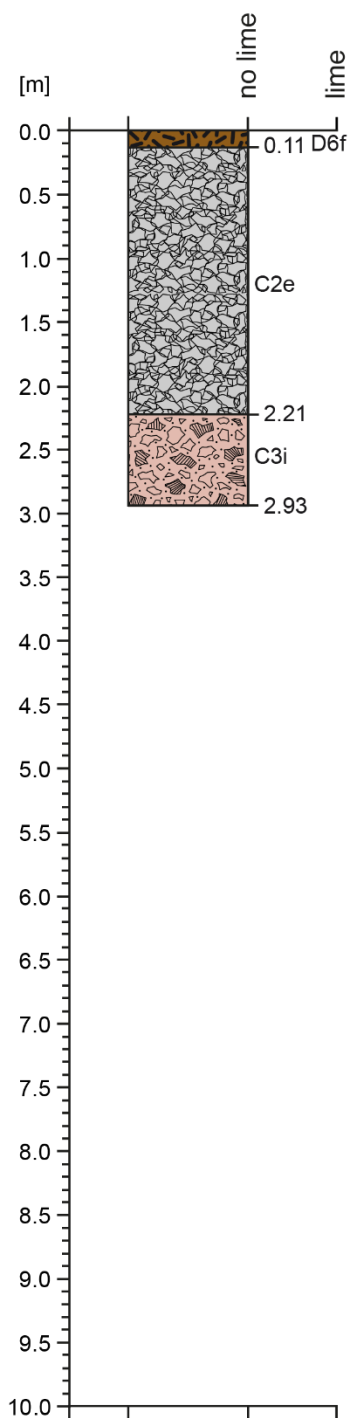
F) Tephra

- 1 Ash
- 2 Lapilli
- 3 Tuff

Colours

- a** whitish
- b** White
- c** Dark grey
- d** Grey
- e** Light grey
- f** Brown
- g** Brown/Yellow
- h** Yellow
- i** Reddish

Core: AU7 Auel



A) Interglacial/Interstadial

- 1 Gyttja
- 2 Sapropel
- 3 Diatom gyttja

B) Glacial

- 1 Silt lamination
- 2 Silt-Clay lamination

C) Detrital

- 1 Rounded
- 2 Angular
- 3 Matrix supported

D) Rearrangement

- 1 Sand layer
- 2 Dark sand layer
- 3 Clay layer
- 4 Turbidite
- 5 Cross-bedding
- 6 Soil horizon

E) Slump

- 1 folded
- 2 Mottled appearance

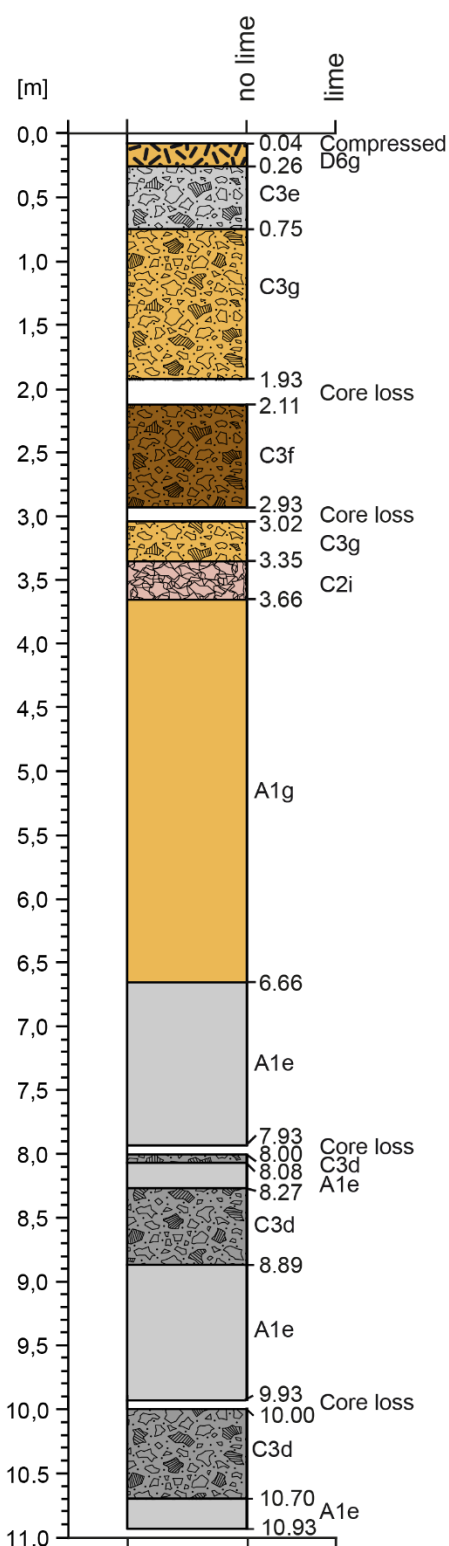
F) Tephra

- 1 Ash
- 2 Lapilli
- 3 Tuff

Colours

- a** whitish
- b** White
- c** Dark grey
- d** Grey
- e** Light grey
- f** Brown
- g** Brown/Yellow
- h** Yellow
- i** Reddish

Core: AU8 Auel



A) Interglacial/Interstadial

- 1 Gyttja
- 2 Sapropel
- 3 Diatom gyttja

B) Glacial

- 1 Silt lamination
- 2 Silt-Clay lamination

C) Detrital

- 1 Rounded
- 2 Angular
- 3 Matrix supported

D) Rearrangement

- 1 Sand layer
- 2 Dark sand layer
- 3 Clay layer
- 4 Turbidite
- 5 Cross-bedding
- 6 Soil horizon

E) Slump

- 1 folded
- 2 Mottled appearance

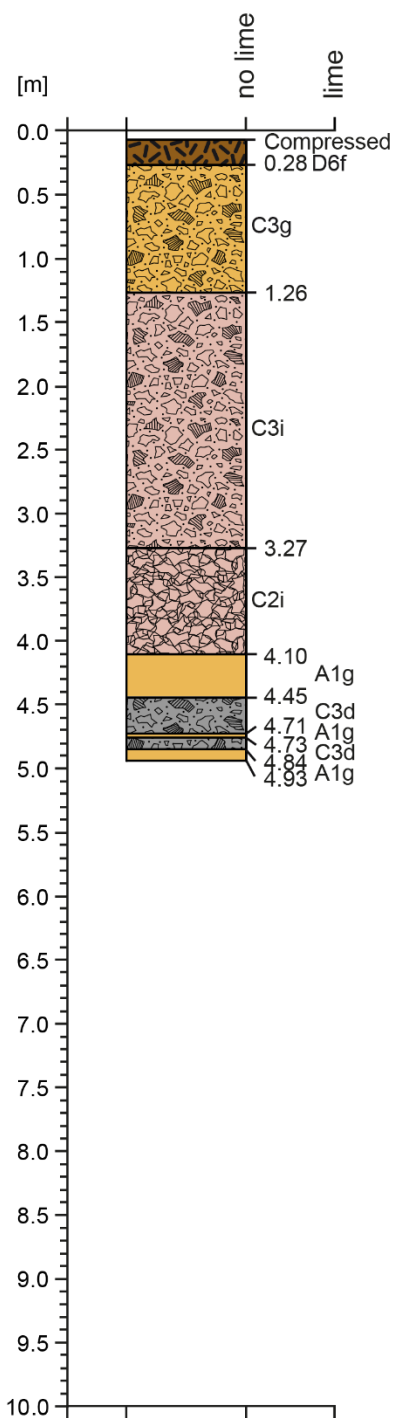
F) Tephra

- 1 Ash
- 2 Lapilli
- 3 Tuff

Colours

- a** whitish
- b** White
- c** Dark grey
- d** Grey
- e** Light grey
- f** Brown
- g** Brown/Yellow
- h** Yellow
- i** Reddish

Core: AU9 Auel



A) Interglacial/Interstadial

- 1 Gyttja
- 2 Sapropel
- 3 Diatom gyttja

B) Glacial

- 1 Silt lamination
- 2 Silt-Clay lamination

C) Detrital

- 1 Rounded
- 2 Angular
- 3 Matrix supported

D) Rearrangement

- 1 Sand layer
- 2 Dark sand layer
- 3 Clay layer
- 4 Turbidite
- 5 Cross-bedding
- 6 Soil horizon

E) Slump

- 1 folded
- 2 Mottled appearance

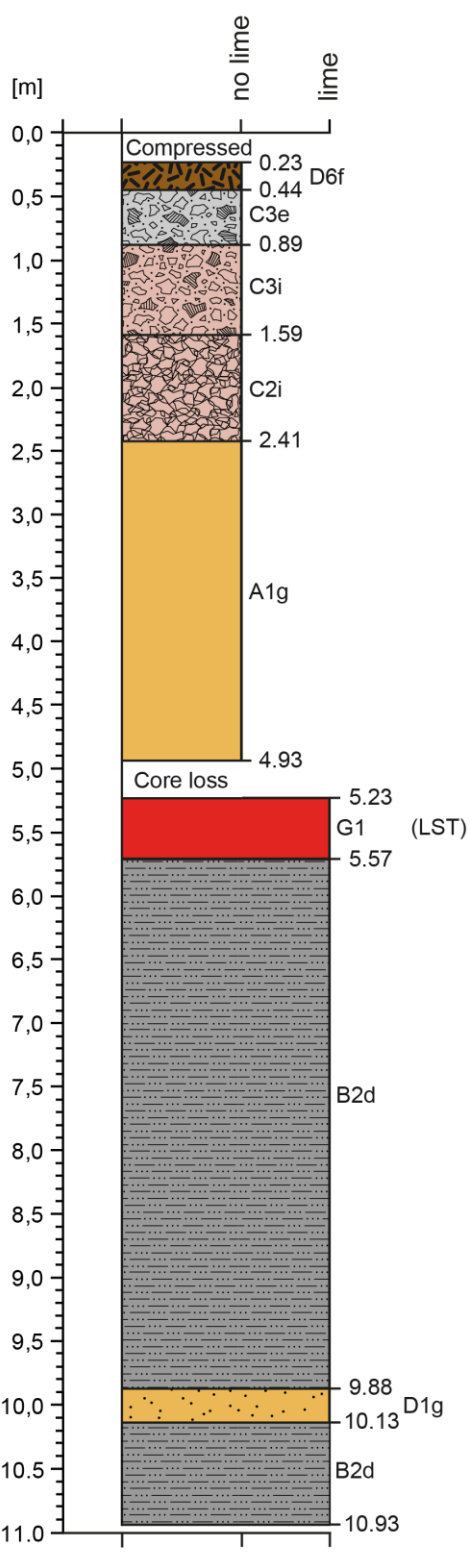
F) Tephra

- 1 Ash
- 2 Lapilli
- 3 Tuff

Colours

- a** whitish
- b** White
- c** Dark grey
- d** Grey
- e** Light grey
- f** Brown
- g** Brown/Yellow
- h** Yellow
- i** Reddish

Core: AU10 Auel



A) Interglacial/Interstadial

- 1 Gyttja
- 2 Sapropel
- 3 Diatom gyttja

B) Glacial

- 1 Silt lamination
- 2 Silt-Cley lamination

C) Detrital

- 1 Rounded
- 2 Angular
- 3 Matrix supported

D) Rearrangement

- 1 Sand layer
- 2 Dark sand layer
- 3 Clay layer
- 4 Turbidite
- 5 Cross-bedding
- 6 Soil horizon

E) Slump

- 1 folded
- 2 Mottled appearance

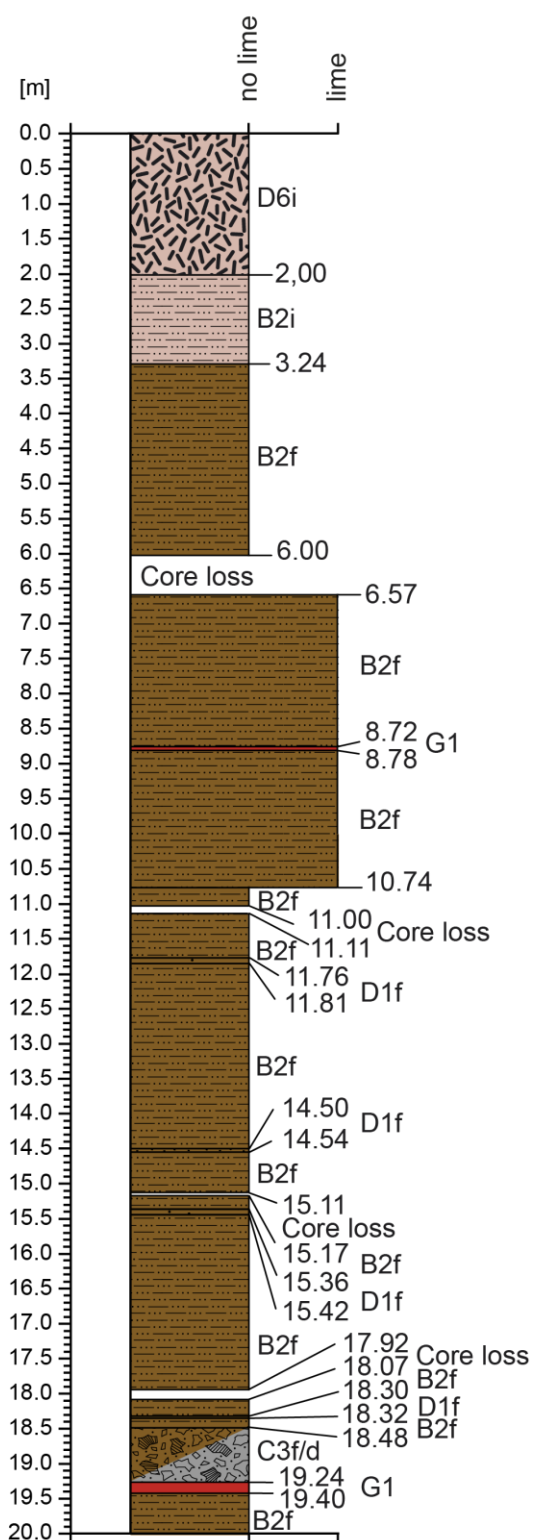
F) Tephra

- 1 Ash
- 2 Lapilli
- 3 Tuff

Colours

- a** whitish
- b** White
- c** Dark grey
- d** Grey
- e** Light grey
- f** Brown
- g** Brown/Yellow
- h** Yellow
- i** Reddish

Core: MS1 Merscheid



A) Interglacial/Interstadial

- 1 Gyttja
- 2 Sapropel
- 3 Diatom gyttja

B) Glacial

- 1 Silt lamination
- 2 Silt-Clay lamination

C) Detrital

- 1 Rounded
- 2 Angular
- 3 Matrix supported

D) Rearrangement

- 1 Sand layer
- 2 Dark sand layer
- 3 Clay layer
- 4 Turbidite
- 5 Cross-bedding
- 6 Soil horizon

E) Slump

- 1 folded
- 2 Mottled appearance

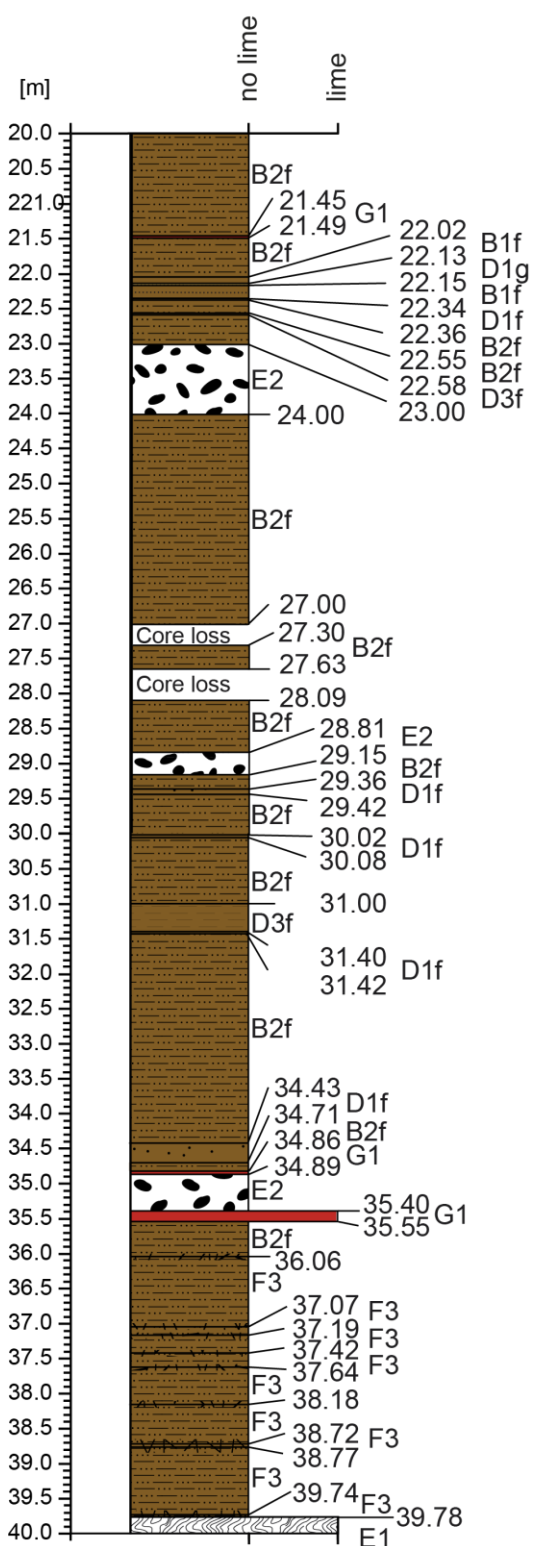
F) Tephra

- 1 Ash
- 2 Lapilli
- 3 Tuff

Colours

- a whitish
- b White
- c Dark grey
- d Grey
- e Light grey
- f Brown
- g Brown/Yellow
- h Yellow
- i Reddish

Core: MS1 Merscheid



25.00 - 30.00
lamination
25.79 - 26.10
no lamination

A) Interglacial/Interstadial

- 1 Gyttja
- 2 Sapropel
- 3 Diatom gyttja

B) Glacial

- 1 Silt lamination
- 2 Silt-Clay lamination

C) Detrital

- 1 Rounded
- 2 Angular
- 3 Matrix supported

D) Rearrangement

- 1 Sand layer
- 2 Dark sand layer
- 3 Clay layer
- 4 Turbidite
- 5 Cross-bedding
- 6 Soil horizon

E) Slump

- 1 folded
- 2 Mottled appearance

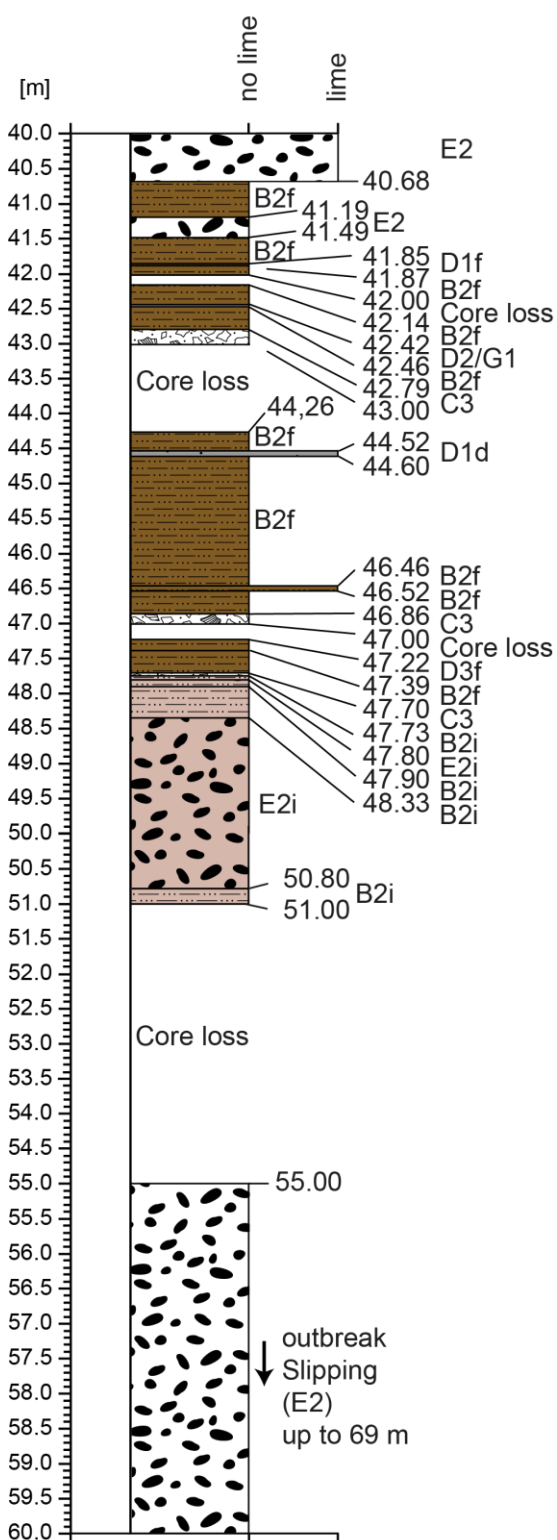
F) Tephra

- 1 Ash
- 2 Lapilli
- 3 Tuff

Colours

- a whitish
- b White
- c Dark grey
- d Grey
- e Light grey
- f Brown
- g Brown/Yellow
- h Yellow
- i Reddish

Core: MS1 Merscheid



A) Interglacial/Interstadial

- 1 Gyttja
- 2 Sapropel
- 3 Diatom gyttja

B) Glacial

- 1 Silt lamination
- 2 Silt-Clay lamination

C) Detrital

- 1 Rounded
- 2 Angular
- 3 Matrix supported

D) Rearrangement

- 1 Sand layer
- 2 Dark sand layer
- 3 Clay layer
- 4 Turbidite
- 5 Cross-bedding
- 6 Soil horizon

E) Slump

- 1 folded
- 2 Mottled appearance

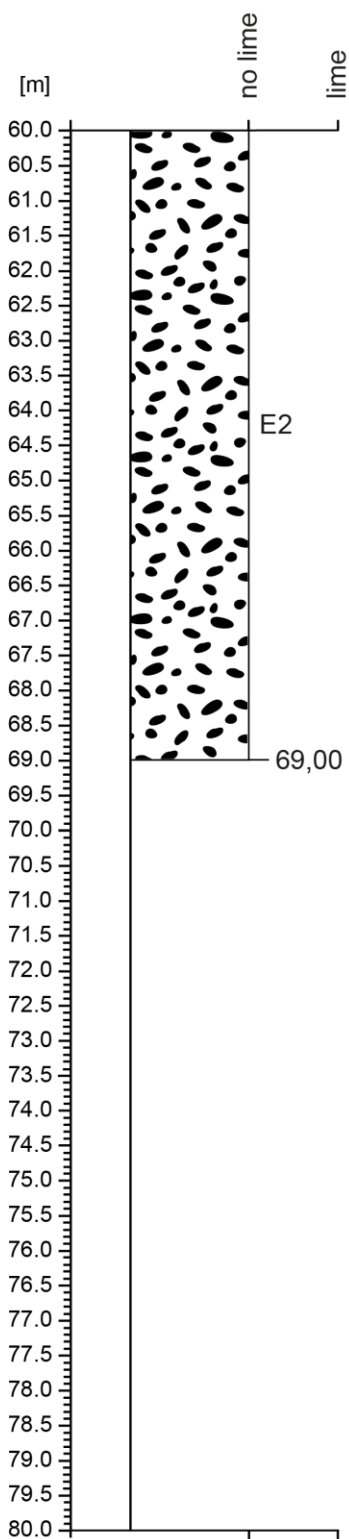
F) Tephra

- 1 Ash
- 2 Lapilli
- 3 Tuff

Colours

- a whitish
- b White
- c Dark grey
- d Grey
- e Light grey
- f Brown
- g Brown/Yellow
- h Yellow
- i Reddish

Core: MS1 Merscheid



A) Interglacial/Interstadial

- 1 Gyttja
- 2 Sapropel
- 3 Diatom gyttja

B) Glacial

- 1 Silt lamination
- 2 Silt-Clay lamination

C) Detrital

- 1 Rounded
- 2 Angular
- 3 Matrix supported

D) Rearrangement

- 1 Sand layer
- 2 Dark sand layer
- 3 Clay layer
- 4 Turbidite
- 5 Cross-bedding
- 6 Soil horizon

E) Slump

- 1 folded
- 2 Mottled appearance

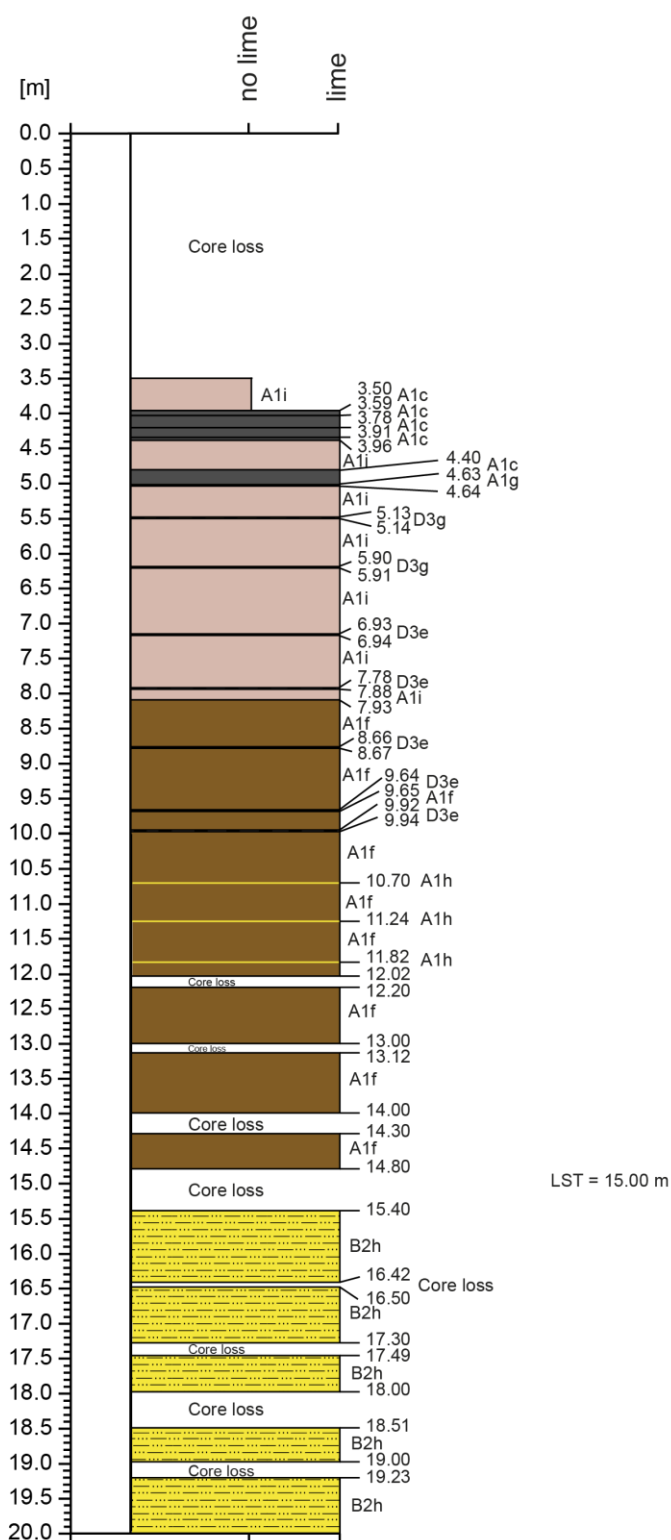
F) Tephra

- 1 Ash
- 2 Lapilli
- 3 Tuff

Colours

- a** whitish
- b** White
- c** Dark grey
- d** Grey
- e** Light grey
- f** Brown
- g** Brown/Yellow
- h** Yellow
- i** Reddish

Core: RM2 Rother Maar



A) Interglacial/Interstadial

- 1 Gyttja
- 2 Sapropel
- 3 Diatom gyttja

B) Glacial

- 1 Silt lamination
- 2 Silt-Clay lamination

C) Detrital

- 1 Rounded
- 2 Angular
- 3 Matrix supported

D) Rearrangement

- 1 Sand layer
- 2 Dark sand layer
- 3 Clay layer
- 4 Turbidite
- 5 Cross-bedding
- 6 Soil horizon

E) Slump

- 1 folded
- 2 Mottled appearance

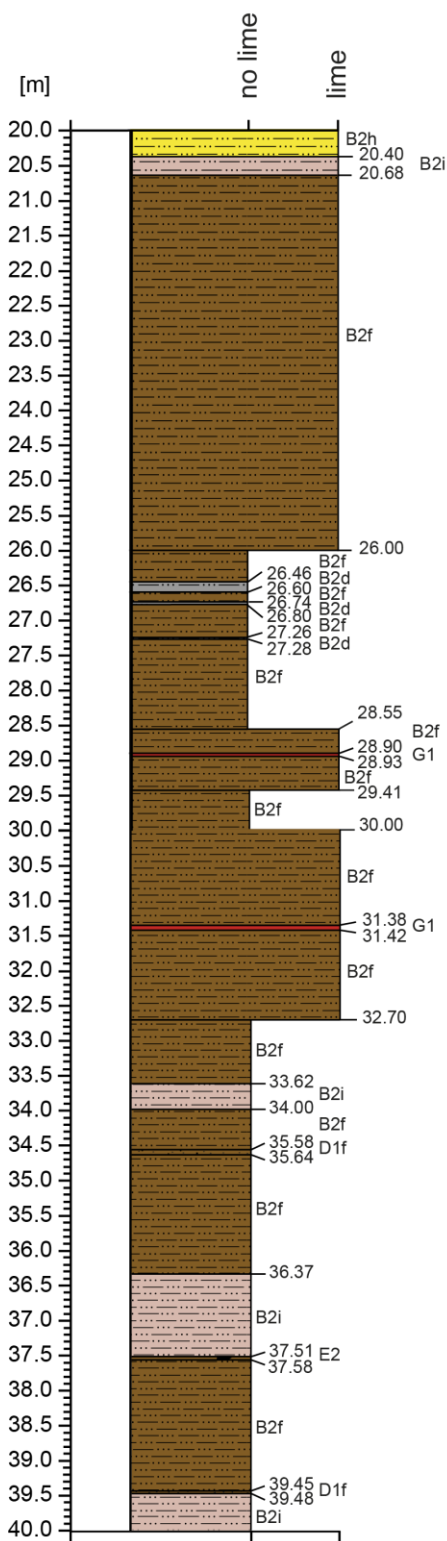
F) Tephra

- 1 Ash
- 2 Lapilli
- 3 Tuff

Colours

- a whitish
- b White
- c Dark grey
- d Grey
- e Light grey
- f Brown
- g Brown/Yellow
- h Yellow
- i Reddish

Core: RM2 Rother Maar



A) Interglacial/Interstadial

- 1 Gyttja
- 2 Sapropel
- 3 Diatom gyttja

B) Glacial

- 1 Silt lamination
- 2 Silt-Cley lamination

C) Detrital

- 1 Rounded
- 2 Angular
- 3 Matrix supported

D) Rearrangement

- 1 Sand layer
- 2 Dark sand layer
- 3 Clay layer
- 4 Turbidite
- 5 Cross-bedding
- 6 Soil horizon

E) Slump

- 1 folded
- 2 Mottled appearance

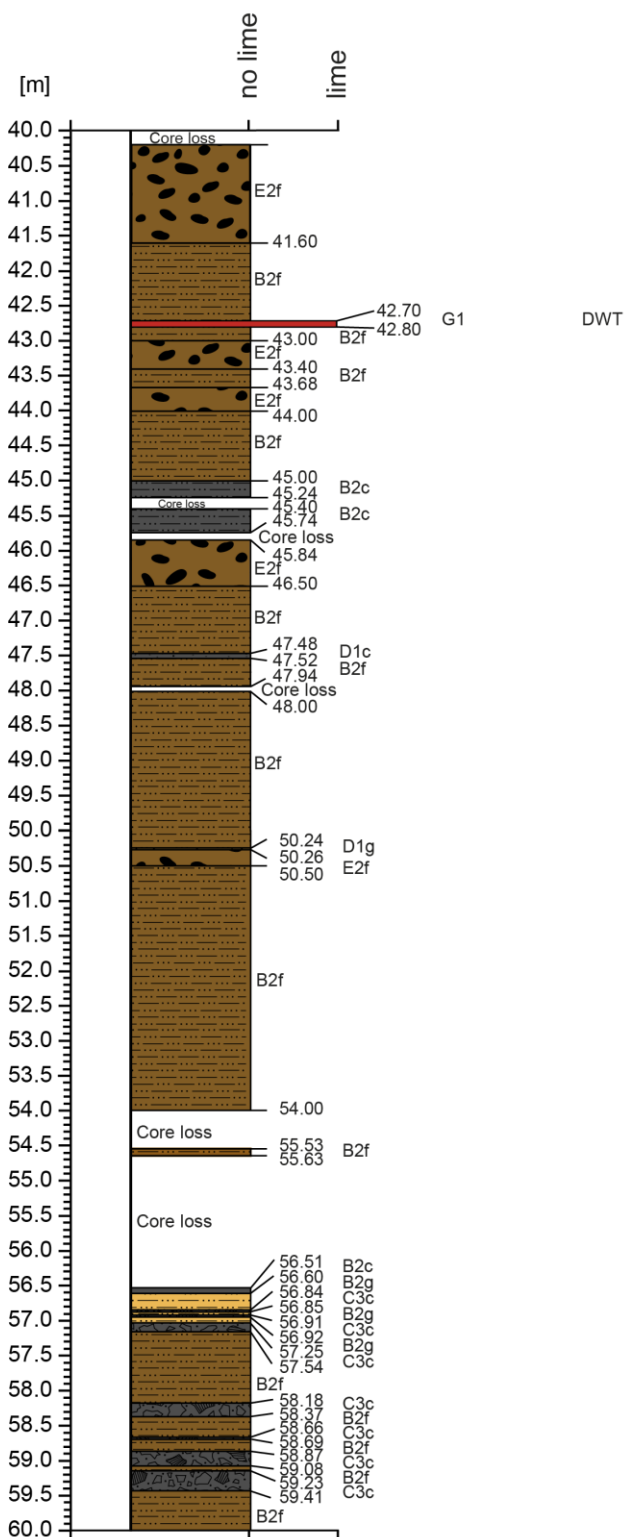
F) Tephra

- 1 Ash
- 2 Lapilli
- 3 Tuff

Colours

- a whitish
- b White
- c Dark grey
- d Grey
- e Light grey
- f Brown
- g Brown/Yellow
- h Yellow
- i Reddish

Core: RM2 Rother Maar



A) Interglacial/Interstadial

- 1 Gyttja
- 2 Sapropel
- 3 Diatom gyttja

B) Glacial

- 1 Silt lamination
- 2 Silt-Clay lamination

C) Detrital

- 1 Rounded
- 2 Angular
- 3 Matrix supported

D) Rearrangement

- 1 Sand layer
- 2 Dark sand layer
- 3 Clay layer
- 4 Turbidite
- 5 Cross-bedding
- 6 Soil horizon

E) Slump

- 1 folded
- 2 Mottled appearance

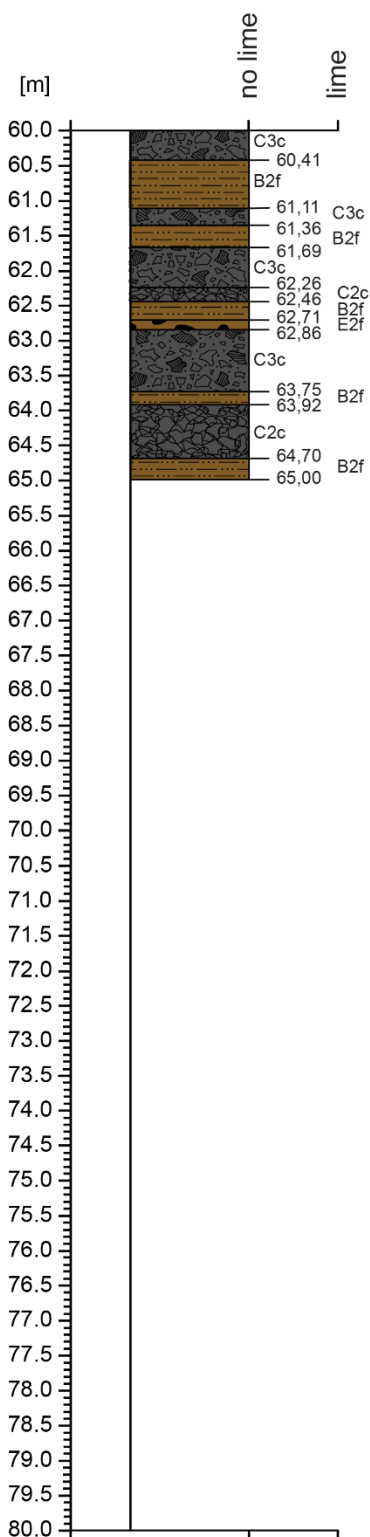
F) Tephra

- 1 Ash
- 2 Lapilli
- 3 Tuff

Colours

- a** whitish
- b** White
- c** Dark grey
- d** Grey
- e** Light grey
- f** Brown
- g** Brown/Yellow
- h** Yellow
- i** Reddish

Core: RM2 Rother Maar



A) Interglacial/Interstadial

- 1 Gyttja
- 2 Sapropel
- 3 Diatom gyttja

B) Glacial

- 1 Silt lamination
- 2 Silt-Clay lamination

C) Detrital

- 1 Rounded
- 2 Angular
- 3 Matrix supported

D) Rearrangement

- 1 Sand layer
- 2 Dark sand layer
- 3 Clay layer
- 4 Turbidite
- 5 Cross-bedding
- 6 Soil horizon

E) Slump

- 1 folded
- 2 Mottled appearance

F) Tephra

- 1 Ash
- 2 Lapilli
- 3 Tuff

Colours

- a** whitish
- b** White
- c** Dark grey
- d** Grey
- e** Light grey
- f** Brown
- g** Brown/Yellow
- h** Yellow
- i** Reddish

Appendix C Flood layer table

Gauge analysis Cologne
Period: 2014 – 1800 [AD]

Recurrence interval	Recurrence interval
25 years	10 years
1995	2011
1993	2003
1988	1997
1948	1995
1926	1993
1920	1988
1882	1984
1845	1983
	1970
	1955
	1948
	1926
	1924
	1920
	1883
	1882
	1876
	1850
	1845
	1819

Core: SMf2**Flood layers over 0.75 cm****Period: 1950 – 1000 [AD]/ 50 – 1000 [b2k]**

Number	Depth from [m]	Depth to [m]	Average [m]	Thickness [cm]	Average-Year [AD]	Average-Year [b2k]
1	0.128	0.162	0.145	3.3160	1945	55
2	0.226	0.235	0.230	0.0092	1917	83
3	0.326	0.337	0.331	0.0115	1858	142
4	0.797	0.806	0.802	0.0086	1559	441
5	0.825	0.851	0.838	0.0258	1547	453
6	0.876	0.919	0.897	0.0425	1532	468
7	0.984	0.997	0.991	0.0126	1499	501
8	0.997	1.016	1.007	0.0186	1498	502
9	1.016	1.047	1.032	0.0303	1497	503
10	1.090	1.098	1.094	0.0087	1470	530
11	1.114	1.178	1.146	0.0635	1462	538
12	1.233	1.249	1.241	0.0166	1440	560
13	1.268	1.283	1.276	0.0148	1429	571
14	1.297	1.307	1.302	0.0102	1423	577
15	1.425	1.454	1.439	0.0293	1359	641
16	1.492	1.530	1.511	0.0388	1342	658
17	1.561	1.572	1.567	0.0111	1324	676
18	1.584	1.599	1.592	0.0152	1316	684
19	1.645	1.654	1.650	0.0086	1278	722
20	1.657	1.665	1.661	0.0075	1274	726
21	1.677	1.729	1.703	0.0519	1265	735
22	1.736	1.757	1.747	0.0212	1259	741
23	1.798	1.872	1.835	0.0737	1226	774
24	1.988	2.009	1.999	0.0219	1134	866
25	2.014	2.025	2.020	0.0102	1131	869

Core: HM1**Flood layers over 0.75 cm****Period: 0 – 13000 [b2k]**

Number	Depth from [m]	Depth to [m]	Average [m]	Thickness [cm]	Average-Year [b2k]
1	0.66	0.69	0.675	3	243
2	0.96	0.971	0.966	1.1	347
3	0.998	1.006	1.002	0.8	360
4	1.82	1.836	1.828	1.6	658
5	1.921	1.932	1.927	1.1	721
6	2.225	2.241	2.233	1.6	920
7	3.197	3.205	3.201	0.8	1549
8	3.627	3.641	3.634	1.4	2038
9	3.946	3.954	3.950	0.8	2429
10	4.223	4.305	4.264	8.2	2827
11	4.4	4.432	4.416	3.2	3117
12	5.42	5.428	5.424	0.8	5124
13	8.893	8.905	8.899	1.2	11704
14	9.413	9.422	9.418	0.9	12643

Core: UM2**Flood layers over 0.75 cm****Period: 0 – 8600 [b2k]**

Number	Depth from [m]	Depth to [m]	Average [m]	Thickness [cm]	Average-Year [b2k]
1	1.528	2.426	1.977	89.8	658
2	2.555	2.563	2.559	0.8	720
3	2.72	2.831	2.776	11.1	805
4	2.886	2.896	2.891	1	851
5	3.004	3.015	3.010	1.1	897
6	3.024	3.036	3.030	1.2	905
7	3.117	3.126	3.122	0.9	941
8	3.194	3.219	3.207	2.5	975
9	3.272	3.281	3.277	0.9	1002
10	3.3	3.311	3.306	1.1	1013
11	3.32	3.333	3.327	1.3	1022
12	3.389	3.4	3.395	1.1	1048
13	3.447	3.464	3.456	1.7	1072
14	3.476	3.487	3.482	1.1	1082
15	3.577	3.589	3.583	1.2	1122
16	3.604	3.613	3.609	0.9	1132
17	3.637	3.649	3.643	1.2	1146
18	3.765	3.9	3.833	13.5	1220
19	4.068	4.077	4.073	0.9	1314
20	4.106	4.118	4.112	1.2	1330
21	4.26	4.279	4.270	1.9	1392
22	4.364	4.376	4.370	1.2	1431
23	4.557	4.585	4.571	2.8	1510
24	4.639	4.667	4.653	2.8	1542
25	4.691	4.723	4.707	3.2	1563
26	4.745	4.76	4.753	1.5	1581
27	4.901	4.928	4.915	2.7	1689
28	5.067	5.081	5.074	1.4	1812
29	5.115	5.132	5.124	1.7	1850
30	5.32	5.329	5.325	0.9	2006
31	5.416	5.428	5.422	1.2	2082
32	5.53	5.558	5.544	2.8	2176
33	5.673	5.681	5.677	0.8	2279
34	5.709	5.725	5.717	1.6	2310
35	5.786	5.795	5.791	0.9	2367
36	5.831	5.839	5.835	0.8	2401
37	5.855	5.864	5.860	0.9	2420

Number	Depth from [m]	Depth to [m]	Average [m]	Thickness [cm]	Average-Year [b2k]
38	6.044	6.052	6.048	0.8	2566
39	6.31	6.371	6.341	6.1	2792
40	6.4	6.43	6.415	3	2844
41	6.486	6.5	6.493	1.4	2897
42	6.571	6.6	6.586	2.9	2960
43	6.709	6.741	6.725	3.2	3054
44	6.814	6.828	6.821	1.4	3119
45	6.844	6.857	6.851	1.3	3139
46	6.863	6.883	6.873	2	3154
47	7.017	7.046	7.032	2.9	3262
48	7.226	7.237	7.232	1.1	3397
49	7.251	7.265	7.258	1.4	3415
50	7.328	7.338	7.333	1	3466
51	7.364	7.382	7.373	1.8	3493
52	7.41	7.421	7.416	1.1	3522
53	7.46	7.499	7.480	3.9	3565
54	7.606	7.617	7.612	1.1	3655
55	7.636	7.664	7.650	2.8	3681
56	7.717	7.748	7.733	3.1	3737
57	7.779	7.797	7.788	1.8	3774
58	8.027	8.036	8.032	0.9	4040
59	8.135	8.162	8.149	2.7	4208
60	8.227	8.235	8.231	0.8	4327
61	8.379	8.413	8.396	3.4	4565
62	8.453	8.463	8.458	1	4654
63	8.535	8.545	8.540	1	4772
64	8.583	8.592	8.588	0.9	4841
65	8.6	8.612	8.606	1.2	4867
66	8.64	8.652	8.646	1.2	4925
67	8.727	8.75	8.739	2.3	5058
68	8.91	8.918	8.914	0.8	5311
69	8.935	8.95	8.943	1.5	5352
70	9.117	9.133	9.125	1.6	5615
71	9.3	9.321	9.311	2.1	5883
72	9.373	9.383	9.378	1	6001
73	9.435	9.443	9.439	0.8	6068
74	9.464	9.481	9.473	1.7	6116
75	9.513	9.521	9.517	0.8	6180
76	9.563	9.579	9.571	1.6	6258
77	9.606	9.617	9.612	1.1	6311
78	9.684	9.692	9.688	0.8	6384

Number	Depth from [m]	Depth to [m]	Average [m]	Thickness [cm]	Average-Year [b2k]
79	9.753	9.767	9.760	1.4	6453
80	9.788	9.8	9.794	1.2	6486
81	9.886	9.898	9.892	1.2	6580
82	10.06	10.077	10.069	1.7	6749
83	10.13	10.139	10.135	0.9	6812
84	10.345	10.362	10.354	1.7	6991
85	10.389	10.401	10.395	1.2	7061
86	10.431	10.446	10.439	1.5	7103
87	10.471	10.485	10.478	1.4	7141
88	10.495	10.503	10.499	0.8	7161
89	10.541	10.566	10.554	2.5	7213
90	10.72	10.73	10.725	1	7377
91	10.779	10.789	10.784	1	7434
92	10.831	10.84	10.836	0.9	7483
93	11	11.01	11.005	1	7645
94	11.233	11.248	11.241	1.5	7871
95	11.269	11.281	11.275	1.2	7904
96	11.319	11.422	11.371	10.3	7995
97	11.488	11.499	11.494	1.1	8113
98	11.615	11.624	11.620	0.9	8234
99	11.642	11.65	11.646	0.8	8259
100	11.7	11.71	11.705	1	8315
101	11.745	11.755	11.750	1	8359
102	11.801	11.811	11.806	1	8412
103	11.837	11.846	11.842	0.9	8446
104	11.862	11.874	11.868	1.2	8471
105	11.923	12	11.962	7.7	8561

Core: AU2**Flood layers over 0.75 cm****Period: 10000 – 60000 [b2k]**

Number	Depth from [m]	Depth to [m]	Average [m]	Thickness [cm]	Average-Year [b2k]
1	8.051	8.11	8.081	5.9	10649
2	8.355	8.379	8.367	2.4	10760
3	9.696	9.72	9.708	2.4	11280
4	9.833	9.85	9.842	1.7	11332
5	9.875	9.884	9.880	0.9	11347
6	10.439	10.449	10.444	1	11566
7	10.476	10.515	10.496	3.9	11586
8	10.614	10.622	10.618	0.8	11634
9	11.07	11.092	11.081	2.2	11813
10	11.618	11.628	11.623	1	12024
11	11.852	11.9	11.876	4.8	12122
12	12.197	12.22	12.209	2.3	12251
13	13.249	13.281	13.265	3.2	12661
14	13.426	13.463	13.445	3.7	12731
15	14.138	14.152	14.145	1.4	13065
16	15.385	15.442	15.414	5.7	13858
17	15.622	15.634	15.628	1.2	13991
18	15.698	15.709	15.704	1.1	14039
19	15.77	15.789	15.780	1.9	14086
20	16.305	16.313	16.309	0.8	14417
21	17.027	17.043	17.035	1.6	14982
22	17.42	17.433	17.427	1.3	15380
23	17.506	17.517	17.512	1.1	15467
24	17.575	17.608	17.592	3.3	15548
25	18.402	18.424	18.413	2.2	16384
26	18.457	18.478	18.468	2.1	16439
27	18.513	18.539	18.526	2.6	16499
28	18.622	18.646	18.634	2.4	16609
29	19.717	19.732	19.725	1.5	17718
30	19.807	19.837	19.822	3	17817
31	19.853	19.863	19.858	1	17854
32	24.347	24.37	24.359	2.3	22433
33	24.585	24.597	24.591	1.2	22670
34	26.36	26.378	26.369	1.8	23886
35	26.391	26.406	26.399	1.5	23900
36	26.577	26.592	26.585	1.5	23991
37	26.697	26.705	26.701	0.8	24048

Number	Depth from [m]	Depth to [m]	Average [m]	Thickness [cm]	Average-Year [b2k]
38	26.74	26.774	26.757	3.4	24075
39	26.896	26.929	26.913	3.3	24151
40	27.236	27.261	27.249	2.5	24315
41	27.34	27.351	27.346	1.1	24362
42	27.509	27.517	27.513	0.8	24444
43	27.789	27.814	27.802	2.5	24585
44	28.043	28.052	28.048	0.9	24705
45	37.036	37.046	37.041	1	28358
46	37.683	37.695	37.689	1.2	28488
47	41.599	41.621	41.610	2.2	29258
48	42.096	42.106	42.101	1	29352
49	42.643	42.66	42.652	1.7	29458
50	42.822	42.838	42.830	1.6	29492
51	43.738	43.747	43.743	0.9	29668
52	44.345	44.361	44.353	1.6	29785
53	44.613	44.621	44.617	0.8	29836
54	44.837	44.846	44.842	0.9	29879
55	46.27	46.321	46.296	5.1	30159
56	46.777	46.834	46.806	5.7	30280
57	47.688	47.706	47.697	1.8	30520
58	48.296	48.33	48.313	3.4	30686
59	48.49	48.51	48.500	2	30736
60	48.72	48.736	48.728	1.6	30797
61	49.097	49.161	49.129	6.4	30905
62	50.061	50.078	50.070	1.7	31159
63	50.165	50.192	50.179	2.7	31188
64	50.335	50.394	50.365	5.9	31238
65	50.603	50.617	50.610	1.4	31304
66	50.858	50.868	50.863	1	31372
67	51.386	51.42	51.403	3.4	31518
68	52.818	52.837	52.828	1.9	31901
69	53.193	53.202	53.198	0.9	32001
70	54.62	54.634	54.627	1.4	32386
71	55.875	55.886	55.881	1.1	33015
72	58.488	58.503	58.496	1.5	34166
73	59.558	59.574	59.566	1.6	34482
74	59.686	59.697	59.692	1.1	34519
75	60.378	60.407	60.393	2.9	34726
76	60.52	60.542	60.531	2.2	34767
77	61.393	61.42	61.407	2.7	35025
78	61.524	61.539	61.532	1.5	35062

Number	Depth from [m]	Depth to [m]	Average [m]	Thickness [cm]	Average-Year [b2k]
79	62.344	62.362	62.353	2.8	35304
80	62.818	62.834	62.826	2.6	35443
81	82.4	82.409	82.405	0.9	44092
82	83.373	83.396	83.385	2.3	44381
83	83.467	83.495	83.481	2.8	44409
84	84.447	84.457	84.452	1	44695
85	84.785	84.848	84.817	6.3	44802
86	86.355	86.39	86.373	3.5	45451
87	86.684	86.692	86.688	0.8	45593
88	86.737	86.749	86.743	1.2	45618

Core: MS1**Flood layers over 0.75 cm****Period: 25000 – 70000 [b2k]**

Number	Depth from [m]	Depth to [m]	Average [m]	Thickness [cm]	Average-Year [b2k]
1	4.97	4.988	4.979	1.8	26648
2	5.738	5.749	5.744	1.1	26901
3	9.428	9.437	9.433	0.9	28045
4	11.767	11.811	11.789	4.4	28555
5	14.527	14.538	14.533	1.1	29148
6	15.363	15.419	15.391	5.6	29333
7	16.455	16.468	16.462	1.3	29565
8	18.304	18.328	18.316	2.4	29966
9	22.128	22.138	22.133	1	41285
10	22.327	22.341	22.334	1.4	41373
11	25.981	26	25.991	1.9	42970
12	28.706	28.72	28.713	1.4	44590
13	29.391	29.428	29.410	3.7	45401
14	29.543	29.555	29.549	1.2	45564
15	29.744	29.752	29.748	0.8	45797
16	30.069	30.078	30.074	0.9	46175
17	34.871	34.898	34.885	2.7	52577
18	35.404	35.415	35.410	1.1	53364
19	35.448	35.463	35.456	1.5	53433
20	40.816	40.828	40.822	1.2	60699
21	41.851	41.868	41.860	1.7	61247
22	42.445	42.471	42.458	2.6	61563
23	44.512	44.597	44.555	8.5	62671
24	46.493	46.519	46.506	2.6	63702

Core: RM2**Flood layers over 0.75 cm****Period: 10000 – 70000 [b2k]**

Number	Depth from [m]	Depth to [m]	Average [m]	Thickness [cm]	Average-Year [b2k]
1	4.63	4.646	4.638	1.6	10206
2	4.667	4.675	4.671	0.8	10214
3	6.467	6.481	6.474	1.4	10683
4	6.846	6.857	6.852	1.1	10781
5	7.065	7.082	7.074	1.7	10839
6	8.568	8.579	8.574	1.1	11229
7	9.642	9.65	9.646	0.8	11508
8	9.693	9.701	9.697	0.8	11521
9	10.907	10.946	10.927	3.9	11841
10	12.083	12.112	12.098	2.9	12145
11	13.726	13.741	13.734	1.5	12571
12	15.913	15.921	15.917	0.8	13888
13	16.261	16.271	16.266	1	14264
14	22.273	22.298	22.286	2.5	21751
15	22.647	22.659	22.653	1.2	22147
16	27.273	27.282	27.278	0.9	26130
17	28.512	28.52	28.516	0.8	27465
18	29.781	29.792	29.787	1.1	28710
19	30.161	30.173	30.167	1.2	29066
20	30.631	30.639	30.635	0.8	29503
21	31.113	31.122	31.118	0.9	29955
22	40.831	40.843	40.837	1.2	39239
23	41.441	41.456	41.449	1.5	39823
24	41.562	41.581	41.572	1.9	39941
25	43.482	43.494	43.488	1.2	42007
26	43.615	43.637	43.626	2.2	42179
27	45.337	45.352	45.345	1.5	44320
28	45.742	45.756	45.749	1.4	44824
29	46.915	46.924	46.920	0.9	46283
30	47.492	47.501	47.497	0.9	46993
31	50.247	50.259	50.253	1.2	51553
32	51.401	51.409	51.405	0.8	54104
33	51.595	51.603	51.599	0.8	54534
34	56.839	56.848	56.844	0.9	61817
35	56.913	56.922	56.918	0.9	61863
36	57.247	57.262	57.255	1.5	62071
37	58.527	58.535	58.531	0.8	62859

Number	Depth from [m]	Depth to [m]	Average [m]	Thickness [cm]	Average-Year [b2k]
38	58.671	58.681	58.676	1	62948
39	59.458	59.469	59.464	1.1	63434
40	59.503	59.514	59.509	1.1	63462

Appendix D Core correlation table

LEZ-Zone	Time marker	Event	Age	UM _f	SM _{f2}	HM _f	UM2	HM1	GM1	SM2	SM3	SM4	SM5	SM6	SM7	SM8	SM9	SM10	
			[b2k]	[m]	[m]	[m]	[m]	[m]	[m]	[m]	[m]	[m]	[m]	[m]	[m]	[m]	[m]	[m]	
LEZ 1		Tschernobyl 137Cs peak	14	0.18	0.09		0.11												
		Colour change 1												0.36	0.44		0.12	0.12	
		137Cs peak	37	0.28	0.18														
		AD 1342	Flood event 1342 Top				1.53	1.82	1.11		1.61								
			Flood event 1342 Basis	658		1.51	1.74	2.43	1.84	1.18		1.69	1.45		1.08	1.12	0.95	0.92	0.85
			Start Carpinus peak	1 570			4.80	3.28	3.30		2.70								
			Colour change 2											0.95	1.88	1.77	1.67	1.57	1.59
			Betula peak	1 590			4.90	3.30			2.80								
			Colour change 3								3.28	2.84	3.14	1.89					
			Increase Cereal	2 700			6.00	4.20			3.35	3.35							
			Flood event 800 BC	2 800			6.35	4.25	4.07	3.38	3.40	3.34							
		Subboreal	Increase of Fagus	3 850			7.90	4.80	4.70	3.90									
			Elm fall	6 300			9.60	6.00	5.25	4.19	4.60			3.18					
	LEZ 2	8,2 ka event		8 200				11.50	7.00										
		Hazel decrease	8 600				11.60	7.20	5.70	5.10	5.40								
	10.500 b2k	Oaks and elms	10 500					8.24			5.78								
LEZ 3		Hazel increase	10 850					8.40		6.00									
	UMT		11 000				12.00	8.51	6.36		5.88	5.98							
	11 600 BP	Colour change 4	11 650					8.80	6.45	6.10	6.00								
		Increase of grass pollen	12 850					9.40	6.65	6.30									
		LST Top						9.53	6.72	6.44	6.24	6.20							
	LST Basis		12 900				9.66	6.80	6.53	6.33	6.26								

LEZ-Zone	Time marker	Event	Age [b2k]	AU2 [m]	DE2 [m]	DE3 [m]	MS1 [m]	OW1 [m]	RM2 [m]	JW2 [m]	JW3 [m]
LEZ 3	LST Top			13.80		3.40					
	LST Basis		12 900	13.95		3.49		2.65	15.00		1.14
	14 700 b2k		14 700	16.96		7.60			16.67		
LEZ 4	Glacial Max	Dark sediment colour	22 700	25.25		26.105					
	23 000 b2k		23000	23.49					22.52		
LEZ 5		Start red layer zone		30.26		36.76		15.45			
		End red layer zone		30.42		37.69		26.10			
	GI 3		27 780	34.35							
	WBT Top			36.70	37.30	37.80	8.72	27.76	28.80		
	WBT Basis		28 300	36.90	37.37	37.92	8.80	27.78	28.92		
	GI 4		28 900	39.75							
LEZ 6	28 500 b2k	Start red layer zone				40.49	12.72	28.05			21.29
		End red layer zone				42.08	15.56	29.37			
	UT1 Top			46.50		42.80	19.24	30.27	31.34		
	UT1 Basis		30 200	46.60		42.93	19.40	30.30	31.41		
	GI 5		32 500	55.05							
	GI 6		33 740	57.05							
	GI 7		35 480	62.95							
		Start red layer zone				43.37		34.33			
		End red layer zone				45.59		34.85			41.70
		Start slide zone		63.86		47.43					42,03
		End slide zone		64.14		47.63					45,00
	36500 b2k		36 500	64.33			20.61		37.97		
LEZ 7	Beginn GI 8		38 220	66.35							
	Beginn GI 9		40 160	69.35							
	DWT Top			71.12		47.63	21.46	39.40	42.68	51.38	49.39
	DWT Basis		40 800	71.20		47.66	21.50	39.45	42.70	51.52	49.42
	GI 10		41 460	73.15							
		Start vivianite zone				48.22	21.57				
		End vivianite zone				50.12	21.91				

LEZ-Zone	Time marker	Event	Age	AU2	DE2	DE3	MS1	OW1	RM2	JW2	JW3
			[b2k]	[m]	[m]	[m]	[m]	[m]	[m]	[m]	[m]
		Start slide zone		77.19			23.12				
	GI 11		43 340	77.55							
		End slide zone		79.47			24.28				
	UT2 Top			81.59		50.67	28.07	43.02			
	UT2 Basis		43 900	81.63		50.68	28.14	43.08			
		Start slide zone				55.29	28.84	47.00			
		End slide zone				56.98	29.15	47.56			
		Start red layer zone				57.02					65.66
		End red layer zone				58.37					67.28
	GI 12		46 860	89.50							
	48 700 b2k	End Picea + Carpinus zone	48 700	91.50		59.90	32.50		49.10		71.70
LEZ 8		Start vivianite zone		92.28			33.43				72.14
		Start slide zone		92.32		60.30					
	GI 13		49 280	92.55							
		End slide zone		93.36		61.86					
	GI 14		54 220	94.35							
	55200 b2k	Start Picea + Carpinus zone	55 200	96.55		64.80					73.00
LEZ 9		Start slide zone		97.51		70.19			50.5		
	GI 15		55 800	97.95							
		End slide zone		98.86		70.28			50.84		
	GI 16		58 280	99.55							
		End vivianite zone				73.16	39.74				
	60 000 b2k	Start Picea zone	60 000	101.95		73.90	39.50		53.90		74.20

Acknowledgment

Curriculum vitae

Personal Details

Name: Heiko Brunck
Date and Place of Birth: 02/01/1987, Landstuhl
Nationality: German

Education

01/2014 – 12/2016 Johannes Gutenberg-University Mainz
Academic Degree: Doctor of Science
Dissertation: Palaeoflood Project – Floods of Central Europe during the Late Quaternary

10/2007 – 11/2013 Johannes Gutenberg-University Mainz
Academic degree: Diploma Geologist
Focus: Sedimentology, Mineralogy and Environmental Geochemistry
Thesis: Zum Einfluss von Sonnenaktivität und NAO auf das Klima von Mitteleuropa – Rekonstruktion aus historischen Daten und laminierten Maarsedimenten der Eifel

08/1997 – 04/2006 Gymnasium Ramstein-Miesenbach, higher education entrance qualification

Eidesstattliche Erklärung

Hiermit versichere ich gemäß § 10 Abs. 3d der Promotionsordnung vom 24.07.2007, dass ich die jetzt als Dissertation vorgelegte Arbeit selbst angefertigt und alle benutzten Hilfsmittel (Literatur, Apparaturen, Material) in der Arbeit angegeben habe. Des Weiteren habe oder hatte ich die jetzt als Dissertation vorgelegte Arbeit nicht als Prüfungsarbeit für eine staatliche oder andere wissenschaftliche Prüfung eingereicht. Außerdem hatte ich weder die jetzt als Dissertation vorgelegte Arbeit noch Teile davon bei einer anderen Fakultät bzw. einem anderen Fachbereich als Dissertation eingereicht.

Mainz, Januar 2017

Handwritten signature of Heiko Brunk in black ink.